



Hydrodynamic Modelling Report

**San Jacinto River Waste Pits - Northern
Impoundment**

June 17, 2024

→ **The Power of Commitment**

Contents

1. Introduction	1
1.1 Background	1
1.2 Site Description	2
2. Data Sources and Description	3
2.1 Bathymetry and Coastline Data	3
2.2 Water Level Data	3
2.3 Wind Data	5
2.4 Flow Data	5
2.5 Lake Houston Data	7
2.6 Sediment Samples	9
3. Model Description	9
3.1 Background	9
3.2 Model Setup	10
3.3 Modeled Scenarios	13
3.3.1 Cofferdam Effects on Floodplain	13
3.3.2 Sedimentation Analysis	13
3.3.2.1 Existing Condition	13
3.3.2.2 Cofferdam Present	14
3.3.2.3 End-State Condition	14
4. Model Scenario Results	14
4.1 Cofferdam Effects on the Floodplain	14
4.2 Sedimentation Study	23
4.2.1 Sedimentation Study with Cofferdam Analysis	24
4.2.2 End-State Conditions Analysis	29
4.2.3 Cofferdam Effects on I-10	33
5. Summary and Conclusions	34
5.1 Cofferdam Effects on Floodplain	35
5.2 Sedimentation Analysis - Cofferdam	35
5.3 Sedimentation Analysis - End-State	35
6. References	36

Table index

Table 1	NOAA Gauge # 8770613 Datums and Tides	4
Table 2	Surge levels in ft for the corresponding return period based on Gumbel regression	5
Table 3	Streamflow Data	5
Table 4	Velocity Data	5
Table 5	Rating Curve for Lake Houston Dam Spillway (Anchor QEA)	8

Table 6	Sediment Samples Mean Particle Size Distribution (d_{50}) Statistics	9
Table 7	Water Depth Differences	16
Table 8	Critical Shear Stress Classification	24
Table 9	Maximum and Average Shear Stress “With Cofferdam”	25
Table 10	Maximum and Average Shear Stress Differences “With Cofferdam”	25
Table 11	Maximum and Average Velocities for Conditions with Cofferdam	27
Table 12	Percentage Maximum and Average Velocity Differences for Conditions with Cofferdam	28
Table 13	Maximum and Average Shear Stresses for End-State Conditions	30
Table 14	Maximum and Average Shear Stresses Differences for End-State Minus Existing Conditions	30
Table 15	Maximum and Average Velocities for End-State Conditions	32
Table 16	Maximum and Average Velocity Differences for End-State Minus Existing Condition	32

Figure index

Figure 1	Site Location	2
Figure 2	Project Location Watershed (Green: Upper San Jacinto River Basin Watershed; Light Blue: Lower San Jacinto Watershed)	3
Figure 3	NOAA 8770613 Datums	4
Figure 4	USGS 08072050 Highway US-90 / San Jacinto River Near Sheldon, Texas (USGS) The Northern Impoundment is located to the South and Not Shown in Image.	6
Figure 5	USGS 08074000 Buffalo Bayou at Houston, Texas (USGS); The Northern Impoundment and Immediate Surroundings are Identified with the Black Box.	6
Figure 6	USGS 08073700 Buffalo Bayou at Piney Point, Texas (USGS); The Northern Impoundment and Immediate Surroundings are Identified with the Black box.	7
Figure 7	USGS 08072000 Lake Houston River Near Sheldon, Texas (USGS); The Northern Impoundment is located to the South and Not Shown in Image.	8
Figure 8	Sediment Sample Locations	9
Figure 9	Model Domain with Bathymetry	10
Figure 10	Model Grid Showing Delineation of Cofferdam and Cell Models Defining the Northern Impoundment	11
Figure 11	Model Grid Showing location of the Open Boundary Condition at Fred Hartman Bridge	12
Figure 12	Estimated End State Bathymetry Changes with Respect to Existing Conditions	13
Figure 13	Stations for Water Depth Comparisons	15
Figure 14	Station 1 Water Depth Comparison “With and Without Cofferdam” for 2-Year Storm	16
Figure 15	Station 2 Water Depth Comparison “With and Without Cofferdam” for 2-Year Storm	17
Figure 16	Station 1 Water Depth Comparison “With and Without Cofferdam” for 10-Year Storm	17
Figure 17	Station 2 Water Depth Comparison “With and Without Cofferdam” for 10-Year Storm	18
Figure 18	Station 1 Water Depth Comparison “With and Without Cofferdam” for 100-Year Storm	18
Figure 19	Station 2 Water Depth Comparison “With and Without Cofferdam” for 100-Year Storm	19
Figure 20	Maximum Water Surface Elevation for the 2-Year Storm	20

Figure 21	Maximum Water Surface Elevation for the 10-Year Storm	21
Figure 22	Maximum Water Surface Elevation for the 100-Year Storm	22
Figure 23	Area Used for the Computation of Statistics for the Conditions Around the Cofferdam	23
Figure 24	Maximum Shear Stresses “With Cofferdam” for the 100-Year flow	26
Figure 25	Maximum Shear Stress Differences Between “With Cofferdam” and Existing Conditions for the 100-Year flow	27
Figure 26	Maximum Velocities “With Cofferdam” for the 100-Year flow	28
Figure 27	Maximum Velocity Differences Between “With Cofferdam” and Existing Conditions for the 100-Year flow	29
Figure 28	Maximum Shear Stresses with End-State During 100-Year flow	30
Figure 29	Maximum Shear Stress Differences Between End-State and Existing Condition for the 100-Year flow	31
Figure 30	Maximum Velocities with End State Condition During the 2 Year Storm	32
Figure 31	Maximum Velocity Differences Between End-State and Existing Condition for the 2-Year Storm	33
Figure 32	Maximum Shear Stresses “With Cofferdam” for the 2-Year Storm at I-10	34

Appendices

Appendix A	Correspondence to HCFCD - Overview of Floodplain Drainage Impact Analysis
Appendix B	Correspondence to TxDOT - Velocity and Shear Stress Analysis
Appendix C	Shear Stress and Velocity Model Results for All Scenarios

1. Introduction

This updated Hydrodynamic Modelling Report (Report) was prepared by GHD Services Inc. (GHD) to summarize activities conducted to model different scenarios in support of the Remedial Design (RD) for the Northern Impoundment of the San Jacinto River Waste Pits Site, located in Channelview, Texas (Northern Impoundment). In accordance with the 2017 United States Environmental Protection Agency (EPA) Record of Decision (ROD; EPA, 2017), Remedial Action (RA) at the Northern Impoundment will include installation of an engineered cofferdam wall surrounding the Northern Impoundment. The cofferdam will be a temporary structure and will be present in the San Jacinto River (River) for the duration of the RA.

1.1 Background

GHD utilized an Environmental Fluid Dynamic Model (EFDC) of the San Jacinto River (River), originally developed by Anchor QEA (AQEA, 2012), to evaluate the various modelling scenarios related to the presence of the cofferdam in the River. The following scenarios were evaluated to support the RD:

- **Effects of the Cofferdam on the Floodplain.** Hydrodynamic modelling was conducted to evaluate the effects the cofferdam might have on the surrounding floodplain. At the request of the Harris County Flood Control District (HCFCD) in an e-mail to Gary Baumgarten, EPA Remedial Project Manager, dated October 20, 2020, GHD conducted hydrodynamic modelling to assess potential impacts of the cofferdam on the surrounding floodplain. A letter summarizing the results of the Floodplain Drainage Impact Analysis was submitted to the HCFCD on March 30, 2022. The HCFCD sent comments on the letter on April 8, 2022. The comments were addressed in a revised letter submitted to the HCFCD on May 6, 2022, and the HCFCD indicated there were no further comments regarding the revised submittal on May 20, 2022. The revised letter is included as Appendix A and a summary of that evaluation is included herein.
- **Effects of the Cofferdam on Velocity and Shear Stress on the Interstate Highway 10 Bridge (I-10).** As requested by the Texas Department of Transportation (TxDOT) in a TWG meeting held March 10, 2022, GHD prepared a velocity and shear stress analysis to evaluate the potential effects of the cofferdam on the flow of the River as it flows under I-10. TxDOT requested this analysis to confirm the design assumptions being used for a planned TxDOT dolphin/fender repair project underneath I-10. GHD provided the results of this analysis on April 11, 2022. The submittal is included as Appendix B and a summary of that evaluation is included herein.
- **Velocity and Shear Stress Around the Perimeter of the Cofferdam.** As previously mentioned, the cofferdam structure will be in place for the duration of the RA. Modelling was conducted to evaluate potential scour around the outer perimeter of the cofferdam, to inform potential armoring or reinforcement of the base of the cofferdam. The results of that evaluation are included herein. The figures for the 2-, 10-, 100-, and 500-year storm event velocity and shear stresses are found in Appendix C.
- **Velocity and Shear Stress under End-State Conditions.** RA activities include removal of approximately 230,000 cubic yards of impacted material from the Northern Impoundment for off-site disposal (excluding the northwest corner). With the exception of the restoration along the southern side of the impoundment, the excavation area will not be backfilled. On the southern side of the impoundment, a backfilled slope will be installed to support the southern slope of the excavation along the extent of the TxDOT right-of-way (ROW) adjacent to I-10. Modelling was performed to evaluate the effects on the velocity and shear stress of the River assuming an end-state excavated condition. This modelling was also requested by TxDOT in a March 10, 2022, meeting and was previously provided to TxDOT. The results of that evaluation are included herein.

1.2 Site Description

The Northern Impoundment is located alongside the San Jacinto River, north of the Houston Ship Channel (HSC), immediately northeast of I-10 to the east of the City of Houston (see Figure 1, below). The San Jacinto River is tidally influenced running from the Lake Houston Dam to Galveston Bay for a total of 28 miles. The Northern Impoundment is located within the San Jacinto Watershed, shown on Figure 2. The upper San Jacinto River Basin Watershed extends from Huntsville, Texas to Lake Houston and represents ten bayous/creeks. The lower San Jacinto Watershed located south of Lake Houston, is the floodplain area assessed for impact.

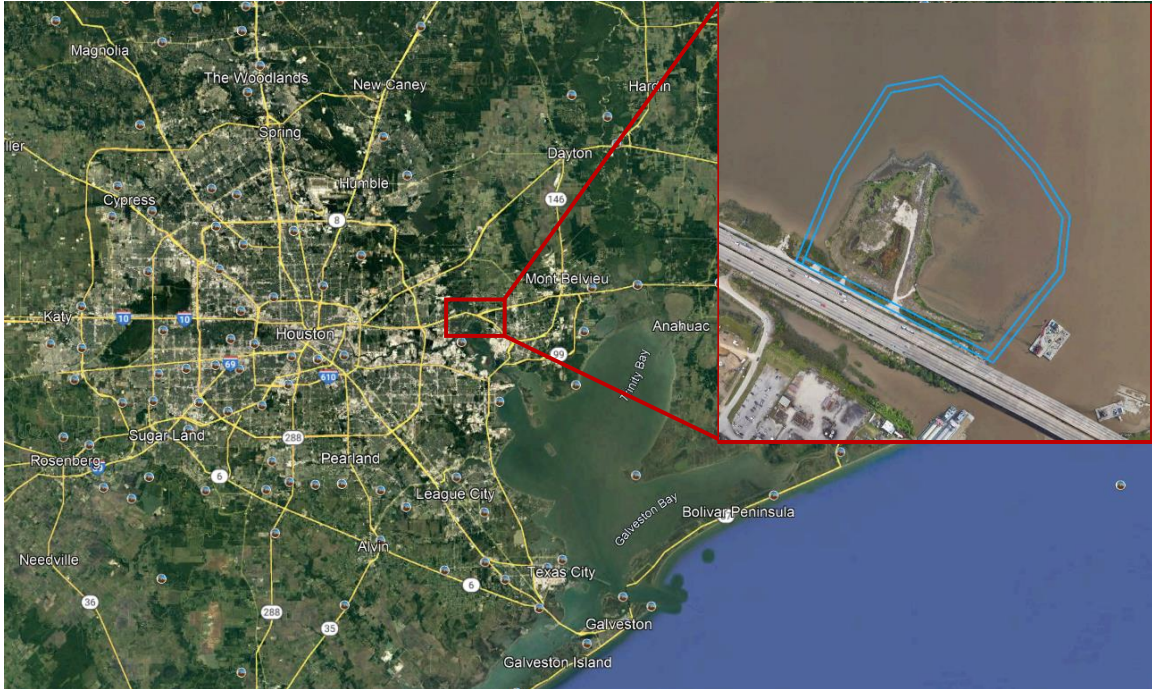


Figure 1 **Site Location**



Figure 2 Project Location Watershed (Green: Upper San Jacinto River Basin Watershed; Light Blue: Lower San Jacinto Watershed)

2. Data Sources and Description

To properly model conditions associated with the Northern Impoundment, a series of data were collected to be used as inputs for the model. The collected data used for the model are discussed in this Section and include bathymetry, water level, wind, streamflow, stream velocity, and sediment data.

2.1 Bathymetry and Coastline Data

Bathymetry and coastline data were acquired from the National Oceanic and Atmospheric Administration's (NOAA) National Centers for Environmental Information (NCEI). The bathymetric topographic data tiles are NCEI continuously updated digital elevation model (CUDEM) with ninth arc second resolution. The data was downloaded as a tif file and converted to an ascii file using ArcMap 10.8.1. Additionally, due to the large size of the data tile, the tile was cut into smaller pieces. The projection is set to the State Plane 1983, with the horizontal and vertical datums being North American Datum of 1983 (NAD83) and North American Vertical Datum of 1988 (NAVD88), respectively.

Detailed bathymetry data of the existing conditions and the estimated end-state of the planned excavation of the Northern Impoundment were obtained. The data was critical for completing the shear stress analysis and velocity assessments.

2.2 Water Level Data

Water level data was collected from the Morgans Point, Texas NOAA gauge #8770613 from NOAA's Tides and Currents website (NOAA, 2021). The water level data is provided in feet relative to the mean lower low water (MLLW)

datum in the 1983 to 2001 epoch. The datum values are listed in Table 1 and shown graphically on Figure 3. The highest observed (max) tide, 6.62 ft occurred on September 12, 2008, at 21:00 with the lowest observed (min) tide, -3.27 ft occurring on January 19, 1996, at 18:00. Morgans Point experiences both diurnal and semidiurnal tides. Diurnal tides have one high and one low tide per day, while semidiurnal tides have two highs and two low tides per day. Verified hourly tidal data from January 6, 1998, through September 16, 2021, was downloaded with data from 2010 through 2020 utilized for the hydrodynamic model.

Table 1 NOAA Gauge # 8770613 Datums and Tides

Datum	Description	MLLW (ft)	NAVD88 (ft)
Highest Observed Tide		6.62	6.63
MHHW	Mean Higher High Water	1.33	1.34
MHW	Mean High Water	1.26	1.27
DHQ	Mean Diurnal High Water Inequality	0.07	0.08
MSL	Mean Sea Level	0.73	0.74
MTL	Mean Tide Level	0.69	0.70
DTL	Mean Diurnal Tide Level	0.67	0.68
MN	Mean Range of Tide	1.13	1.14
GT	Great Diurnal Range	1.33	1.34
MLW	Mean Low Water	0.13	0.14
DLQ	Mean Diurnal Low Water Inequality	0.12	0.13
MLLW	Mean Lower Low Water	0.00	0.01
NAVD88	North American Vertical Datum	-0.01	0.00
Lowest Observed Tide		-3.27	-3.26

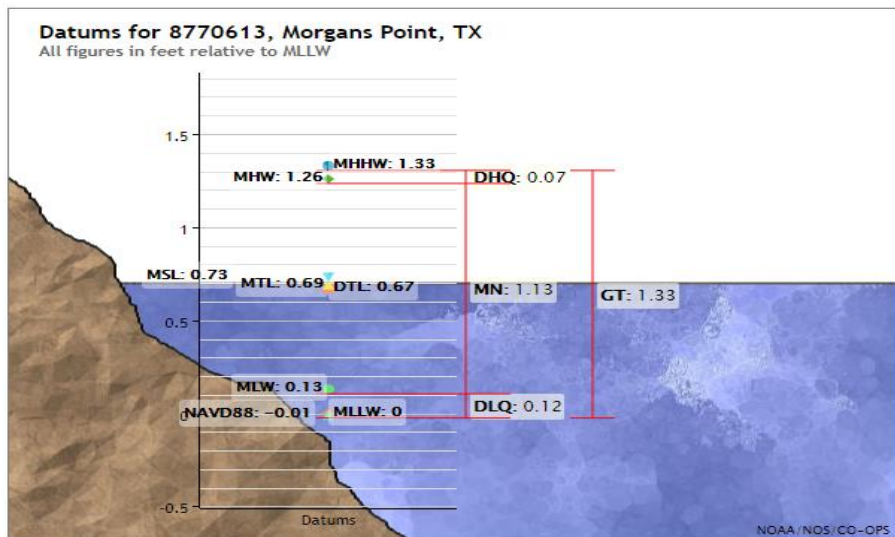


Figure 3 NOAA 8770613 Datums

The surge data at Galveston Bay was also considered for boundary conditions in the model. The surge statistics were obtained from <http://www.u-surge.net/galveston.html>, where the surge values for 85 storms were considered. Values of the surge for the corresponding return period are presented in Table 2 below. As a reference, a 2-year return period approximately corresponds to a tropical storm and a 20-year return period approximately corresponds to a Category 2 hurricane. However, this correlation is affected both by the strength of the storm and its landfall location.

Table 2 Surge levels in ft for the corresponding return period based on Gumbel regression

Return Period (years)	Surge level (feet) using Gumbel regression
20	18.3
10	15.9
5	13.3
2	9.5

2.3 Wind Data

Wind data was acquired from the Morgans Point, Texas NOAA gauge #8770613 from NOAA’s Tides and Currents website (NOAA, 2021). Hourly wind data from October 17, 1995, to September 18, 2008, was collected along with data from June 8, 2010, to September 15, 2021.

2.4 Flow Data

Streamflow data south of Lake Houston is limited with the majority of USGS (United States Geological Survey) gauges measuring water surface elevation and velocity data only. Table 3 lists the USGS gauges with streamflow data (in cubic feet per second, cfs) downloaded along with the gauge location, dates collected, and sample intervals. The velocity data (in feet per second, ft/s) details downloaded at the same gauges are shown in Table 4. Maps of the three gauges with streamflow and velocity are shown on Figure 4 through Figure 6.

Additionally, the drainage area from which precipitation runoff drains into the Buffalo Bayou upstream of USGS gauge #08074710 at Turning Basin, Texas, is 465 square miles and 336 square miles at USGS gauge #08074000.

Table 3 Streamflow Data

USGS Gauge	Location	Start Date	End Date	Interval	Units
08072050	Highway US-90/San Jacinto River near Sheldon, Texas	May 19, 1989	June 11, 2021	Peak (33 samples only)	cfs
08074000	Buffalo Bayou at Houston, Texas	January 2, 1991	September 14, 2021	Hourly	cfs
08073700	Buffalo Bayou at Piney Point, Texas	October 1, 1991	September 24, 2021	15 minutes	cfs

Table 4 Velocity Data

USGS Gauge	Location	Start Date	End Date	Interval	Units
08072050	Highway US-90/San Jacinto River near Sheldon, Texas	August 19, 2020	September 24, 2021	5 minutes	ft/s
08074000	Buffalo Bayou at Houston, Texas	September 28, 2018	September 24, 2021	15 minutes	ft/s
08073700	Buffalo Bayou at Piney Point, Texas	August 1, 2018	September 24, 2021	15 minutes	ft/s

Data from gauges 08074000 and 08073700 were used to generate flow boundary conditions along the Buffalo Bayou and HSC, based on normal flow identified for the stations. For the non-gauged tributaries considered along the Bayou and HSC, a watershed area weighted for these tributaries based on those same station was used.

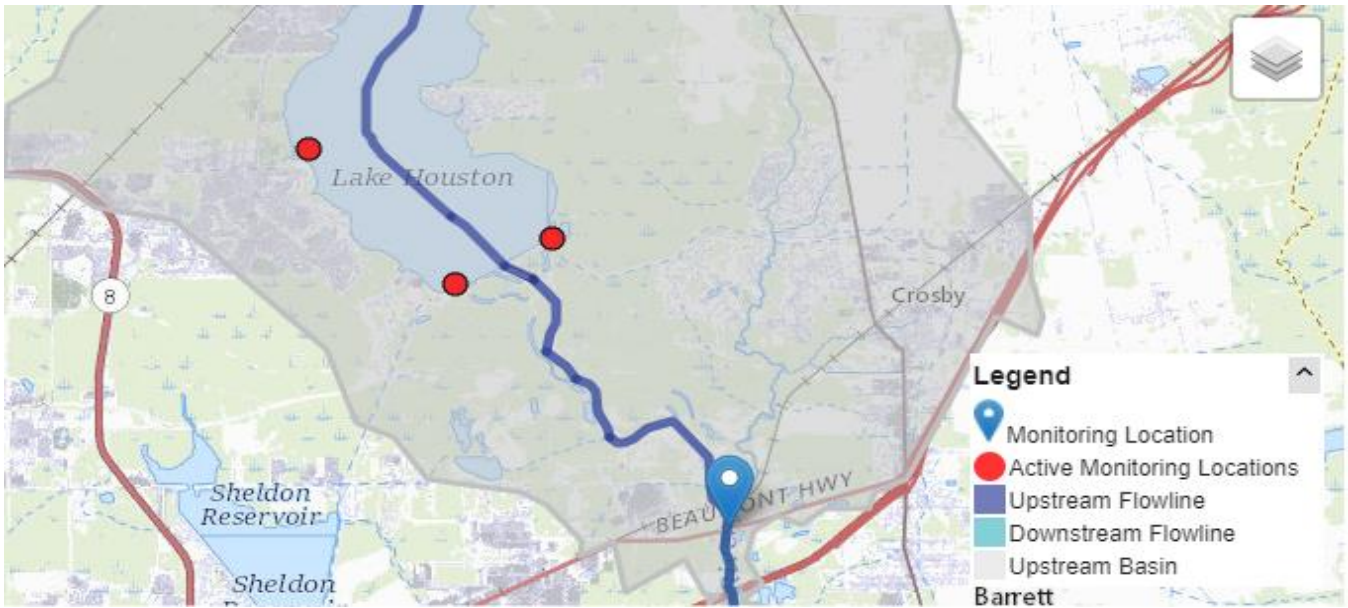


Figure 4 USGS 08072050 Highway US-90 / San Jacinto River Near Sheldon, Texas (USGS) The Northern Impoundment is located to the South and Not Shown in Image.

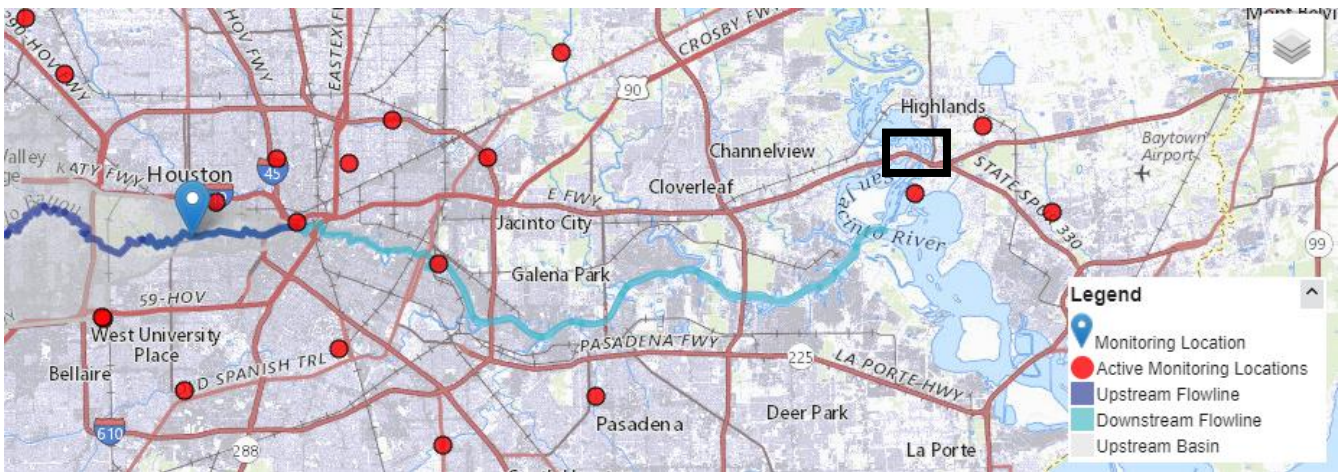


Figure 5 USGS 08074000 Buffalo Bayou at Houston, Texas (USGS); The Northern Impoundment and Immediate Surroundings are Identified with the Black Box.

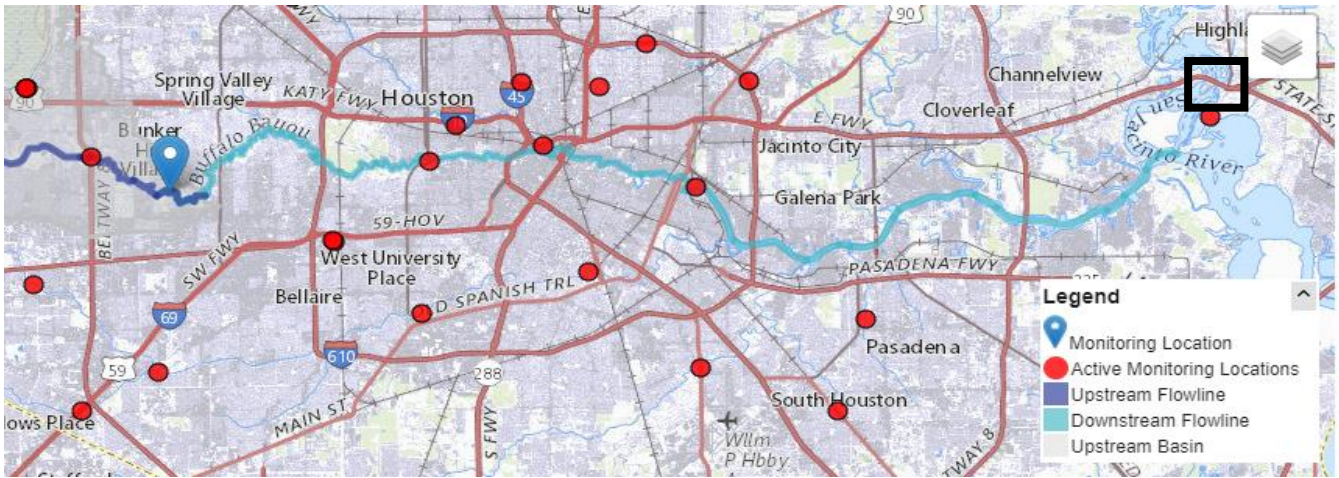


Figure 6 USGS 08073700 Buffalo Bayou at Piney Point, Texas (USGS); The Northern Impoundment and Immediate Surroundings are Identified with the Black box.

2.5 Lake Houston Data

Lake Houston flow data is required to correctly model the flow down the San Jacinto River. Previous hydrodynamic modelling work included obtaining flow rates from CWA (Coastal Water Authority) for the years 2007 through 2011 (AQEA, 2012). For the timeframe prior to 2007, previous modelling used a rating curve, shown in Table 5, to calculate discharge through the gates with the assumption that they were open. In addition, EPA has requested calculated and modeled flow data for the proposed Lake Houston Dam Spillway Improvements from CWA on behalf of GHD, but it has not been provided. In place of CWA data, Lake Houston water levels covering nearly 14 years were downloaded from USGS gauge #08072000, located alongside the dam, as shown on Figure 7. Lake Houston water level data and the rating curve were used to generate flow for the period of data available. These generated flow data showed inconsistencies and therefore the flow rates obtained directly from CWA were deemed more reliable and the extreme values used in the previous modeling work (AQEA,2012) were used.

Table 5 Rating Curve for Lake Houston Dam Spillway (Anchor QEA)

Rating Curve for Lake Houston Dam Spillway			
Lake Stage (ft MSL)	Overflow Spillway Discharge (cfs)	Tainter Gate Discharge (cfs)	Total (cfs)
44.50	0	0	0
45.00	3,500	0	3,500
45.50	9,800	0	9,800
46.00	18,400	9,900	28,300
46.50	28,700	10,300	39,000
47.00	40,600	10,800	51,400
47.50	54,100	11,200	65,300
48.00	68,800	11,700	80,500
48.50	85,000	12,100	97,100
49.00	103,000	12,600	115,600
49.50	121,000	13,100	134,100
50.00	141,000	13,600	154,600
50.50	162,000	14,100	176,100
51.00	184,000	14,500	198,500
51.50	208,000	15,000	223,000
52.00	232,000	15,500	247,500
52.50	257,000	16,000	273,000
53.00	284,000	16,400	300,400
53.50	311,000	16,900	327,900
54.00	339,000	17,300	356,300
54.50	369,000	17,700	386,700
55.00	399,000	18,100	417,100
55.50	430,000	18,500	448,500
56.00	463,000	18,800	481,800
56.50	496,000	19,100	515,100
57.00	530,000	19,400	549,400
57.50	565,000	19,600	584,600
58.00	600,000	19,700	619,700

Notes:
 cfs – cubic feet per second
 MSL – mean sea level

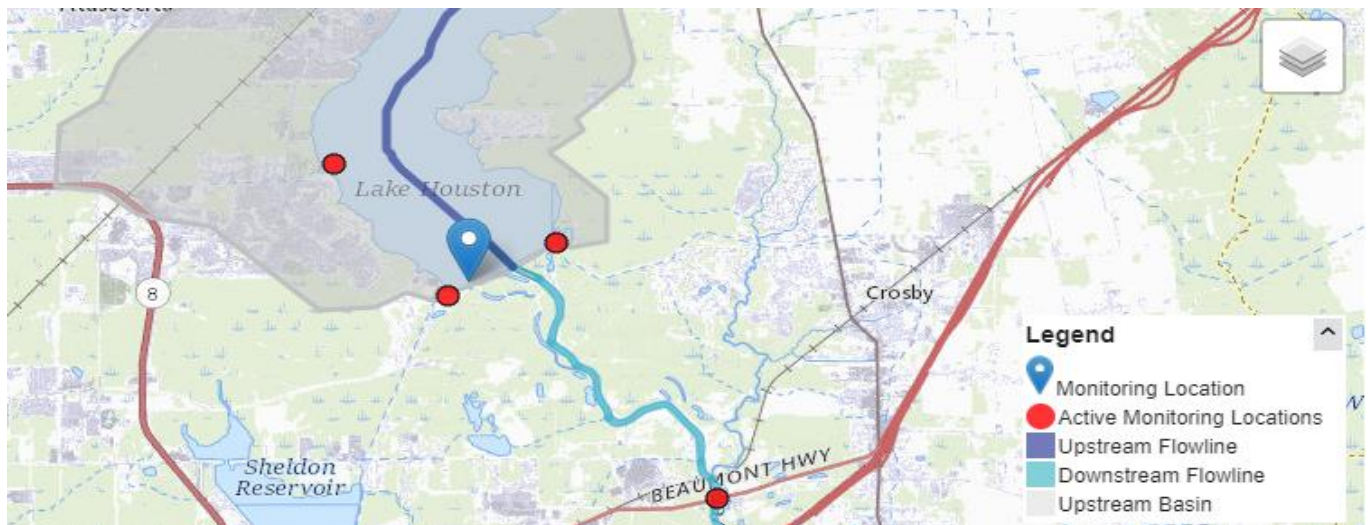


Figure 7 USGS 08072000 Lake Houston River Near Sheldon, Texas (USGS); The Northern Impoundment is located to the South and Not Shown in Image.

2.6 Sediment Samples

As part of the 2021 Supplemental Design Investigation (SDI), shallow sediment samples were collected along the alignment of the planned cofferdam structure, as shown on Figure 8. The sediment was described as a fine to silty sand with clay mixed in. The minimum, maximum and mean particle size distribution (d_{50}) of the sediment samples were calculated (Table 6) and used as input for the sedimentation study described in Section 4.2.

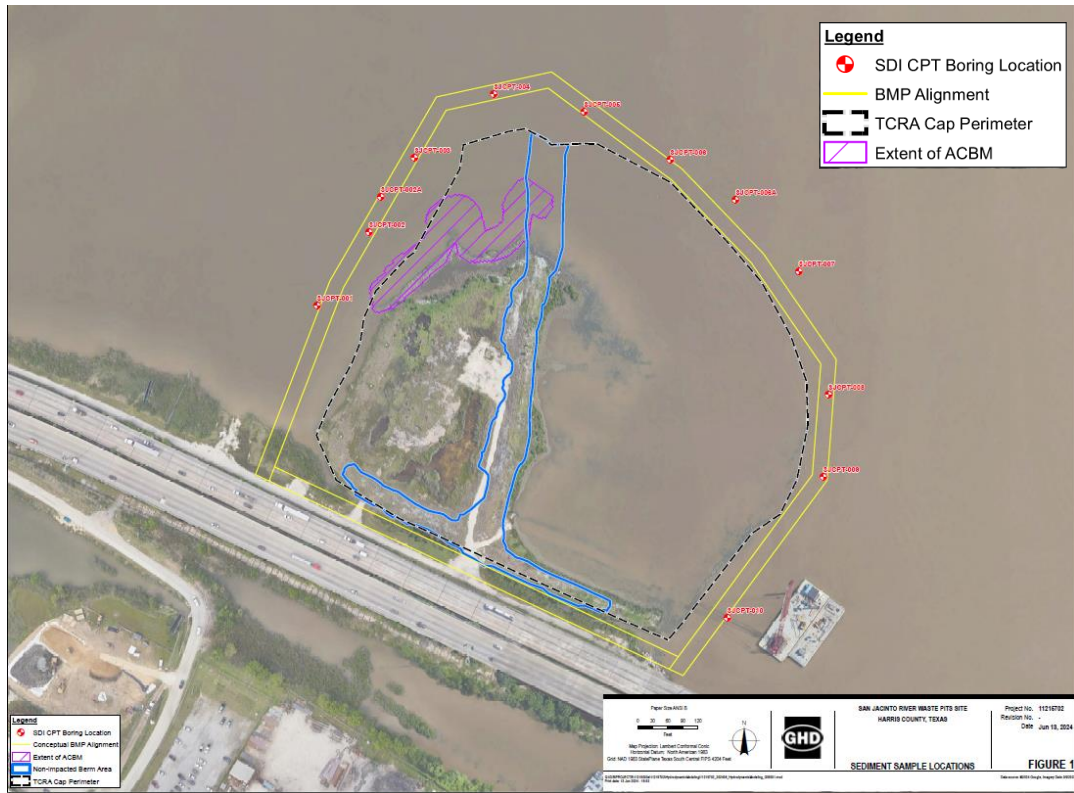


Figure 8 Sediment Sample Locations

Table 6 Sediment Samples Mean Particle Size Distribution (d_{50}) Statistics

Sediment Sample d_{50}	
Minimum	0.0013 mm
Maximum	0.1443 mm
Mean	0.05816 mm

3. Model Description

3.1 Background

GHD set up a hydrodynamic model using the EFDC. EFDC is a general-purpose modelling package for simulating one-, two-, and three-dimensional flow, transport, and bio-geochemical processes in surface water systems which include hydrodynamics, sediment transport, contaminant transport, and water quality-eutrophication components (Hamrick, 1992). The EFDC model can use Cartesian or curvilinear, orthogonal horizontal coordinates. The EFDC numerical scheme uses second order accurate spatial finite differencing on a staggered grid, and second order

accurate three-time level, finite difference scheme with an internal-external mode splitting procedure to separate the internal shear, or baroclinic mode, from the external free surface gravity wave, or barotropic mode. EFDC is supported by the EPA and has been used extensively to simulate hydrodynamic and water quality processes in rivers, lakes, estuaries, reservoirs, wetlands, and coastal regions.

The existing EFDC model for the Northern Impoundment (AQEA, 2012) was used as a base for this work.

3.2 Model Setup

The EFDC hydrodynamic model of the San Jacinto River uses a combined cartesian and orthogonal horizontal grid in a two-dimensional, depth-averaged setup, that simulates flow velocity and water depth in the domain area. The EFDC model does not include a wind wave module and therefore wind waves were not included in the simulation. Wind waves were calculated in a separate analysis based on wind and the more significant fetch for the Northern Impoundment.

The model extends upstream on the San Jacinto River up to Lake Houston Dam and downstream to Fred Hartman Bridge at the Upper San Jacinto Bay. The model covers the San Jacinto River from the Lake Houston Dam to Grennel Slough where it widens, the San Jacinto River from Grennel Slough to the confluence with Buffalo Bayou and HSC, the HSC upstream of the confluence with the San Jacinto River up to the interchange of I-10 and Interstate Highway-69 (I-69) in downtown Houston, and Crystal and Upper San Jacinto Bays, Figure 9, below.

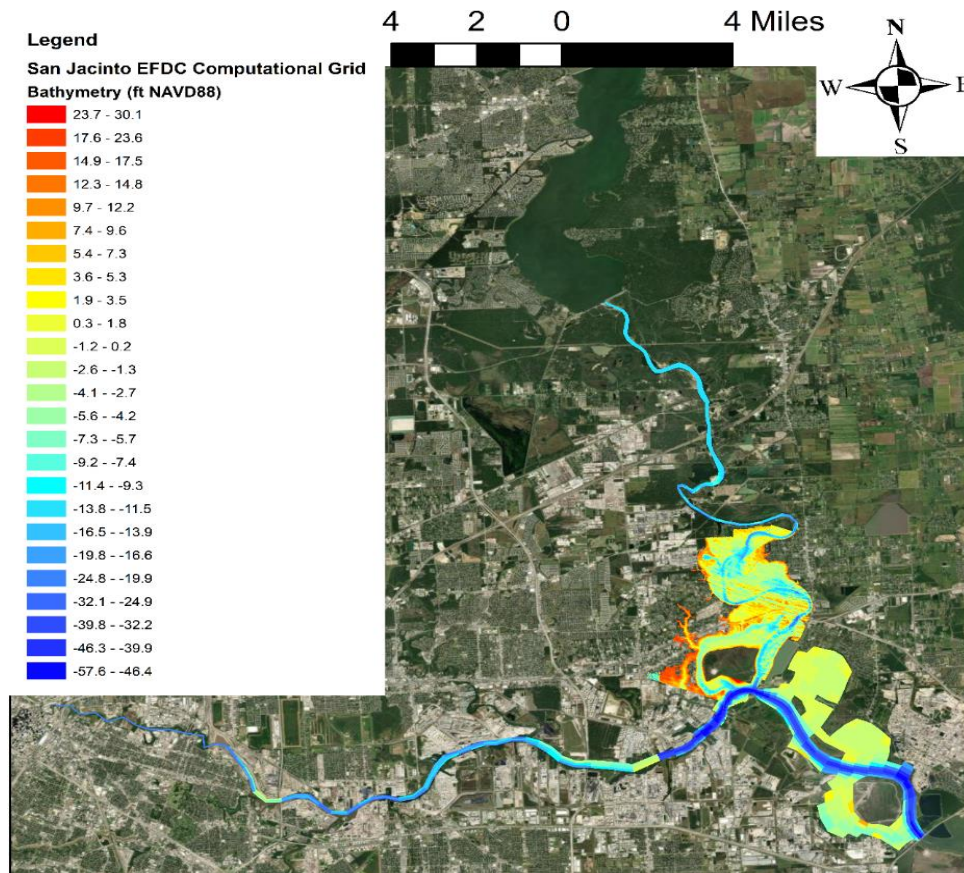


Figure 9 Model Domain with Bathymetry

Anchor QEA (2012) defined two different grids for its study, a denominated coarser grid which covers the whole expanse from Lake Houston to the confluence of the HSC and the HSC to downtown Houston. This grid has a resolution of approximately 100 feet (ft) by 100 ft and was used for longer simulations to reduce simulation time and to generate internal boundary conditions for a finer grid. The finer grid, with a resolution of approximately 50 ft by 50 ft,

does not include the upper San Jacinto River and the HSC. This fine grid requires the running of the coarse grid first to generate the boundary conditions. For this study, the two grids (coarse and fine) were combined into one.

The numerical grid uses rectangular cells (cartesian) with higher resolution (smaller grid cells) in Grennel Slough and areas near the Northern Impoundment and larger orthogonal curvilinear grid cells in areas away from the Northern Impoundment such as the HSC, the upper San Jacinto River, and the bays downstream.

The update of the grid includes the addition of the bays downstream of the confluence of the San Jacinto River with the HSC down to the Fred Hartman Bridge. This area was added to have the open boundary condition at the location of the tidal gage (Section 2.2).

San Jacinto River downstream of the Lake Houston Dam is represented with curvilinear grid cells having an average length and width of 800 ft and 180 ft, respectively. Rectangular grid cells are used in the area of Grennel Slough where the Northern Impoundment is located and down to the confluence with the HSC. Grid cells around the Northern Impoundment have a resolution of 50 ft, increasing to 100 ft moving away from the Northern Impoundment. The curvilinear grid used to represent the HSC has grid cells with an average length and width of 1800 ft and 120 ft, respectively. The curvilinear grid in the bays has cells with an average length and width of 1400 ft and 700 ft, respectively.

The updated model uses bathymetry data from the previous model (AQEA, 2012) together with recent data (Section 2.1) to refine model bathymetry at the Northern Impoundment and define the bathymetry in the bay areas.

The model was simulated with and without the effect of the cofferdam present. Figure 10 shows the cofferdam delineation and its implementation in the model. For the model simulation “with cofferdam,” the model cells highlighted in red on Figure 10 are blocked during the simulation, going dormant and not having any interaction with the rest of the model.



Figure 10 Model Grid Showing Delineation of Cofferdam and Cell Models Defining the Northern Impoundment

The hydrodynamics model uses the parameterization and kinetics from the calibrated (previously developed) models by Anchor QEA (AQEA, 2012).

Deterministic time variable models predict conditions within the computational domain of the model based upon perturbations within the model grid caused by outside forcing functions. The forcing functions need to be described to

the model to predict the perturbations that occur within the model grid. The forcing (inputs) that are required in the hydrodynamic model for the San Jacinto River model include:

- Freshwater flow at the upstream boundary at the Lake Houston Dam.
- Freshwater flow into Buffalo Bayou.
- Water surface elevation at the downstream boundary at Fred Hartman Bridge.

The data described in Section 3 and analyses previously performed by Anchor QEA (AQEA, 2012) were used to determine model boundary condition inputs.

At the San Jacinto river outlet into Galveston Bay, the tides and surges from the bay described in Section 2 were imposed as boundary condition. The location of this boundary condition can be seen in Figure 11.

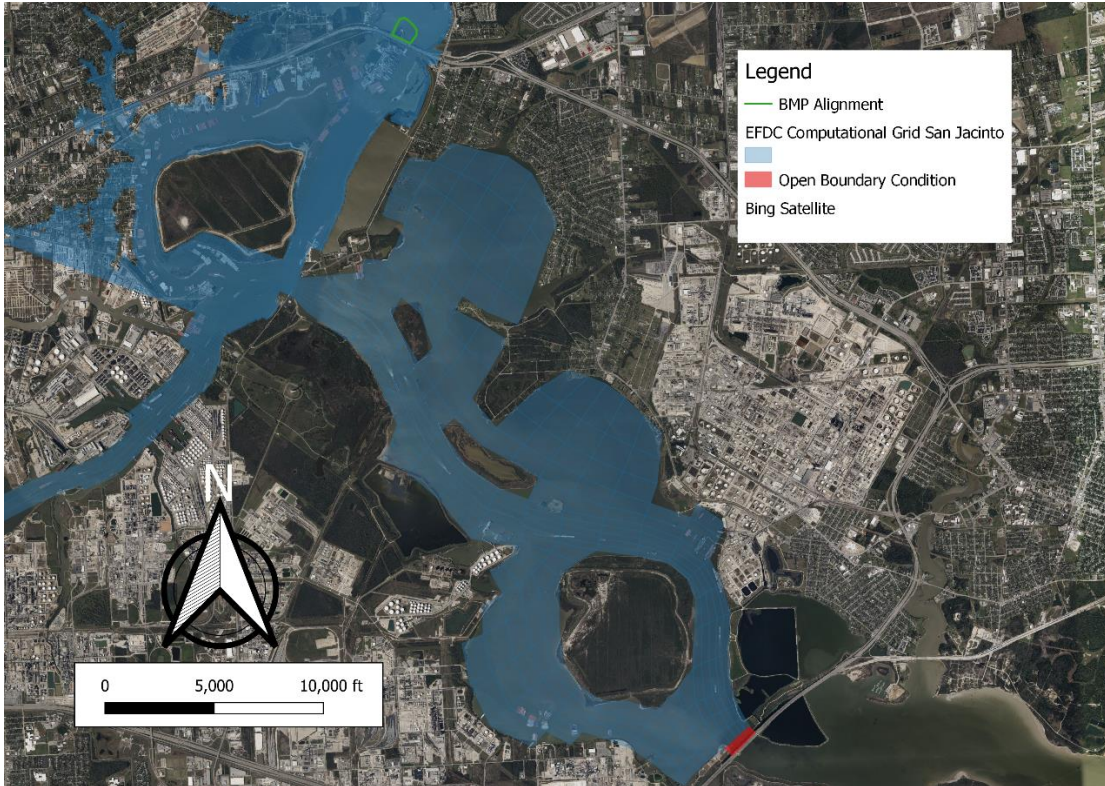


Figure 11 Model Grid Showing location of the Open Boundary Condition at Fred Hartman Bridge

The model was also simulated for the estimated conditions post-RA excavation and removal of the cofferdam (end-state). Based on the design conditions described in Section 2.1, the bathymetry inside the Northern Impoundment area was modified based on the projected depths of excavation and the embankment to be built on the southern side of the impoundment. Figure 12 shows the changes in bathymetry made in the model with respect to existing conditions to simulate the estimated end-state conditions.

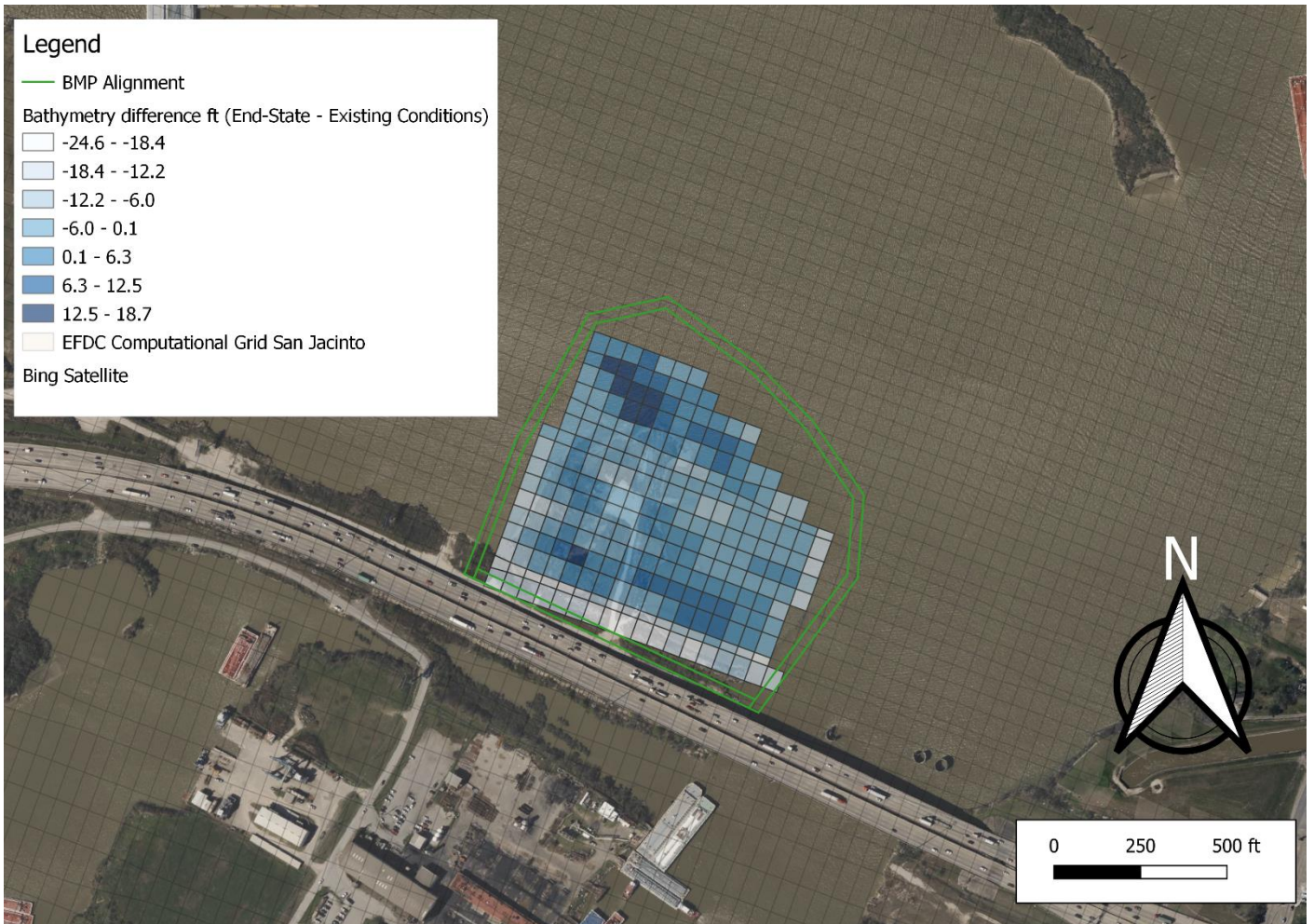


Figure 12 Estimated End State Bathymetry Changes with Respect to Existing Conditions

3.3 Modeled Scenarios

3.3.1 Cofferdam Effects on Floodplain

The developed hydrodynamic model was used to assess any impact that the introduction of the cofferdam would have on the surrounding floodplain. The floodplain impact was assessed for the lower San Jacinto Watershed shown on Figure 2. Data was analyzed to evaluate a change in water surface elevations, for existing conditions (“without cofferdam”) and “with cofferdam,” for the 2-, 10-, and 100-year storm events. The results for the assessment are found in Section 4.1.

3.3.2 Sedimentation Analysis

A series of sedimentation analyses were conducted evaluating the changes, if any, in the shear stresses and velocities in the river surrounding the Northern Impoundment.

3.3.2.1 Existing Condition

Shear stresses and velocities were evaluated for the Northern Impoundment using the existing conditions (“without cofferdam”) under the 2-, 10-, 100-, and 500-year storm events. This provides a baseline to compare data with the cofferdam present and for the end-state condition. Results are discussed in Section 4.2.1.

3.3.2.2 Cofferdam Present

Shear stresses and velocities were analyzed for the condition with the cofferdam at the Northern Impoundment. The model was run for the same 2-, 10-, 100-, and 500-year storm events. Results are discussed in Section 4.2.1.

3.3.2.3 End-State Condition

Shear stresses and velocities were assessed for the Northern Impoundment for the end-state condition after the excavation activities are complete, and the cofferdam is removed. The soil within the cofferdam will be removed, thus leaving a different bathymetry than the existing condition data. The shear stress and velocity data with the estimated end-state bathymetry with no cofferdam present were run for the 2-, 10-, 100-, and 500-year storm events. Estimated end-state bathymetry conditions are subject to change during RA. This set of data was used to evaluate any impacts to I-10. Results are discussed in Section 4.2.2.

4. Model Scenario Results

4.1 Cofferdam Effects on the Floodplain

The model was used with and without the cofferdam to determine the effect on the floodplain.

Three scenarios were simulated corresponding to three different river flow and surge conditions that were selected based on the existing San Jacinto River hydrology and the data from the tidal NOAA gauge #8770613. Each scenario was simulated “without cofferdam” (baseline) and “with cofferdam” to provide relative comparisons between the outcomes.

High-flow events with return periods of 2-, 10-, and 100-year storm events were evaluated during this analysis. Peak flow rates at the Lake Houston Dam for the three high-flow events were determined using a frequency analysis of historical flow data from Lake Houston Dam. Normal flows were considered in the Bayou and HSC for all simulations.

Sensitivity analysis has shown that the surge at the open boundary generates a backwater effect that influences flooding. The higher the surge, the higher the water elevations in the floodplain. For this reason, different surges were considered in combination with Lake Houston Dam flows for the floodplain analysis.

A 2-year flow event of 38,400 cfs at Lake Houston Dam was simulated with a 2-year surge of 9.5 ft at the open boundary with Galveston Bay, 126,000 cfs for the 10-year flow event at the dam was used in conjunction with a 5-year surge of 13.3 ft at the bay, and 372,000 cfs for the 100-year flow event was considered with a 20-year surge at the open boundary. The scenarios are named after the flow event. The synthetic period of 30 days was simulated for all scenarios and conditions, with a 10-day spin up period. The model was simulated with wetting and drying capabilities turned on. Under these conditions a cell is active or dormant depending on the water depth. Water depth must be prescribed for when a cell goes dry (dormant) when it has been active before and for when a cell becomes active in the simulation after being dormant. For the present study, the water depth at which a cell goes dry was 0.1 ft and it became active at a depth of 0.17 ft.

Figure 13 presents the location of two stations that were used to compare results from the model. The two stations were selected at locations less than 800 ft from the planned cofferdam in areas subjected to flooding and drying during the simulation. The model used actual dates for the simulation and synthetic period, without the spin up.

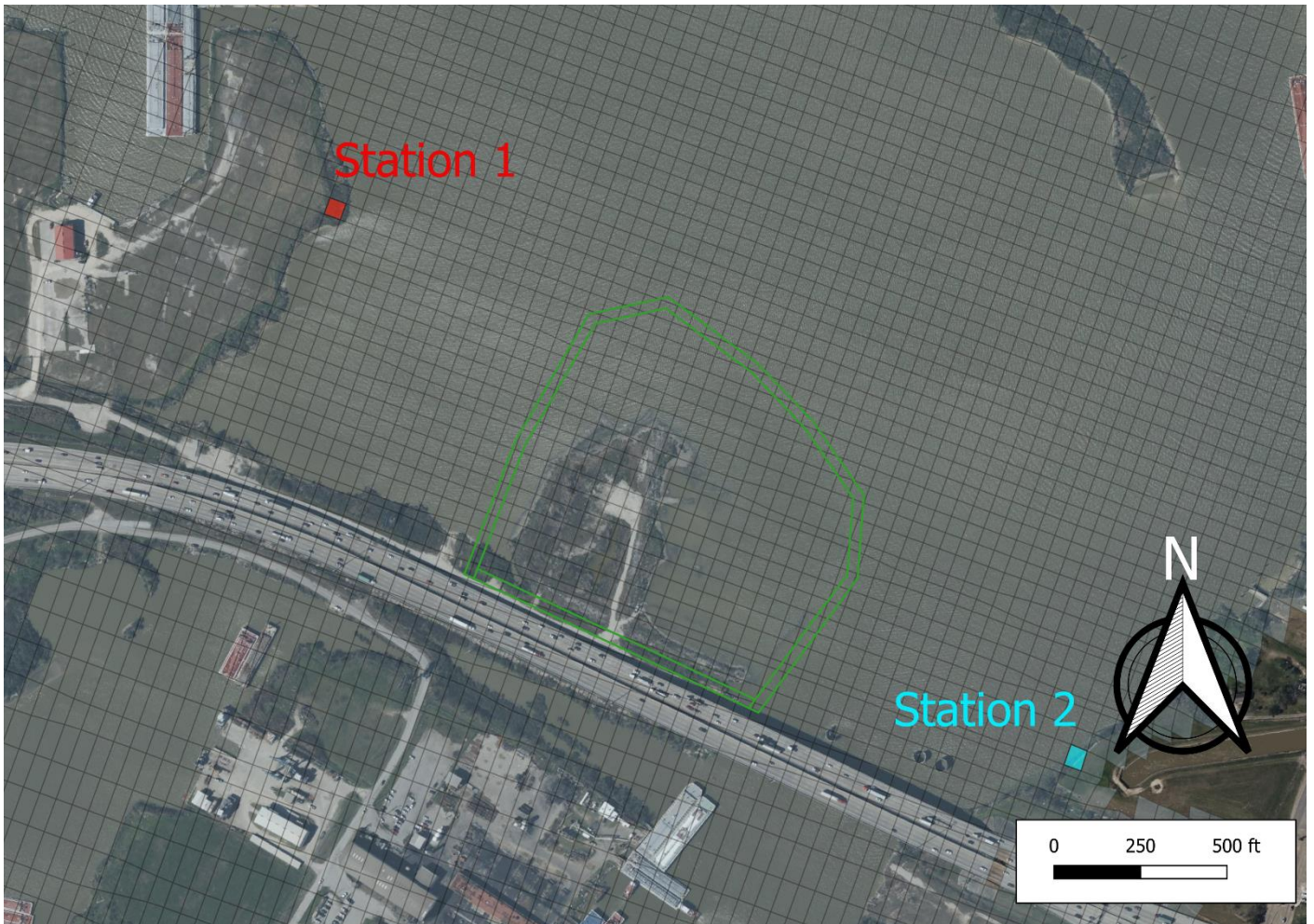


Figure 13 Stations for Water Depth Comparisons

The water depth data at Stations 1 and 2 shows the flooding along the shoreline for each storm event. Both stations are located on the shoreline and are primarily dry during non-storm events. The ground elevation is 2.39 ft North American Vertical Datum of 1988 (NAVD88) for Station 1 and 3.78 ft NAVD88 for Station 2. As the storm progresses and water surface rises, each location starts to experience an increase in water depth. We can see that Station 1 experiences a max of ~2.2 ft water depth during a 2-year storm event while Station 2 experiences a max of ~0.79 ft during the 2-year storm event. Figure 14 and Figure 15 show the 2-year storm water depth comparison between the “with cofferdam” and “without cofferdam” simulations at Stations 1 and 2.

Figure 16 and Figure 17 show the water depth comparison for a 10-year storm event. Figure 18 and Figure 19 show the water depth comparison for a 100-year storm event. The time series comparisons show that there are minimal changes in the water depths for all three storm events between the “without cofferdam” and “with cofferdam” conditions. The difference between the “with cofferdam” conditions and the “without cofferdam” conditions for all three storm events were calculated for the whole modelling domain. Results show no changes in the floodplain inundated areas between the “with cofferdam” and “without cofferdam” conditions. The same cells become wet under both conditions and there are minimal changes in water height in the flooded areas of the floodplain between both conditions. The changes in water depth in flooded areas between both conditions are less than 0.1 ft for all three scenarios, as shown in Table 7.

Table 7 Water Depth Differences

Return Period	Difference Between “With and without cofferdam”	
	(feet)	(inches)
2-year	0.072	0.86
10-year	0.020	0.24
100-year	0.003	0.04

Figure 2020, Figure 211, and Figure 222 show the maximum flooded areas for all three scenarios “with cofferdam” condition.

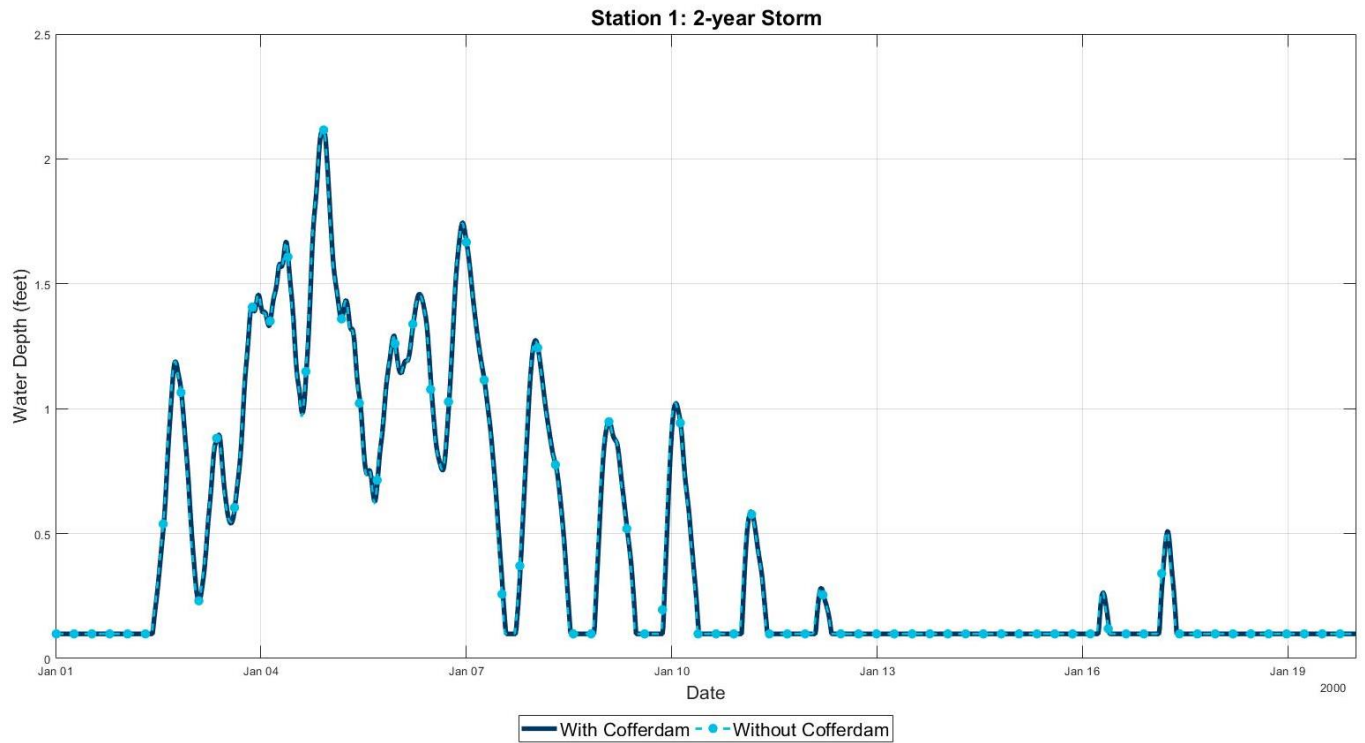


Figure 14 Station 1 Water Depth Comparison “With and Without Cofferdam” for 2-Year Storm

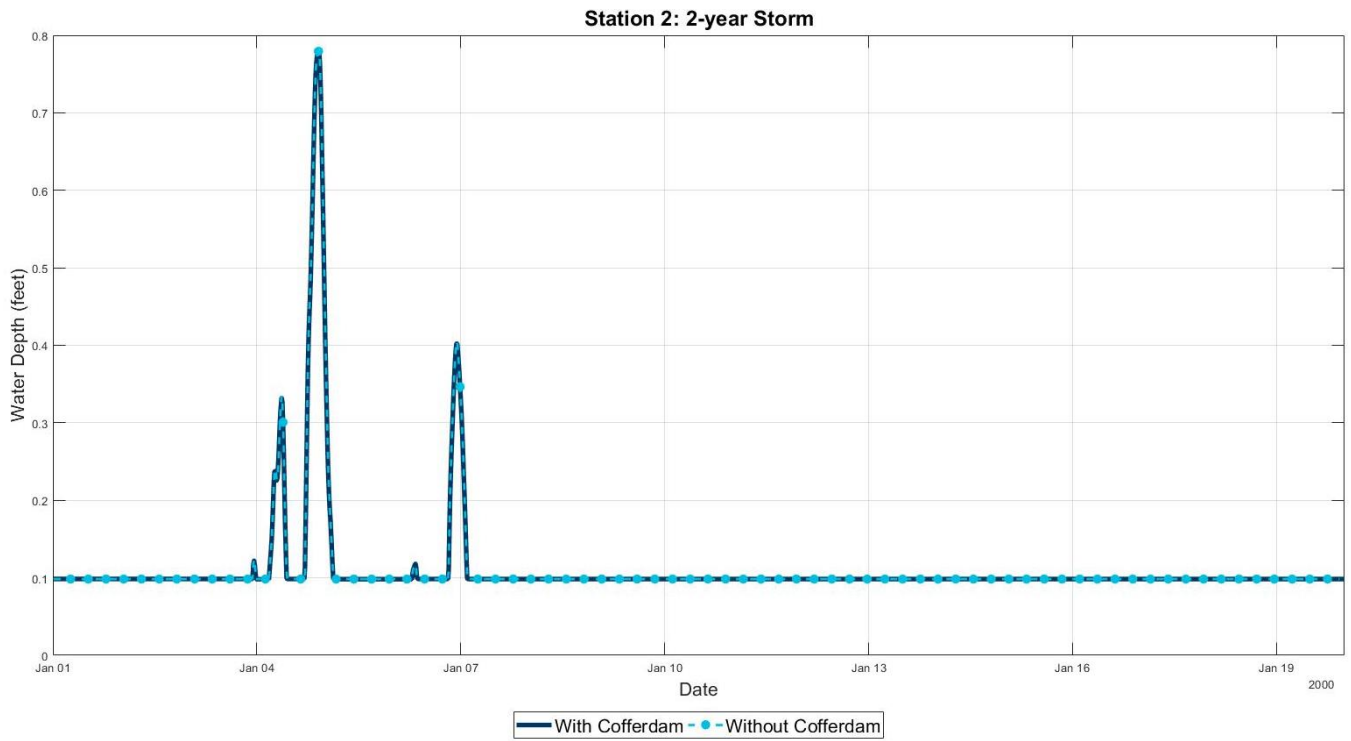


Figure 15 Station 2 Water Depth Comparison “With and Without Cofferdam” for 2-Year Storm

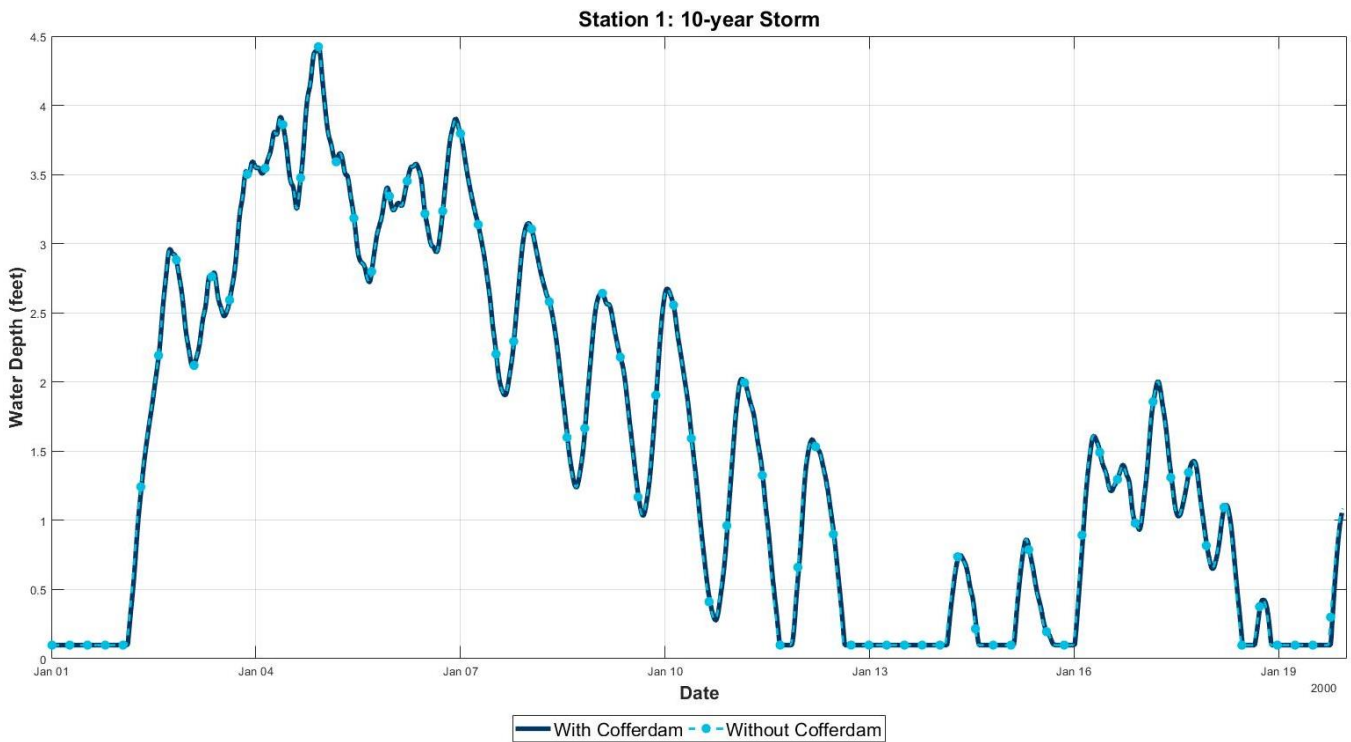


Figure 16 Station 1 Water Depth Comparison “With and Without Cofferdam” for 10-Year Storm

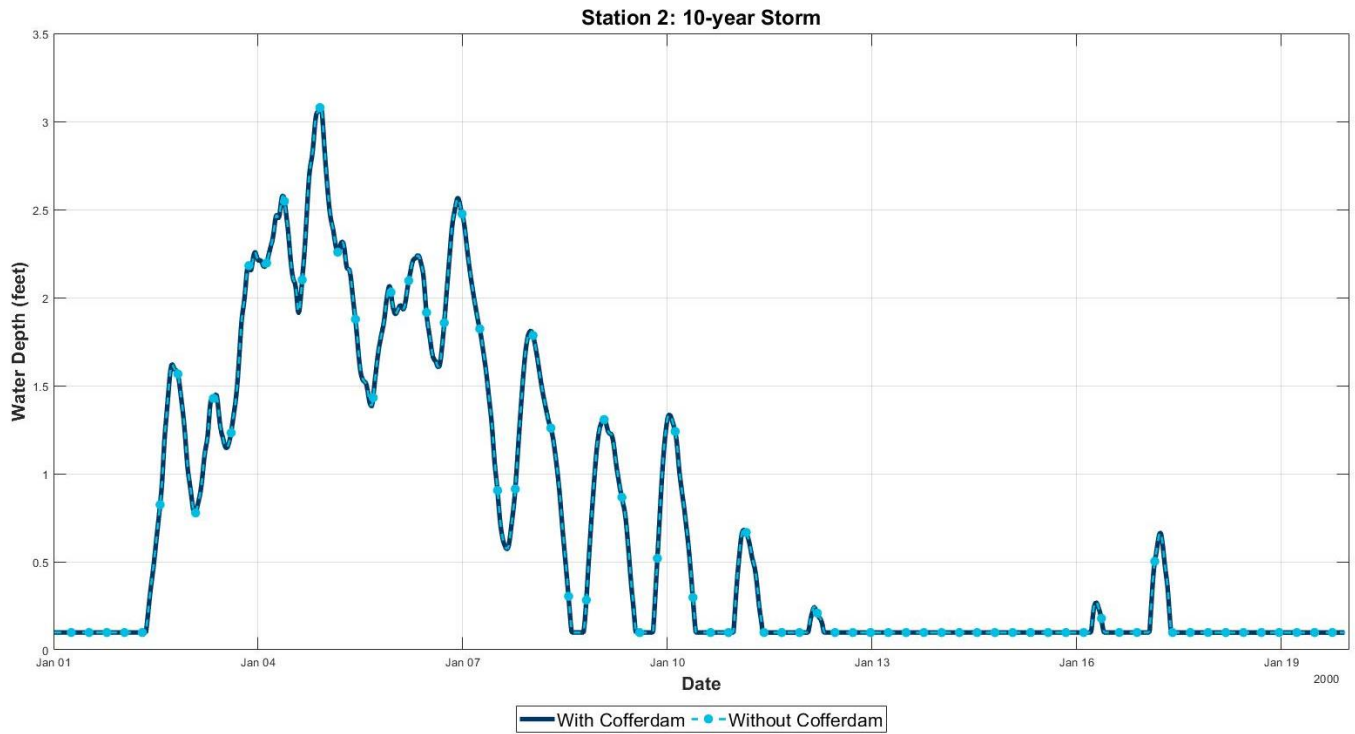


Figure 17 Station 2 Water Depth Comparison “With and Without Cofferdam” for 10-Year Storm

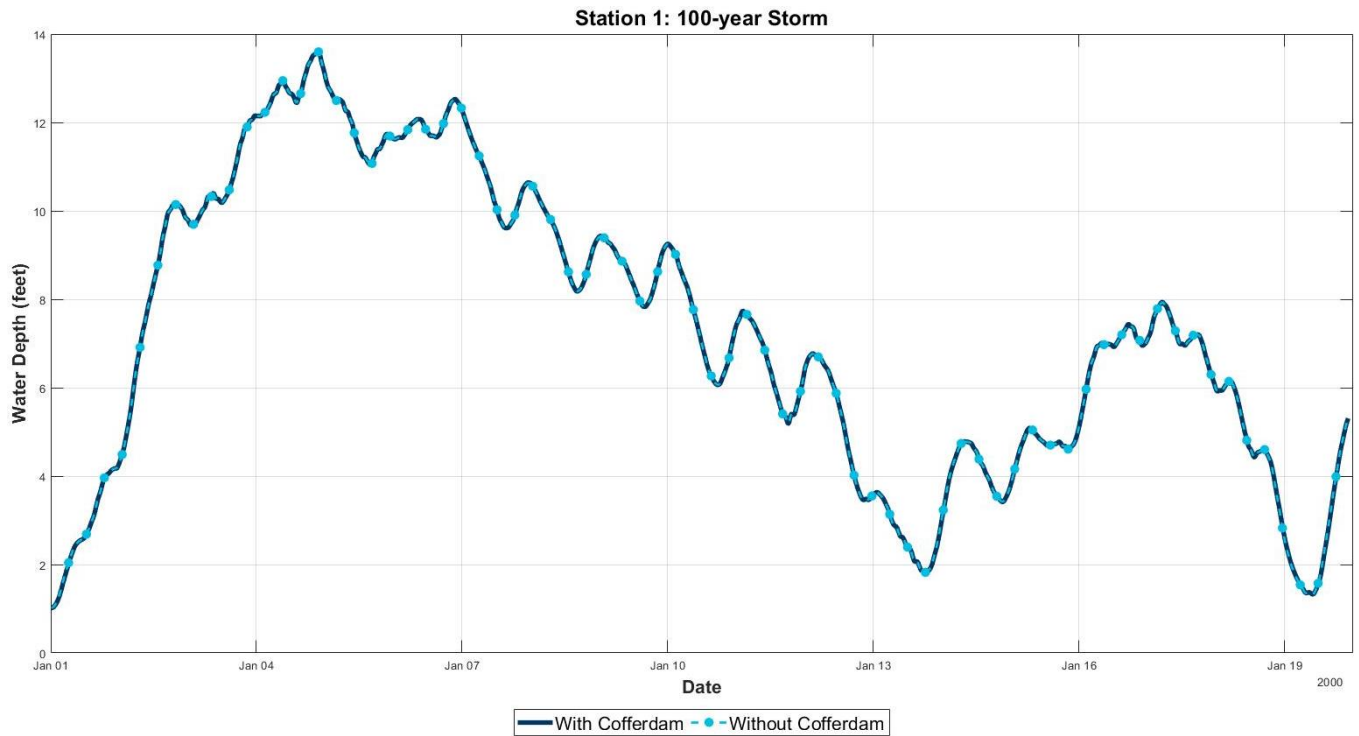


Figure 18 Station 1 Water Depth Comparison “With and Without Cofferdam” for 100-Year Storm

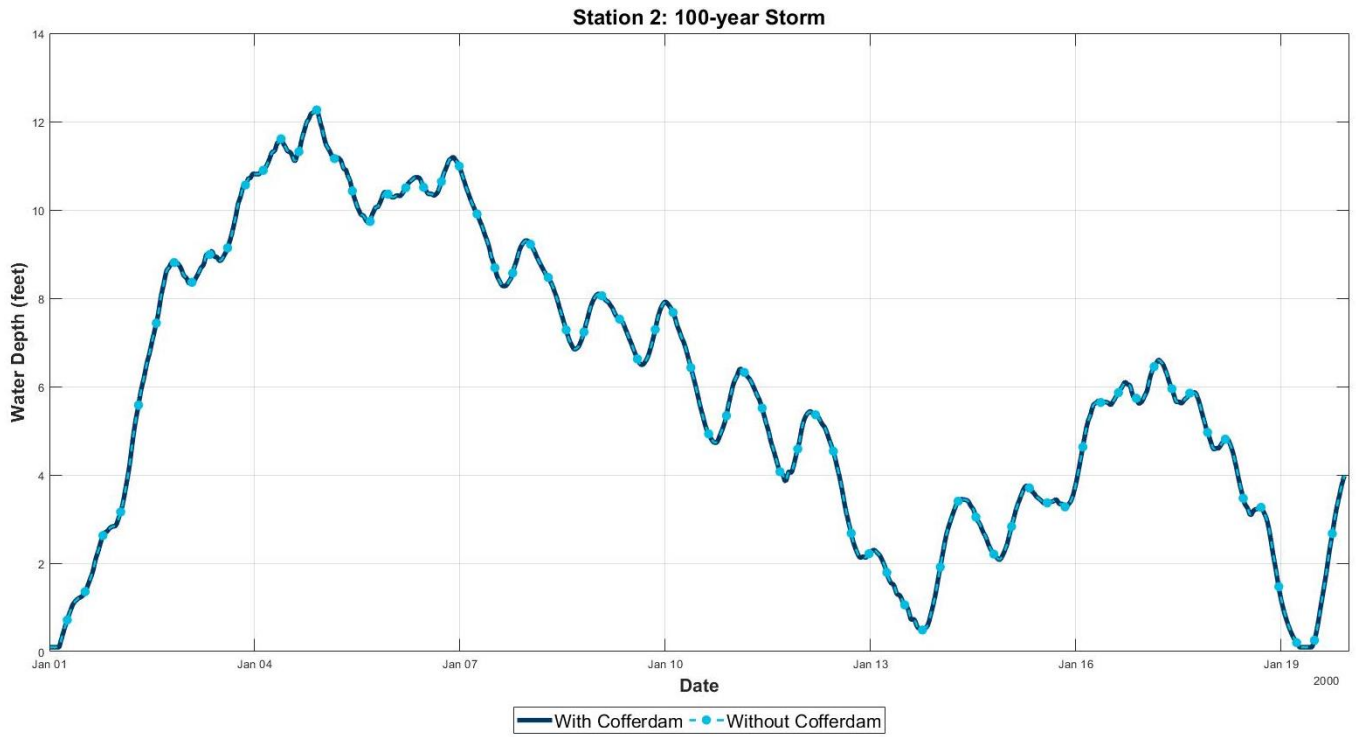


Figure 19 Station 2 Water Depth Comparison “With and Without Cofferdam” for 100-Year Storm

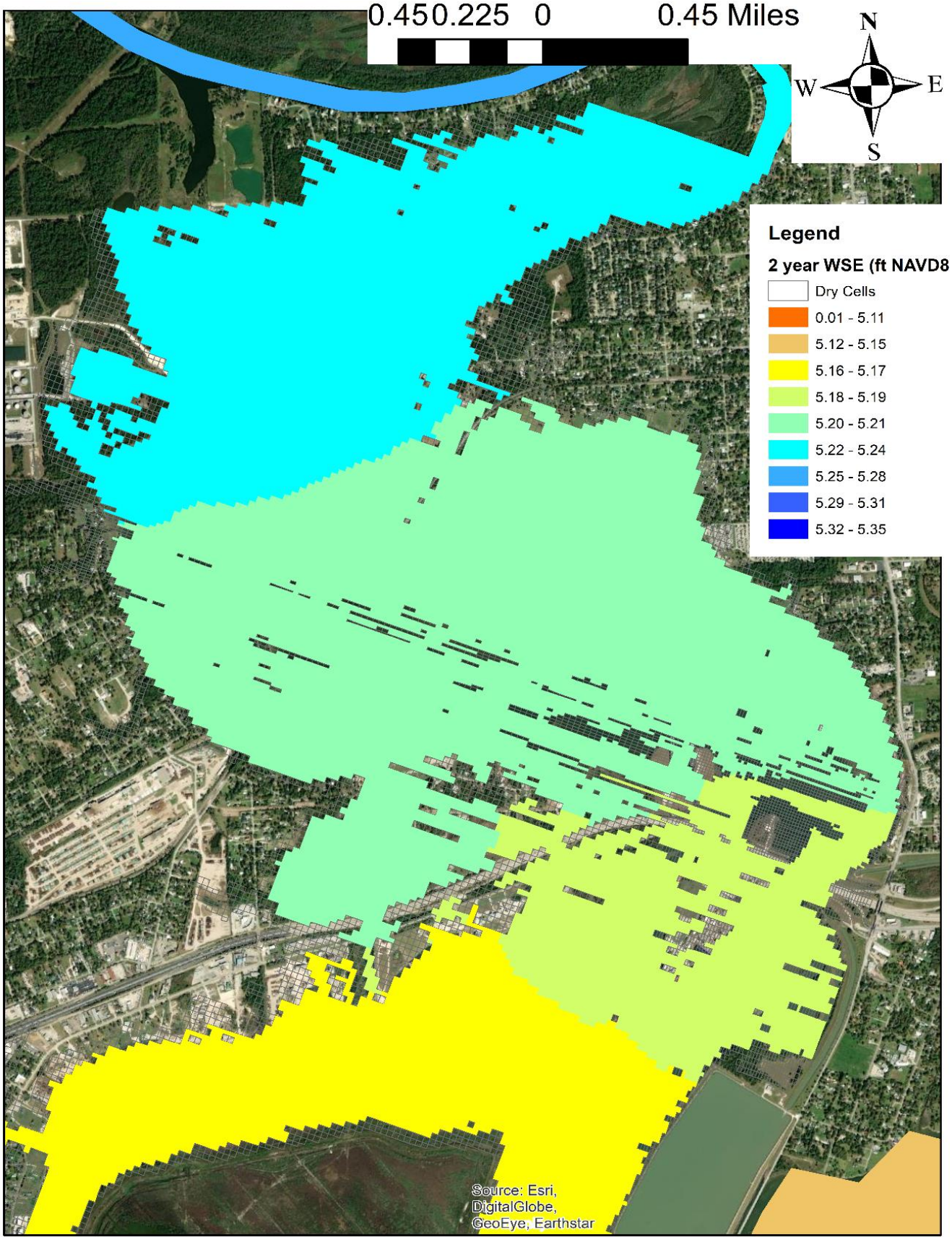


Figure 20 Maximum Water Surface Elevation for the 2-Year Storm

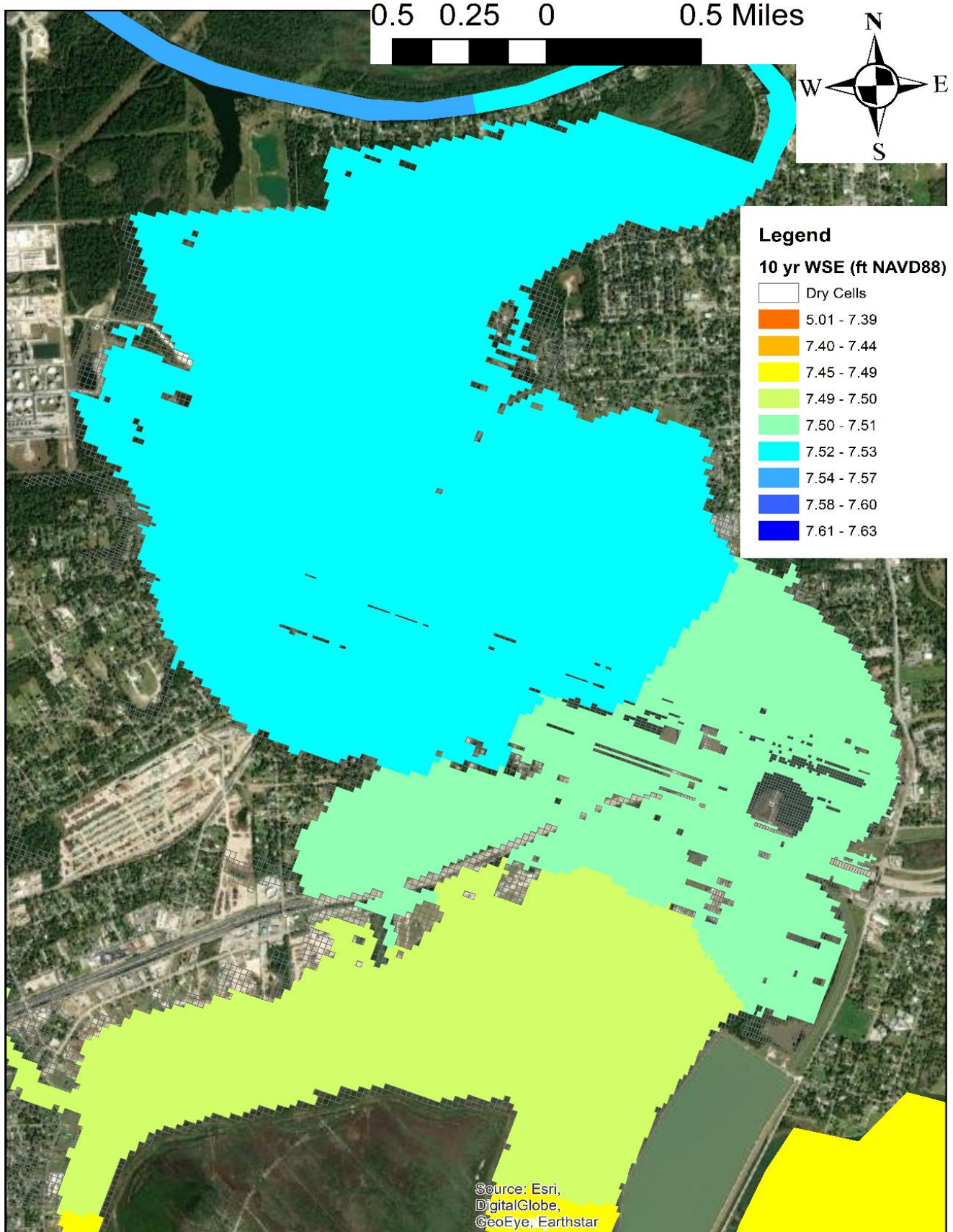


Figure 21 Maximum Water Surface Elevation for the 10-Year Storm

Legend

100 yr WSE (ft NAVD88)

- Dry Cells
- 10.001 - 16.610
- 16.611 - 16.620
- 16.621 - 16.630
- 16.631 - 16.640
- 16.641 - 16.650
- 16.651 - 16.660
- 16.661 - 16.680
- 16.681 - 16.690
- 16.691 - 16.700

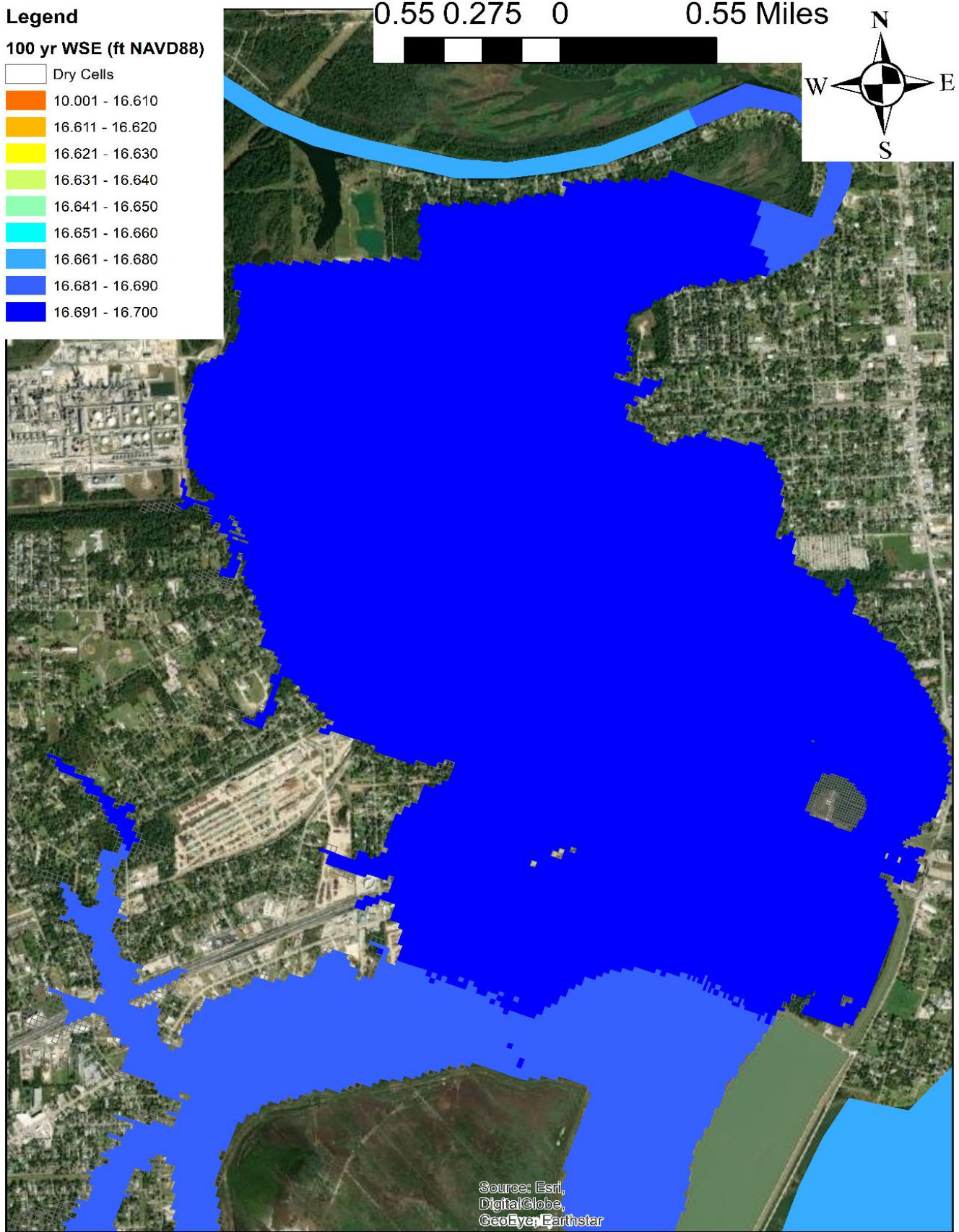


Figure 22 Maximum Water Surface Elevation for the 100-Year Storm

4.2 Sedimentation Study

Sediment transport was not simulated with the model. A qualitative sedimentation study was conducted based on shear stresses and velocities simulated with the hydrodynamic model. The purpose of the sedimentation study is to qualitatively assess effects on sedimentation of the cofferdam and the effects on sedimentation of the changes in bathymetry from the baseline to the estimated end-state conditions. The study focused on potential modifications in local erosion and deposition patterns, velocity changes affecting circulation in the area, and potential scour around the cofferdam. The study utilizes the calibrated hydrodynamic model discussed in Section 3 to determine bottom shear stresses and velocities in and around the vicinity of the Northern Impoundment.

Model results for the estimated end-state, “with cofferdam,” and existing conditions were processed and compared for shear stresses and velocity. Statistics for shear stresses and velocities were calculated in an area around the Northern Impoundment as shown on Figure 23.

A sensitivity analysis was performed to determine how the surge at the open boundary affects stresses and velocities in the study area. It was found that higher storm surges with the same dam flow create lower velocities in the study area. Therefore, for the shear stress and velocity analysis a fixed open boundary condition with a 2-year storm surge was used for all dam flow conditions. For the analysis, the maximum value of the time series at each model cell in the area shown in Figure 23 were considered. Then the maximum and average values in the area were calculated.



Figure 23 Area Used for the Computation of Statistics for the Conditions Around the Cofferdam

Based on the geotechnical studies described in Section 2.6, the bed sediment at the Northern Impoundment is fine and can be described as sandy silt and silty sand. The bed grain size has a maximum d_{50} of 0.14 millimeters (mm), which is on the lower range for fine sand, and was used for reference.

Shear stresses determine the capability of a flow to move material. Non-cohesive sediment movement occurs when the boundary threshold is exceeded (Julien, 2002). The threshold is referred to as the critical shear stress, T_c .

The model-simulating bed shear stress was used to qualitatively assess sediment mobility. Sediment mobility for a given particle size occurs when the bed shear stress (T_b) exerted by the flow on the bed exceeds critical shear stress, $T_b > T_c$. This determines only whether a given particle size is potentially mobile. Sediment mobility provides an indication of whether sediment movement (transport) occurs. However, bed erosion and deposition also depend on sediment supply.

The critical shear stress for particle motion was determined based on the Shields diagram for each particle size. Table 8 shows critical shear stresses for the particle-size and sediment classifications.

This analysis determines whether a given grain size is mobile but does not calculate erosion or deposition. This study analyzed changes in shear stresses and velocities to give an indication of potential erosion and deposition, but the actual erosion and deposition depends on the total sediment transport which can be altered by other factors.

Based on the previous sediment mobility computations, the reference sediment of 0.14 mm grain size has a critical bed shear stress of 0.15 Pascals (Pa). A bed shear stress exceeding 0.15 Pa has the potential to mobilize the sediment encountered in the vicinity of the Northern Impoundment and could result in scour.

Table 8 Critical Shear Stress Classification

Classification	Particle Diameter (mm)	Critical Shear Stress T_c (Pa)
Medium sand	0.25 - 0.5	0.19 - 0.27
Fine sand	0.125 - 0.25	0.14 - 0.19
Very fine sand	0.063 - 0.125	0.11 - 0.14
Silt and Clay	< 0.063	< 0.11

Simulated depth average flow velocities, which are average velocities at any vertical section of a channel, were also analyzed. Average flow velocities increase as river discharge increases and decrease with an increase in water surface elevation, like backwater conditions caused by surges. In this analysis, velocity was expressed only by magnitude (speed).

4.2.1 Sedimentation Study with Cofferdam Analysis

The model was used with and without the designed cofferdam to determine the changes in circulation around the cofferdam. Shear stresses and velocities for four scenarios (2-, 10-, 100, and 500-year flow event) with and without the cofferdam wall, were analyzed.

Figure 24 shows the maximum shear stresses for the cofferdam and Figure 25 shows the differences, with and without the cofferdam, of the maximum shear stresses for the 100-year flow conditions. Figure 26 shows the maximum velocities for the 100-year flow with the cofferdam while Figure 27 shows the differences, with and without the cofferdam, for the maximum velocities. Table 9 and Table 10 present the statistics for shear stresses for the cofferdam and differences with existing conditions, respectively.

The shear stress for the cofferdam conditions have a maximum value of 4.34 Pa and an average value of 0.24 Pa, both shown in green in Table 9. The difference in the maximum value of the shear stress with existing conditions is 2.65 Pa with a difference in the average value of 0.03 Pa. Maximum shear stress differences were observed in two locations at the southwest corner of the cofferdam, and the other at the north side of the cofferdam. The elevated shear stress in the southwest corner is due to a concentration of flow in the area due to the presence of the cofferdam. The model bathymetry does not accurately account for modifications of the access road for purposes of the RA which

will increase its height and prevent flow and shear stress from occurring at that location. Large differences both in shear stresses and velocities occur since the flow, previously distributed across the area of the impoundment, is now constricted to the north, to an area with lower flow under existing conditions. At the northern boundary of the cofferdam, the shear stress values are large compared to the critical shear stress value of 0.15 Pa and could potentially generate scour.

The relatively small value for the maximum shear stress indicates that, except for the locations discussed above, the average conditions of the area are comparable to existing conditions. The pattern is similar for all flow conditions with only small differences in magnitude.

Table 9 *Maximum and Average Shear Stress “With Cofferdam”*

Shear Stress (Pa)	Existing Conditions				With Cofferdam Wall			
	2-year	10-year	100-year	500-year	2-year	10-year	100-year	500-year
Maximum value of cell maximums	3.54	3.85	3.84	3.84	4.34	4.23	4.18	4.16
Average value of cell maximums	0.26	0.25	0.26	0.26	0.23	0.16	0.23	0.24

Table 10 *Maximum and Average Shear Stress Differences “With Cofferdam”*

Shear Stress Difference	2-Year		10-Year		100-Year		500-Year	
	Pa	%	Pa	%	Pa	%	Pa	%
Maximum value of cell maximums	2.65	75%	2.27	59%	2.21	58%	2.18	57%
Average value of cell maximums	0.03	11%	0.02	9%	0.02	7%	0.01	-6%



Figure 24 Maximum Shear Stresses "With Cofferdam" for the 100-Year flow

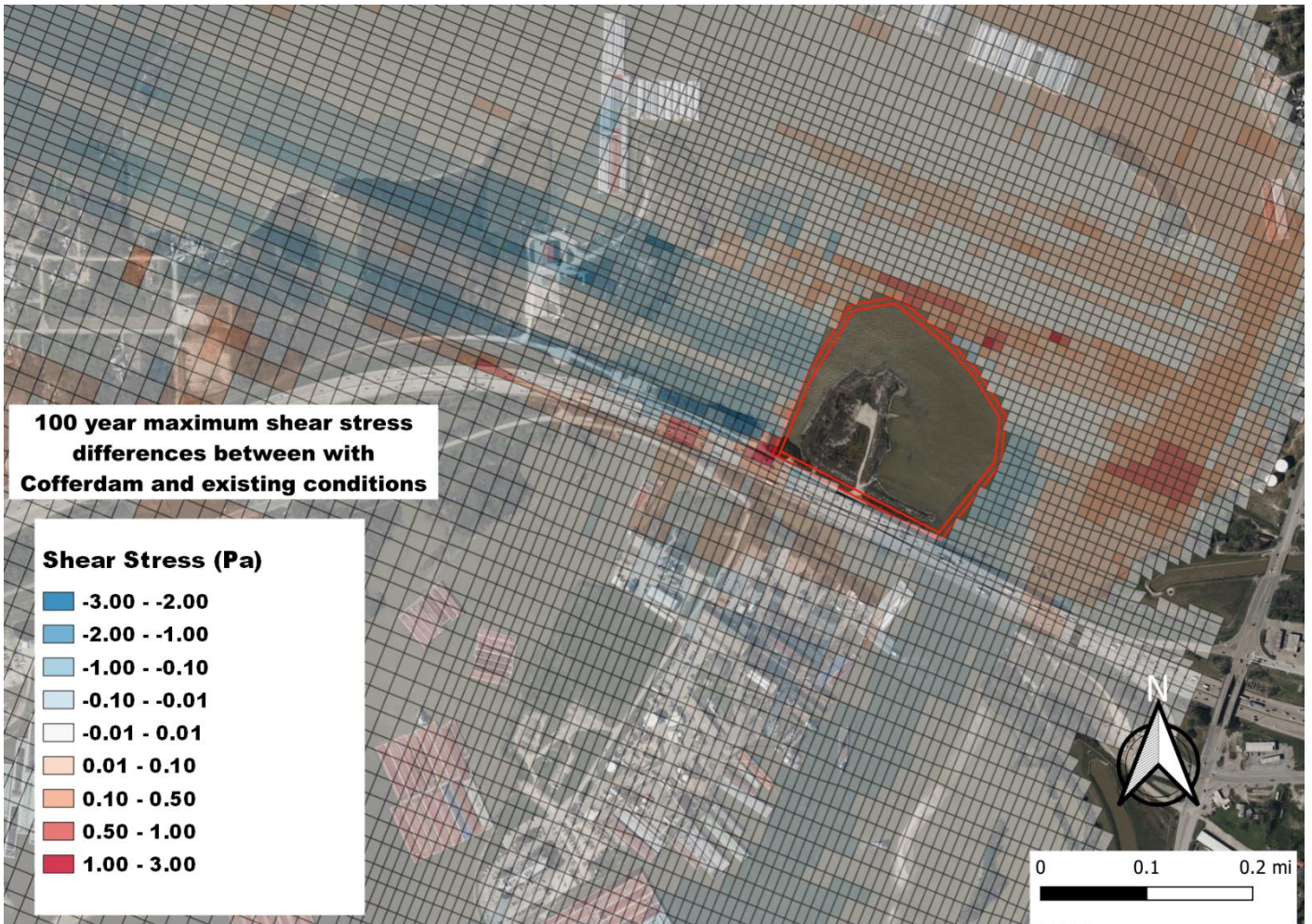


Figure 25 Maximum Shear Stress Differences Between “With Cofferdam” and Existing Conditions for the 100-Year flow

Table 11 and Table 12 present the statistics for velocities for the cofferdam and differences with existing conditions for the 2-, 10-, and 100-year storm events.

The maximum and average values of the maximum velocities are 3.14 ft/s and 0.72 ft/s, respectively. The differences in the maximum and average value of the maximum velocity are 1.67 ft/s and 0.06 ft/s, respectively. Figure 26 indicates that the presence of the cofferdam diverts the flows to the north side, decreasing velocities next to I-10 except right next to the cofferdam wall itself when a sudden large increase occurs creating the large shear stresses and potential scour discussed above.

Table 11 Maximum and Average Velocities for Conditions with Cofferdam

Velocity (ft/s)	Existing conditions				With Cofferdam Wall			
	2-year	10-year	100-year	500-year	2-year	10-year	100-year	500-year
Maximum value of cell maximums	2.79	2.68	2.95	2.95	2.68	2.93	3.14	3.14
Average value of cell maximums	0.56	0.55	0.66	0.68	0.61	0.60	0.71	0.72

Table 12 Percentage Maximum and Average Velocity Differences for Conditions with Cofferdam

Velocity Difference	2-Year		10-Year		100-Year		500-Year	
	ft/s	%	ft/s	%	ft/s	%	ft/s	%
Maximum 95 th Percentile	1.64	61%	1.58	54%	1.54	49%	1.67	53%
Average 95 th Percentile	0.06	10%	0.04	7%	0.03	4%	0.04	5%

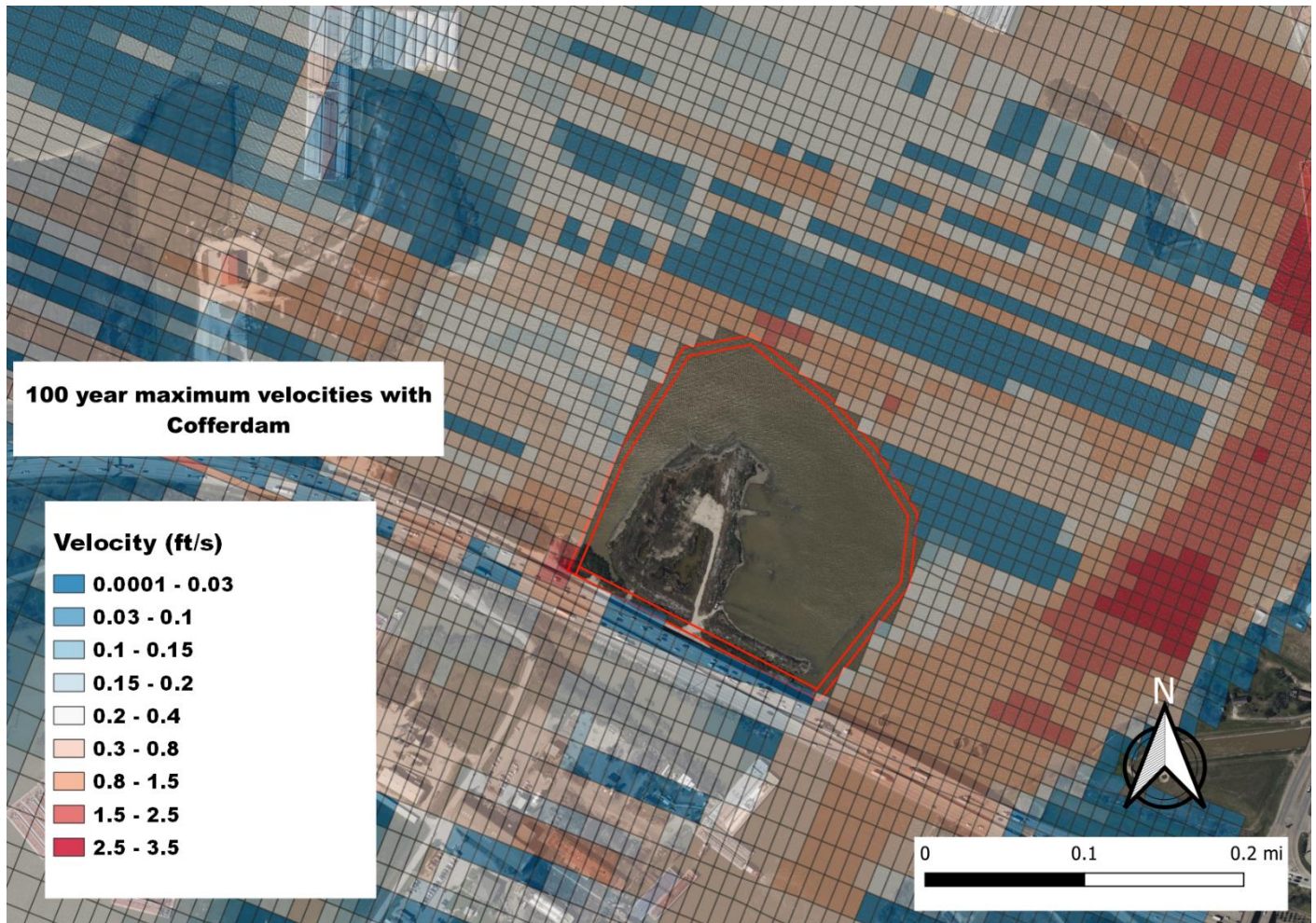


Figure 26 Maximum Velocities "With Cofferdam" for the 100-Year flow

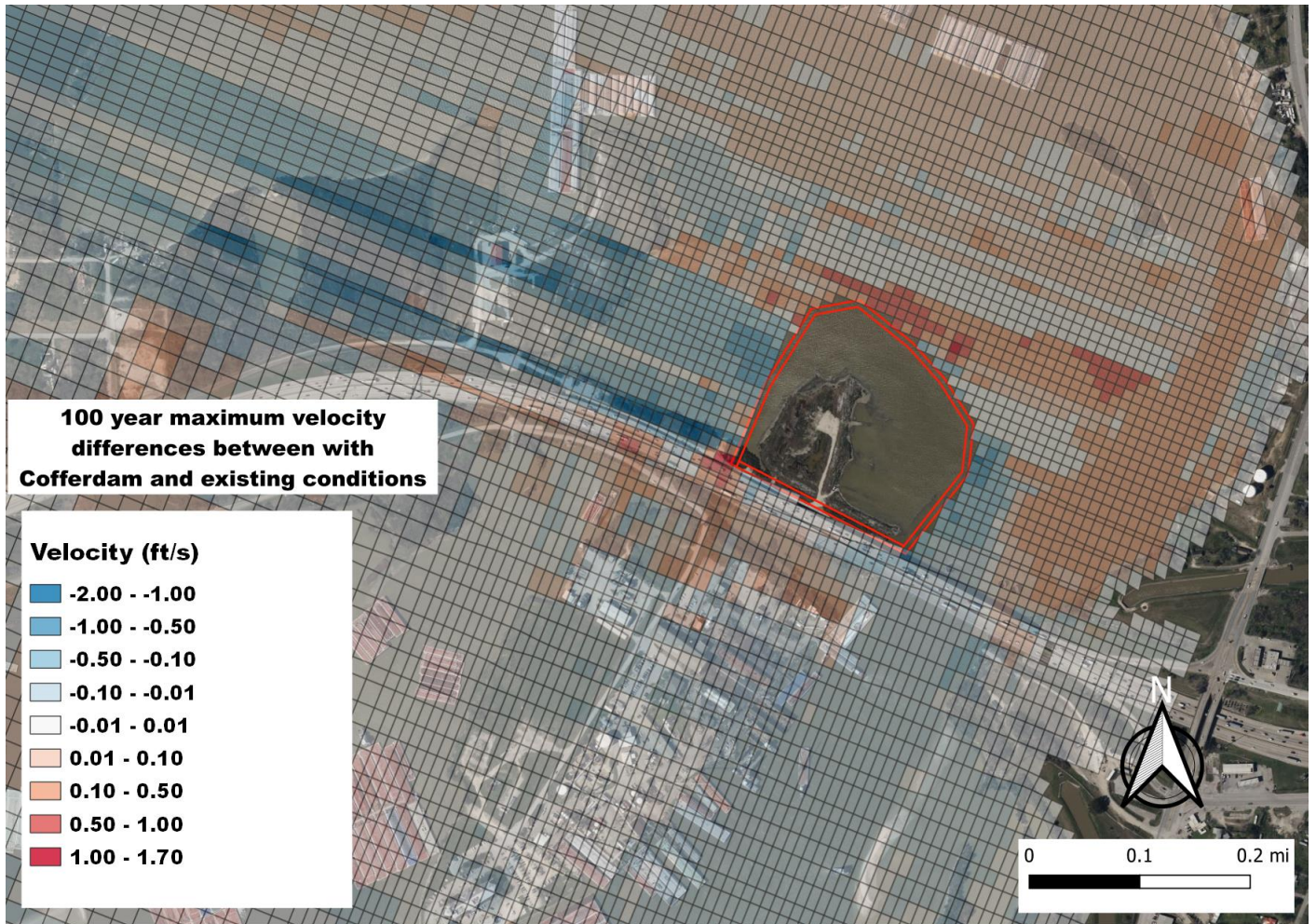


Figure 27 Maximum Velocity Differences Between “With Cofferdam” and Existing Conditions for the 100-Year flow

Appendix C presents the figures for median and maximum shear stress and velocity for the existing condition and cofferdam for the 2-, 10-, 100-year, and 500-year flow events. Appendix C shows the figures for the maximum shear stress and velocity differences between the “with cofferdam” and existing conditions for the 2-, 10-, 100-year, and 500-year flow events. The sedimentation discussion was taken into account for the design of the cofferdam. The analysis of velocities and shear stresses indicates the areas potentially requiring additional scour protection, both during the construction when the cofferdam is present and the end-state situation after cofferdam removal.

4.2.2 End-State Conditions Analysis

Scenarios described in Section 3.3 (2-, 10-, 100-year, and 500-year flow event) without the cofferdam and incorporating the changes in estimated bathymetry resulting from the RA excavation described in Section 2.1 (Figure 12) were simulated to qualitatively assess the potential scour and sedimentation in the end-base situation based on shear stresses and velocities for the considered scenarios.

Figure 28 shows the maximum shear stresses for the estimated end-state condition only for the 100-year flow event. Figure 29 shows the difference in the maximum shear stresses between the estimated end-state and existing conditions for the 100-year flow event. Table 13 and Table 14 present the statistics for the difference in shear stresses between the estimated end-state condition and existing condition for the 2-, 10, 100-, and 500-year storm events, respectively.

The maximum shear stress for the estimated end-state conditions have a maximum value of 4.25 Pa and an average value of 0.45 Pa. The maximum value of the 95th percentile shear stress difference is 1.14 Pa with an average value difference of 0.006 Pa.

The differences in the maximum shear stresses are high in the shoal area north of the Northern Impoundment. Compared to the critical shear stress, the shoal area could potentially be affected by scour (i.e., redistribution of sediments from the shoal area into the estimated end-state excavation of Northern Impoundment).

As expected, as depths increase in the excavation area, the shear stresses decrease (i.e., it becomes a depositional environment). The maximum shear stress values of less than 0.03 Pa, significantly below the critical value of 0.15 Pa, indicate the potential for sedimentation in the excavation area.

Table 13 Maximum and Average Shear Stresses for End-State Conditions

Shear Stress (Pa)	Existing conditions				End-State			
	2-year	10-year	100-year	500-year	2-year	10-year	100-year	500-year
Maximum value of cell maximums	3.54	3.85	3.84	3.83	3.82	4.25	4.23	4.25
Average value of cell maximums	0.26	0.26	0.26	0.26	0.25	0.45	0.25	0.25

Table 14 Maximum and Average Shear Stresses Differences for End-State Minus Existing Conditions

Shear Stress Difference	2-Year		10-Year		100-Year		500-Year	
	Pa	%	Pa	%	Pa	%	Pa	%
Maximum value of cell maximums	0.84	24%	1.10	29%	1.14	30%	1.14	30%
Average value of cell maximums	0.006	2%	0.004	1%	0.004	1%	0.003	1%

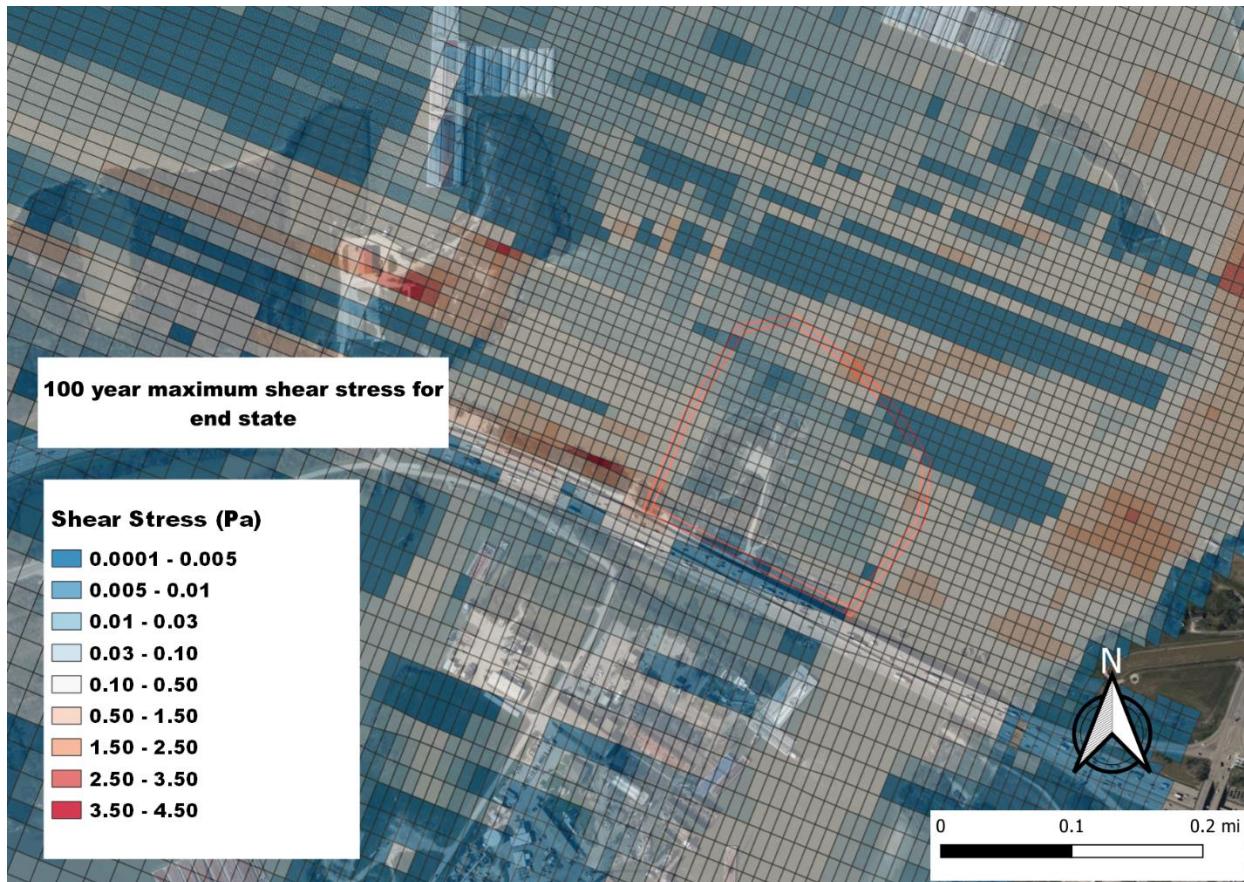


Figure 28 Maximum Shear Stresses with End-State During 100-Year flow

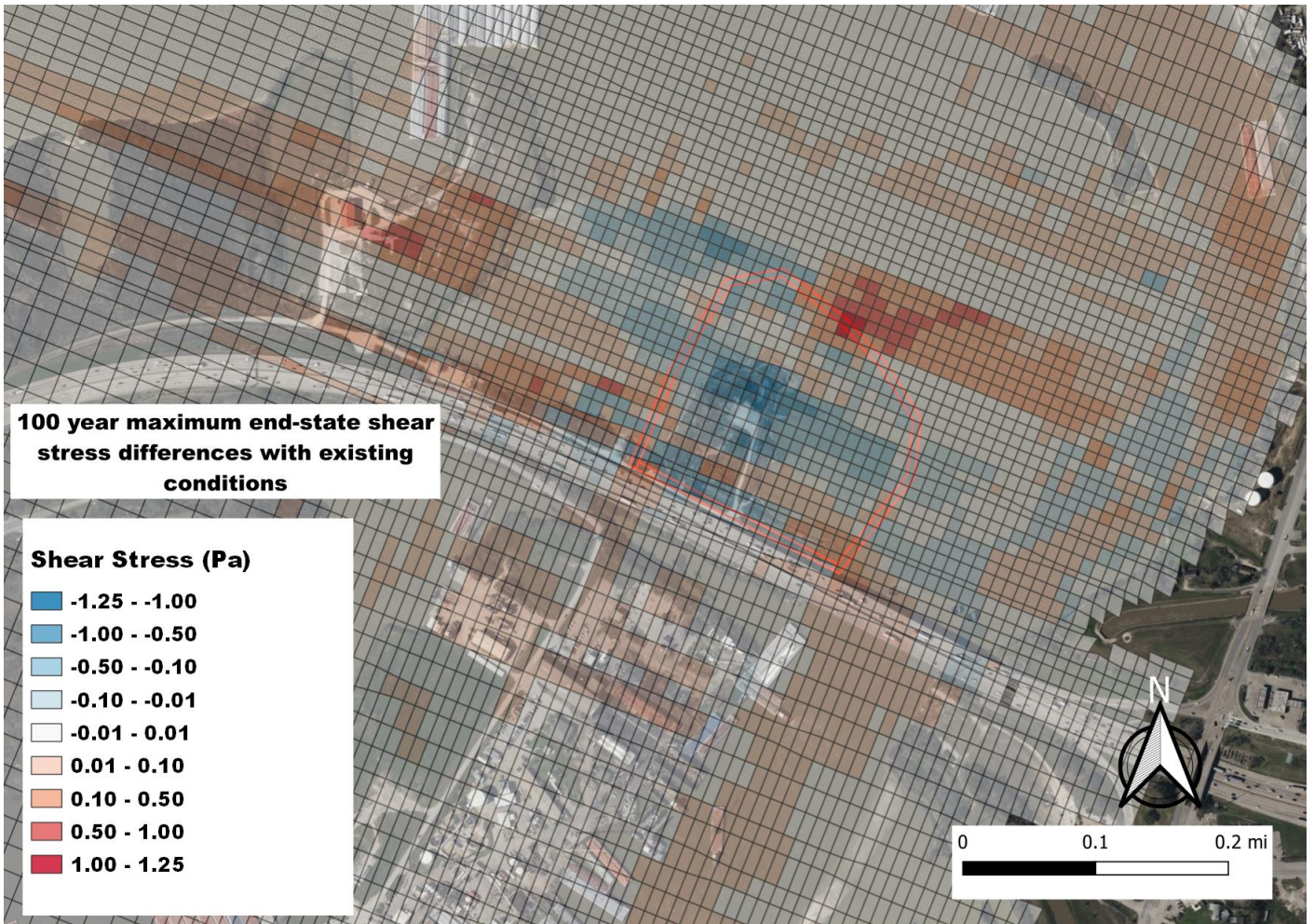


Figure 29 Maximum Shear Stress Differences Between End-State and Existing Condition for the 100-Year flow

Figure 30 shows the maximum velocities for the 100-year storm for end-state conditions and Figure 31 shows the differences for the maximum velocities and Table 15 and Table 16 present the statistics for velocities for the end-state condition and differences with existing conditions for the 2-, 10-, 100-, and 500-year flow events.

The maximum and average values of the maximum velocities are 3.30 ft/s and 0.69 ft/s, respectively. The difference in the maximum value of the maximum velocity is 0.89 ft/s with a maximum difference for the average values of 0.02 ft/s. The velocity pattern shown on Figure 31 indicates that under the estimated end-state conditions there is an increase of flow over the Northern Impoundment location due to a deeper depth because of RA excavation. Figure 31 shows larger maximum velocities on the south and north parts of the Northern Impoundment and slower velocities at the center where larger depths occur. The high velocities do not necessarily translate into higher shear stresses at all locations due to changes in water elevation backwater effects. Figure 29 shows that the greatest difference in shear stresses is at the shoal on the north side of the Northern Impoundment and at the southeast corner of the cofferdam. This is due to an increase in water depth in the estimated end-state condition that permits greater flow and increased velocity to flow through the Northern Impoundment while the shoal and the southeast corner remain relatively shallow. Therefore, the increased maximum velocities and shear stresses over the shoal on the north end and southeast corner of Northern Impoundment, indicate the potential for erosion at these locations.

Table 15 Maximum and Average Velocities for End-State Conditions

Velocity (ft/s)	Existing Conditions				End-State			
	2-year	10-year	100-year	500-year	2-year	10-year	100-year	500-year
Maximum value of cell maximums	2.68	2.93	3.14	3.14	2.80	3.09	3.29	3.30
Average value of cell maximums	0.62	0.61	0.72	0.73	0.59	0.58	0.69	0.69

Table 16 Maximum and Average Velocity Differences for End-State Minus Existing Condition

Velocity Difference	2-Year		10-Year		100-Year		500-Year	
	ft/s	%	ft/s	%	ft/s	%	ft/s	%
Maximum 95 th Percentile	0.82	31%	0.87	30%	0.89	28%	0.86	28%
Average 95 th Percentile	0.02	4%	0.02	3%	0.02	3%	0.01	1%

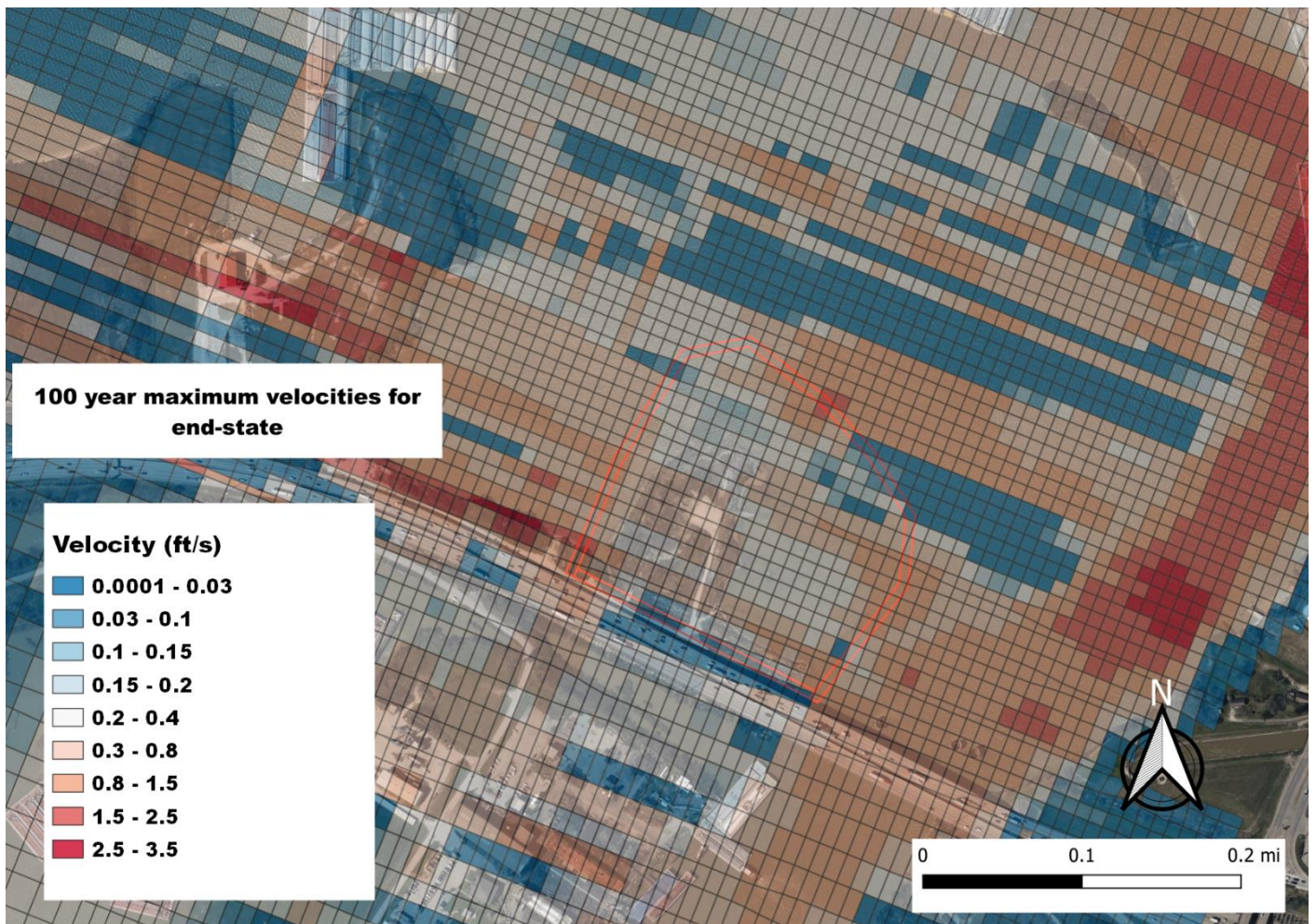


Figure 30 Maximum Velocities with End State Condition During the 2 Year Storm

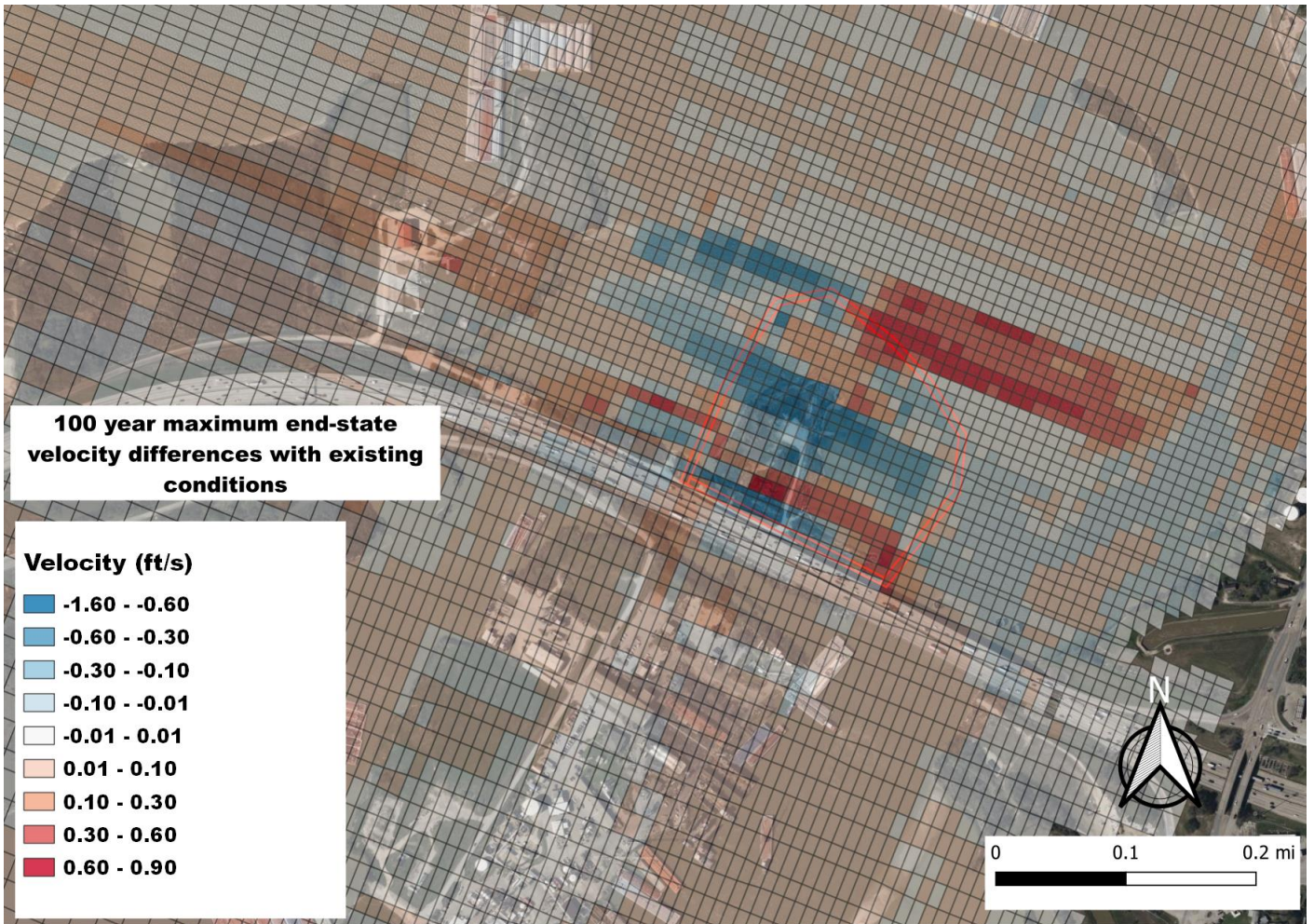


Figure 31 Maximum Velocity Differences Between End-State and Existing Condition for the 2-Year Storm

Appendix C presents the figures for median and maximum of shear stress and velocity for existing and end-state conditions during the 2-, 10-, 100- and 500-year flow events. The figures for the maximum shear stress and velocity differences between end-state and existing conditions for the 2-, 10-, 100-, and 500-year storm events are also included in Appendix C.

4.2.3 Cofferdam Effects on I-10

The model results “with and without” the cofferdam for determining the changes in circulation around the cofferdam, were used for shear stresses and velocities at I-10. The results previously provided to the TxDOT were updated. The model results were applied to the area shown on Figure 32 and the complete results and figures are included as Appendix B.

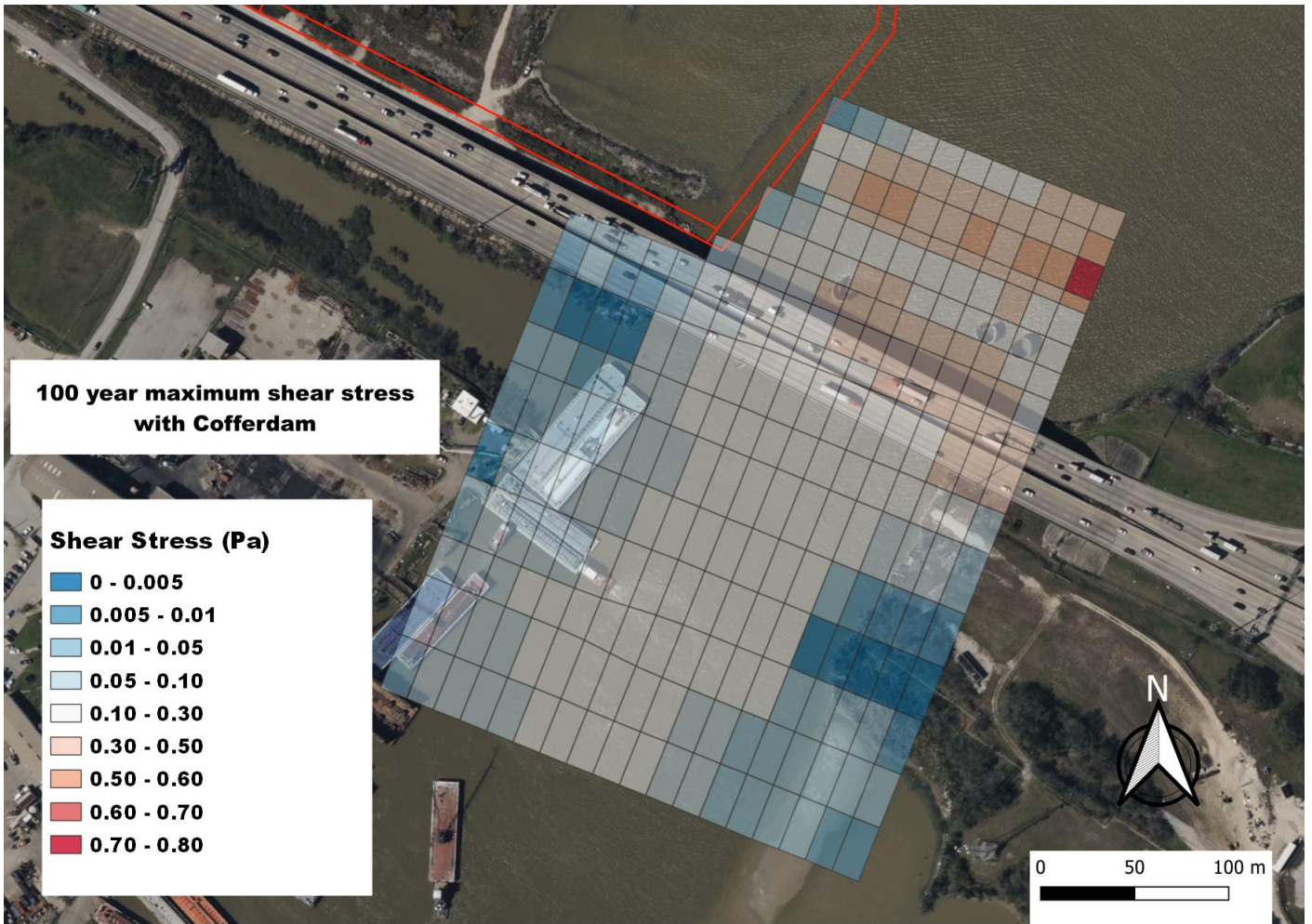


Figure 32 Maximum Shear Stresses “With Cofferdam” for the 2-Year Storm at I-10

5. Summary and Conclusions

This study focused on historical data gathering and depth averaged hydrodynamic modelling of the San Jacinto River. A hydrodynamic model using EFDC was developed to simulate the San Jacinto River from the Lake Houston Dam downstream to the Fred Hartman Bridge including the HSC up to downtown Houston, Texas.

The existing EFDC model for the San Jacinto River (AQEA, 2012) was used as a base for this work, which was updated by combining the coarse and fine grids and by the addition of the bays downstream of the confluence of the San Jacinto River with the HSC down to the Fred Hartman Bridge.

The model was used to determine potential changes in the floodplain inundated areas and in water elevation in flooded areas caused by the cofferdam.

The model was also used to simulate shear stresses and velocities to conduct a sedimentation analysis for the effects of the cofferdam and the end-state conditions.

5.1 Cofferdam Effects on Floodplain

Three scenarios were considered for the hydrodynamic modelling, with 2-, 10-, and a 100-year flow events and the results were compared for two conditions, the existing condition “without cofferdam” and “with cofferdam”, to determine the effect of the cofferdam on the water surface elevation in the floodplain.

Based on results from the numerical model, changes in water height in flooded areas between both conditions are less than 0.1 ft for all three scenarios (Table 7). The results show that there are no changes in the floodplain inundated areas between the “with cofferdam” and “without cofferdam” conditions for all three scenarios.

5.2 Sedimentation Analysis - Cofferdam

Shear stresses and velocities for 2-, 10-, 100-, and 500-year storm events with and without the cofferdam, were simulated with the model and analyzed.

The maximum shear stress for the cofferdam conditions has a maximum value of 4.34 Pa and an average value of 0.72 Pa. The difference in the value of the maximum shear stress is 2.65 Pa with a difference in the average value of less than 0.03 Pa. The shear stress values are large compared to the critical shear stress value of 0.15 Pa at the southwest corner of the cofferdam and at the north side of the cofferdam that could potentially generate scour.

The maximum and average values of the maximum velocities are 3.14 ft/s and 0.72 ft/s, respectively. The differences in the maximum and average value of the maximum velocity are 1.67 ft/s and 0.06 ft/s. The circulation patterns indicate that the presence of the cofferdam generally diverts the flows to the north side of the impoundment, decreasing velocities next to I-10. This is true except for the area north of the cofferdam wall itself (Figure 26 and Figure 27) where an increase in shear stress occurs which could result in potential scour.

5.3 Sedimentation Analysis - End-State

Shear stresses and velocities for the end-state condition were calculated for the 2-, 10-, 100-, and 500-year flow events and compared to the existing condition for sedimentation and circulation analysis. The maximum and median shear stresses and velocities statistics were calculated.

The shear stress for the end-state conditions have a maximum value of 4.25 Pa and an average value of 0.45 Pa. The difference in the maximum value of the maximum shear stress is 1.14 Pa with a difference in average value of 0.006 Pa.

High differences in the maximum shear stresses were found in the shoal area north of the Northern Impoundment which indicates that scouring could potentially occur in the area due to the shallow depth (i.e., redistribution of sediments). An increase in maximum shear stresses is also noticeable close to the west abutment area of the bridge. Although the values are below the critical threshold of 0.15 Pa and range from 0.1 Pa to 0.3 Pa, fine sediment can be mobilized in such areas. The mobilization of sediment leading to scour or accretion depends on the presence of sediment in the system.

As expected, as depth increases in the excavation area shear stresses decrease (i.e., depositional environment). The maximum shear stresses less than 0.03 Pa indicate the potential for sedimentation.

The maximum and average values of the maximum velocities are 3.30 ft/s and 0.69 ft/s, respectively. The difference in the maximum value of the maximum velocity is 0.89 ft/s with negligible differences for the median velocities showing a slight decrease of median velocities for all scenarios of less than 0.02 ft/s. The circulation pattern indicates that underestimated end-state conditions cause an increase of flow over the Northern Impoundment, with larger maximum velocities on the south and north parts of the Northern Impoundment and smaller velocities at the center where larger depths occur. These high velocities do not translate into higher shear stresses because of water elevation backwater effects, except closer to the I-10 abutment. Over the shoal north of the Northern Impoundment, the maximum velocities and shear stresses increase, indicating potential erosion in that area. Once the cofferdam is removed, an

embankment will be built and reinforced with rip-rap on the southern side of the impoundment to account for increases in shear stresses.

6. References

- Anchor QEA, 2012. “Chemical Fate and Transport Modelling Study San Jacinto River Waste Pits Superfund Site,” Ocean Springs, Mississippi.
- EPA, 2017. Record of Decision, San Jacinto River Waste Pits. Harris County, Texas. EPA ID: TXN000606611. U.S. Environmental Protection Agency, Region 6. Dallas, Texas. October 2017.
- Hamrick, J.M., 1992. A Three-Dimensional Environmental Fluid Dynamics Computer Code: Theoretical and Computational Aspects. College of William and Mary, Virginia Institute of Marine Sciences. Special Report 317. 63 pp.
- Julien, P.Y., 2002, River Mechanics: Cambridge, University Press, 434 p.

Appendices

Appendix A

**Correspondence to HCFCD - Overview of
Floodplain Drainage Impact Analysis**

5551 Corporate Boulevard Suite 200
Baton Rouge, Louisiana 70808
United States
www.ghd.com



Our ref: 11215702-Najda-1 Rev. 2

May 06, 2022

Stephania Najda, PE
Harris County Flood Control District
10555 Northwest Freeway, St 170
Houston, TX 77092

Overview of Floodplain Drainage Impact Analysis

Dear Ms. Najda:

On behalf of International Paper Company (IPC) and McGinnes Industrial Maintenance Corporation (MIMC; collectively the Respondents), GHD appreciates the opportunity to submit to the Harris County Flood Control District (HCFCD) this *Overview of Floodplain Drainage Impact Analysis* for the Northern Impoundment of the San Jacinto Waste Pits Superfund Site (Site). The Remedial Design (RD) for the Site is being conducted under the direction of the United States Environmental Protection Agency (EPA) and in accordance with the *Administrative Settlement Agreement and Order on Consent* (AOC; CERCLA Docket No. 06-02-18).

At the request of the HCFCD in an email to Gary Baumgarten, EPA Remedial Project Manager, dated October 20, 2020, GHD conducted hydrodynamic modelling to assess potential impacts of a proposed cofferdam structure to the surrounding floodplain. The design of the cofferdam structure is part of the Northern Impoundment Pre-Final 90% Remedial Design package due to the EPA in June 2022. Per the 2017 EPA Record of Decision (ROD; EPA, 2017), the selected remedy for the Northern Impoundment includes the installation of a cofferdam around the impoundment, dewatering of river water, and excavation of impacted material for off-Site disposal.

GHD provided an overview of the modelling and drainage impact analysis to the HCFCD in a virtual Teams meeting on February 3, 2022. Based upon that discussion, GHD has prepared this letter to provide a summary of the return events modelled, the outputs of the model, and the implications of the results. This letter also describes the model used and how it compares to the HEC-RAS model typically used by the HCFCD.

1. Objective

The objective of this letter is to summarize the numerical hydrodynamic model used to assess the effect of the planned cofferdam on the river hydrodynamics and the results of the modelling. The model was compared to the existing HEC-RAS 3.0.1 G103-00-00SJ San Jacinto Watershed model downloaded from the Harris County Model and Management (M3) website to provide an assessment of the selected model behavior.

2. Background

The Northern Impoundment is located in the San Jacinto River north of Interstate 10 (I-10) to the east of Houston, Texas, Figure 2.1. According to the HCFCD, projects that may impact the floodplain must be modelled up to and including the 500-year flood event. However, the Site is located within a tidally influenced area and is classified by the United States Geological Society (USGS) as a Tidal Stream (USGS, 2022). This means that flow is influenced by the tide and is considered a coastal Site. Therefore, a 500-year flood assessment is not required and was not conducted. The Site is located within the San Jacinto Watershed. As shown in Figure 2.2.1, the upper San Jacinto River Basin Watershed extends from Huntsville, Texas to Lake Houston and represents ten bayous/creeks. South of Lake Houston, Figure 2.2.2 shows the lower San Jacinto Watershed that represents the flood plain south of Lake Houston for the Site.

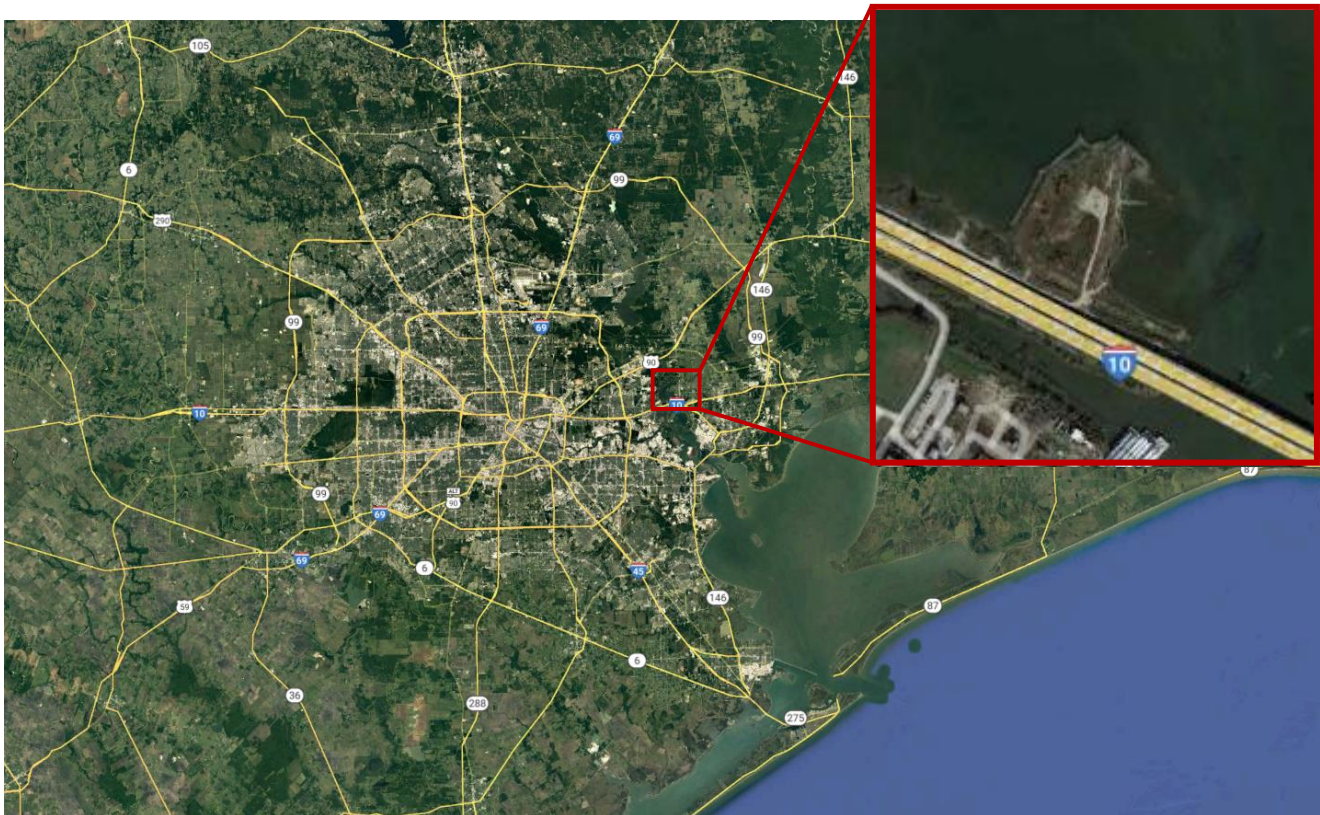


Figure 2.1 Project Location (Site)



Figure 2.2 Project Location Watershed (Green Represents the Upper San Jacinto River Basin Watershed and Blue is the Lower San Jacinto Watershed)

3. EFDC Model

The Environmental Fluid Dynamic Model (EFDC) was used to conduct a numerical hydrodynamic model of the Northern Impoundment. EFDC is a numerical code for 1-, 2- and 3-dimensional hydrodynamic modeling with the ability to calculate sediment and contaminant transport as well as water quality. It has evolved over the past two decades to become one of the most widely used and technically defensible hydrodynamic models in the world. EFDC is used extensively to simulate hydrodynamic and water quality processes in rivers, lakes, estuaries, reservoirs, wetlands, and coastal regions.

The EFDC code solves the three-dimensional primitive variable vertically hydrostatic equations of motion for turbulent flow in a coordinate system which is curvilinear and orthogonal in the horizontal plane and stretched to follow bottom topography and free surface displacement in the vertical direction which is aligned with the gravitational vector. A second moment turbulence closure scheme relates turbulent viscosity and diffusivity to the turbulence intensity and a turbulence length scale. Transport equations for the turbulence intensity and length scale as well as transport equations for salinity, temperature, and suspended sediment are also solved. An equation of state relates density to pressure, salinity, temperature, and suspended sediment concentration.

The EFDC model allows for drying and wetting in shallow areas by a mass conservation scheme for the appropriate representation of marsh and floodplain areas.

A 2-dimensional (2D) depth average EFDC model that simulates flow velocity and water depth in the domain has been developed by Anchor QEA (AQEA, 2012). The EFDC San Jacinto model implementation has been peer reviewed by the US Army Corp of Engineers - Engineer Research and Development Center (ERDC) and approved by EPA for several uses, including hydrodynamic and sediment transport. GHD updated the model for the analysis of the potential impact that the planned cofferdam could have on flooding elevations. The model extends from the Lake Houston Dam south to the Fred Hartman Bridge. A higher resolution grid was implemented near and at the Site, while a lower resolution grid was used in the Houston Ship Channel (HSC), upper San Jacinto River, downstream bays, and down to Fred Hartman bridge.

The bathymetric data used in the AQEA model was updated using the most recent data from the National Oceanic Atmospheric Association (NOAA) National Centers for Environmental Information (NCEI) with the projection set to the State Plane 1983 with horizontal and vertical datums North American Datum of 1983 (NAD83) and North American Vertical Datum of 1988 (NAVD88), respectively. Wind and water levels were downloaded from NOAA’s Tides and Currents gauge #8770613 located at Morgan’s Point, TX. Morgan’s Point is located less than 12 miles from the Site and experiences diurnal and semidiurnal tides (NOAA, 2021).

Flow data for the Lake Houston Dam was obtained from the Coastal Water Authority (CWA) for the years 2007-2011 while the years preceding 2007 were calculated using a rating curve. Streamflow and velocity data for the floodplain south of Lake Houston was downloaded from USGS gauges 08072050, 08074000 and 08073700.

Two stations were used within the model to evaluate results. Both are located less than 800 feet (ft) from the Cofferdam Wall in areas subjected to flooding and drying during the simulation. Station 1 and Station 2 are shown in Figure 3.1.1.

To calculate the impact on the floodplain surrounding the Site, the model was processed using three scenarios, each with and without the cofferdam present. The three flow events processed have return periods of 2-, 10- and 100-years. For all three return periods, the results show that the water height differences expected between “With Cofferdam” and “Without Cofferdam” scenario are less than 0.1 ft as shown in Table .

Table 1 *Water Height Differences*

Return Period	Difference Between With and Without Cofferdam	
	(feet)	(inches)
2-year	0.072	0.864
10-year	0.020	0.24
100-year	0.003	0.036

These results indicate that there should be no adverse effects on the surrounding floodplain caused by the presence of the cofferdam in the river during remedial activities conducted at the Northern Impoundment.

There are no changes in the floodplain inundated areas with or without a cofferdam present. The 2-, 10-, and 100-yr water depth comparison results are shown in Figure 3.23.2, while the calculated water surface elevations at the Site for the three scenarios are shown in Figure 3.33.3.

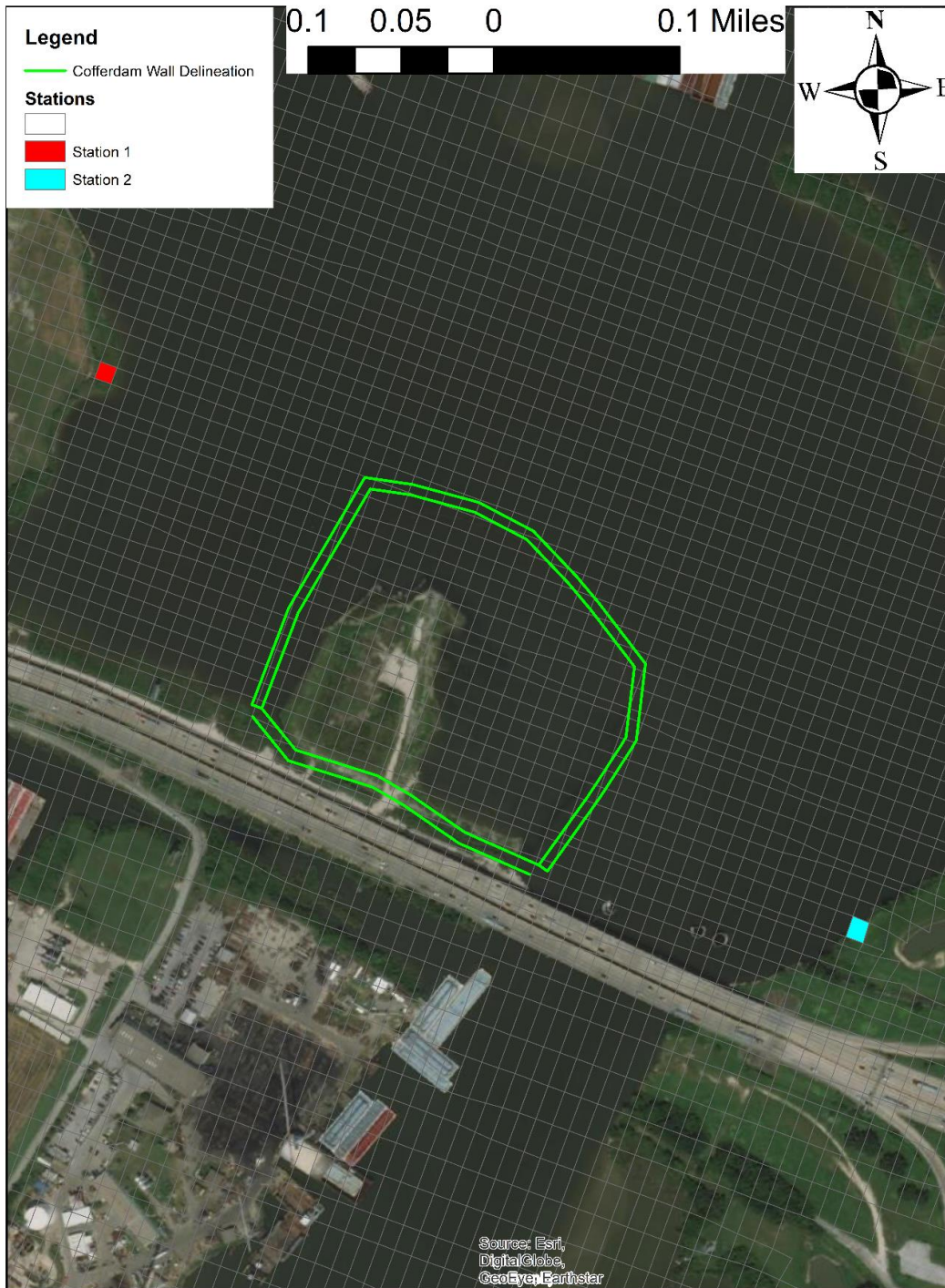


Figure 3.1 Stations for Water Depth Comparisons

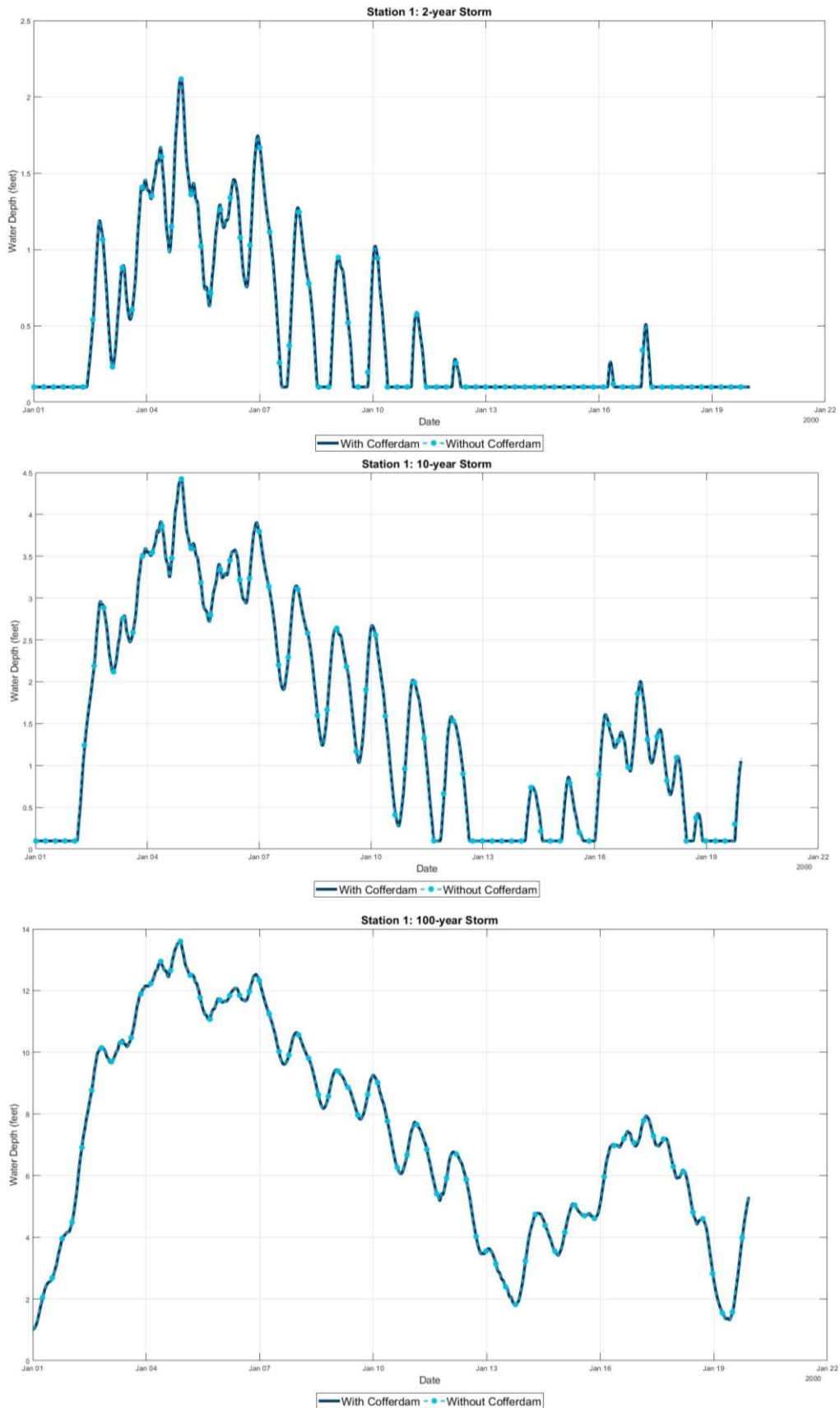


Figure 3.2 Station 1 Water Depth Comparison With and Without Cofferdam Wall for 2-, 10-, and 100-yr Storms

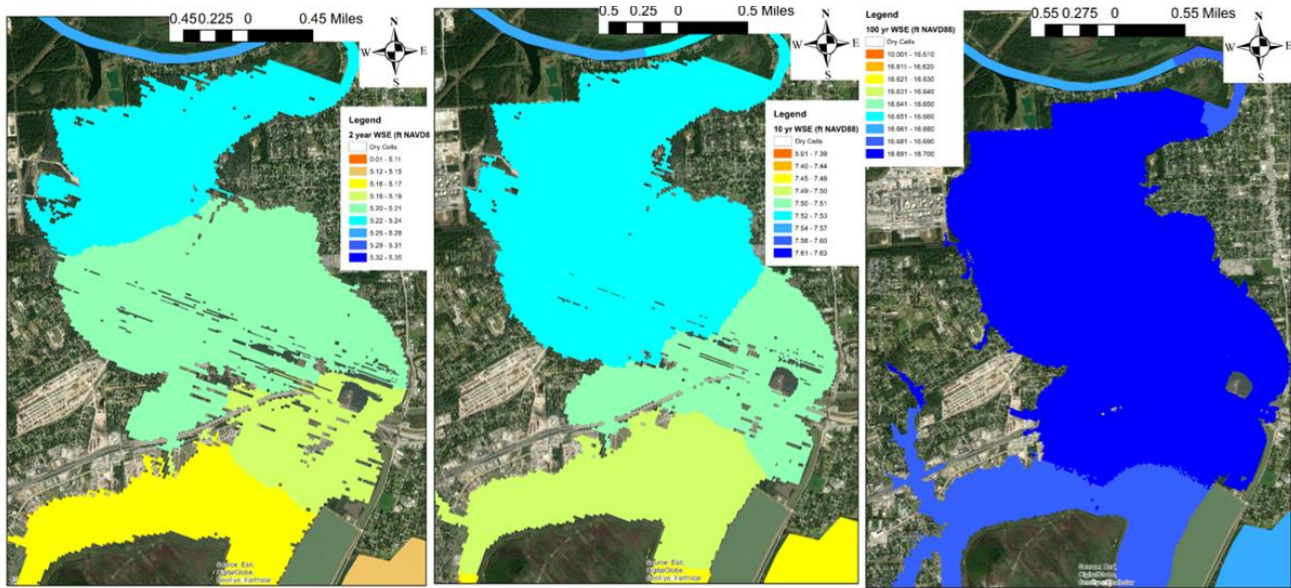


Figure 3.3 Maximum Water Surface Elevations for the 2-, 10- and 100-year Storm

4. HEC-RAS G103-00-00SJ Model

HEC-RAS is an integrated system of software designed to perform one-dimensional and two-dimensional hydraulic calculations for a full network of natural and constructed channels, overbank/floodplain areas, and levee protected areas. The 1D flow calculations are based on the energy equations to solve for steady and unsteady Gradually Varied Flows and can use a solver based on the momentum equation for special cases such as Rapidly Varying Flows or mixed flow regimes. The 2D flow routing capabilities in HEC-RAS have been developed to allow the user to perform 2D or combined 1D/2D modelling. The program solves either the 2D Shallow Water equations (with optional momentum additions for turbulence, wind forces, mud and debris flows, and Coriolis effects) or the 2D Diffusion Wave equations, as selected by the user. The 2D Shallow Water equations are applicable to a wider range of problems and is comparable to the other models used as 2D such as EFDC.

For the San Jacinto River, the G103-00-00SJ data was run through the HEC-RAS 3.0.1 hydraulic model on June 18, 2007, using a steady state flow condition and a vertical datum of NAVD88 (same as EFDC). The HEC-RAS 3.0.1 is a 1-dimensional fluid flow model that computes water surface profiles and floodways for steady, gradually varied flow in channels with the water profile calculated using discharges from the HEC-HMS model.

The data for the San Jacinto River regional watershed was downloaded from the Harris County Flood District Model and M3 System. While all the data sets were pulled for the individual bayous, the data set titled, G103-00-00SJ was compared with the EFDC model results. The G103-00-00SJ data set covers the San Jacinto River from I-10 to the Lake Houston Dam, including the Northern Impoundment location.

5. Model Differences

The key differences between the EFDC model and the HEC-RAS 3.0.1 run model include dimensionality and model boundary conditions. The EFDC model is a 2-dimensional model while the HEC-RAS is 1-dimensional. Additionally, the HEC-RAS model did not take storm surge into account as a boundary condition on the south side of the model boundary which is important as the San Jacinto River is considered a tidally influenced river

The HEC-RAS application assumed normal flow conditions at the downstream boundary of the 1D model neglecting the backwater effect of the storm surge on the area of interest. While the HEC-RAS model was run for the 10-, 50-, 100- and 500-year storm events, the EFDC model was run for the 2-, 10-, and 100-year storm events (the 500-year event was not applicable since the area is considered a coastal area).

6. Result Comparison

Results between the two models were compared from HEC-RAS transect 32 (I-10) upstream to Transect 23 (Bend at Lakeview Terrace/Bluff Gully), as shown boxed in Figure 6.1.1 below.

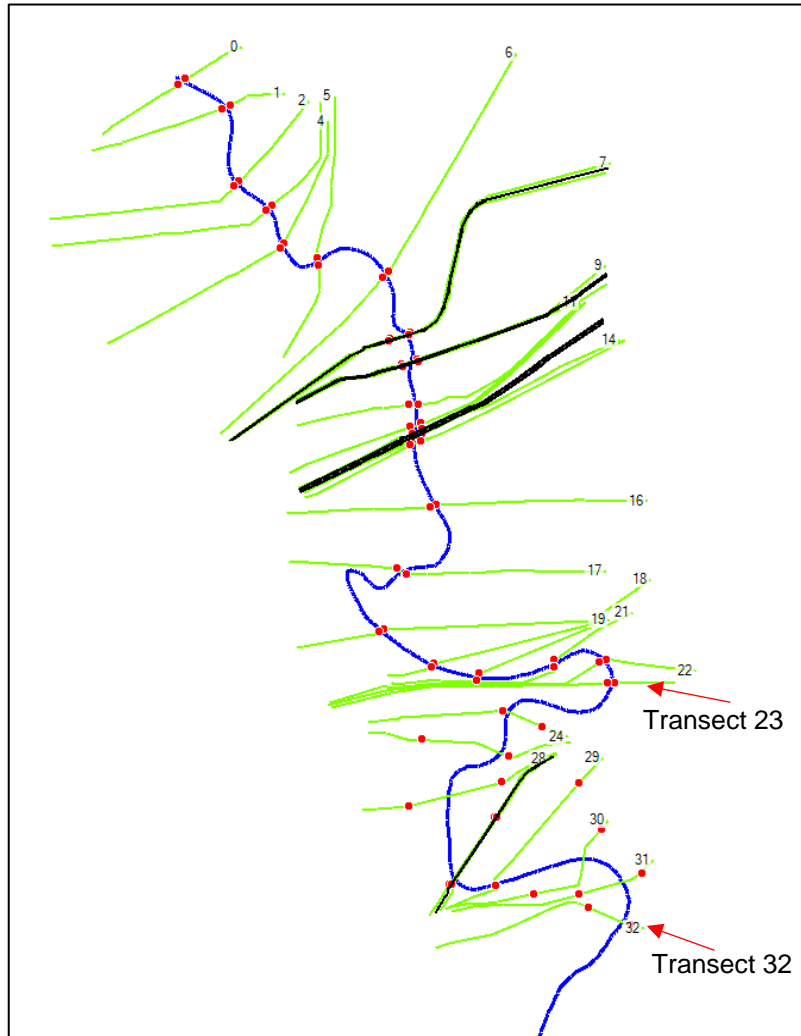


Figure 6.1 G103-00-00SJ River Transect Numbers and Bank Stations (red)

The models were compared for the 10-yr and 100-year return period storm events with results shown in Table 2 below. The EFDC model shows greater water surface elevation at all transect numbers for the 100-yr storm event and for eight of the nine transects for the 10-year storm event. The 23rd transect located north of the Site, has a water surface elevation difference of 0.4-ft or 4.8-inches.

Table 2 G103-00-00SJ River Transects – Model Comparison

Transect Number	River Station	HEC-RAS 10YR	EFDC 10YR	HEC-RAS 50-YR	HEC-RAS 100-YR	EFDC 100-YR
23	93063.22	7.92	7.51-7.52	13.81	16.5	16.661-16.680
24	86250.95	6.80	7.51-7.52	12.76	15.27	16.691-16.7
25	83974.91	6.63	7.51-7.52	12.61	15.11	16.691-16.7
26	79907.59	6.08	7.51-7.52	12.22	14.68	16.691-16.7
27	75450.01	4.96	7.51-7.52	11.51	13.85	16.691-16.7
29	72968.31	4.32	7.51-7.52	11.19	13.43	16.691-16.7
30	67924.46	2.36	7.5-7.51	10.69	12.85	16.691-16.7
31	65261.75	0.36	7.5-7.51	10.21	12.32	16.691-16.7
32	62987.20	-1.24	7.5-7.51	9.33	11.43	16.691-16.7

Given the model differences, the EFDC model is more accurate than the HEC-RAS 3.0.1 model and shows greater water surface elevations at all the transects for the 100-year storm and at eight of the 9 transects for the 10-year storm event. The EFDC model uses storm surge for the water surface elevation, which is crucial, as the Site is located within a tidally influenced section of the San Jacinto River. Additionally, the project is being performed under an AOC under the EPA Superfund program. GHD is confident that the EFDC model gives accurate results that are comparable to what a HEC-RAS 2D application could provide, and with similar results to existing HEC-RAS 1D application in the area with differences mainly related to more accurate boundary conditions enhanced by including storm surge effects.

7. References

San Jacinto River near Sheldon, Texas Monitoring Location 08072050, courtesy of the U.S. Geological Survey. [San Jacinto River near Sheldon, TX - USGS Water Data for the Nation](#). Accessed 11 February 2022.

Model and Map Management (M3) System, Harris County Flood Control District. [Model and Map Management \(M3\) System \(hcfcd.org\)](#). Accessed 11 February 2022.

Hamrick, J. M. (1992) A Three-Dimensional Environmental Fluid Dynamics Computer Code: Theoretical and computational aspects. Special report in applied marine science and ocean engineering; no. 317. Virginia Institute of Marine Science, College of William and Mary.

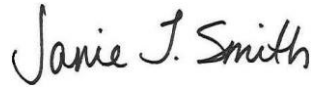
HEC-RAS River Analysis System. HEC-RAS 2D User's Manual. Version 6.0. Exported - February 2022.

USEPA. 2017. Record of Decision. San Jacinto River Waste Pits. Harris County, Texas. USEPA ID TXN000606611. USEPA Region 6. Dallas TX. October 2017.

Regards,



Hugo Rodriguez
Senior Water Resources & Coast
+1 786 431-2914
hugo.rodriguez@ghd.com



Janie Smith
Project Manager
+1 225 296-6550
janie.smith@ghd.com

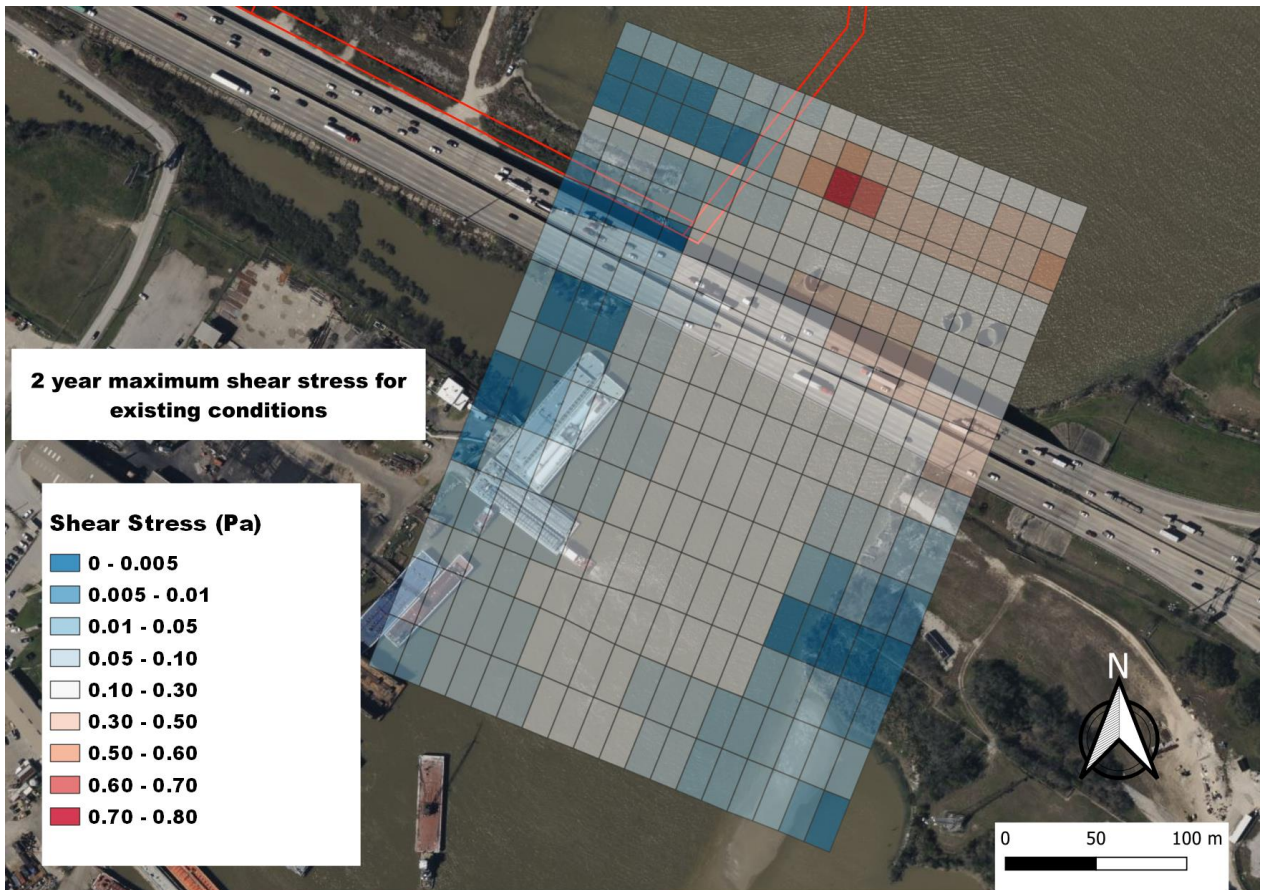
JS/kdn/1

Copy to: Todd Miller, HCFCD
Ashley Howard, USEPA
Phil Slowiak, IPC
Brent Sasser, IPC
Judy Armour, MIMC
Charles Munce, GHD

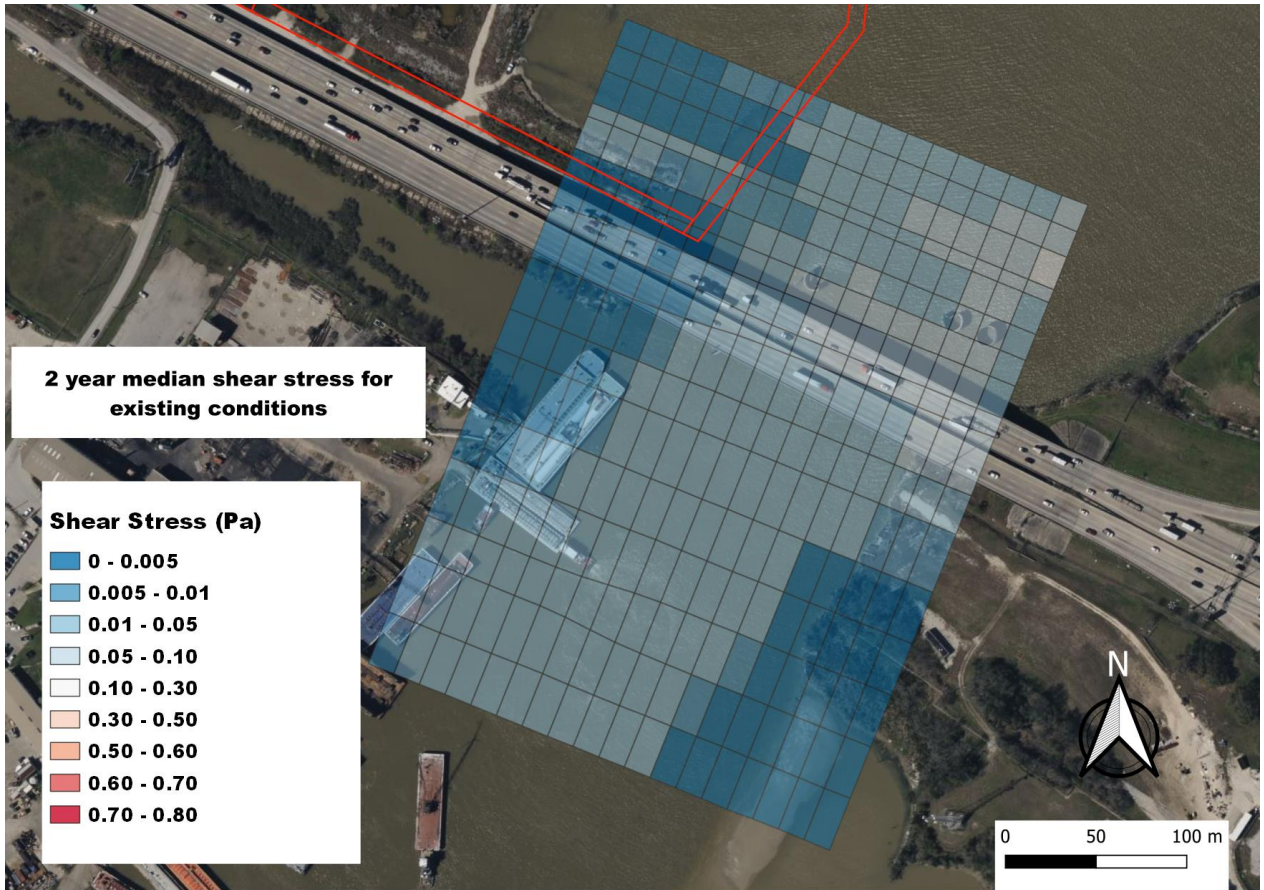
Appendix B

**Correspondence to TxDOT - Velocity and
Shear Stress Analysis**

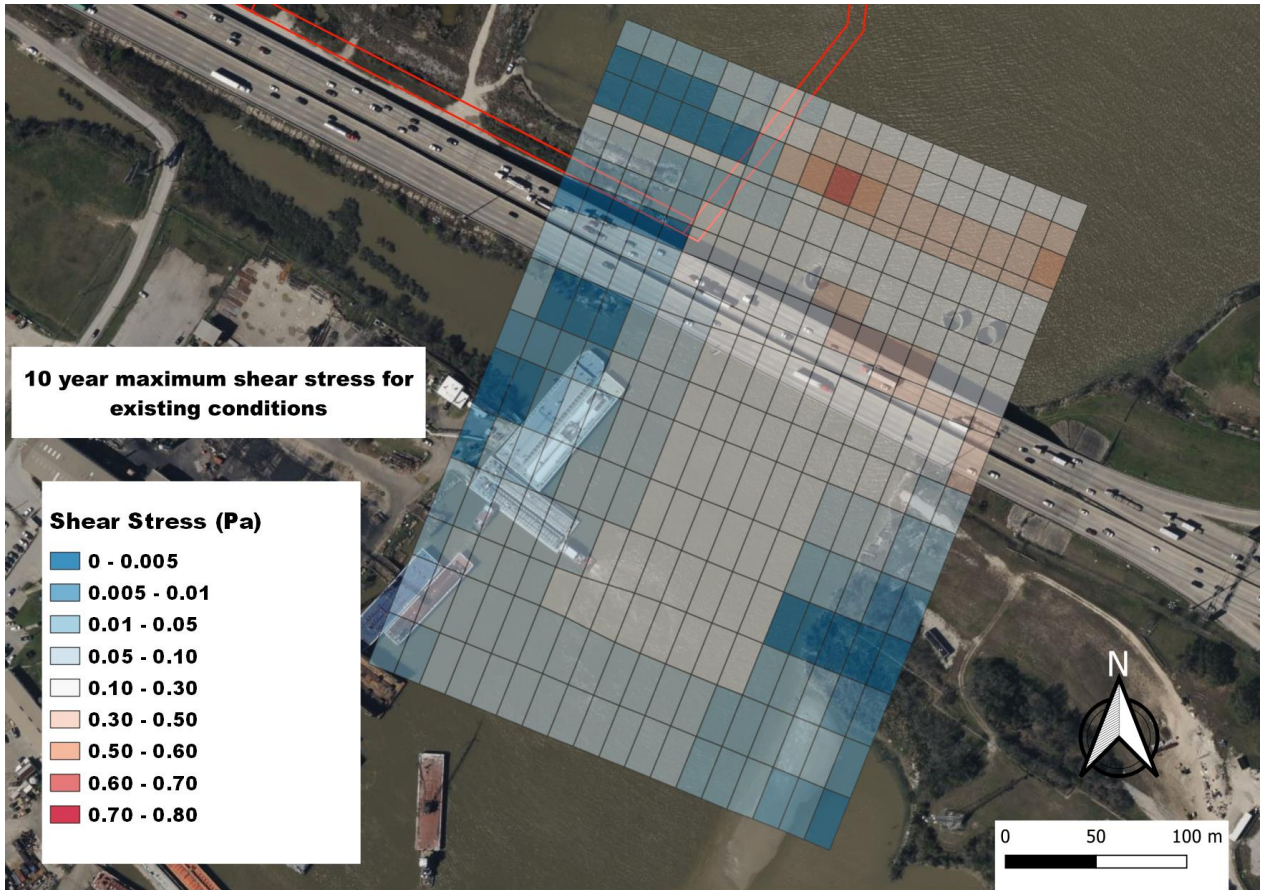
Shear Stress Figures Existing Conditions



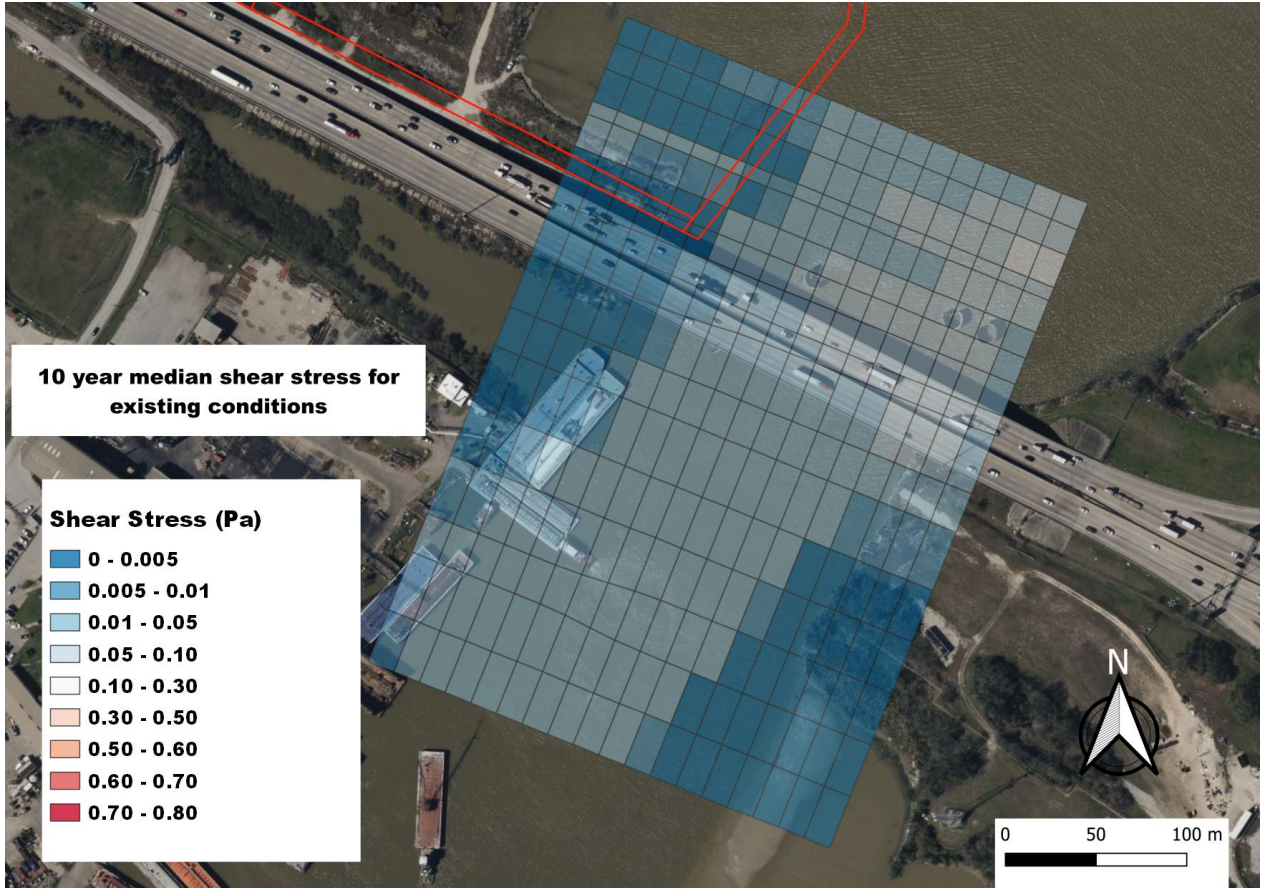
Appendix B - Velocity and Shear Stress Analysis



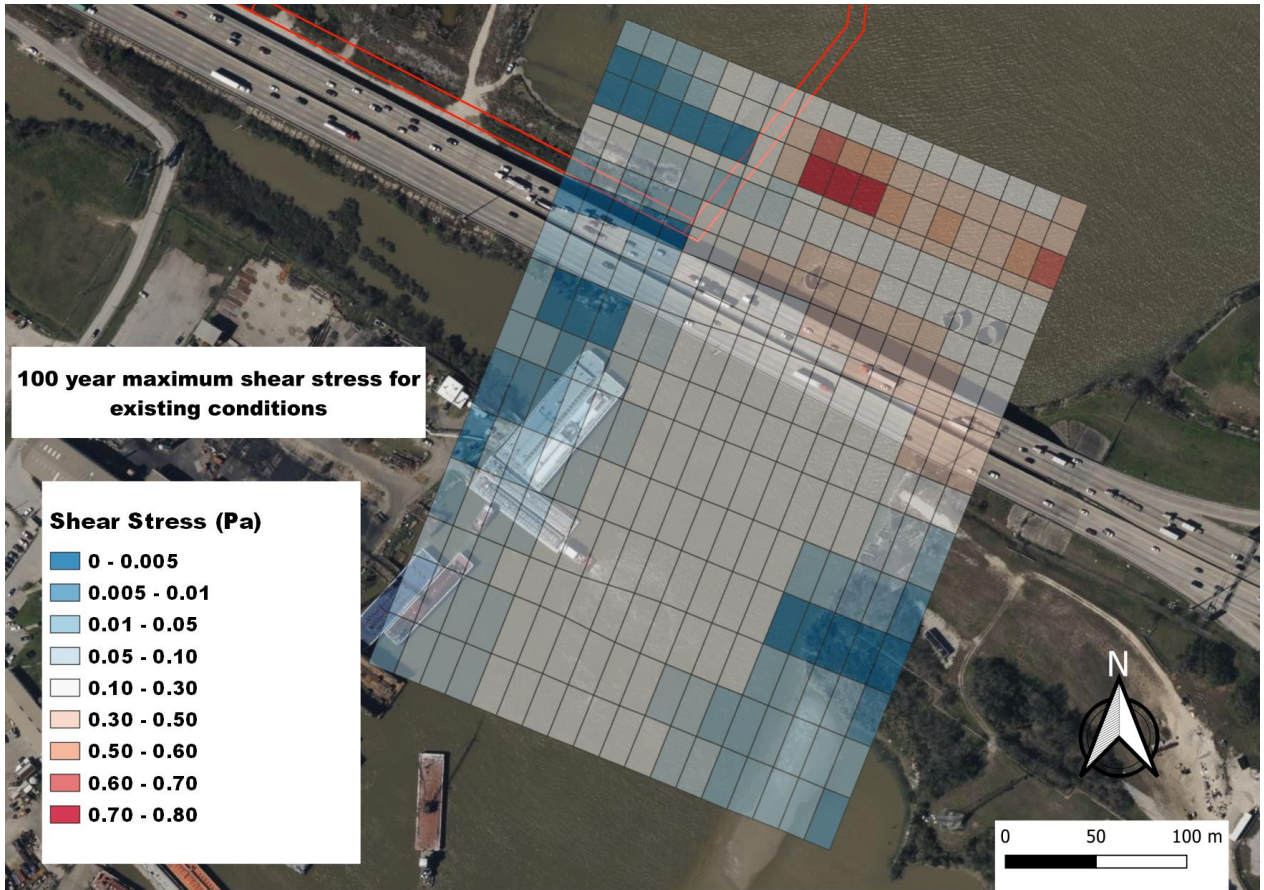
Appendix B - Velocity and Shear Stress Analysis



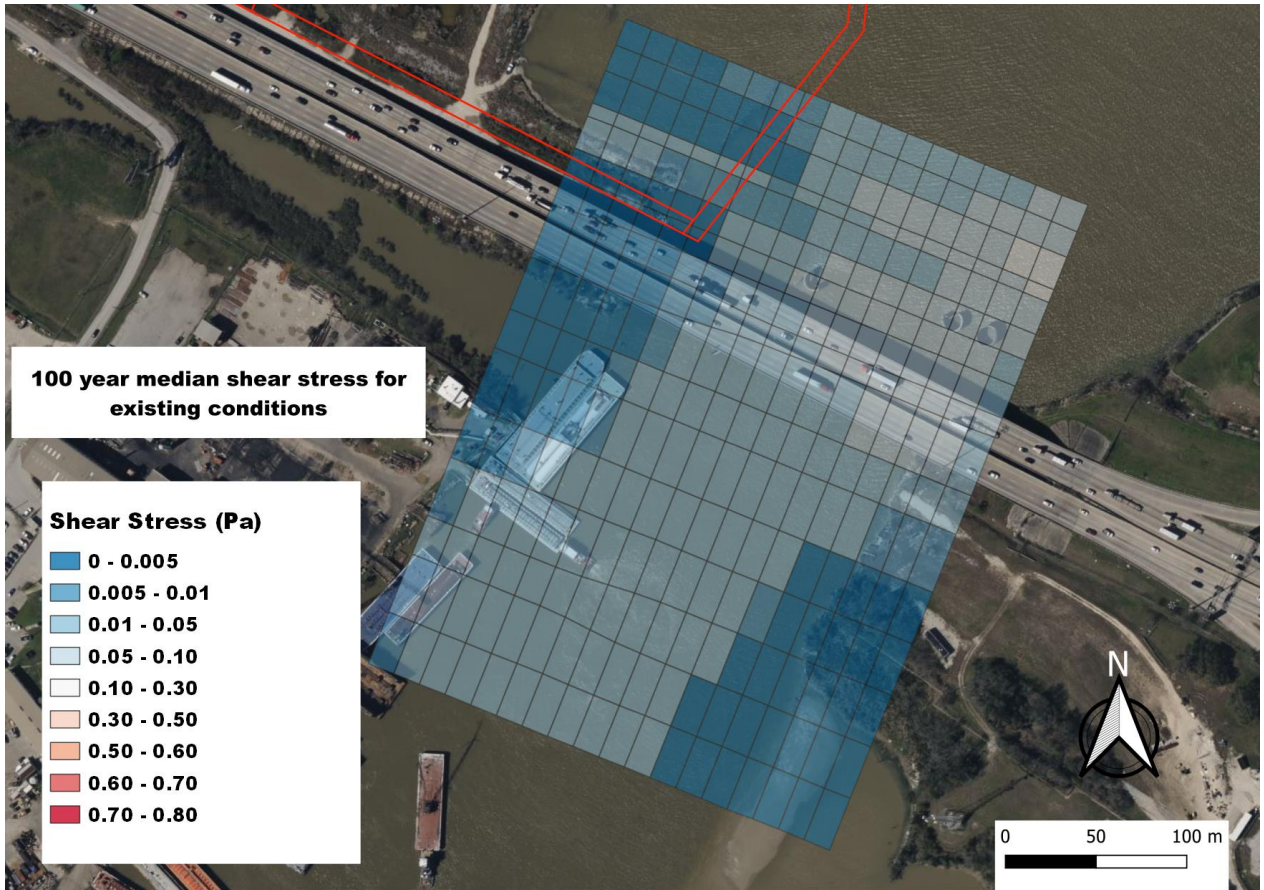
Appendix B - Velocity and Shear Stress Analysis



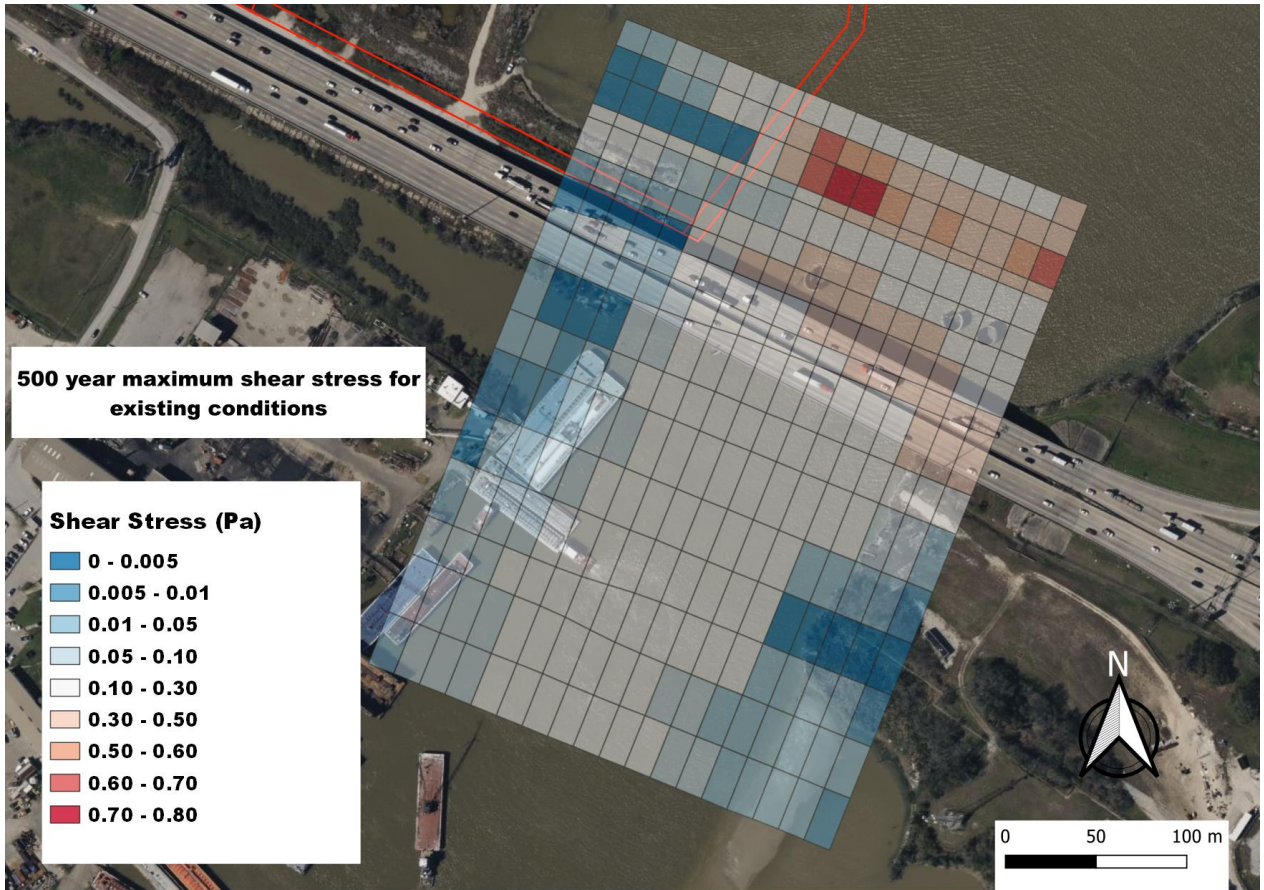
Appendix B - Velocity and Shear Stress Analysis



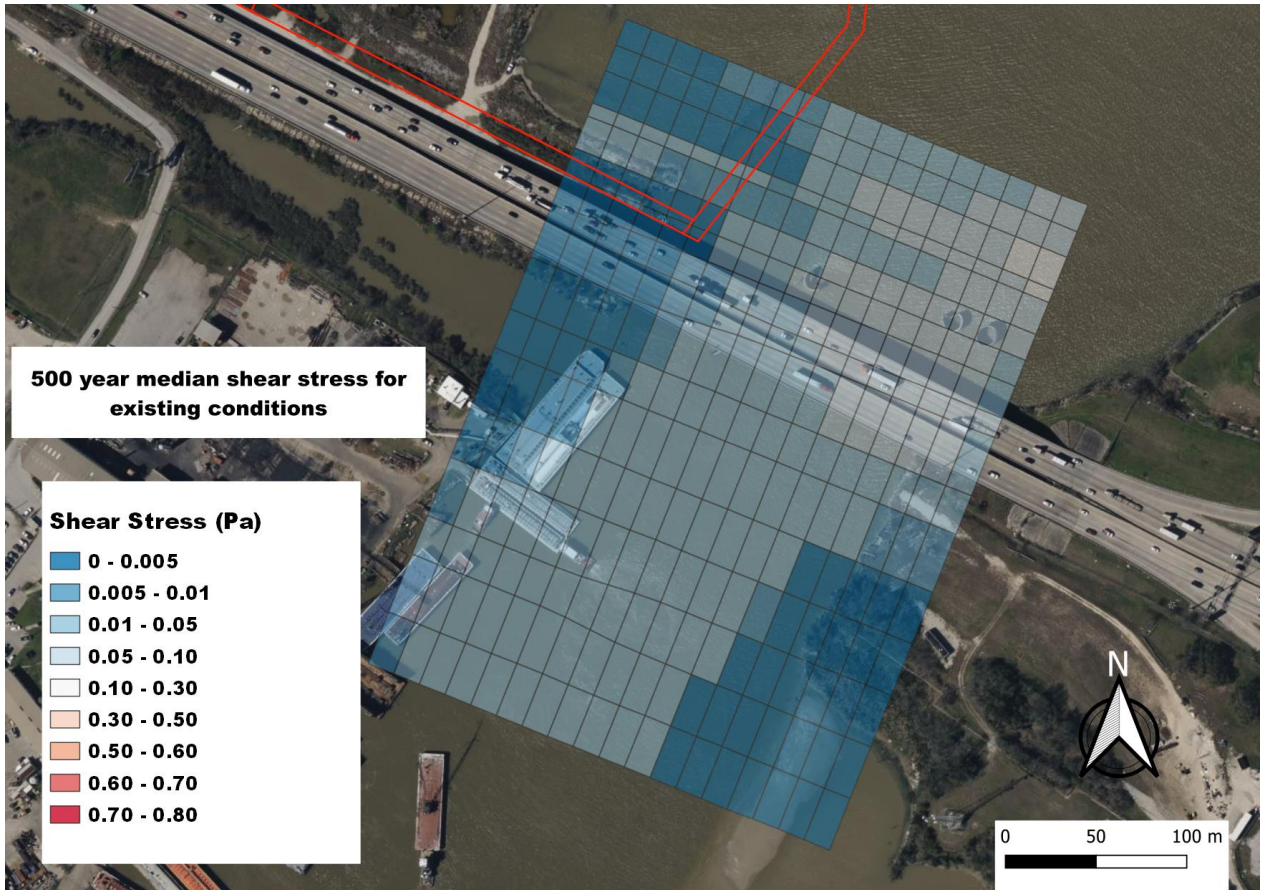
Appendix B - Velocity and Shear Stress Analysis



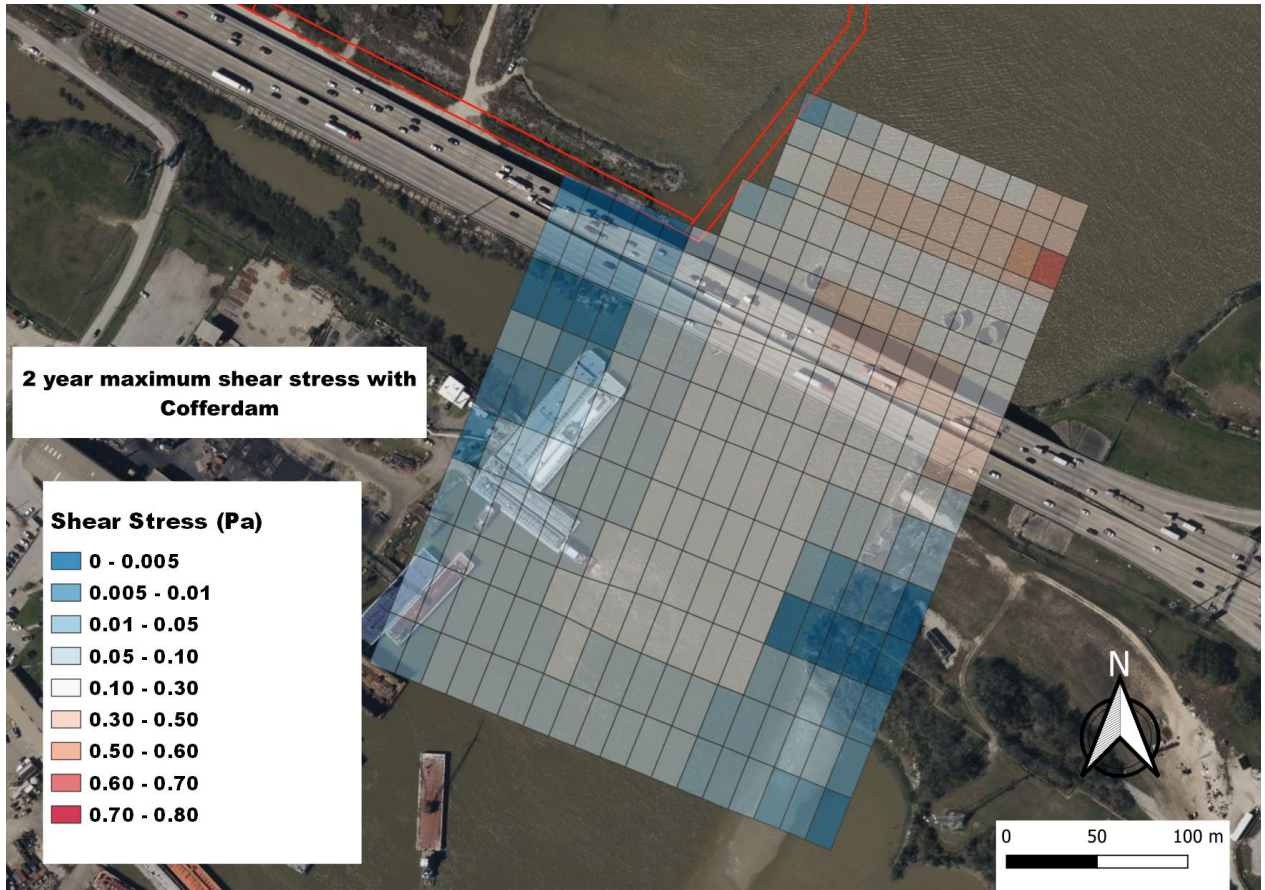
Appendix B - Velocity and Shear Stress Analysis



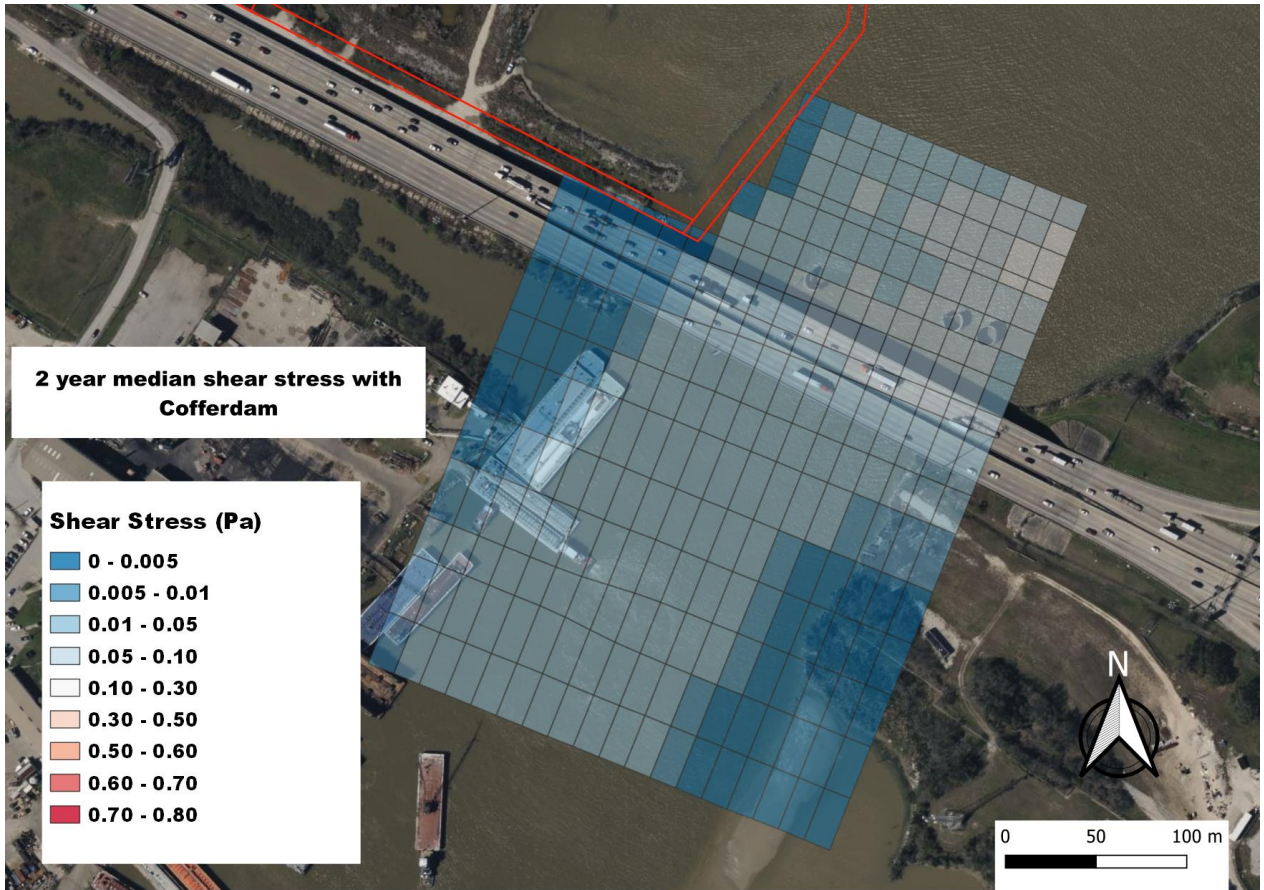
Appendix B - Velocity and Shear Stress Analysis



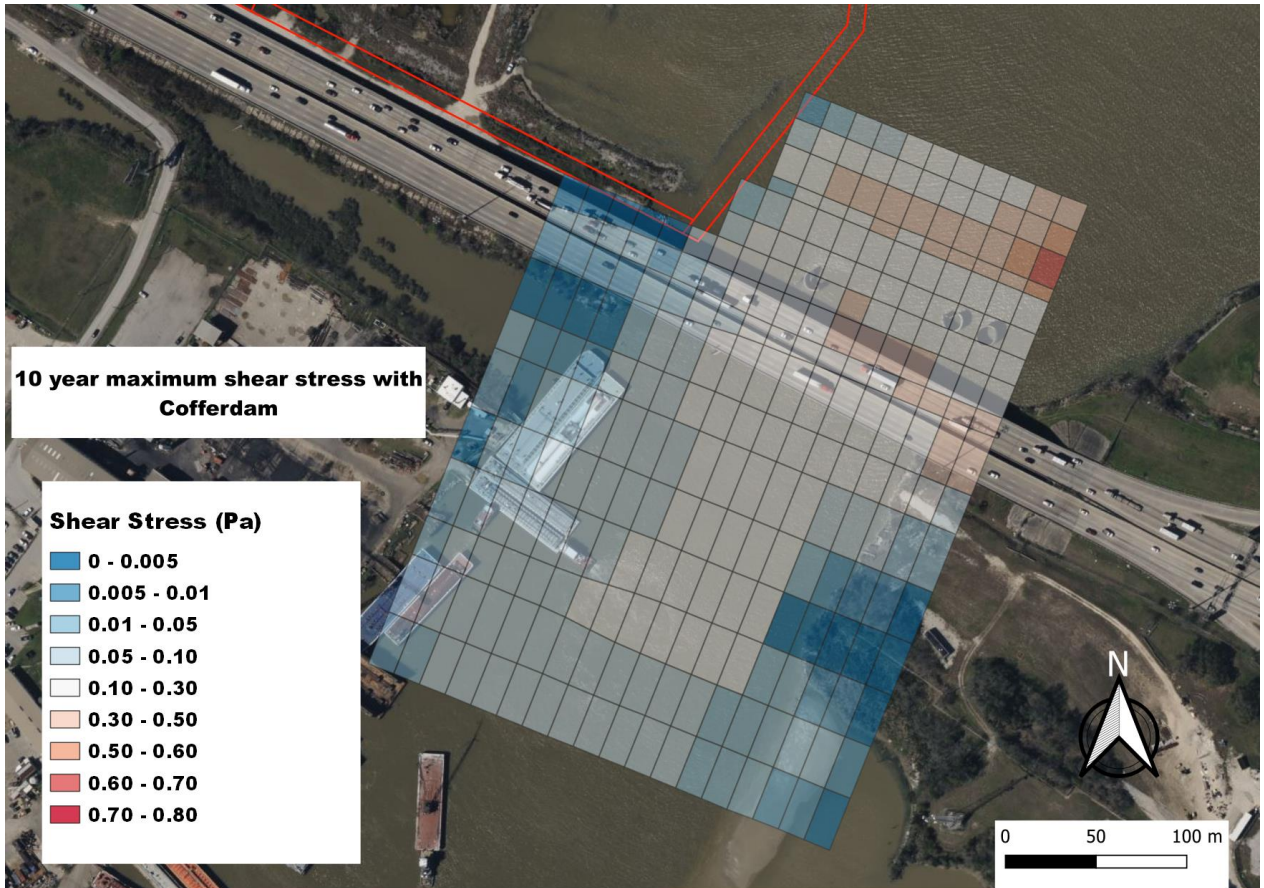
Shear Stress Figures with Cofferdam



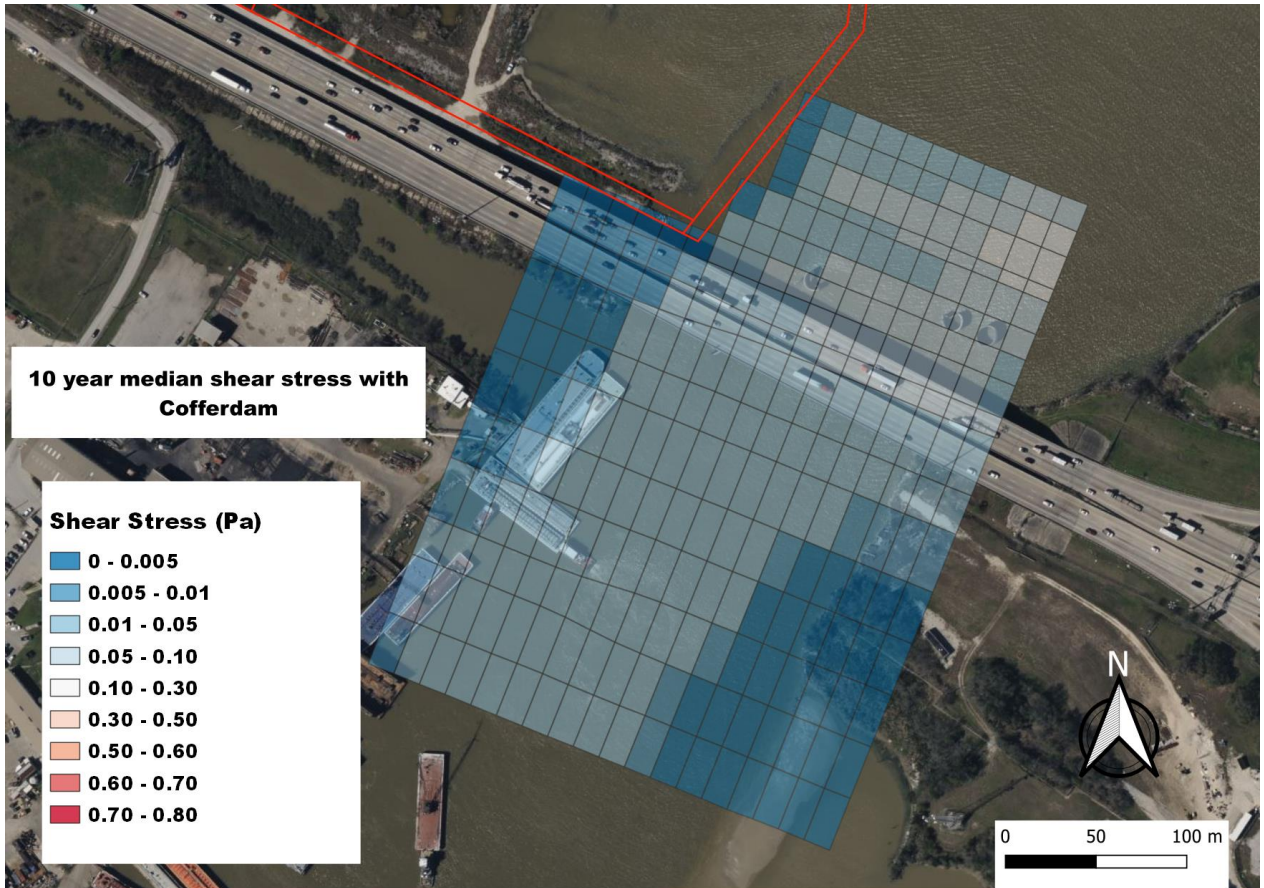
Appendix B - Velocity and Shear Stress Analysis



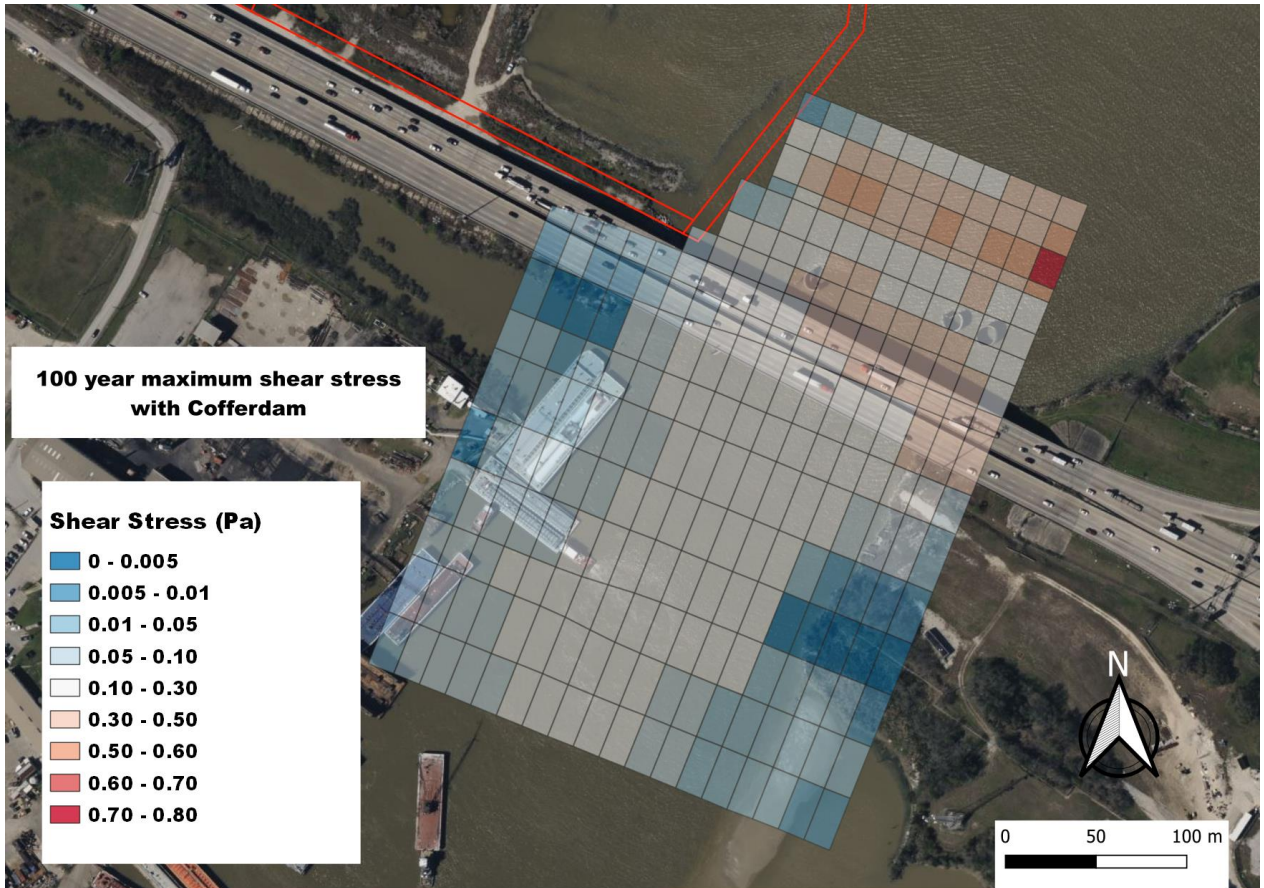
Appendix B - Velocity and Shear Stress Analysis



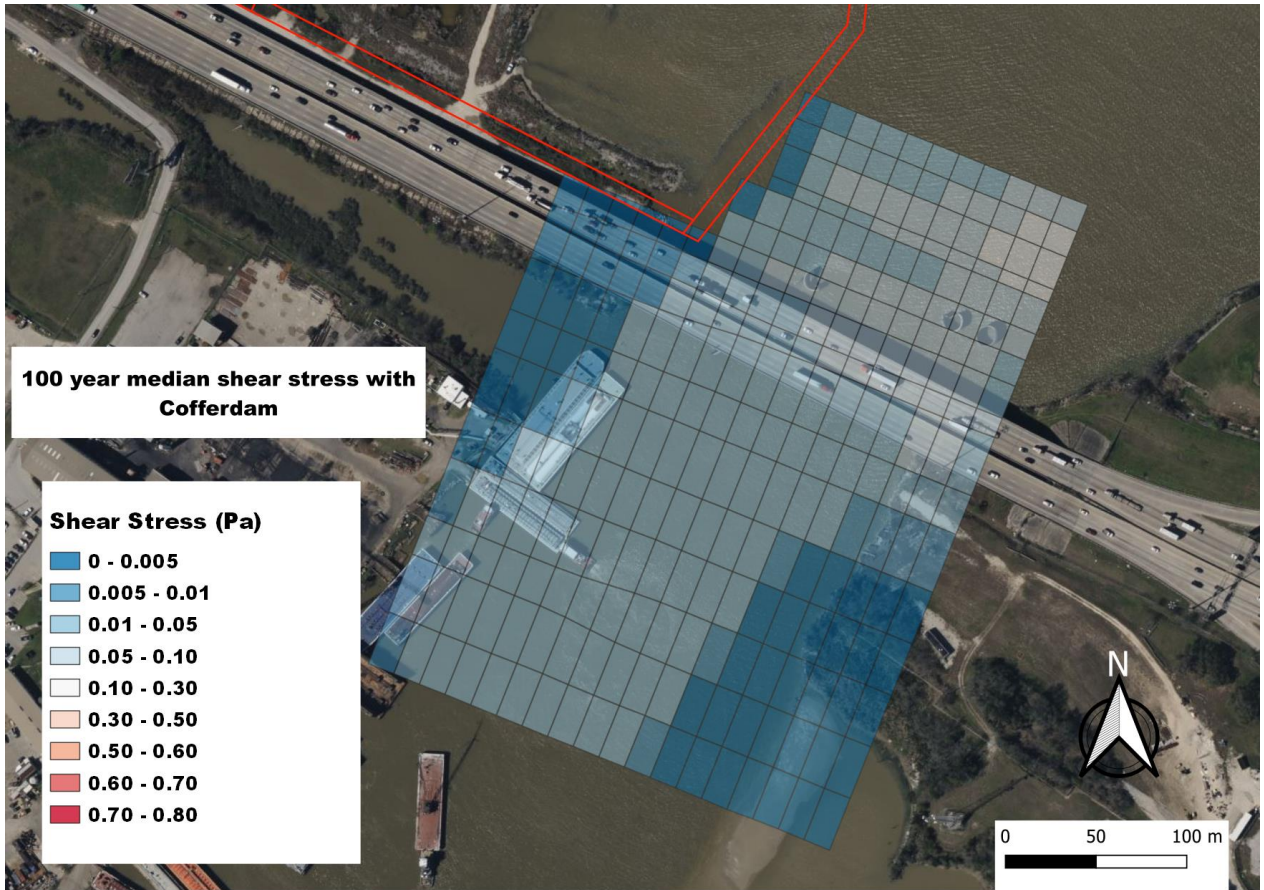
Appendix B - Velocity and Shear Stress Analysis



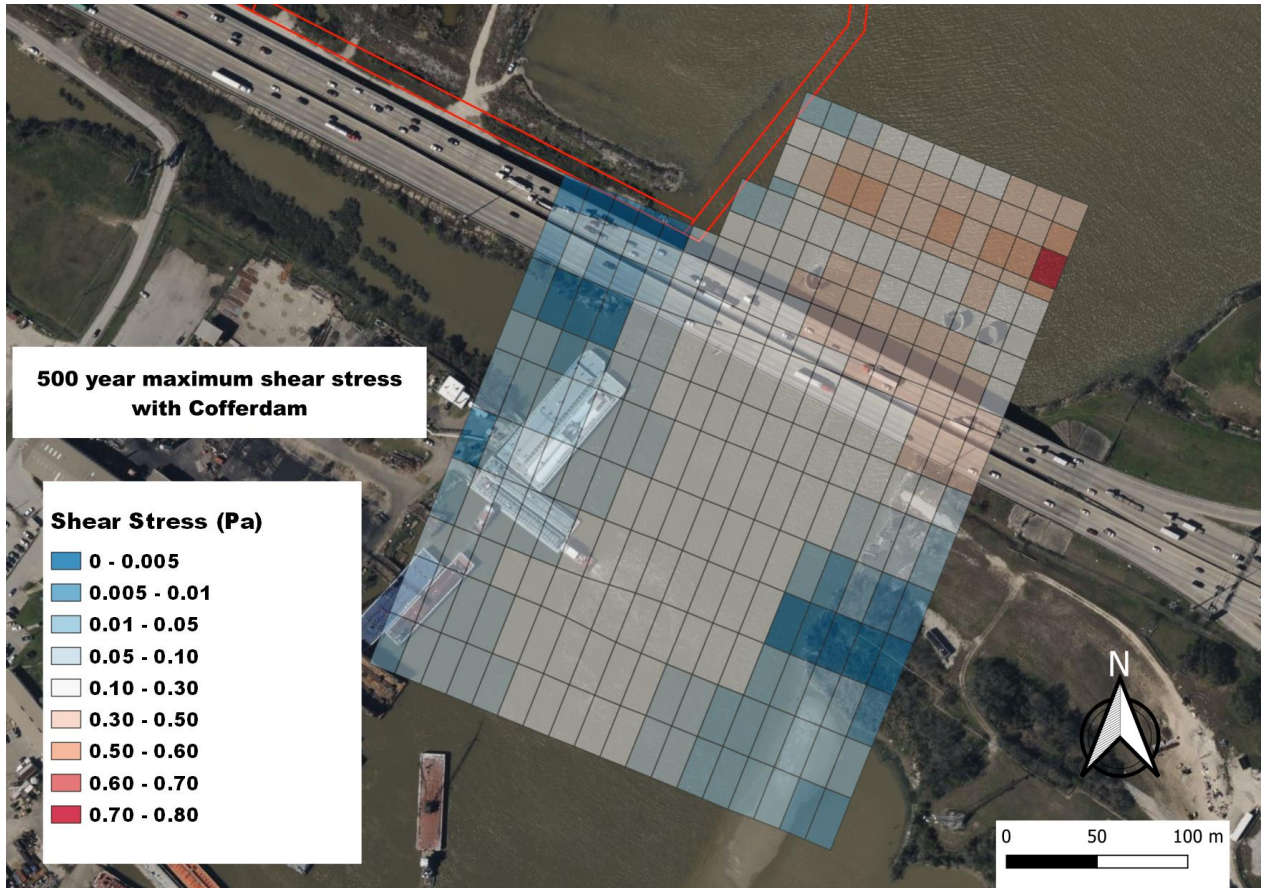
Appendix B - Velocity and Shear Stress Analysis



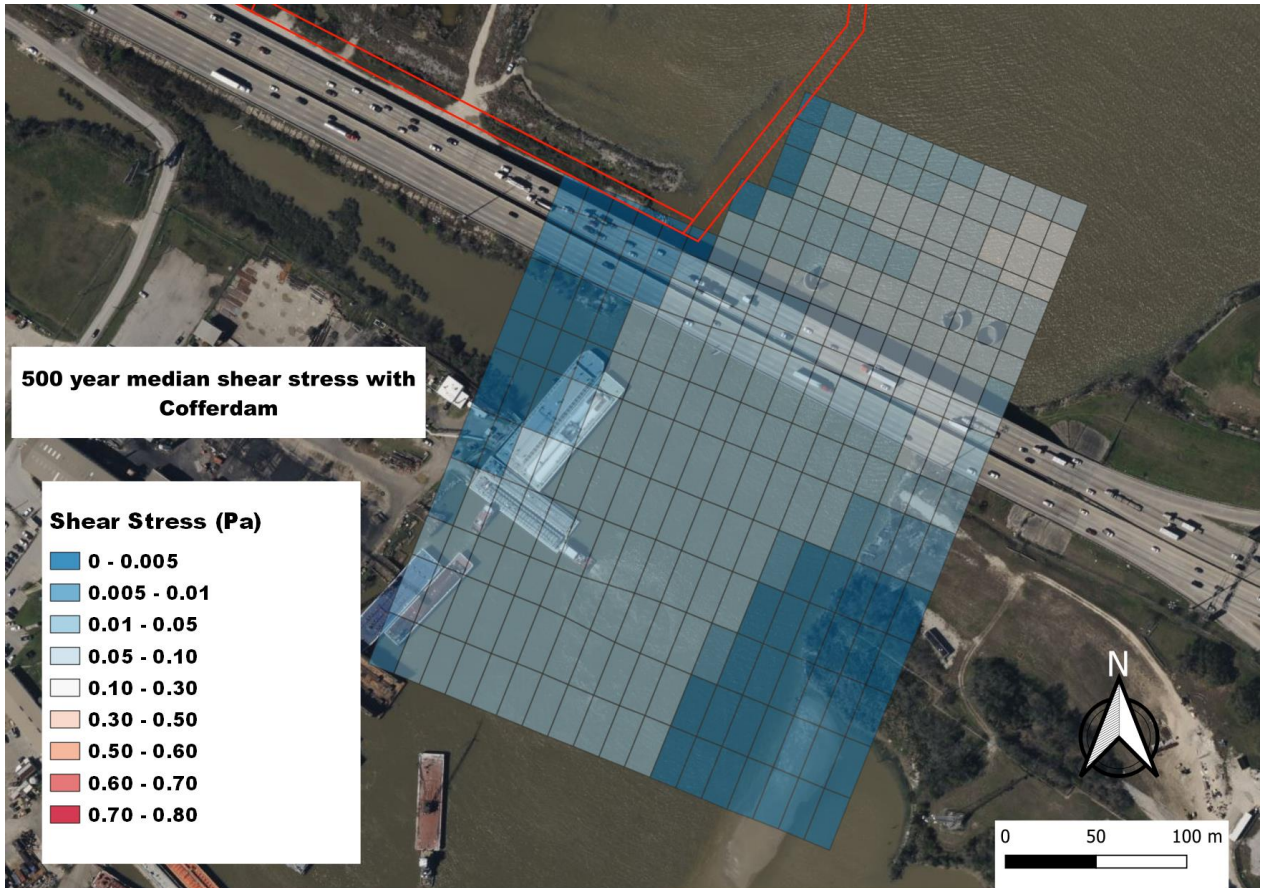
Appendix B - Velocity and Shear Stress Analysis



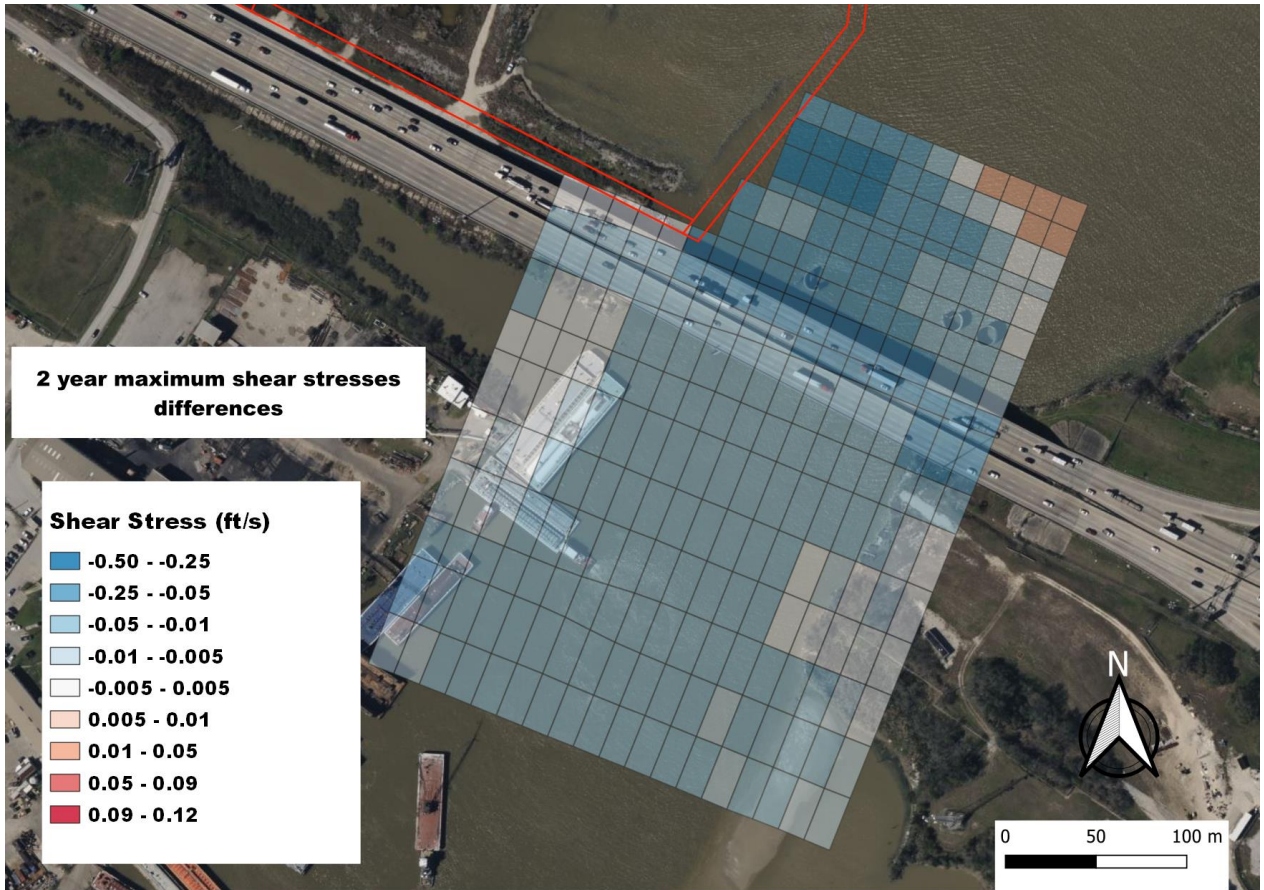
Appendix B - Velocity and Shear Stress Analysis



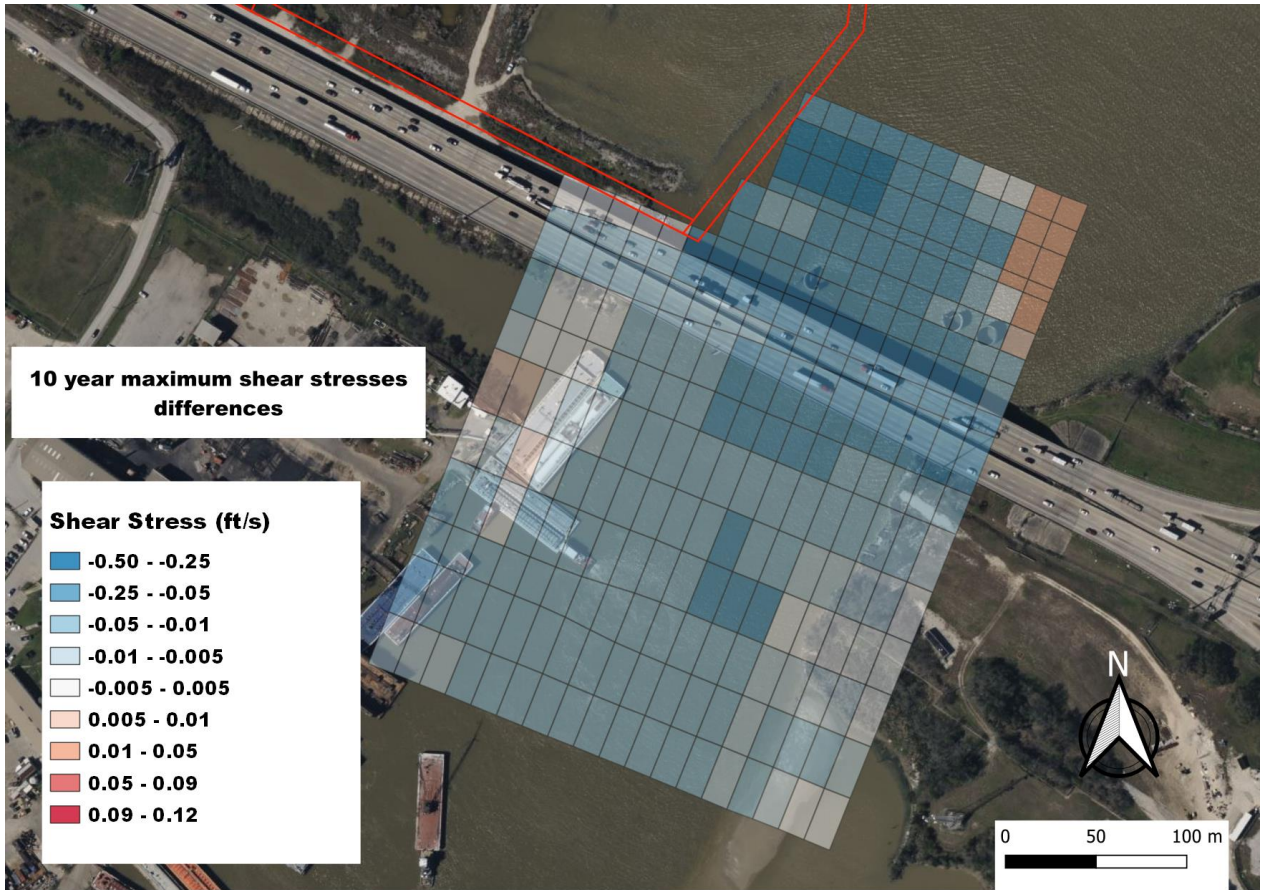
Appendix B - Velocity and Shear Stress Analysis



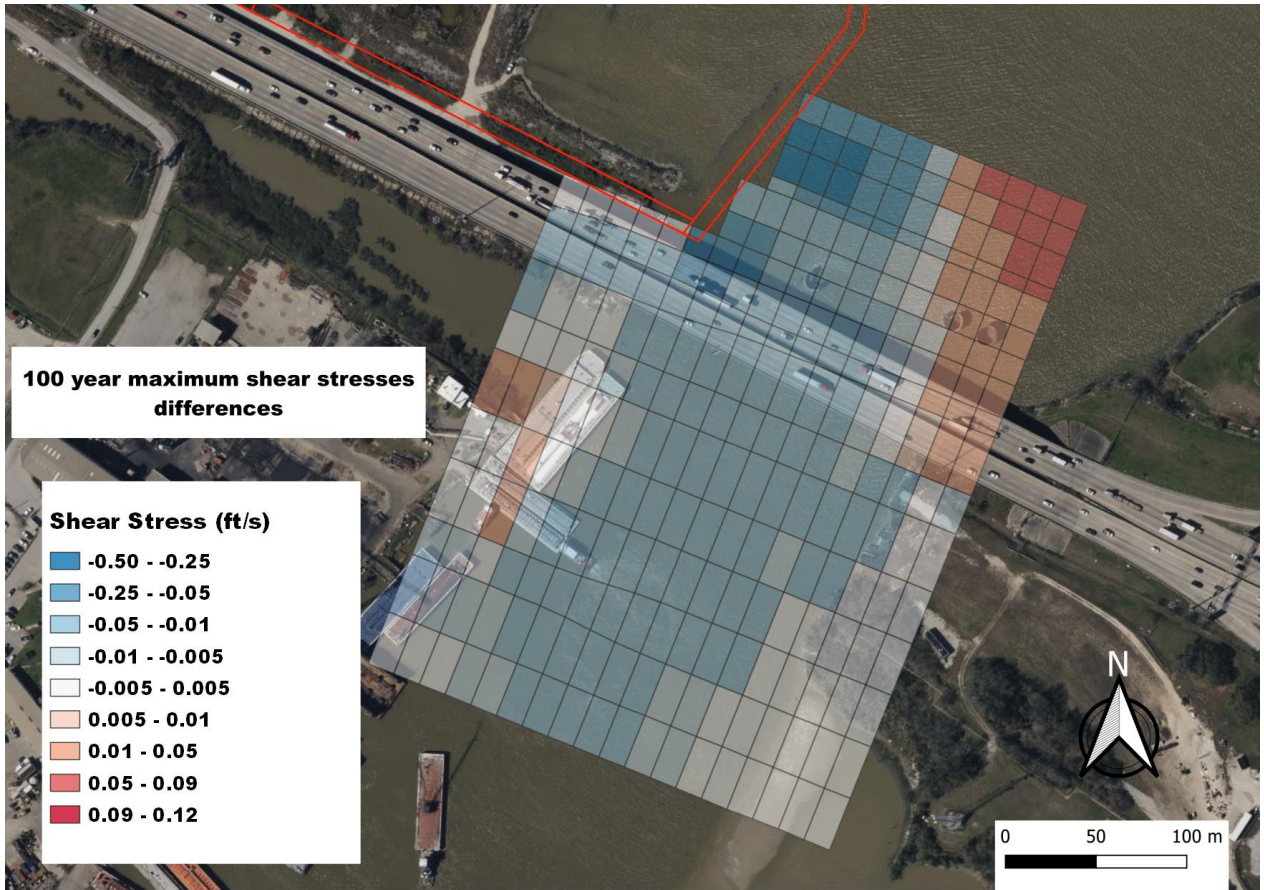
Shear Stress Difference Figures



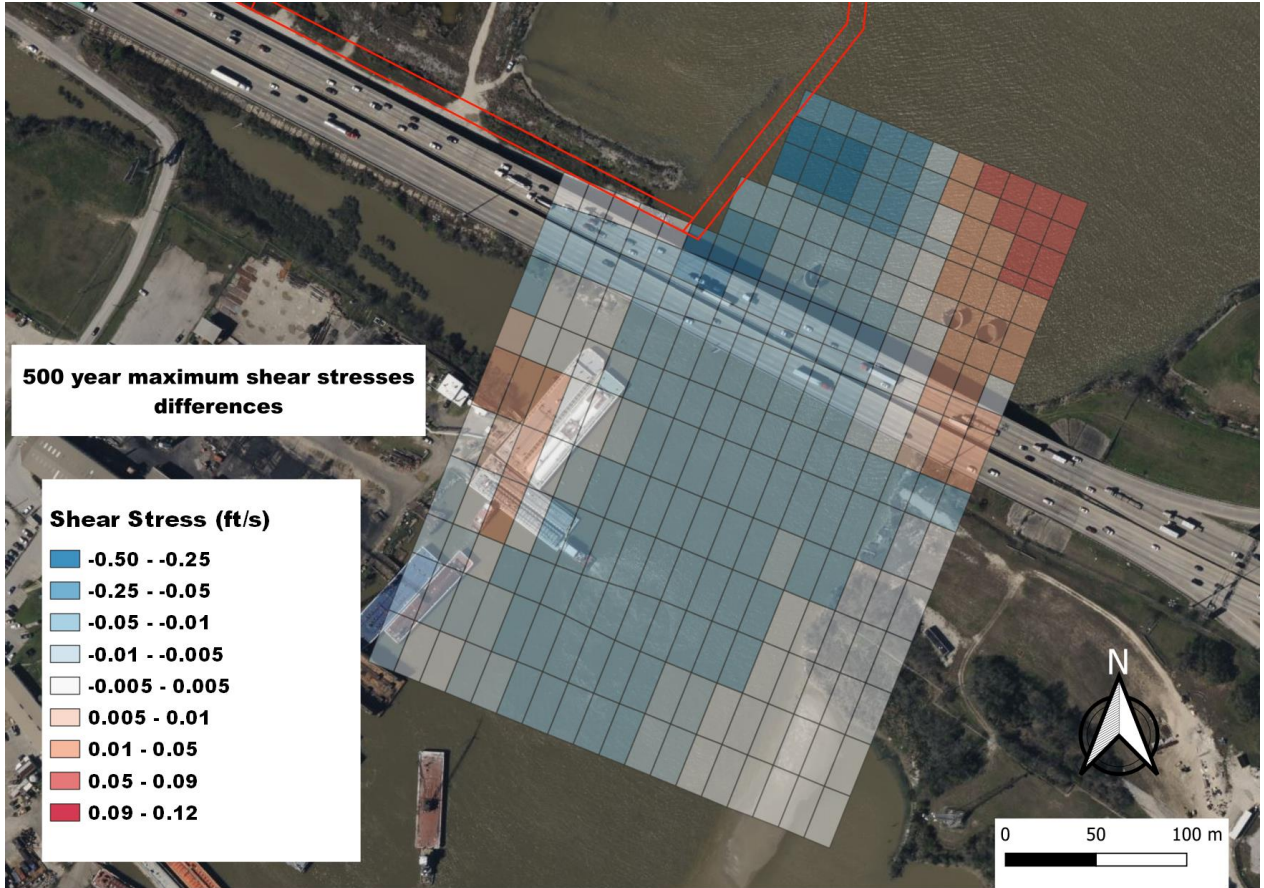
Appendix B - Velocity and Shear Stress Analysis



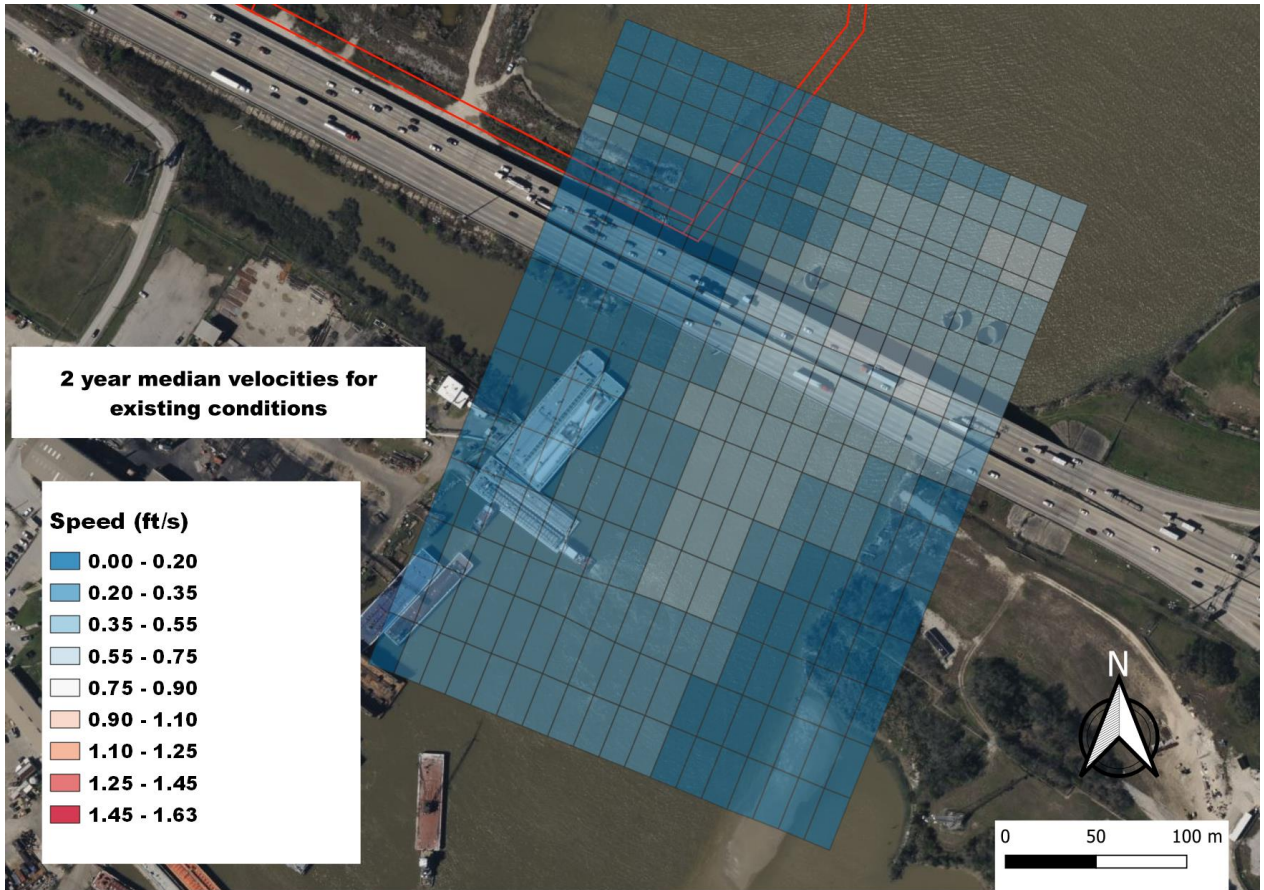
Appendix B - Velocity and Shear Stress Analysis



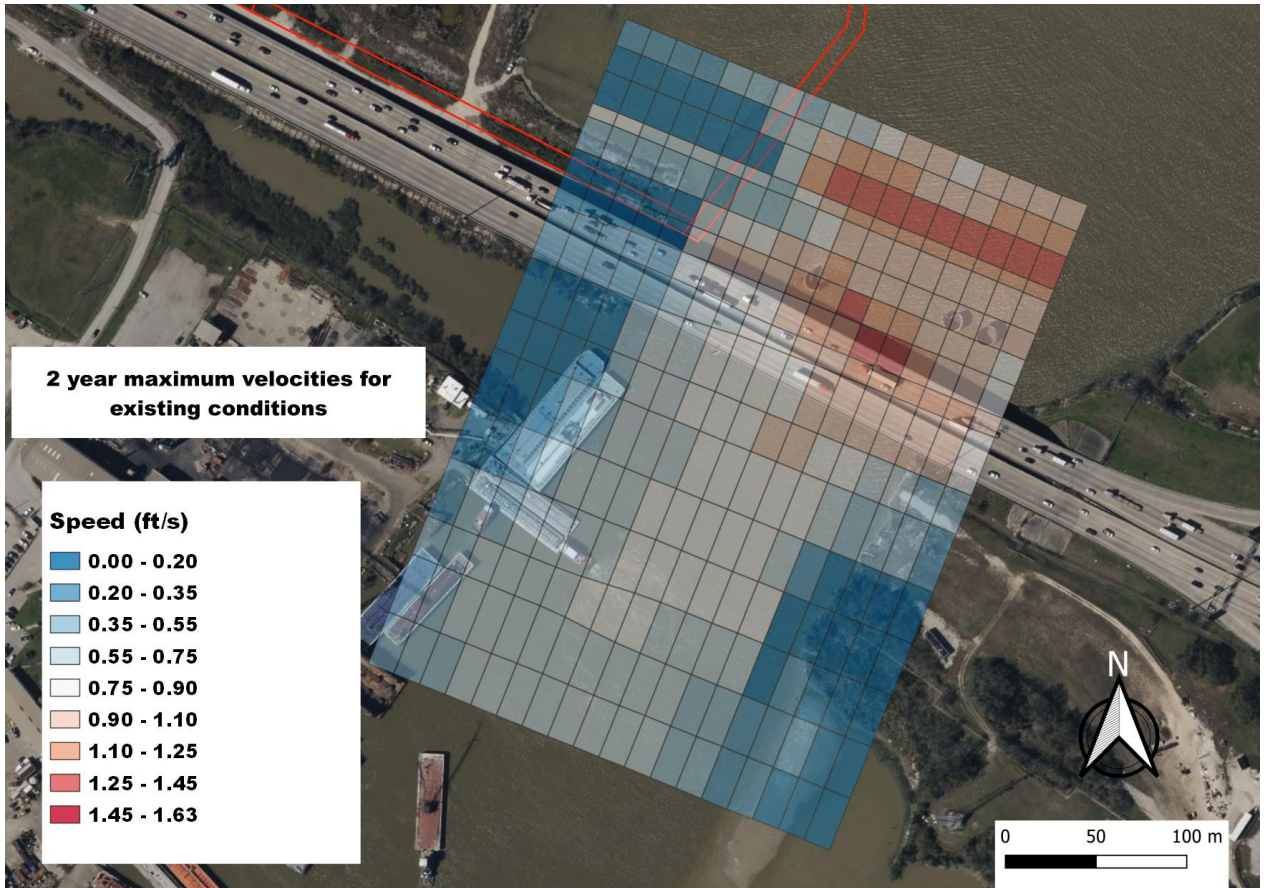
Appendix B - Velocity and Shear Stress Analysis



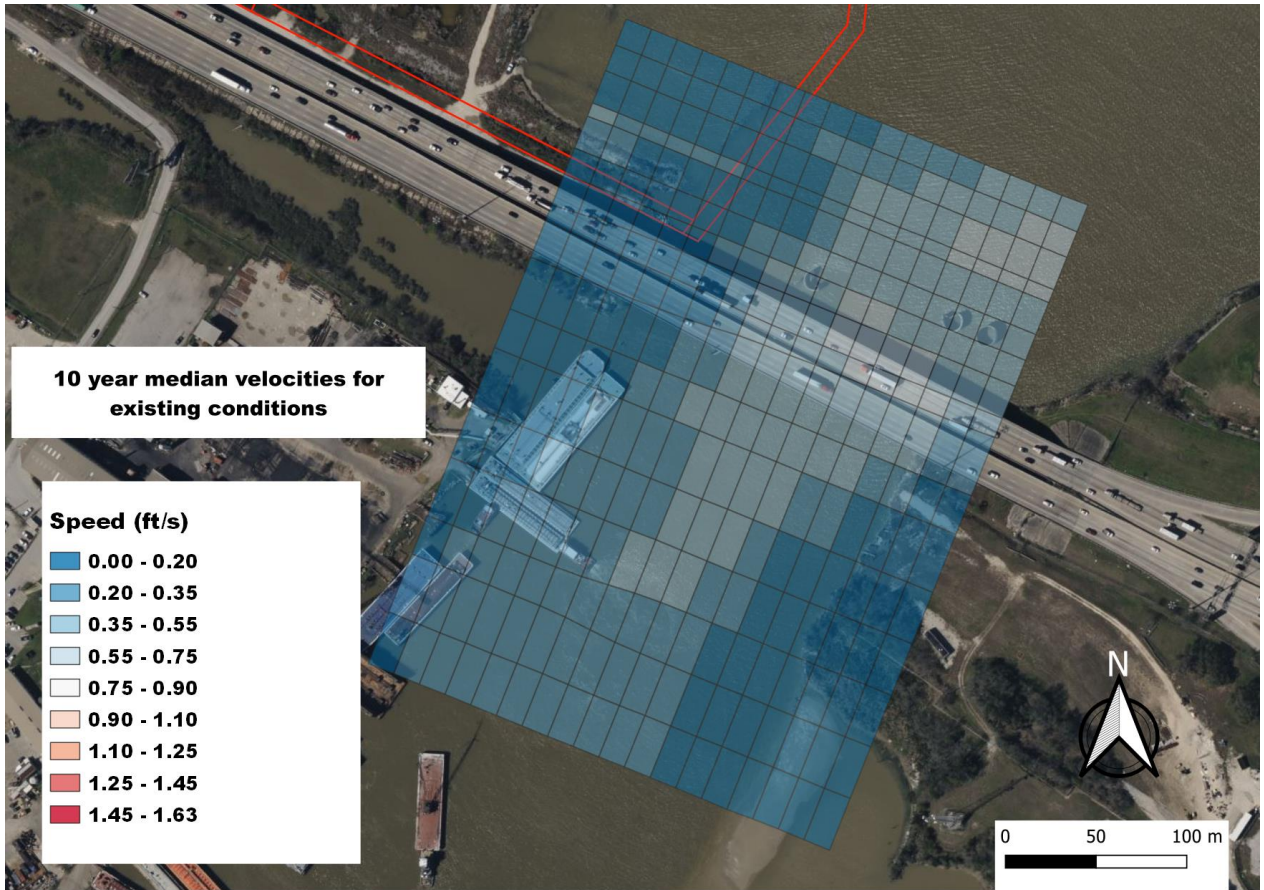
Velocity Figures Existing Conditions



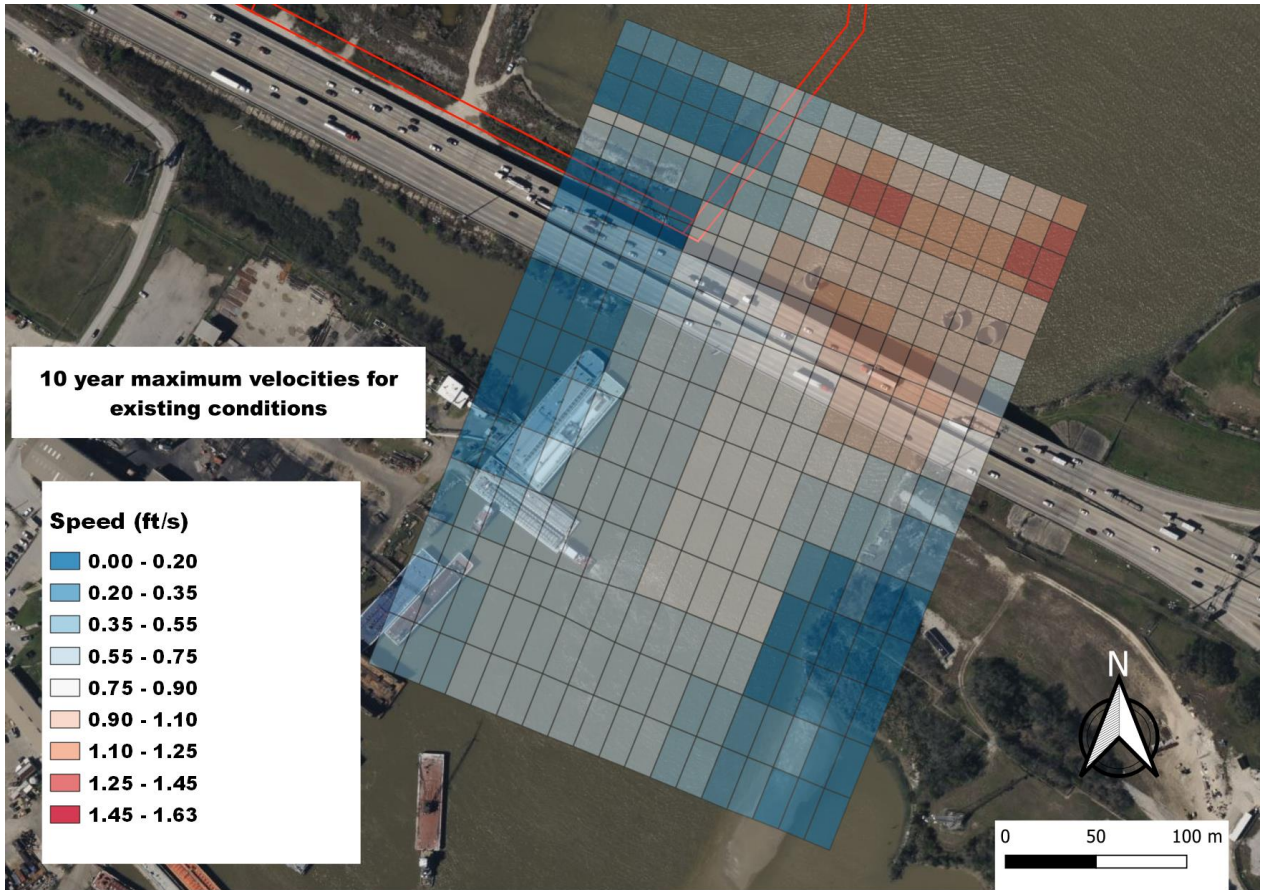
Appendix B - Velocity and Shear Stress Analysis



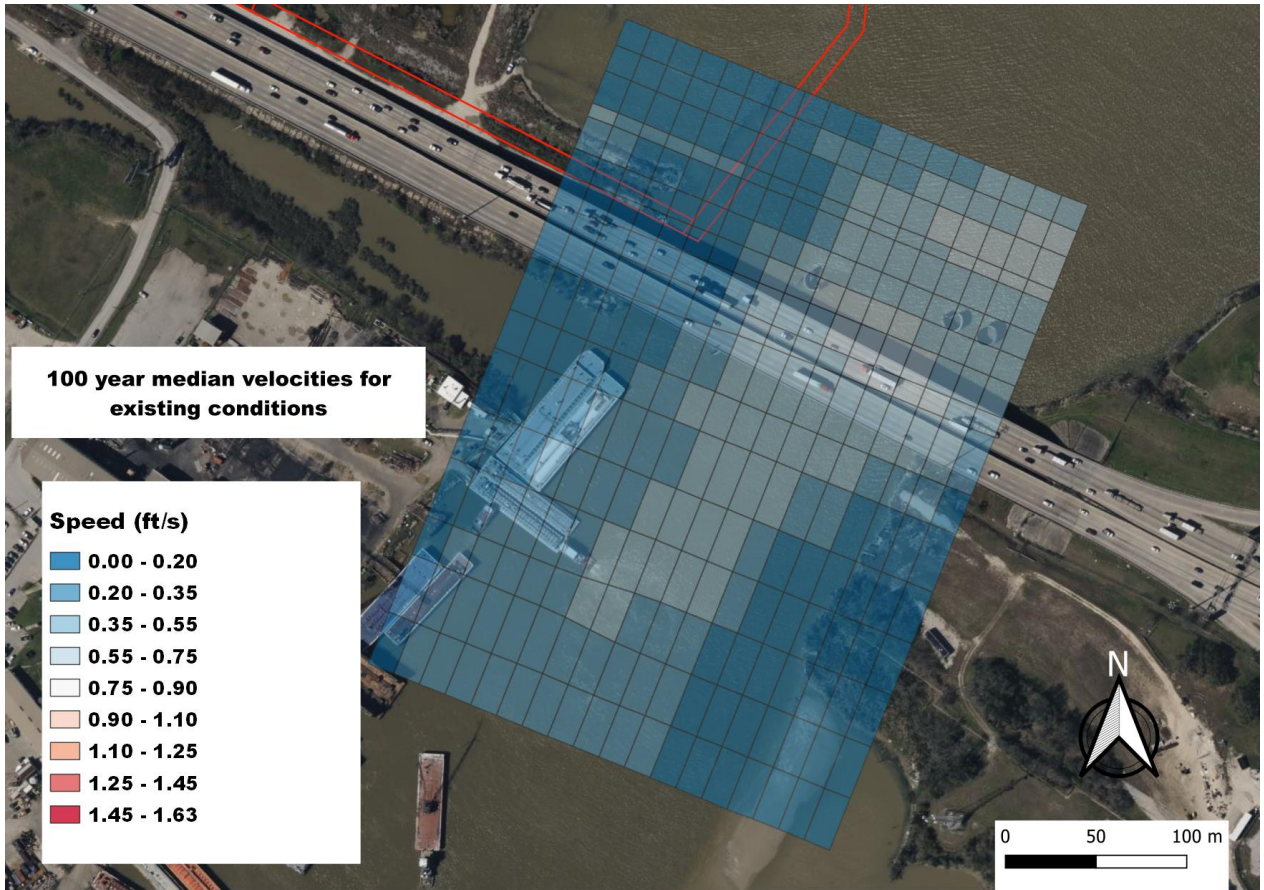
Appendix B - Velocity and Shear Stress Analysis



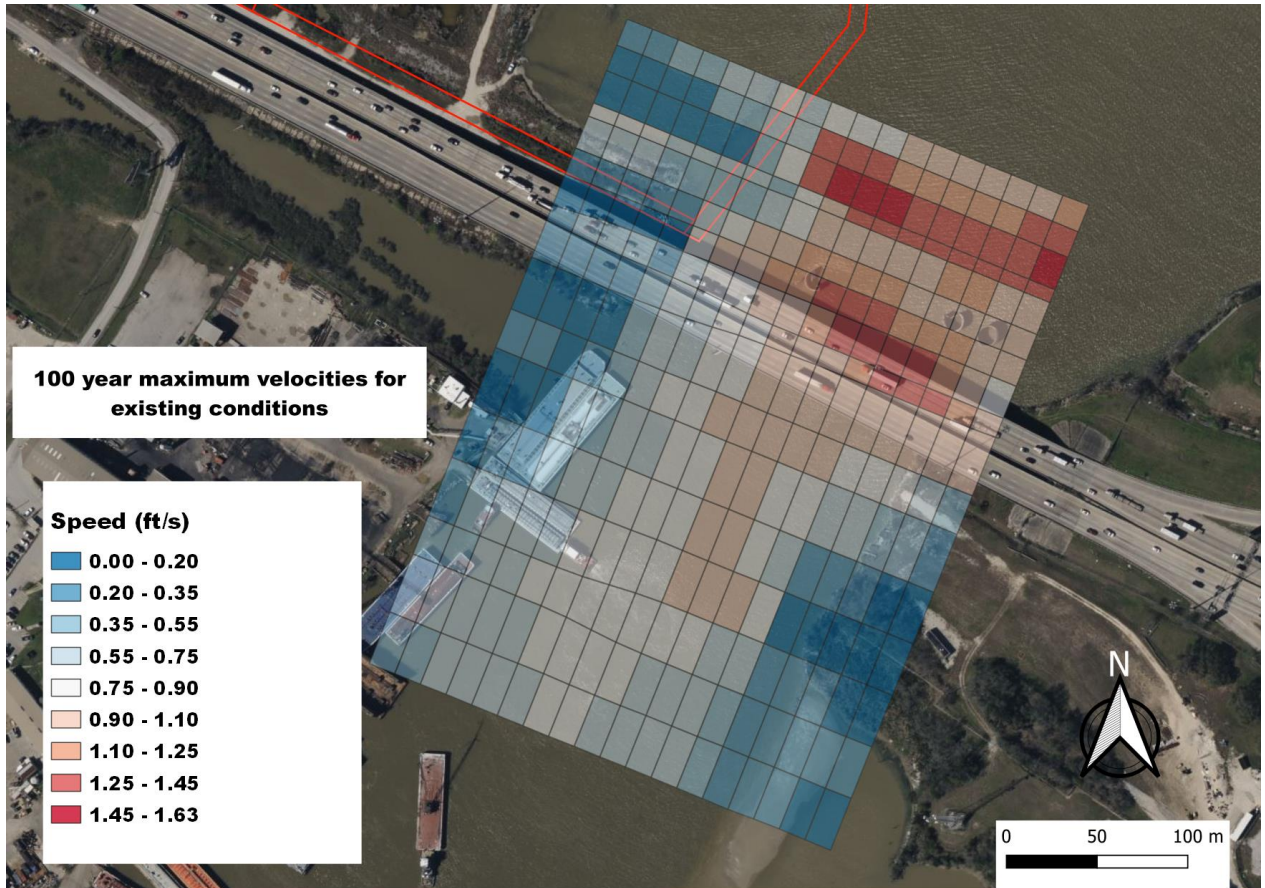
Appendix B - Velocity and Shear Stress Analysis



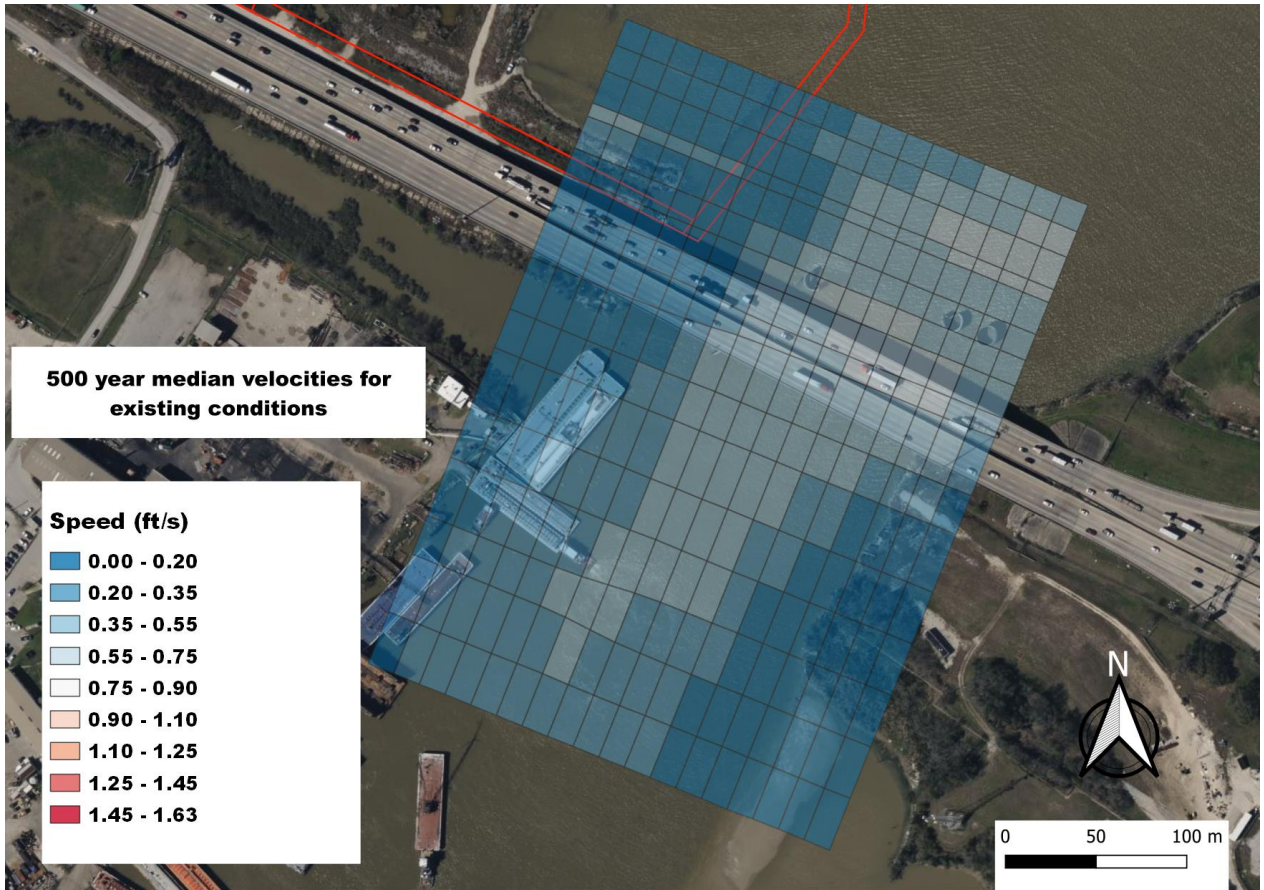
Appendix B - Velocity and Shear Stress Analysis



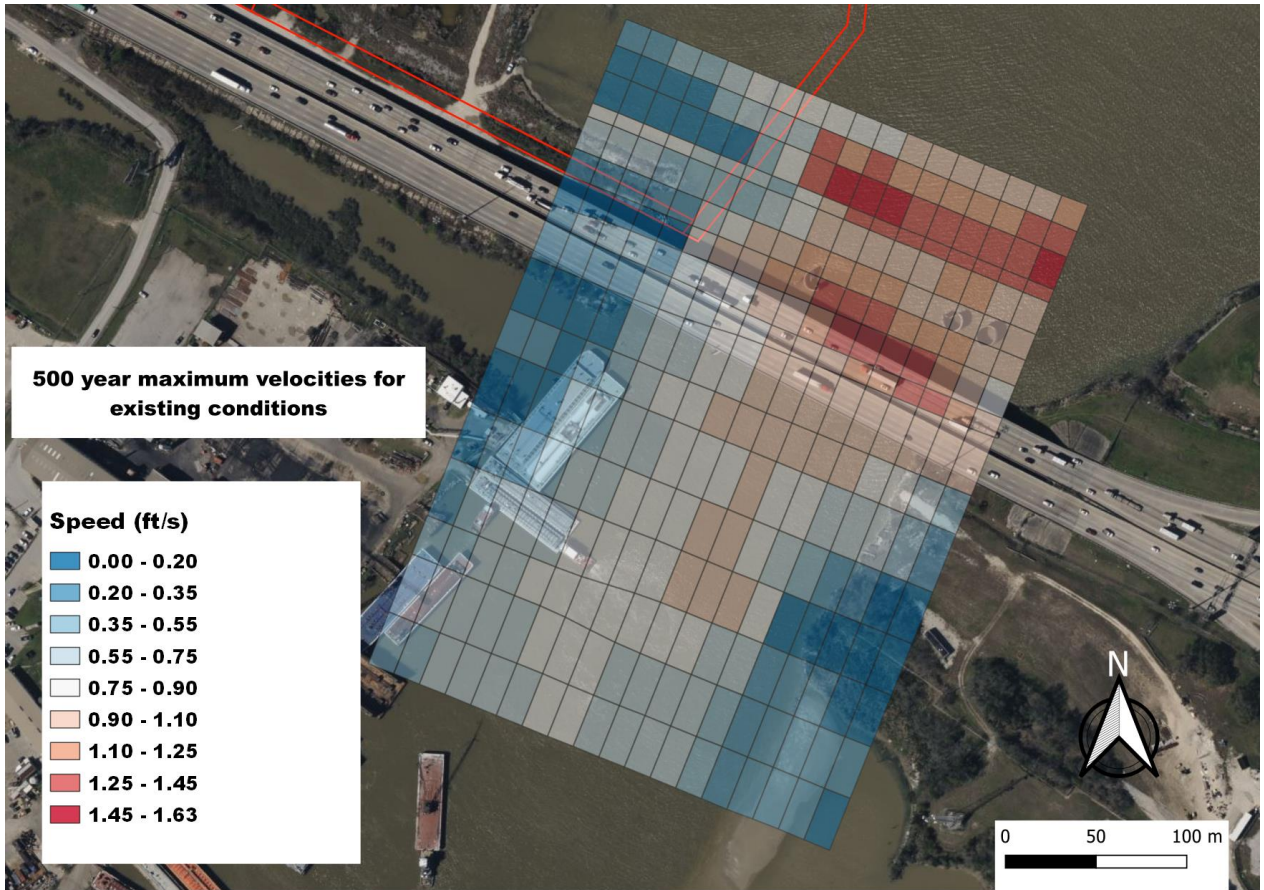
Appendix B - Velocity and Shear Stress Analysis



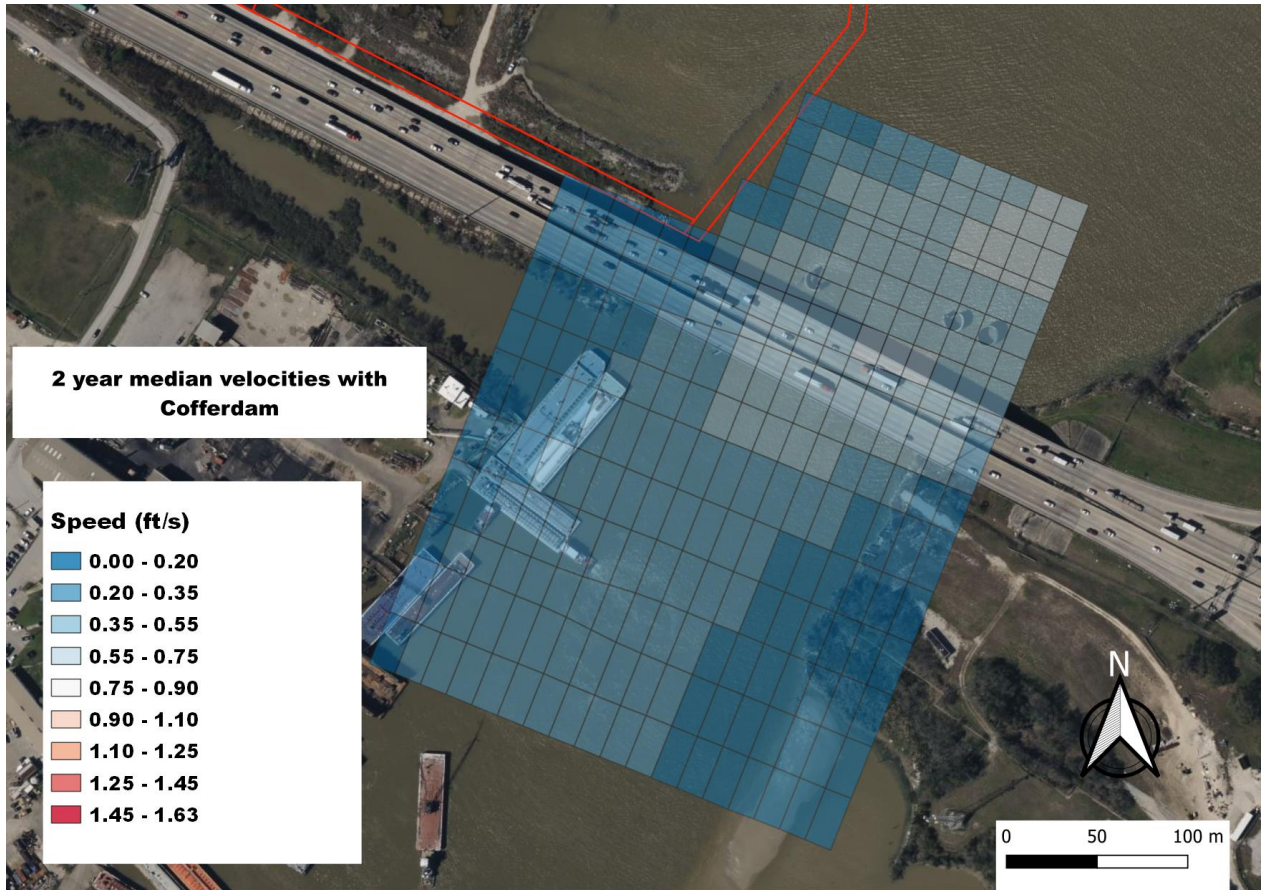
Appendix B - Velocity and Shear Stress Analysis



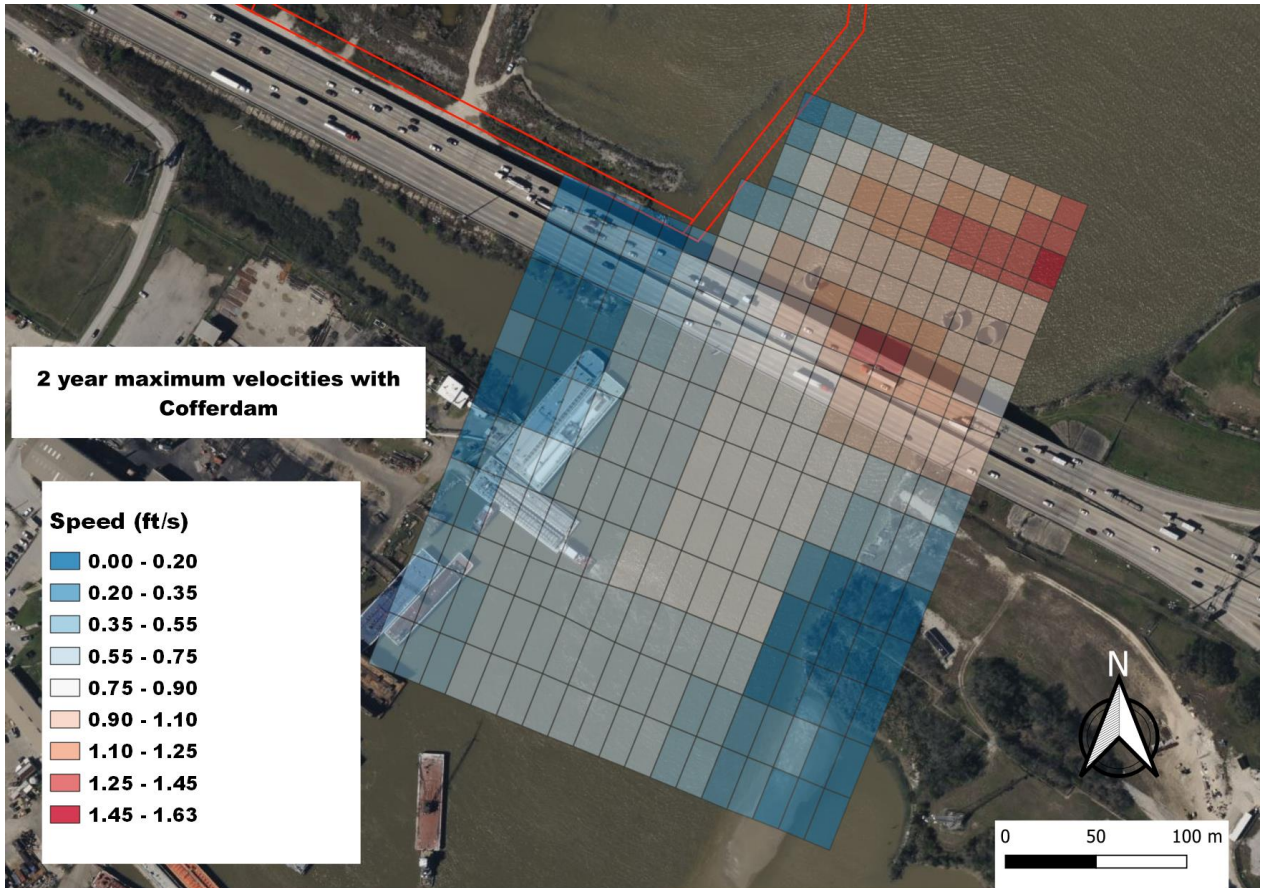
Appendix B - Velocity and Shear Stress Analysis



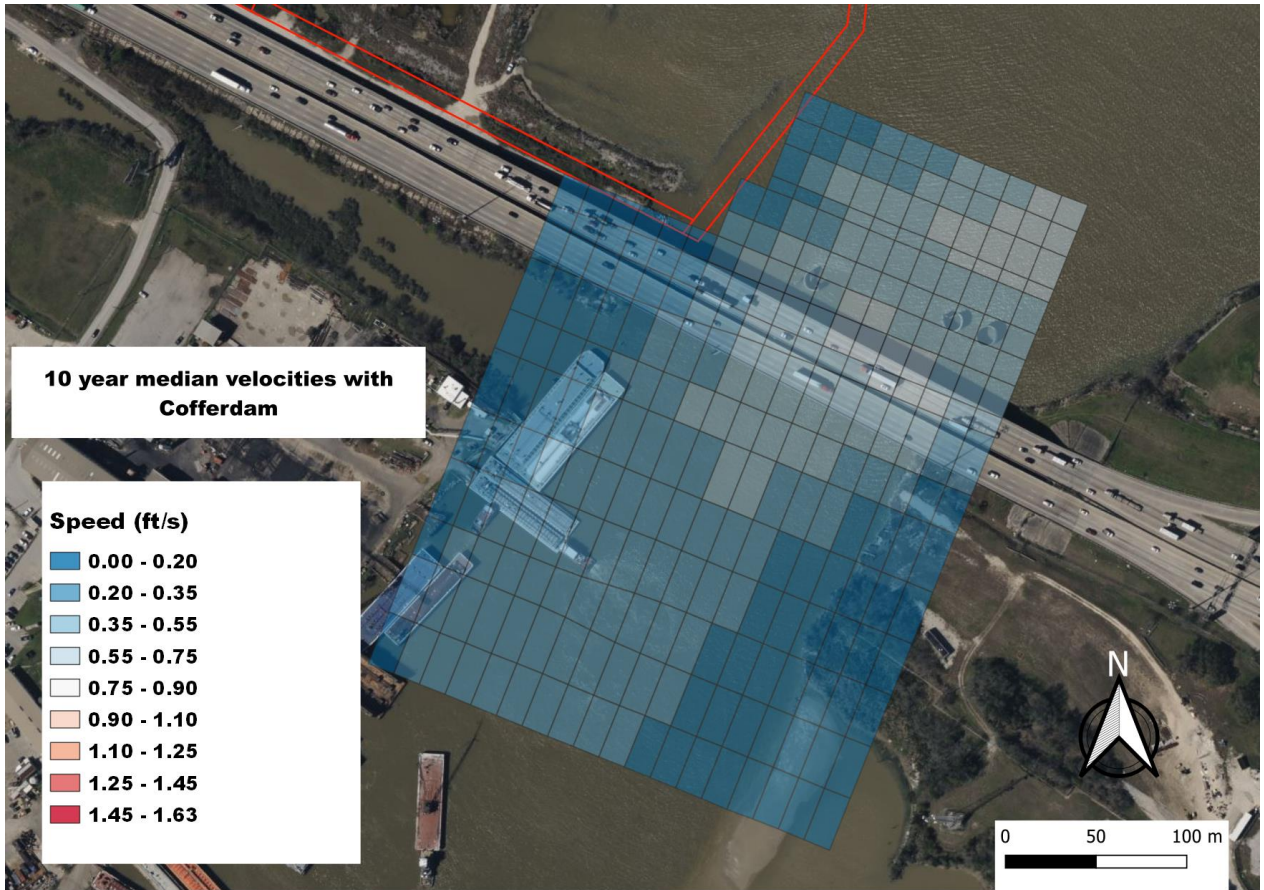
Velocity Figures with Cofferdam



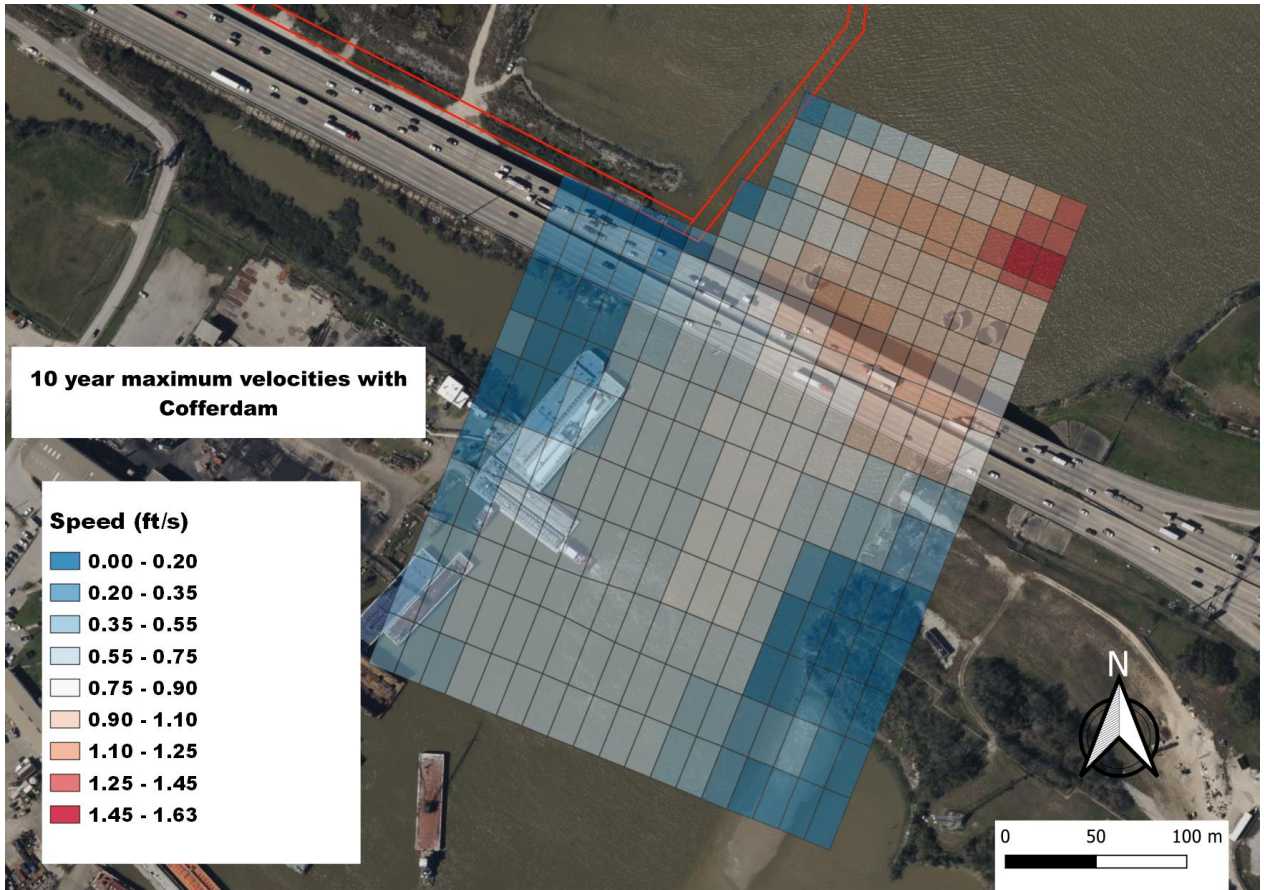
Appendix B - Velocity and Shear Stress Analysis



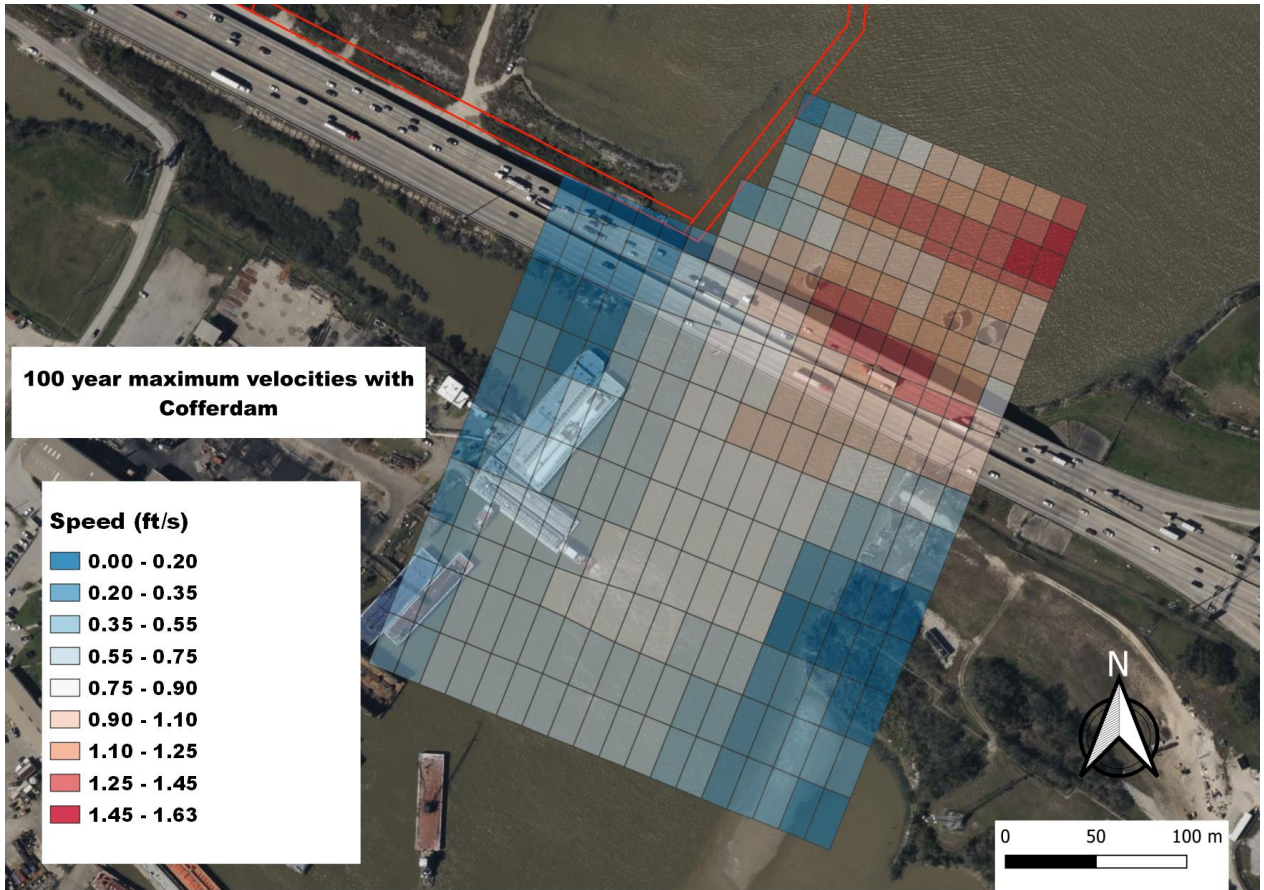
Appendix B - Velocity and Shear Stress Analysis



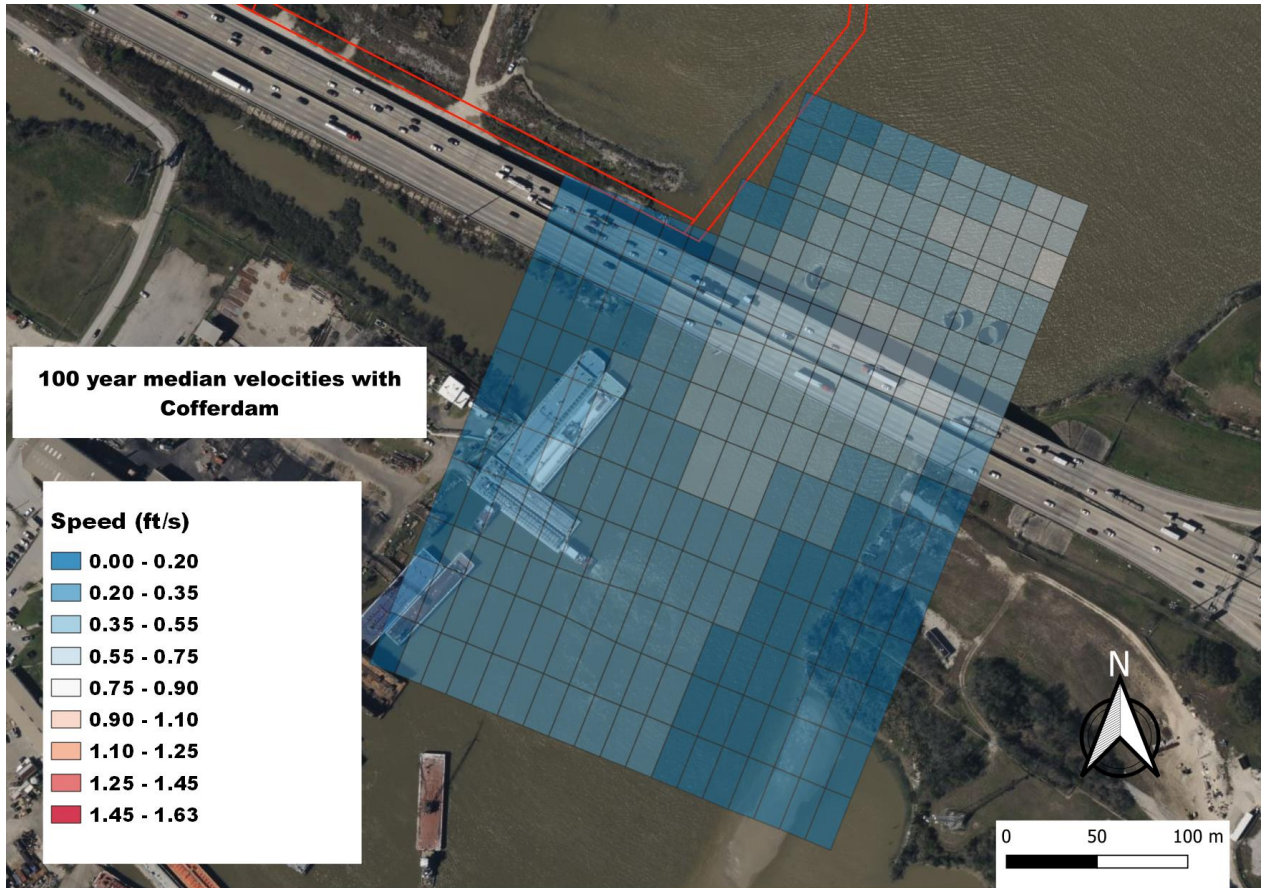
Appendix B - Velocity and Shear Stress Analysis



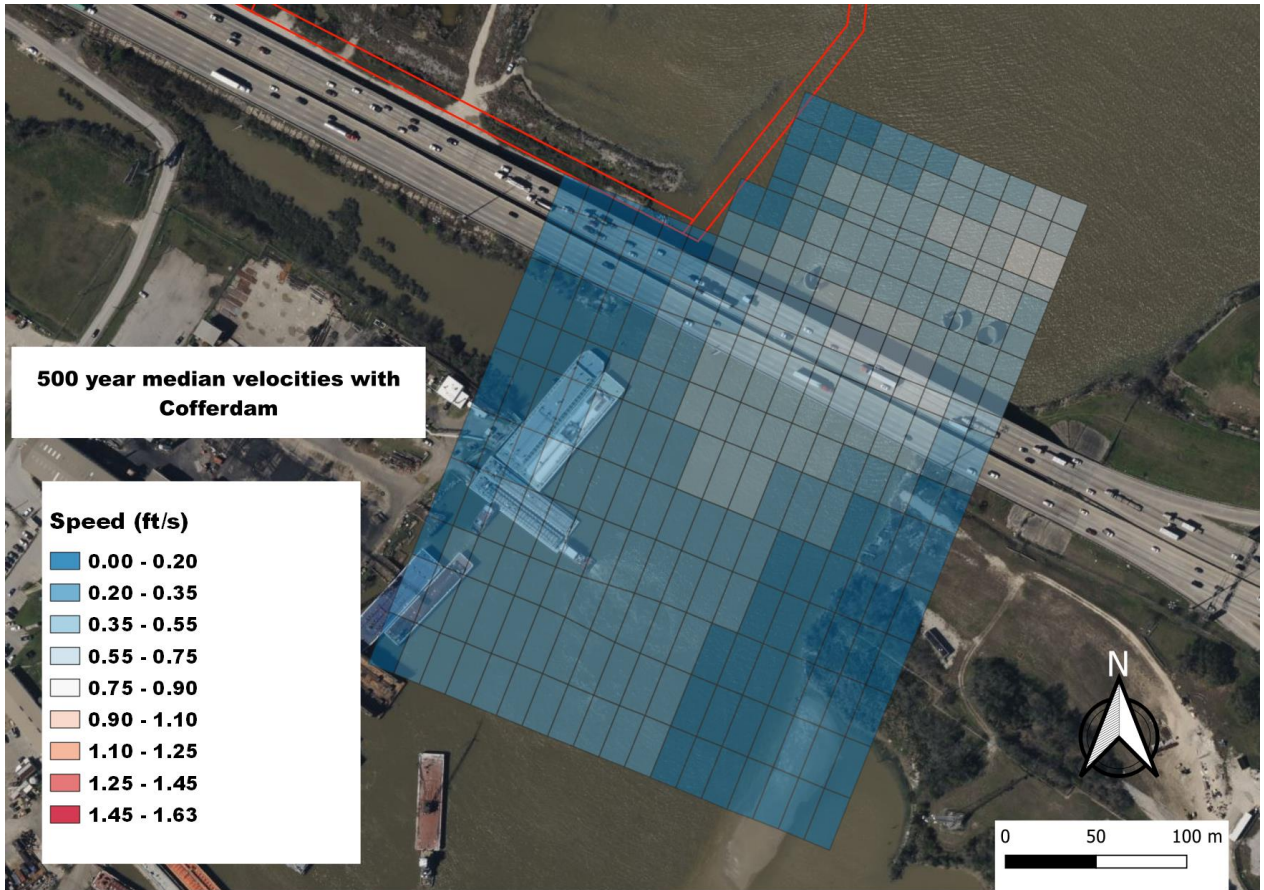
Appendix B - Velocity and Shear Stress Analysis



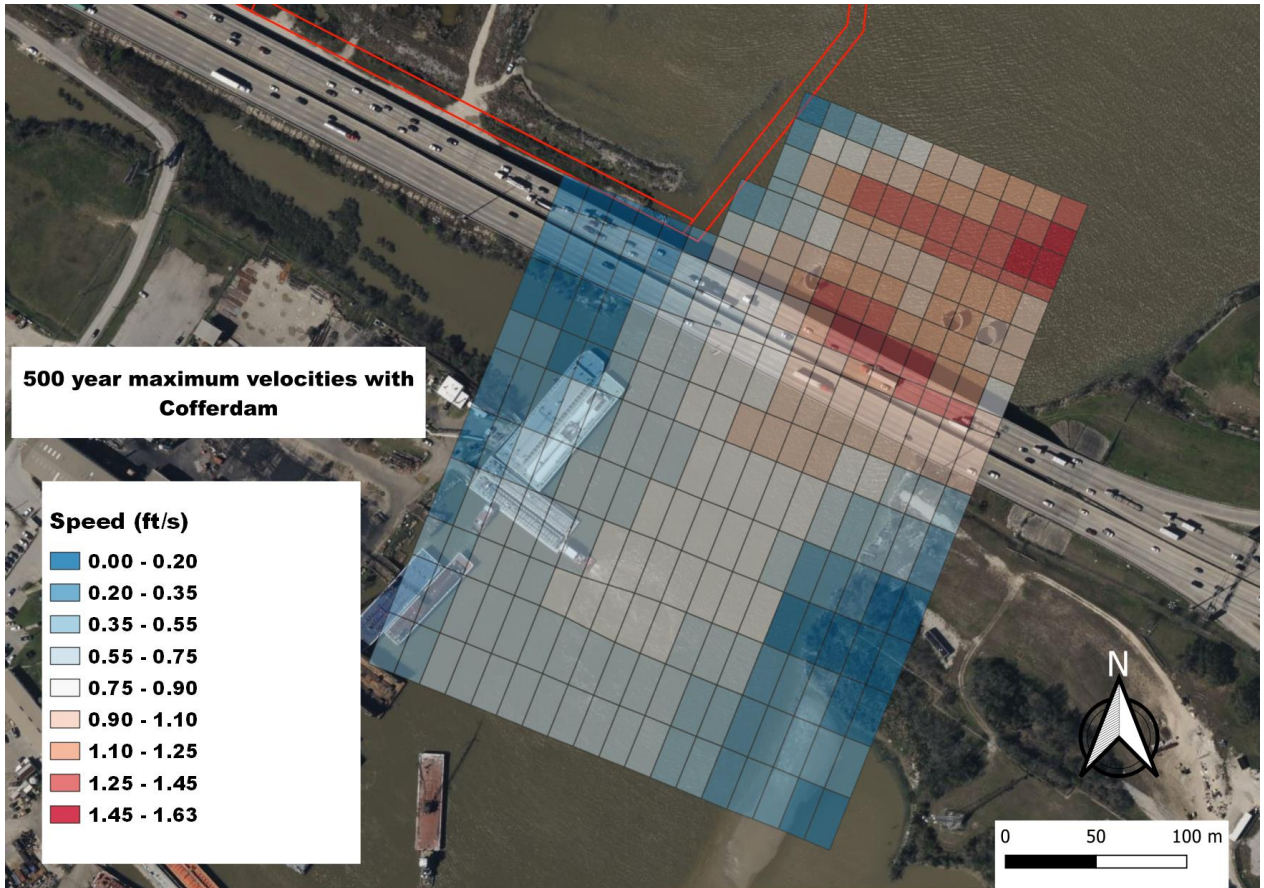
Appendix B - Velocity and Shear Stress Analysis



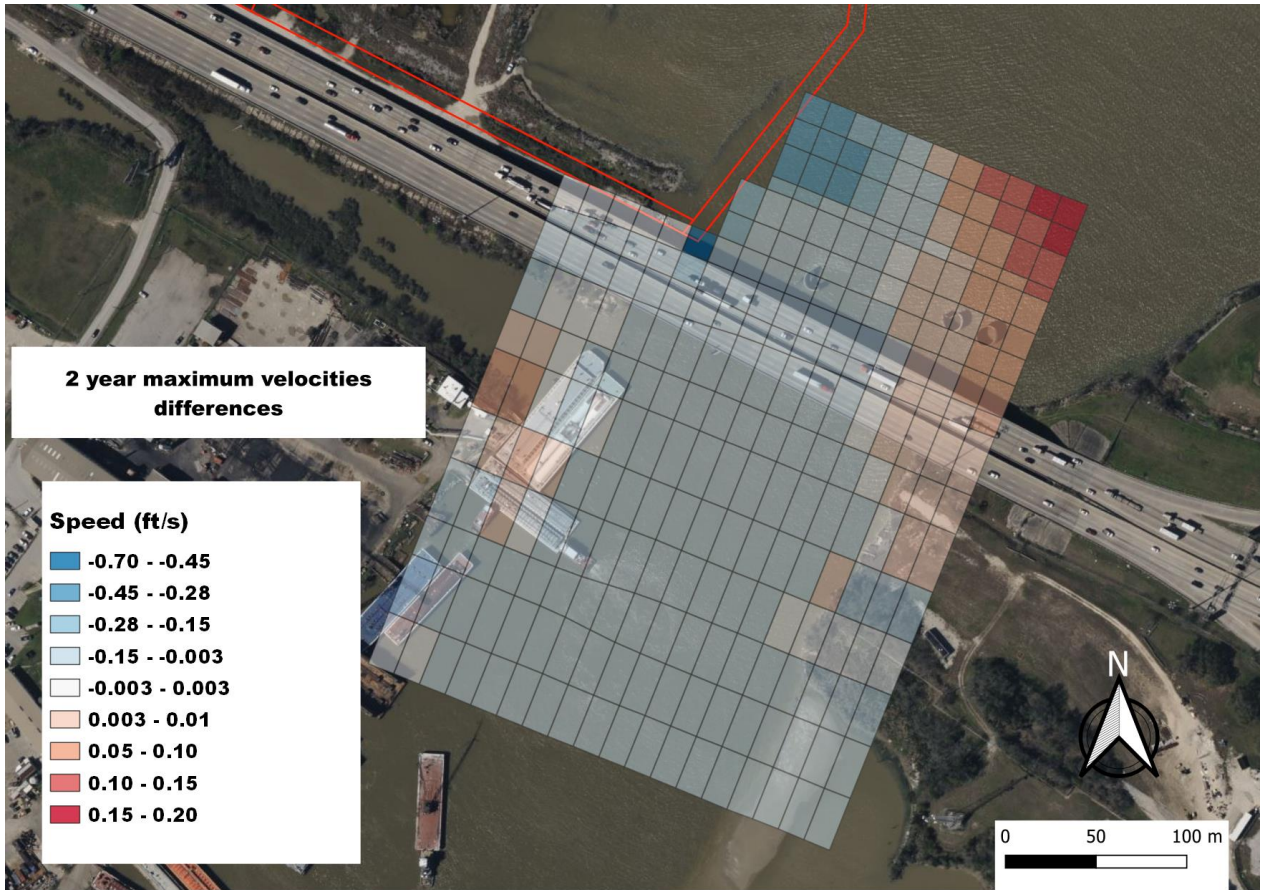
Appendix B - Velocity and Shear Stress Analysis



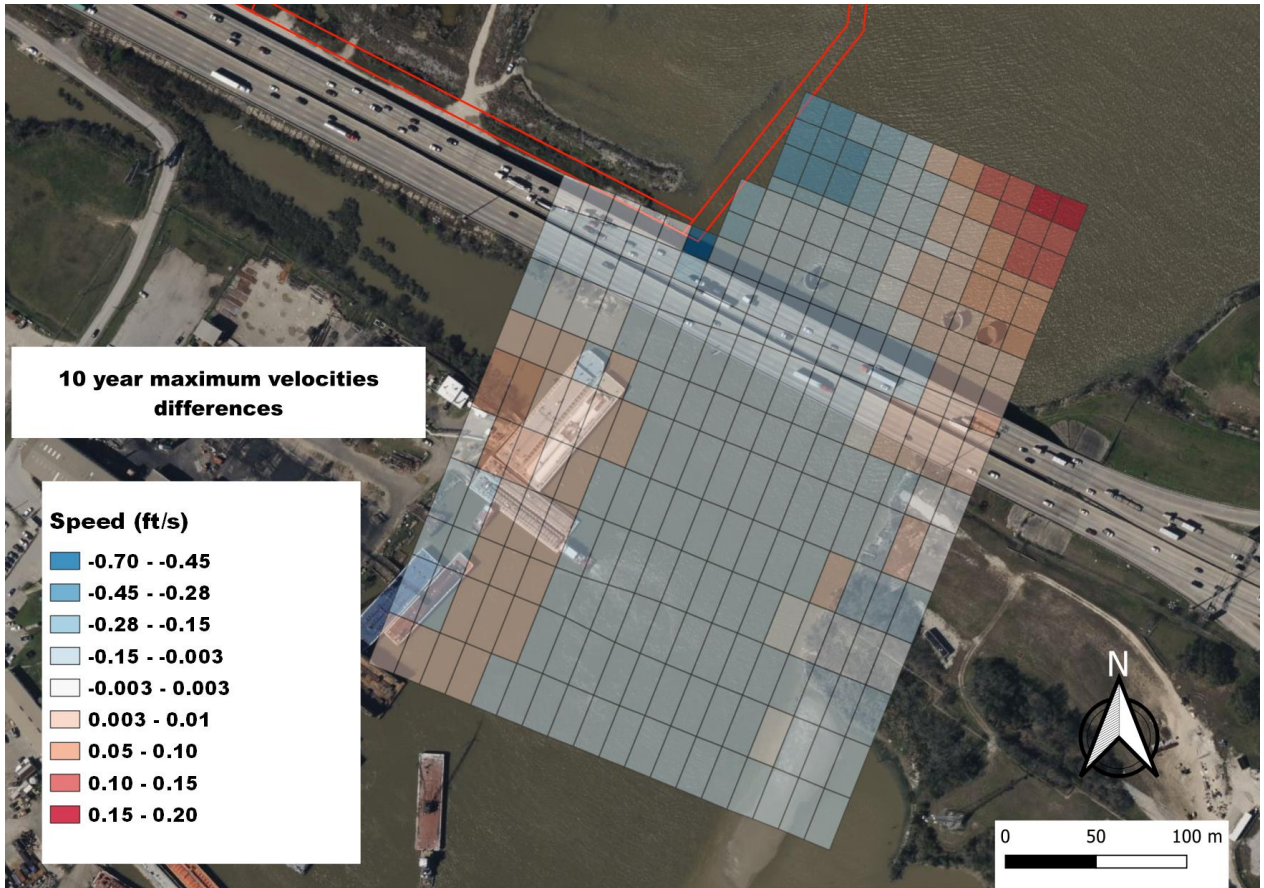
Appendix B - Velocity and Shear Stress Analysis



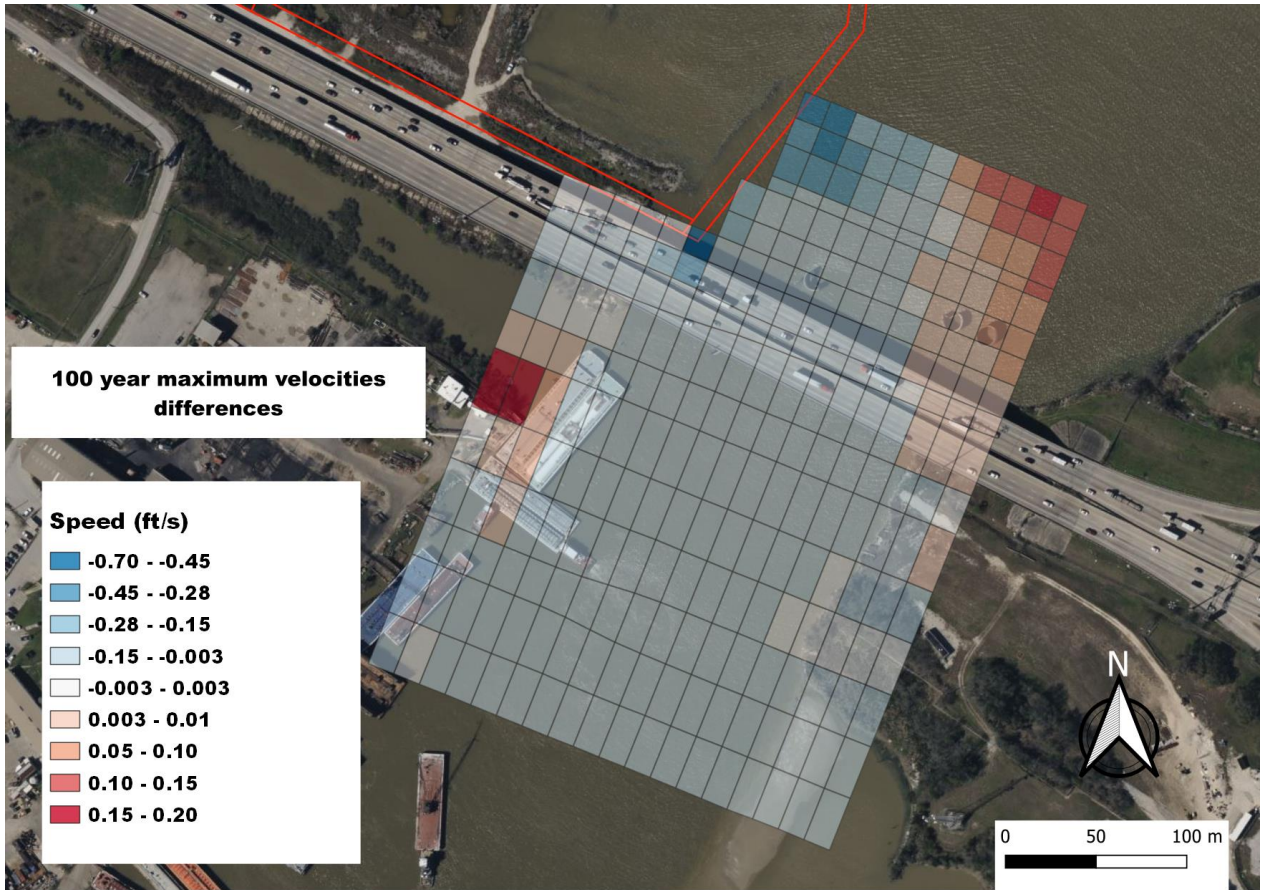
Velocity Difference Figures



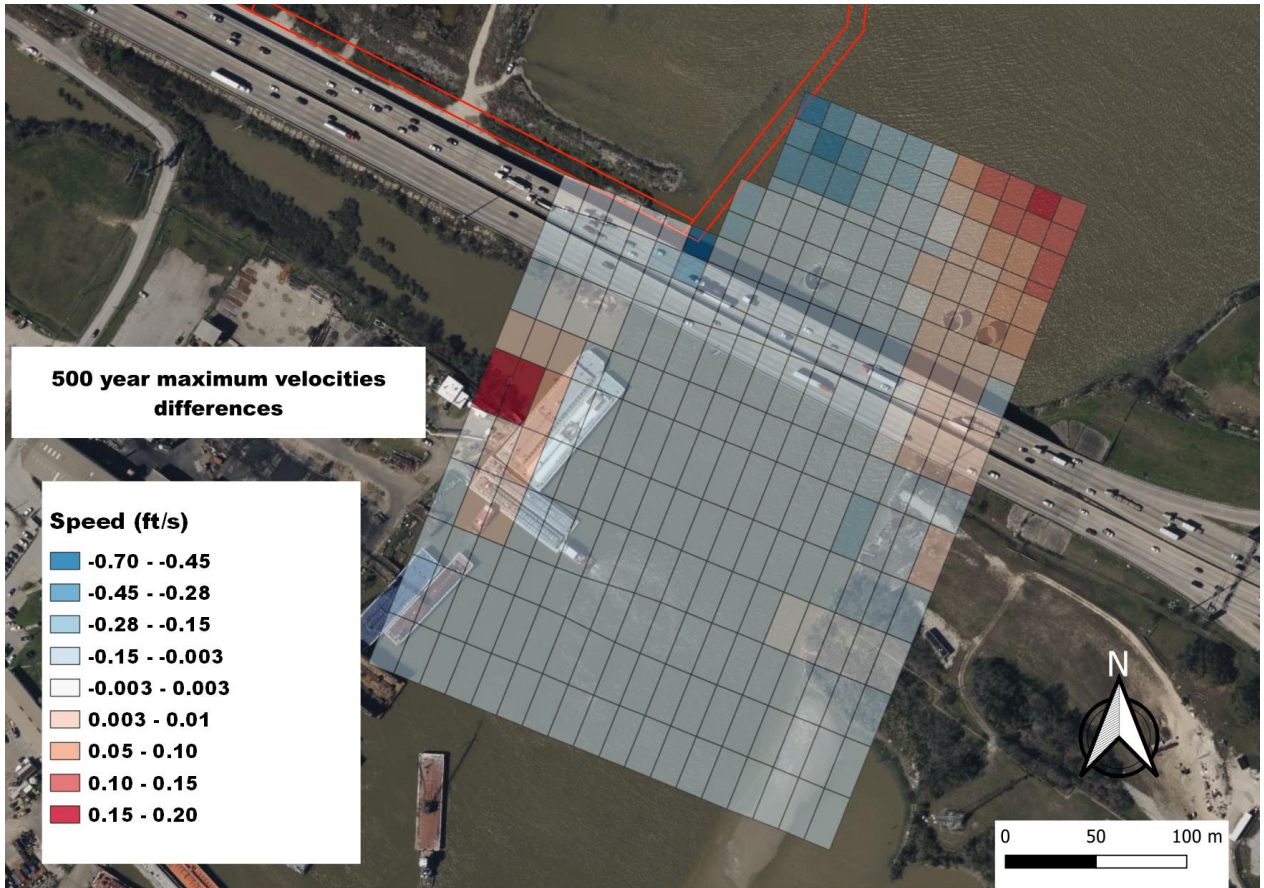
Appendix B - Velocity and Shear Stress Analysis



Appendix B - Velocity and Shear Stress Analysis



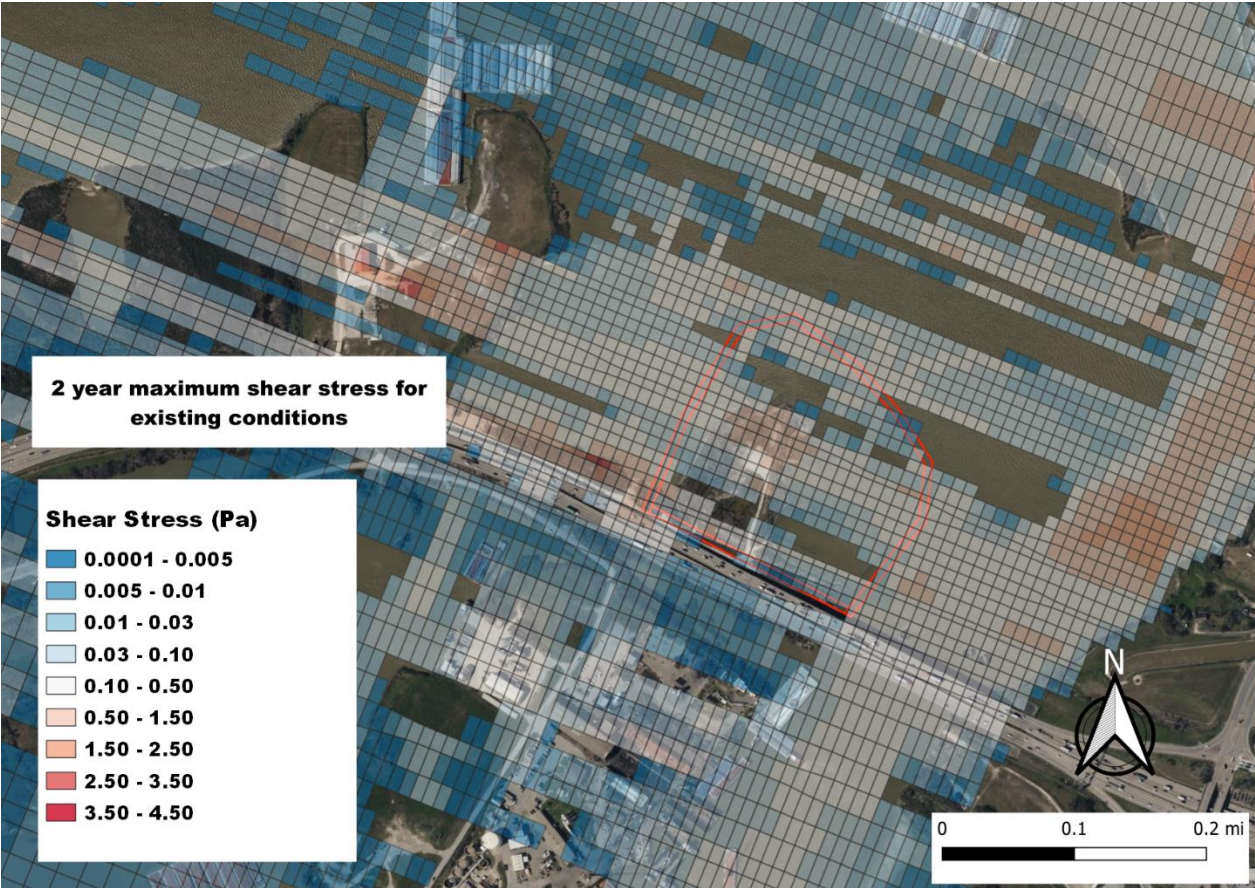
Appendix B - Velocity and Shear Stress Analysis



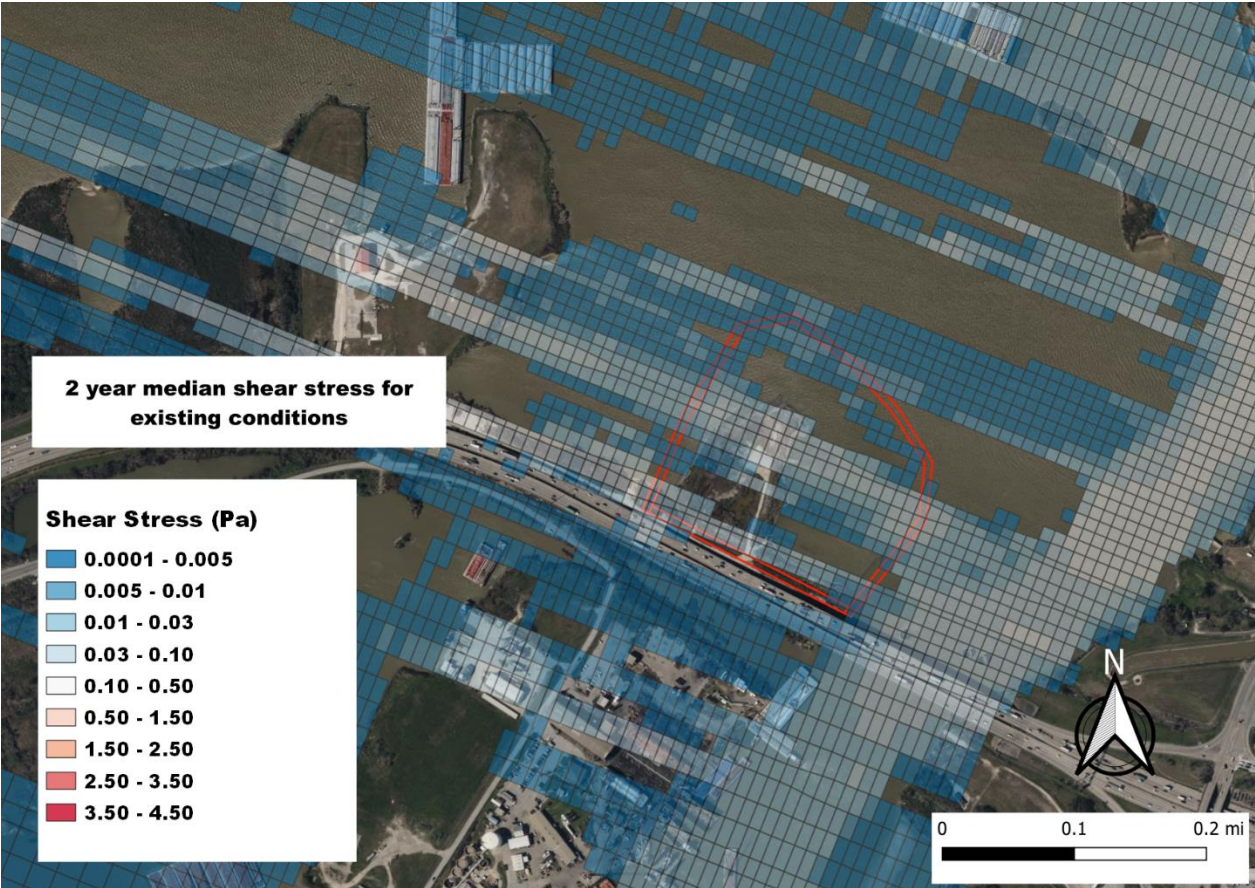
Appendix C

**Shear Stress and Velocity Model Results for
All Scenarios**

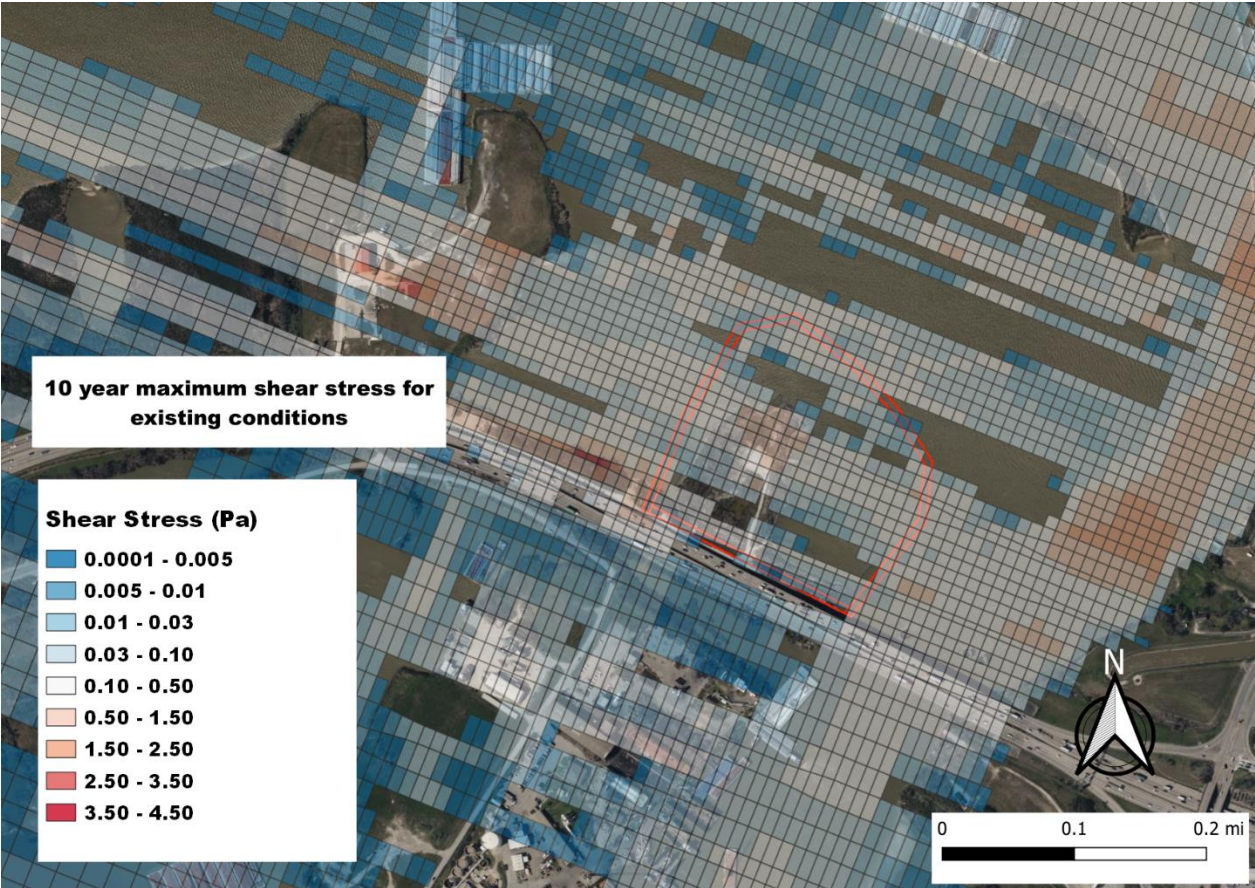
Shear Stress Figures Existing Conditions



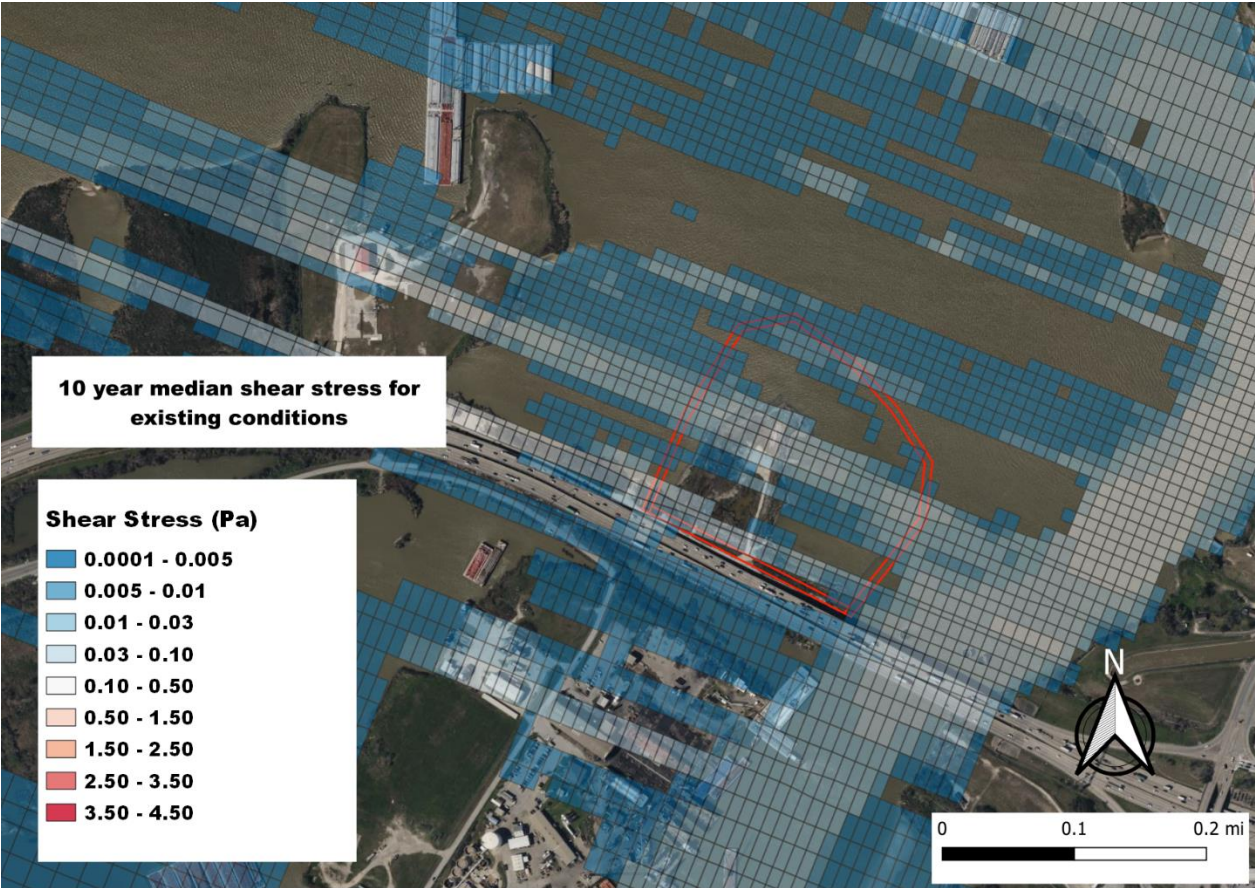
Appendix C - Shear Stress and Velocity Model Results for All Scenarios



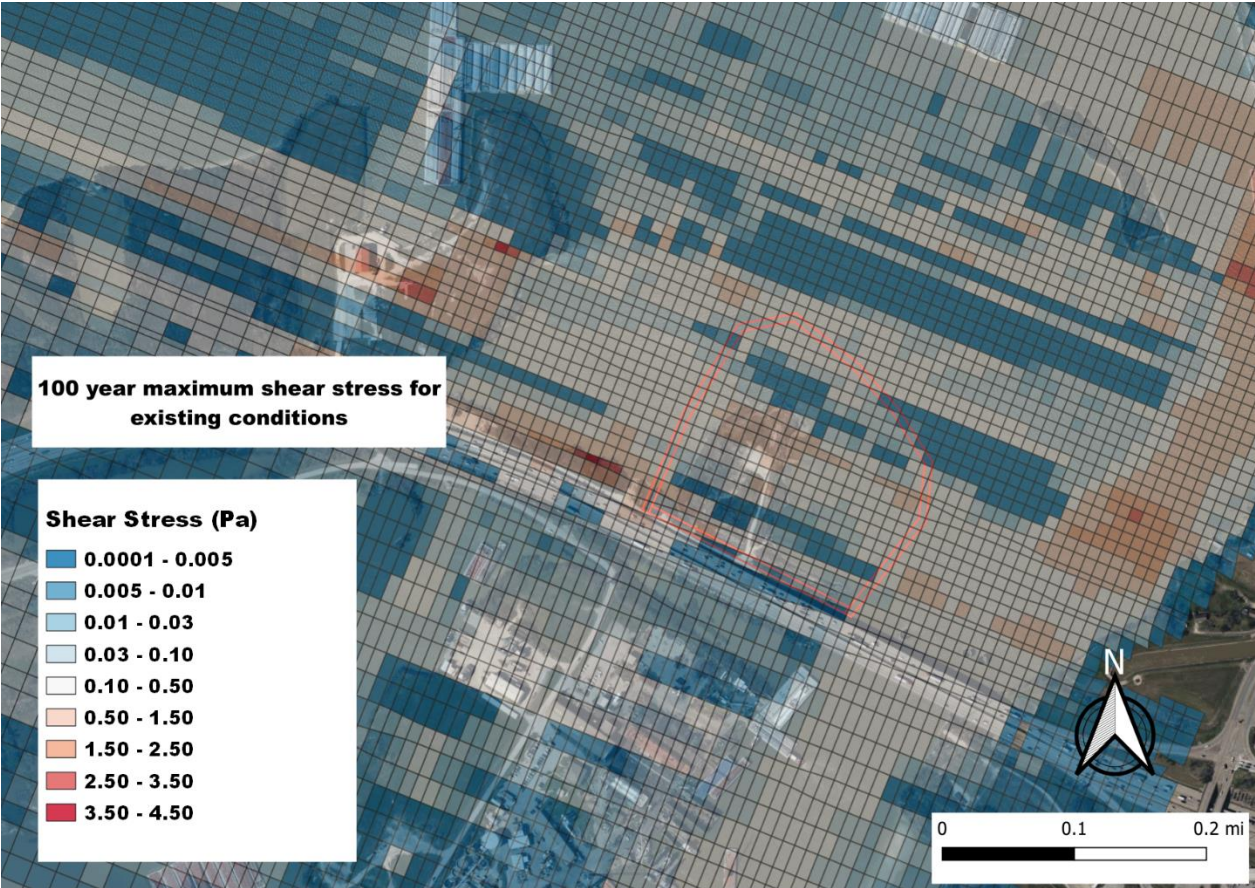
Appendix C - Shear Stress and Velocity Model Results for All Scenarios



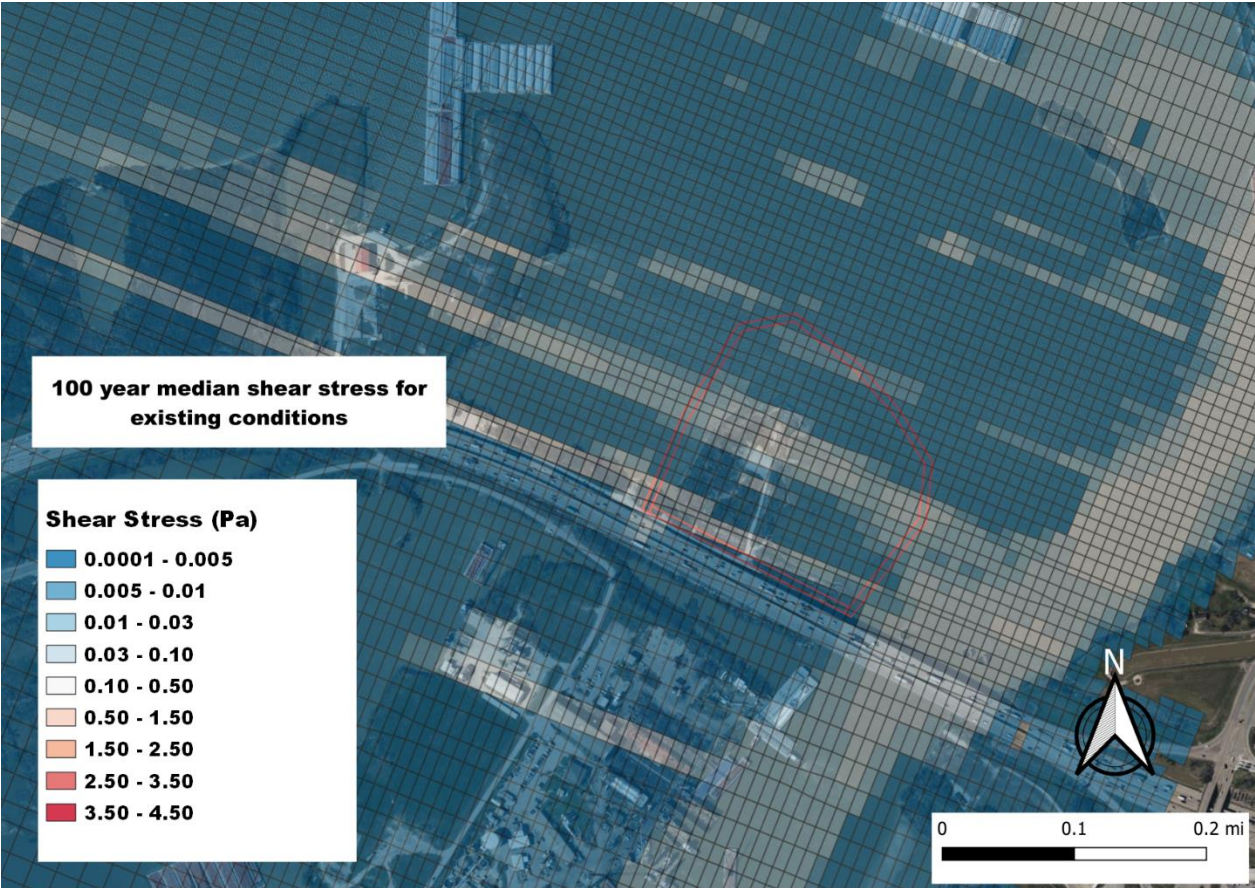
Appendix C - Shear Stress and Velocity Model Results for All Scenarios



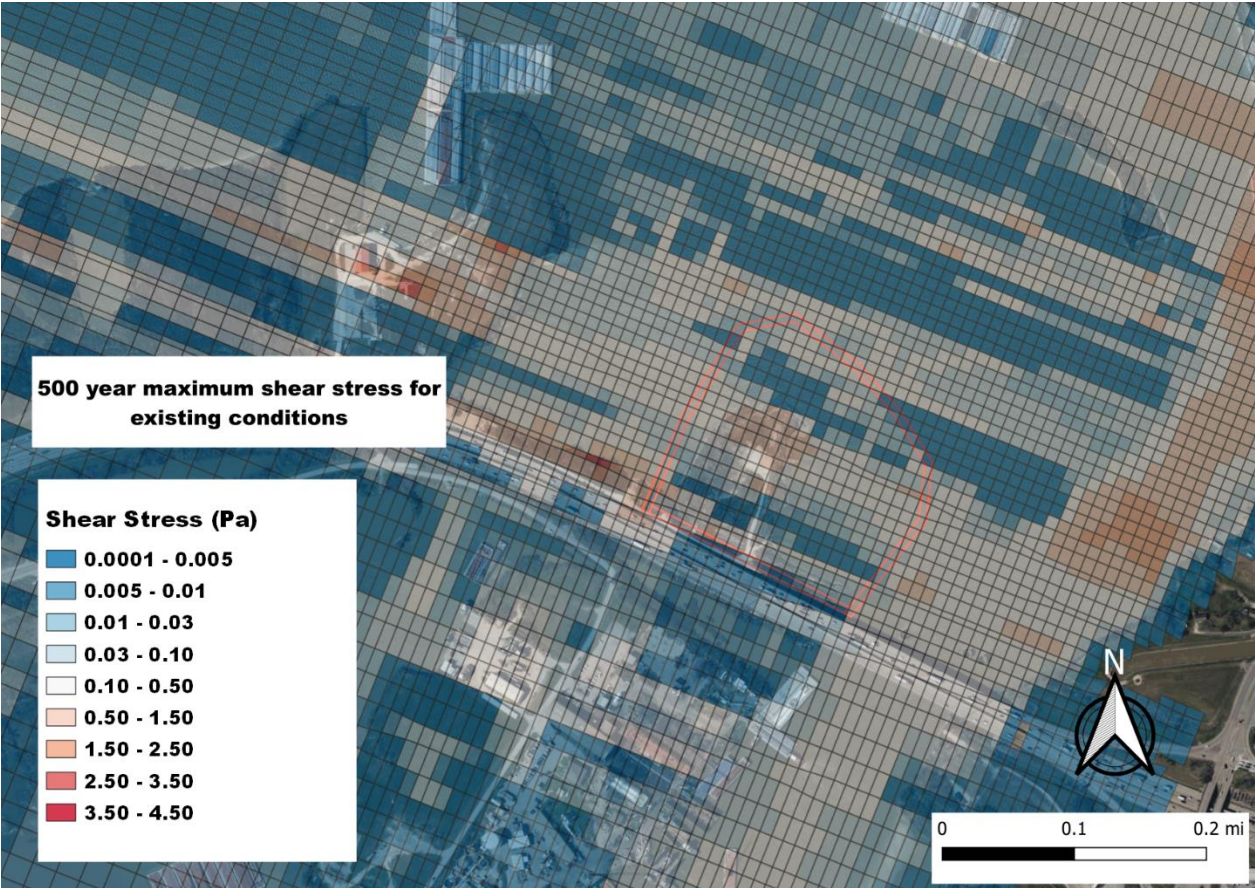
Appendix C - Shear Stress and Velocity Model Results for All Scenarios



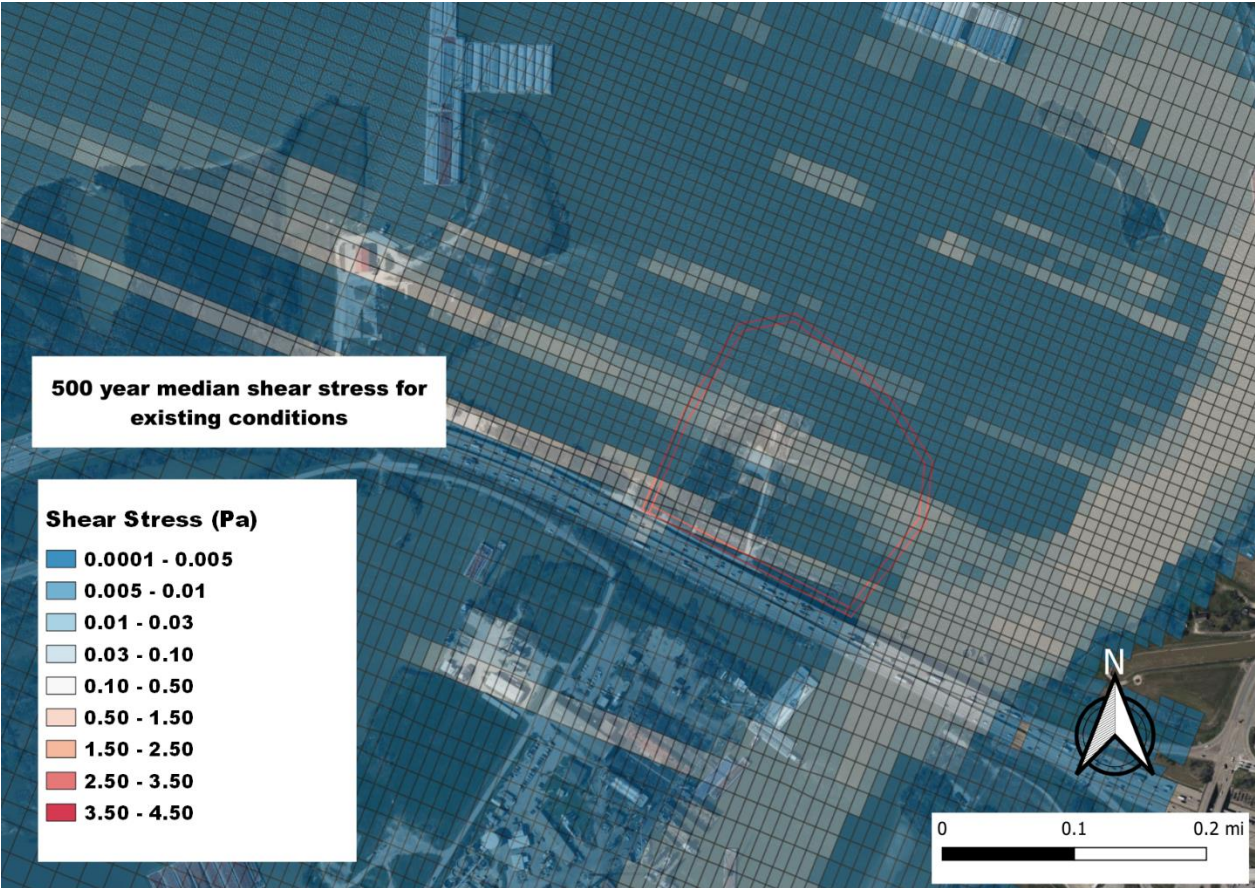
Appendix C - Shear Stress and Velocity Model Results for All Scenarios



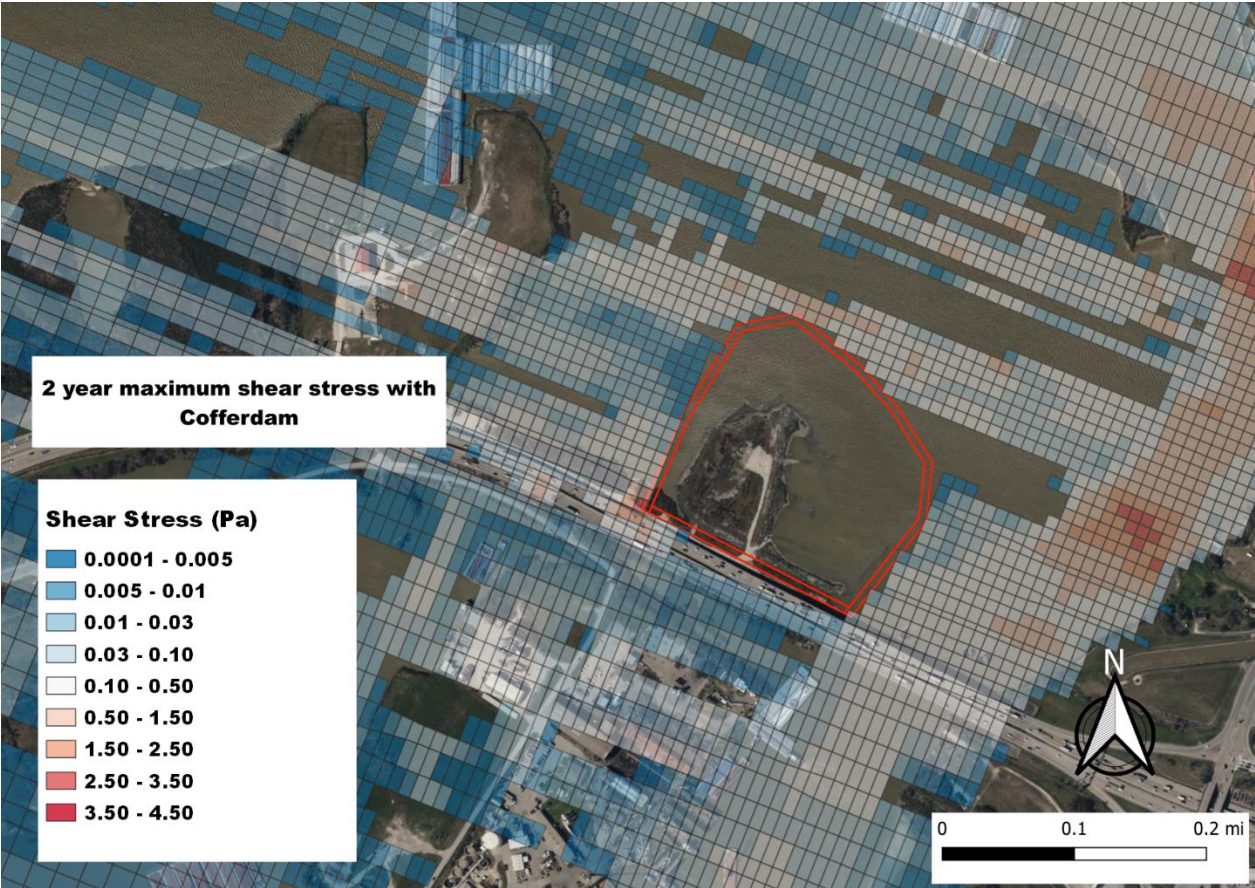
Appendix C - Shear Stress and Velocity Model Results for All Scenarios



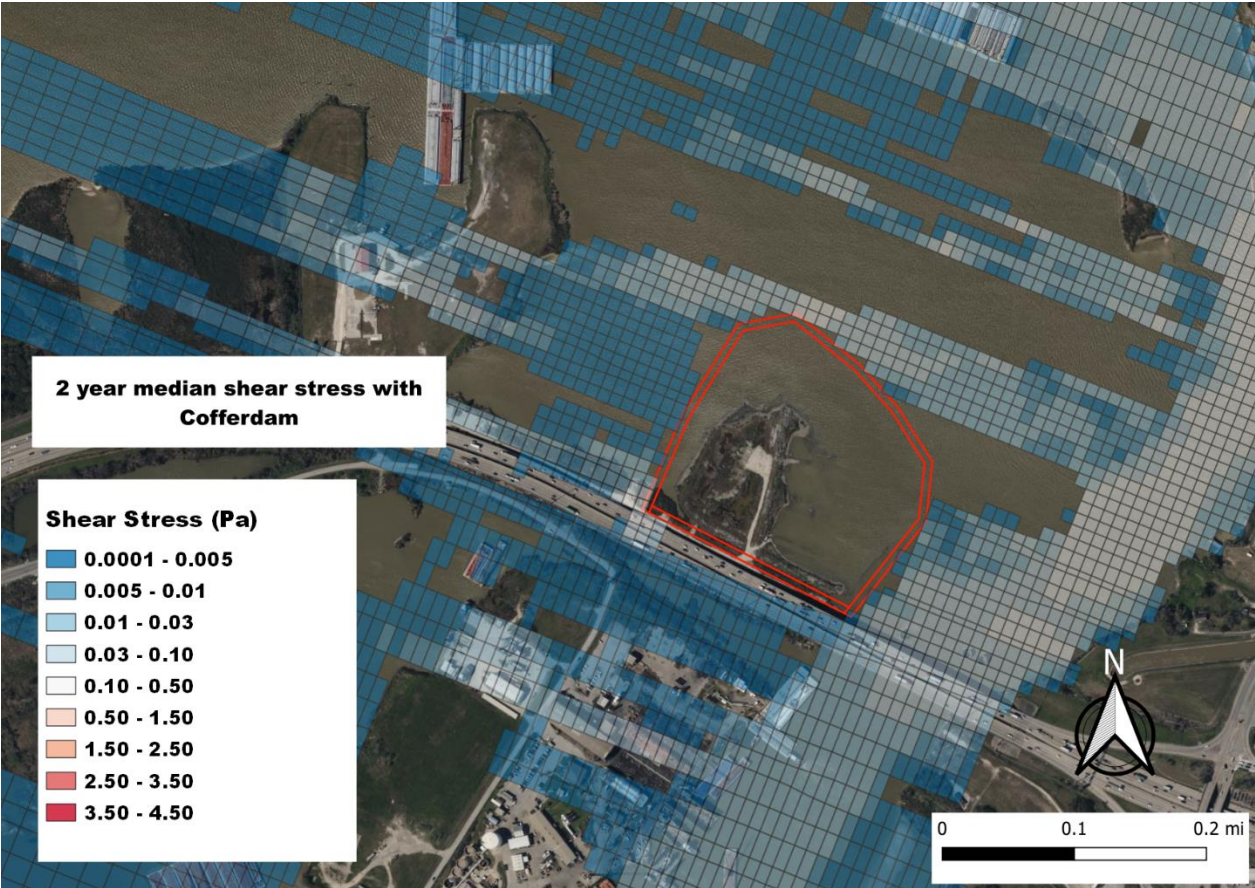
Appendix C - Shear Stress and Velocity Model Results for All Scenarios



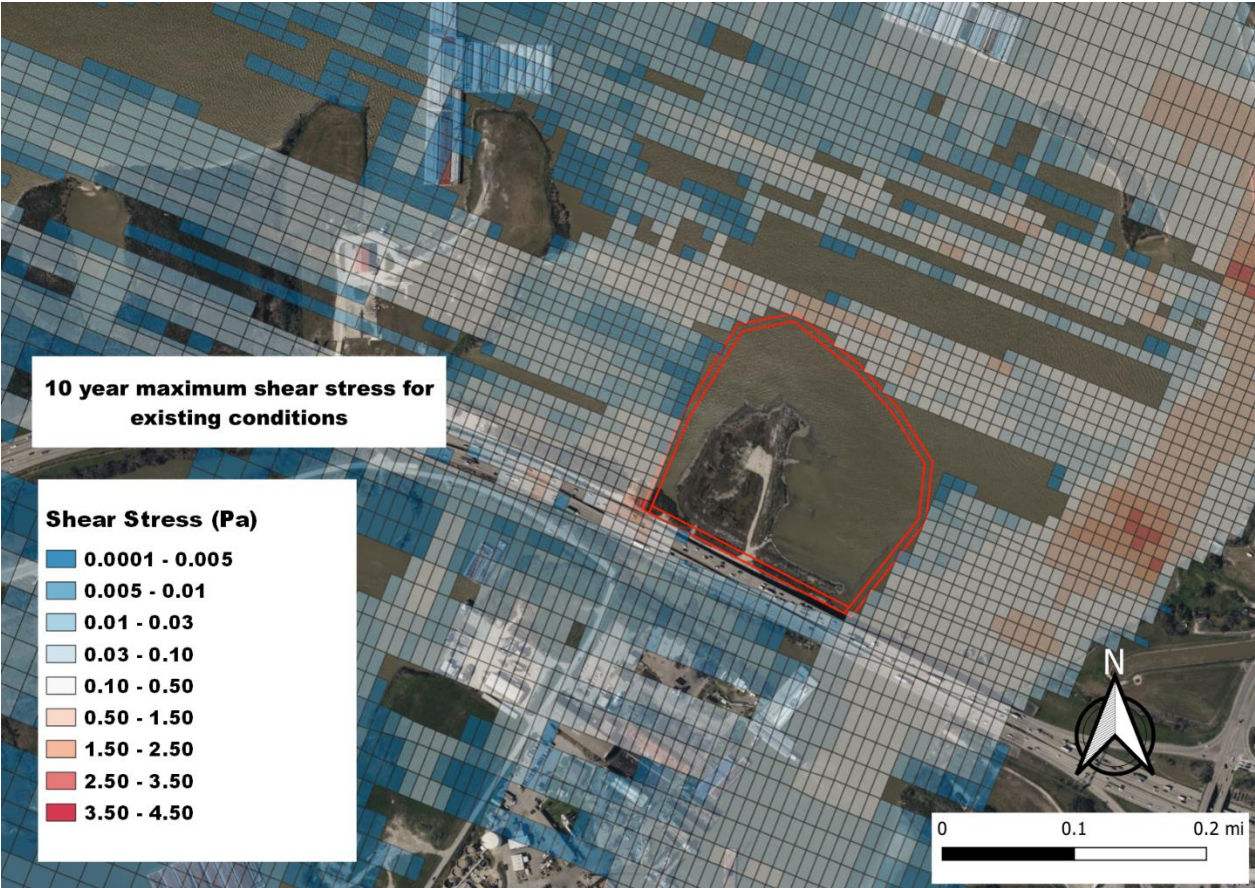
Shear Stress Figures with Cofferdam



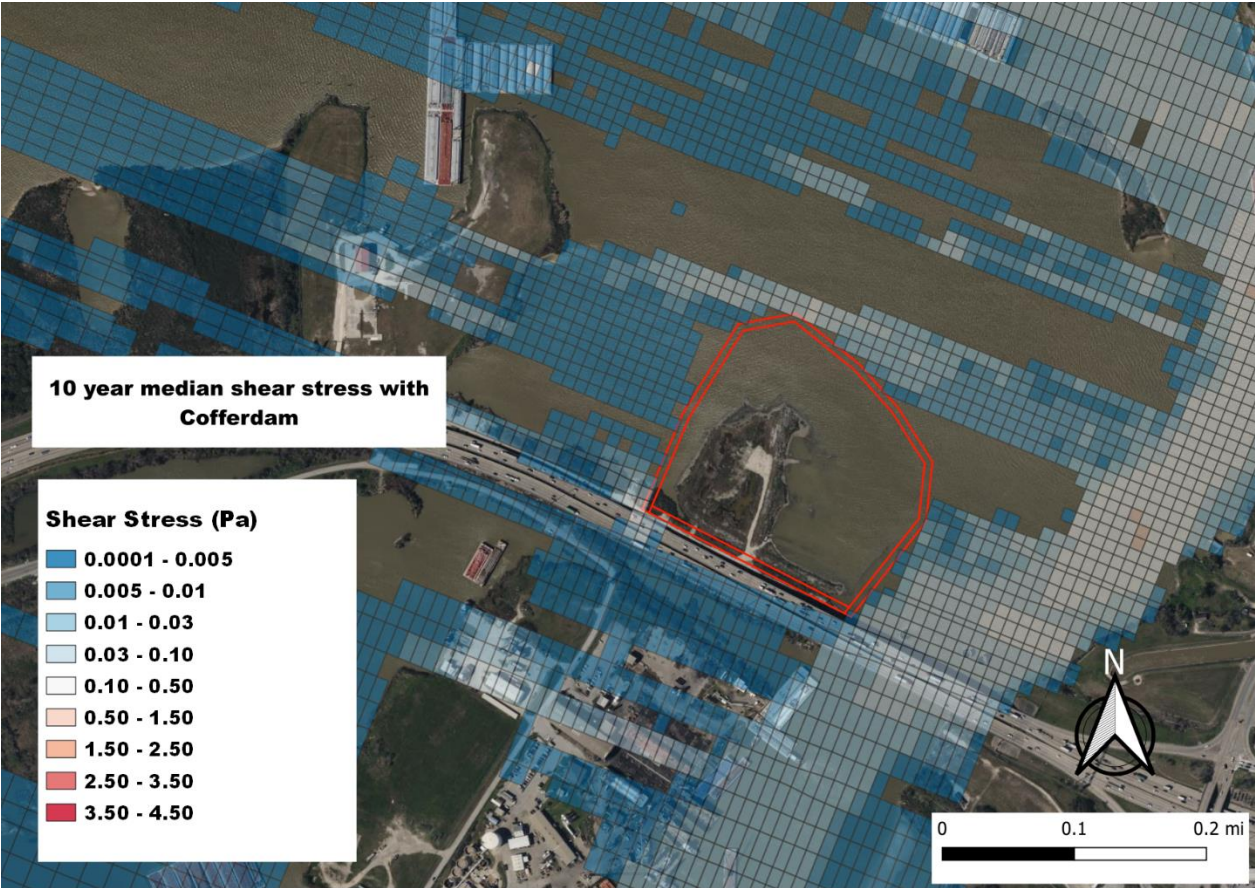
Appendix C - Shear Stress and Velocity Model Results for All Scenarios



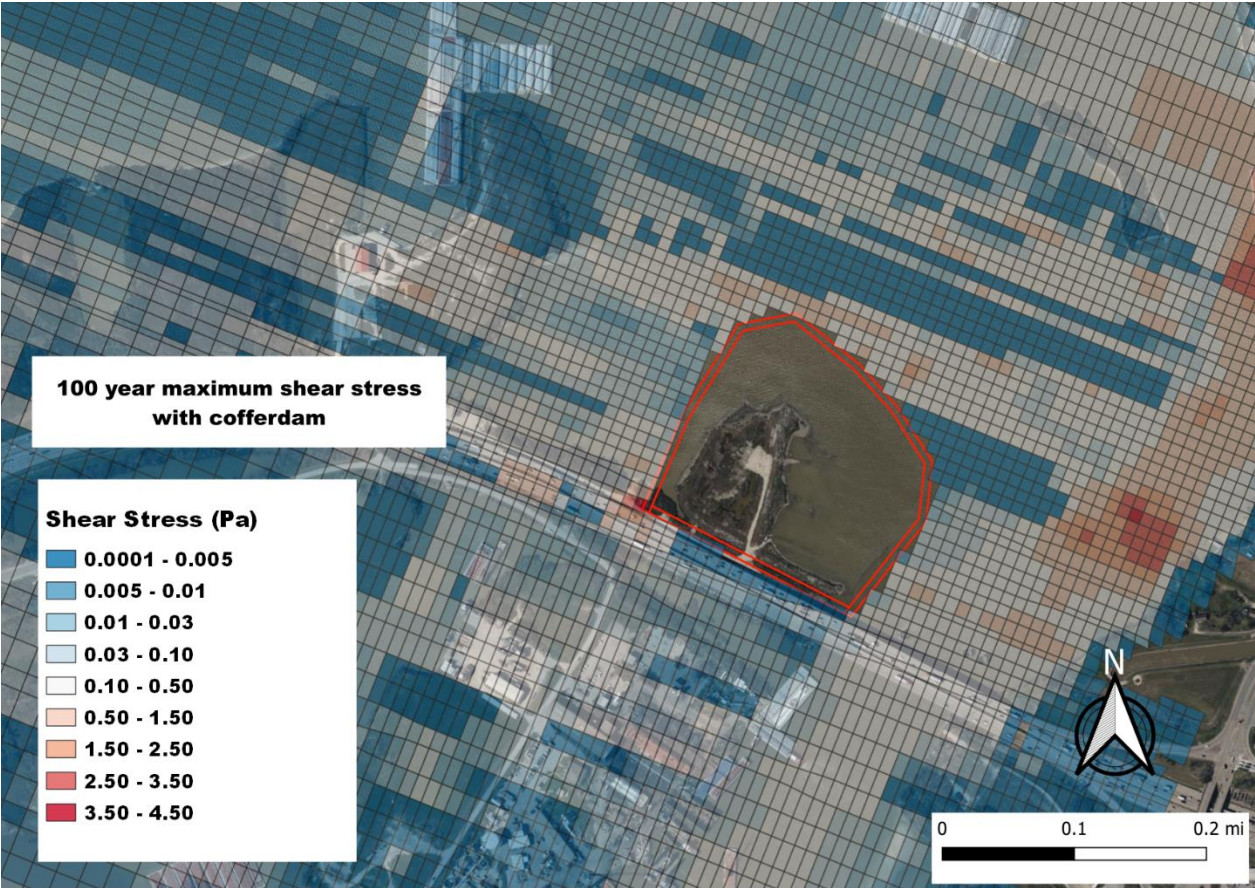
Appendix C - Shear Stress and Velocity Model Results for All Scenarios



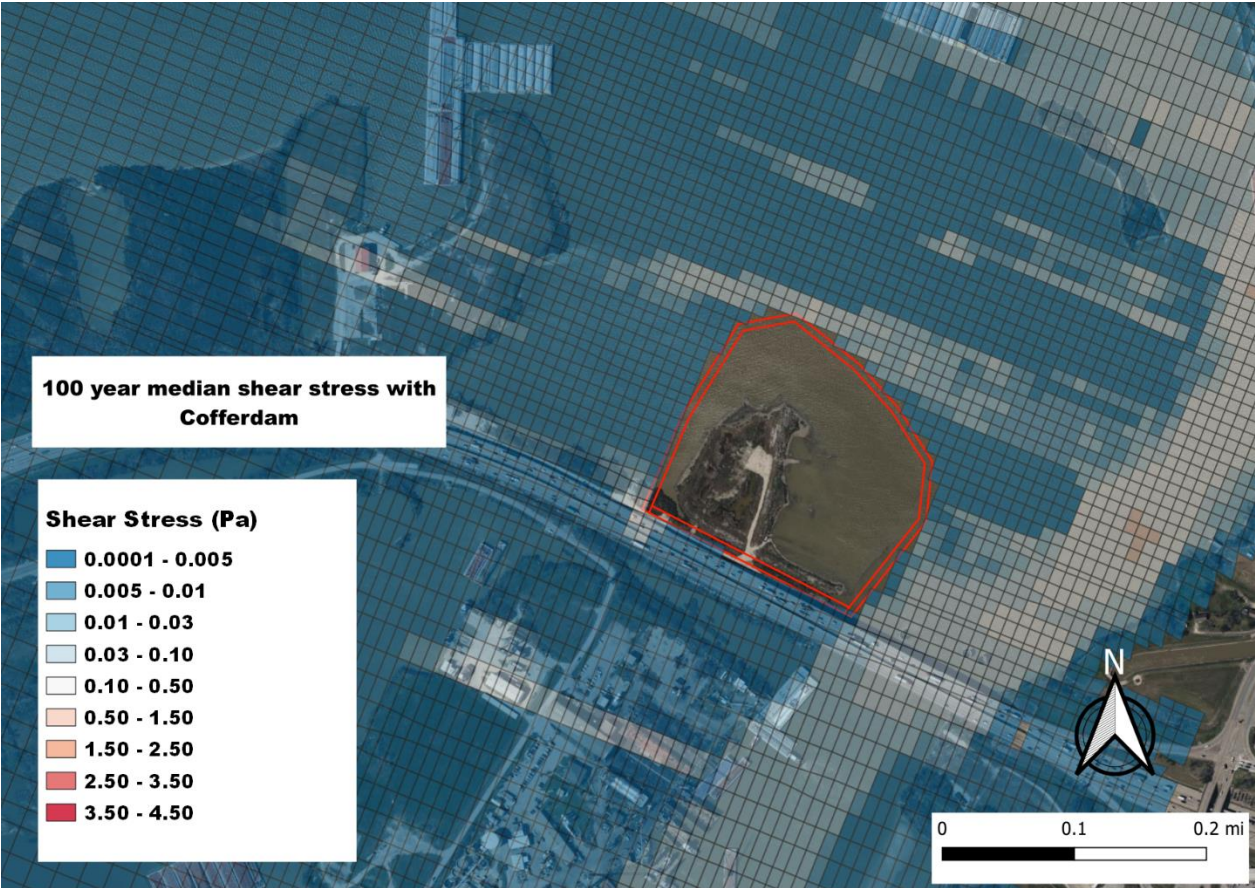
Appendix C - Shear Stress and Velocity Model Results for All Scenarios



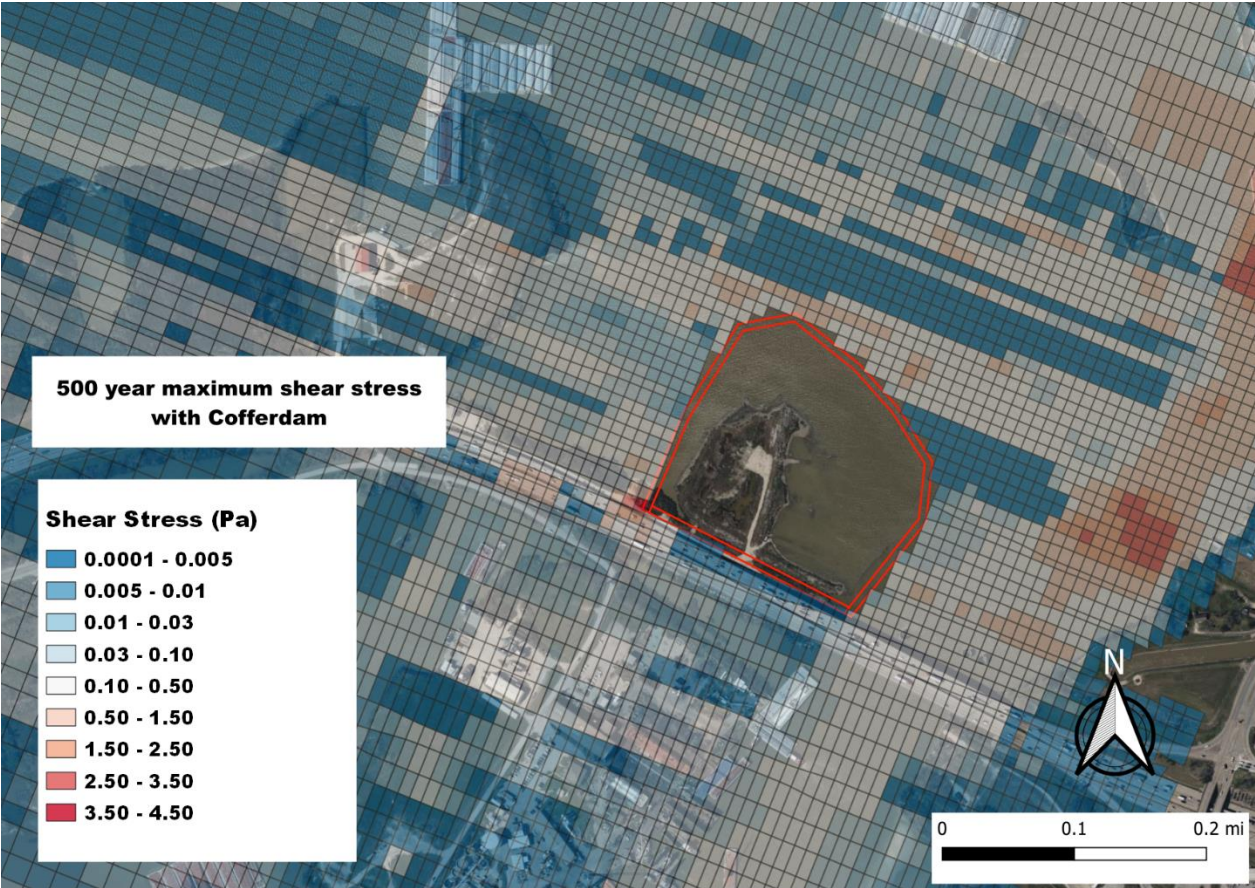
Appendix C - Shear Stress and Velocity Model Results for All Scenarios



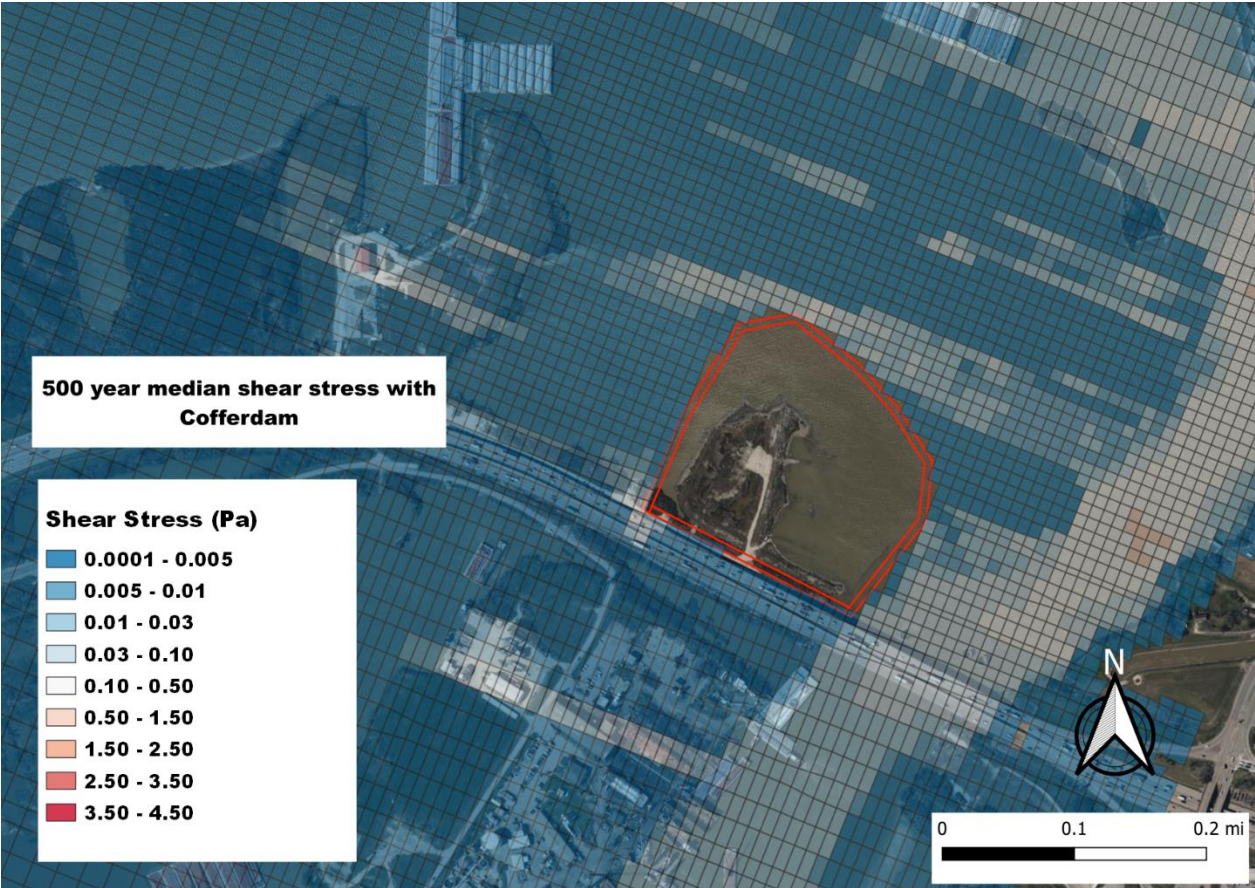
Appendix C - Shear Stress and Velocity Model Results for All Scenarios



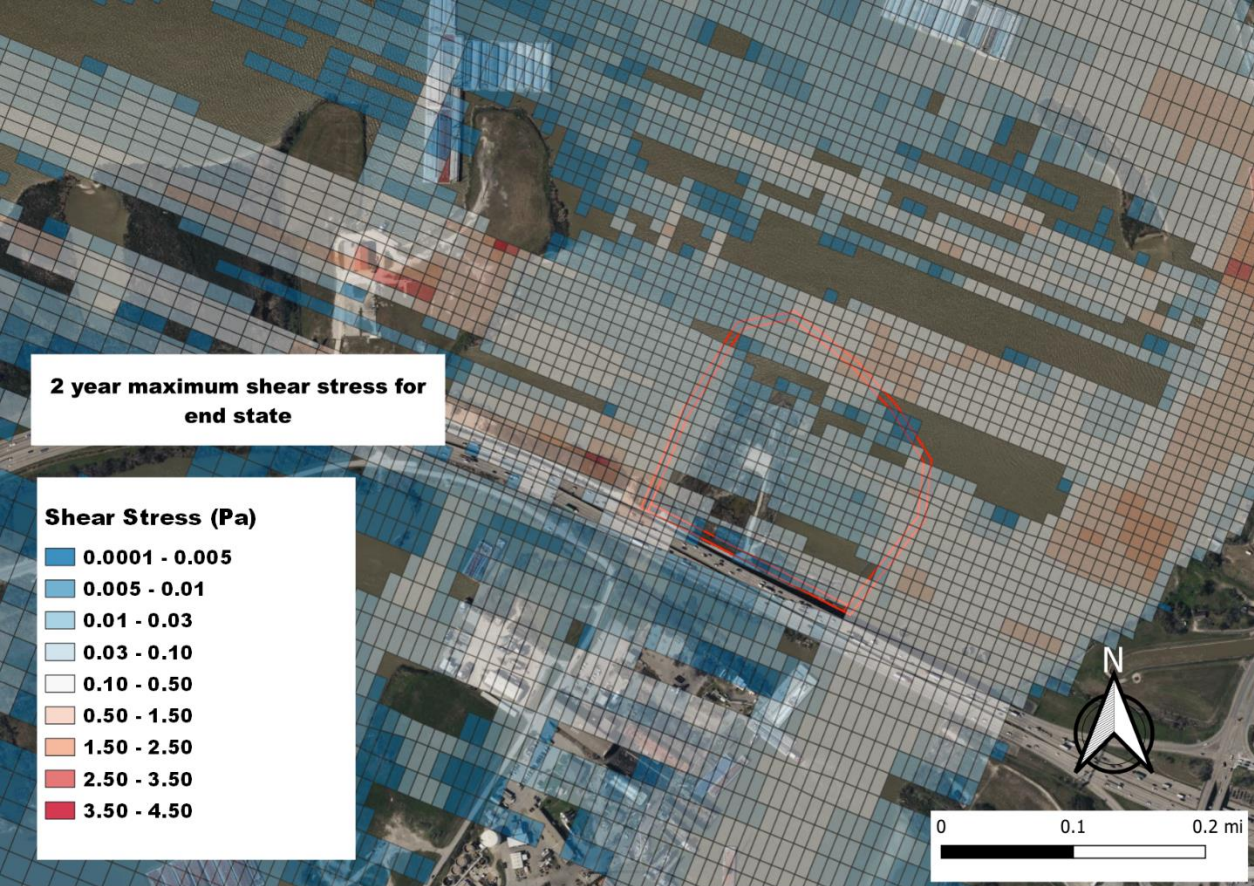
Appendix C - Shear Stress and Velocity Model Results for All Scenarios



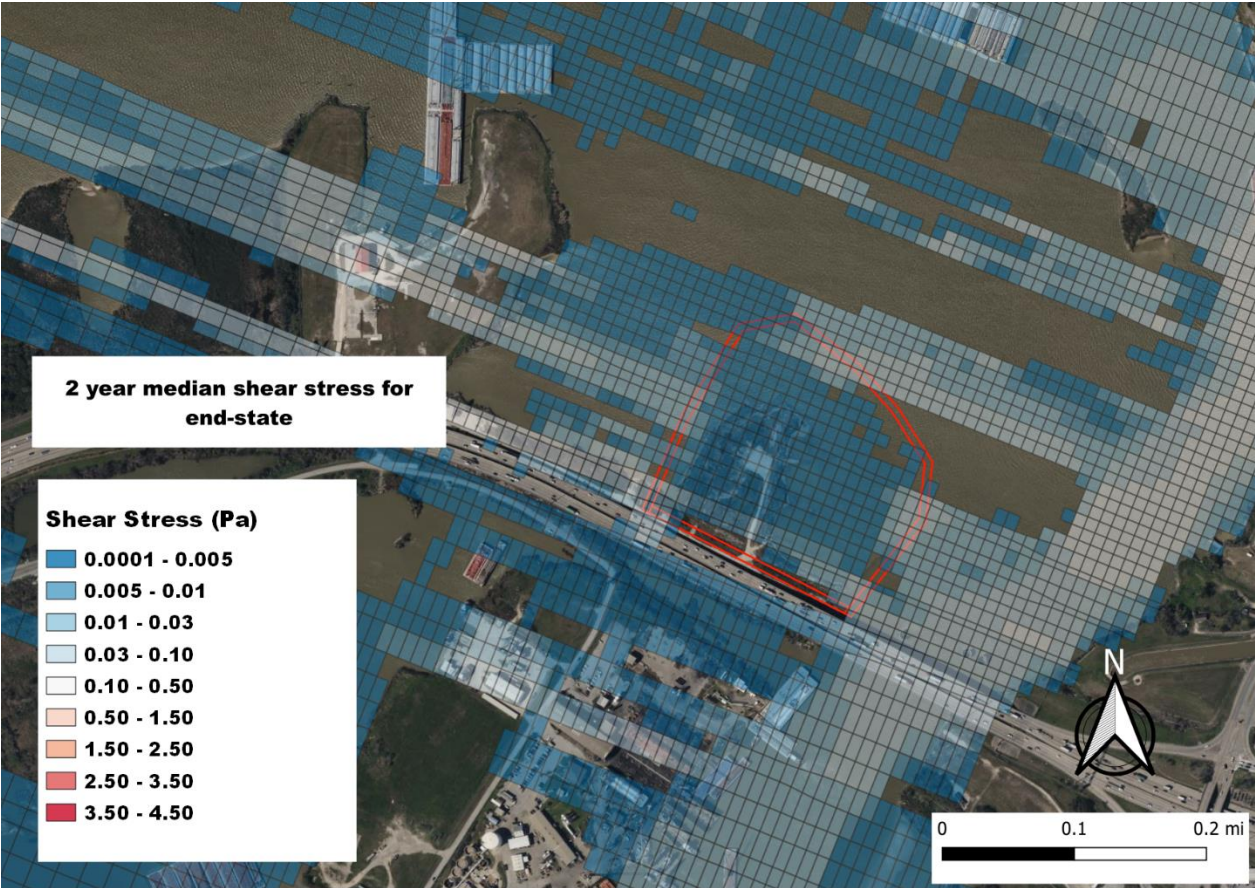
Appendix C - Shear Stress and Velocity Model Results for All Scenarios



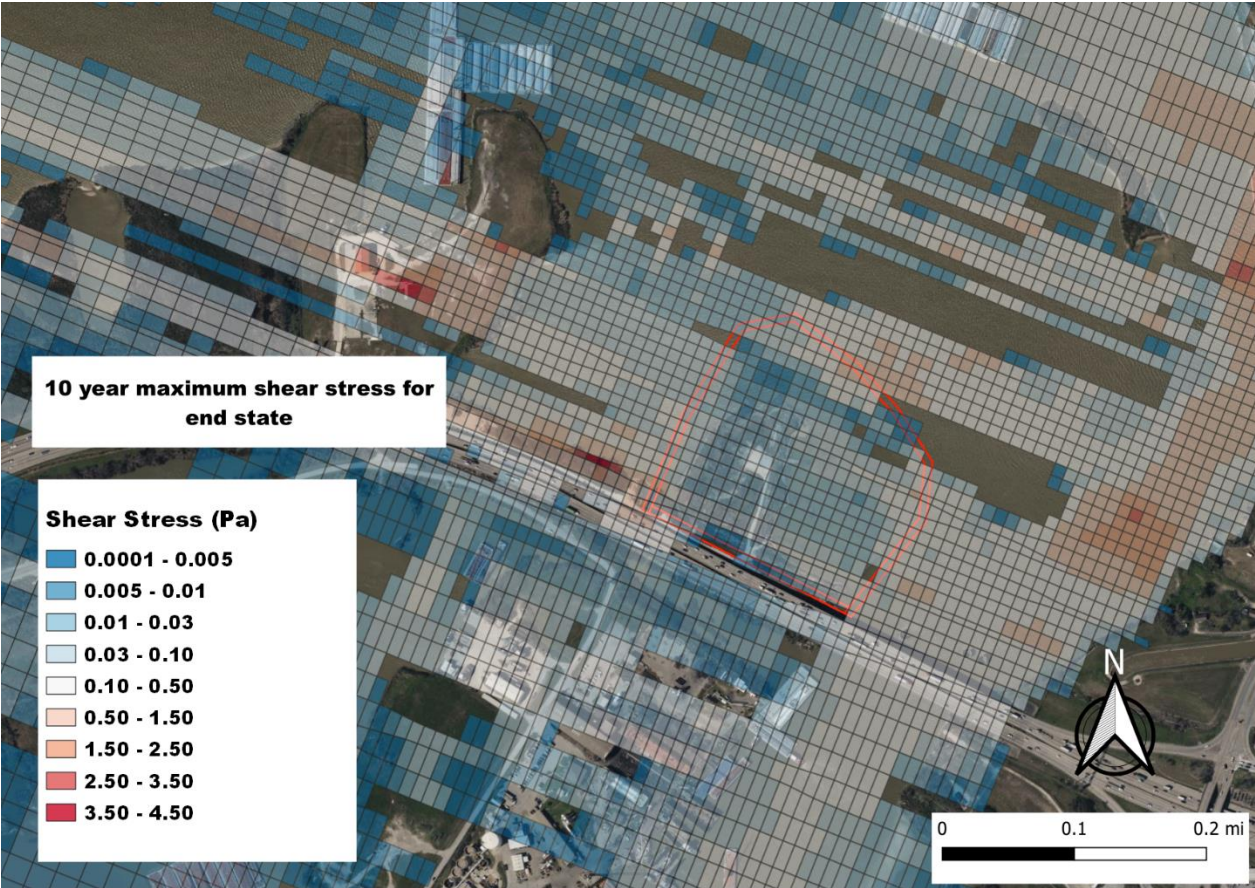
End-State Shear Stress Figures



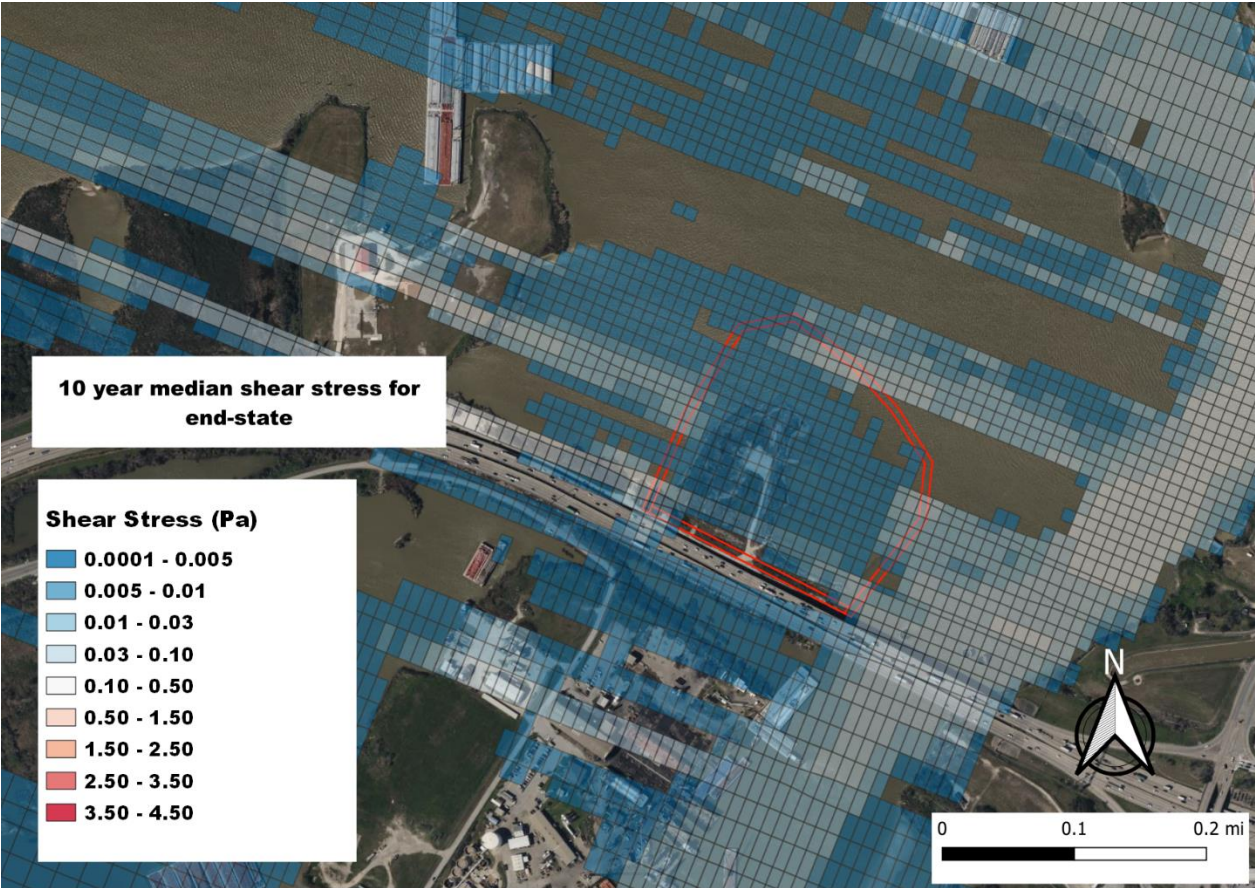
Appendix C - Shear Stress and Velocity Model Results for All Scenarios



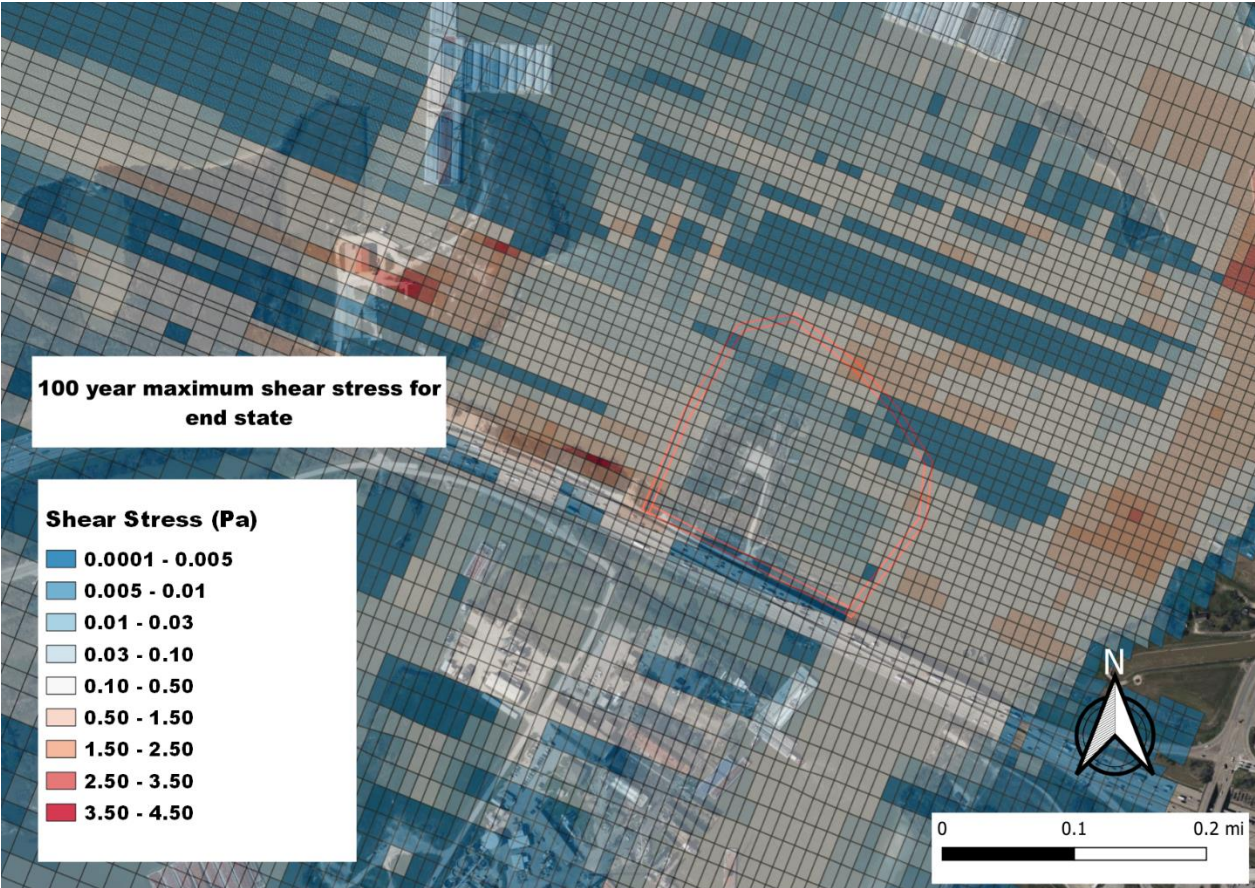
Appendix C - Shear Stress and Velocity Model Results for All Scenarios



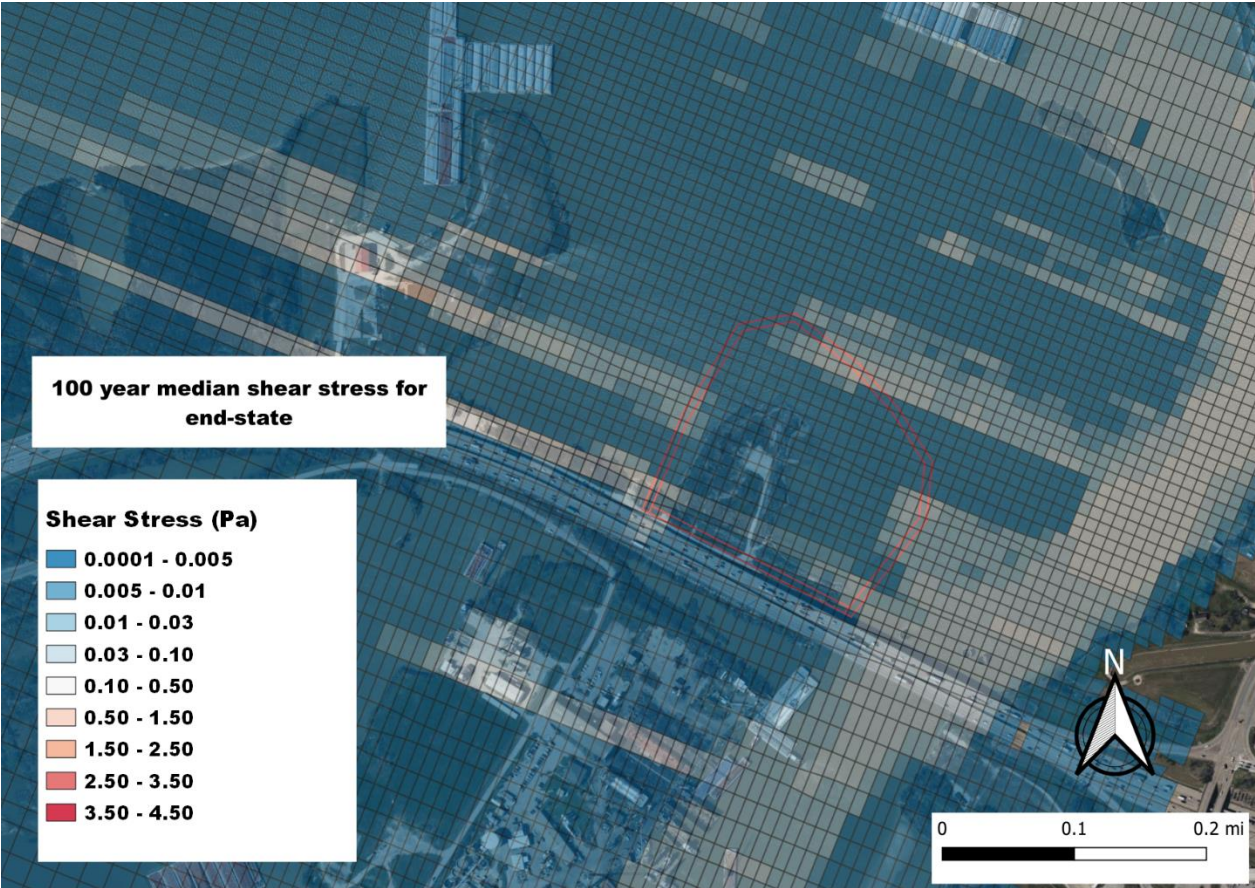
Appendix C - Shear Stress and Velocity Model Results for All Scenarios



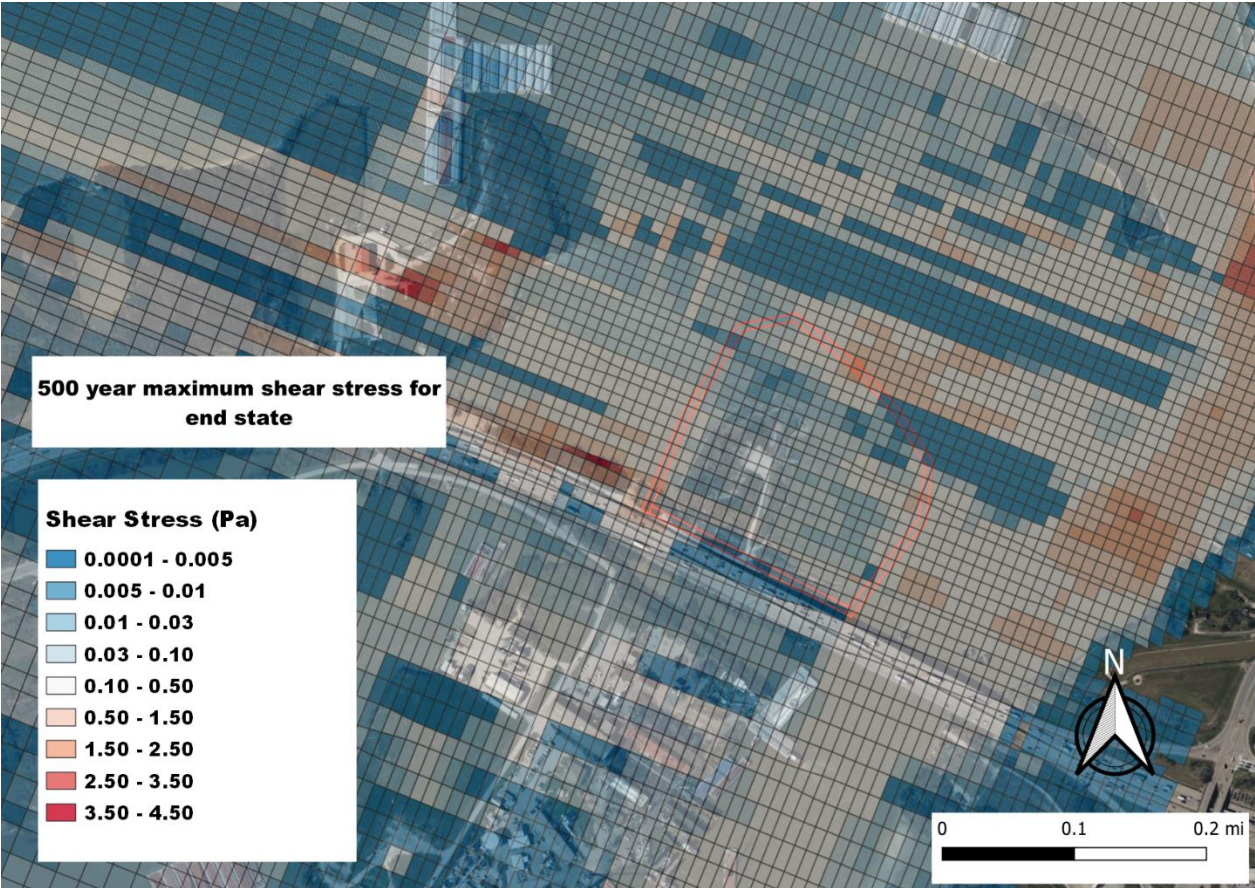
Appendix C - Shear Stress and Velocity Model Results for All Scenarios



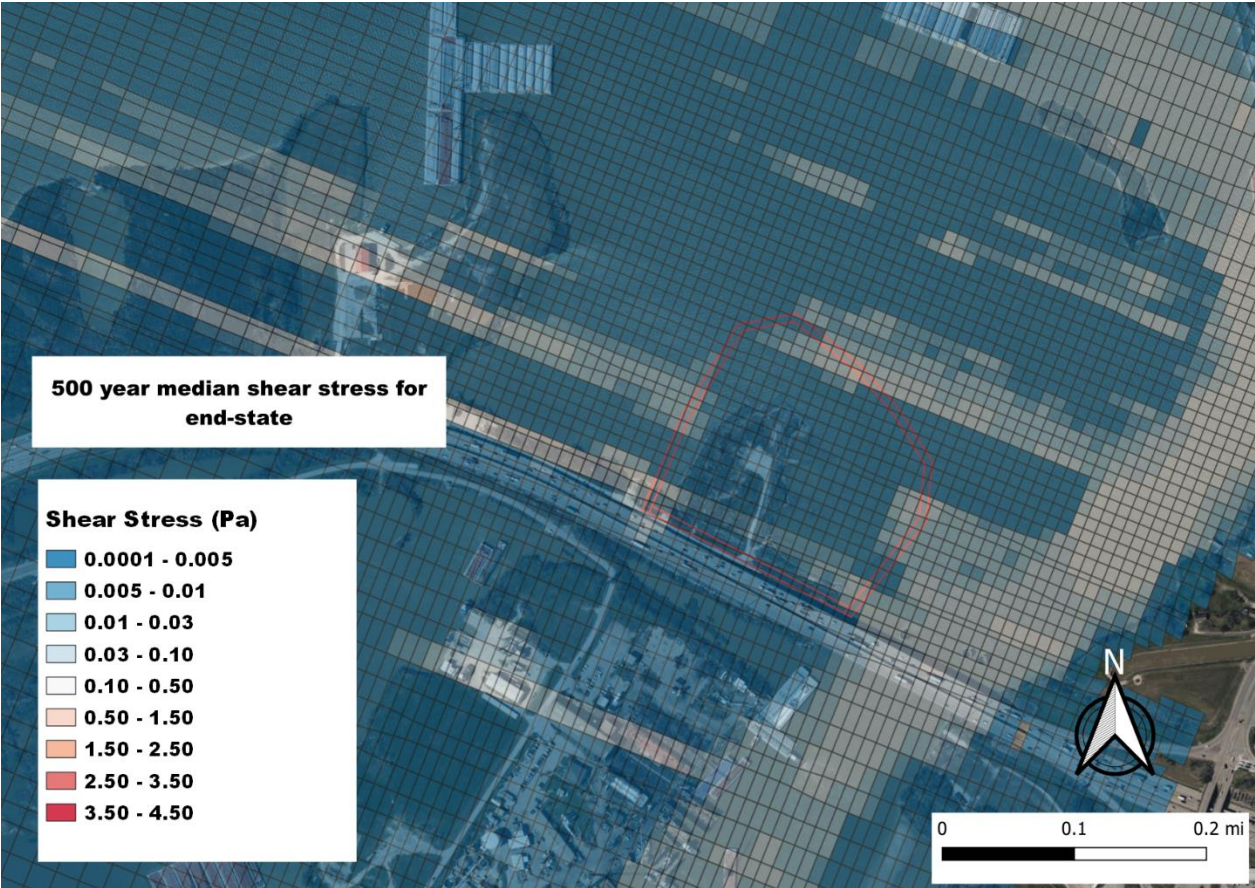
Appendix C - Shear Stress and Velocity Model Results for All Scenarios



Appendix C - Shear Stress and Velocity Model Results for All Scenarios

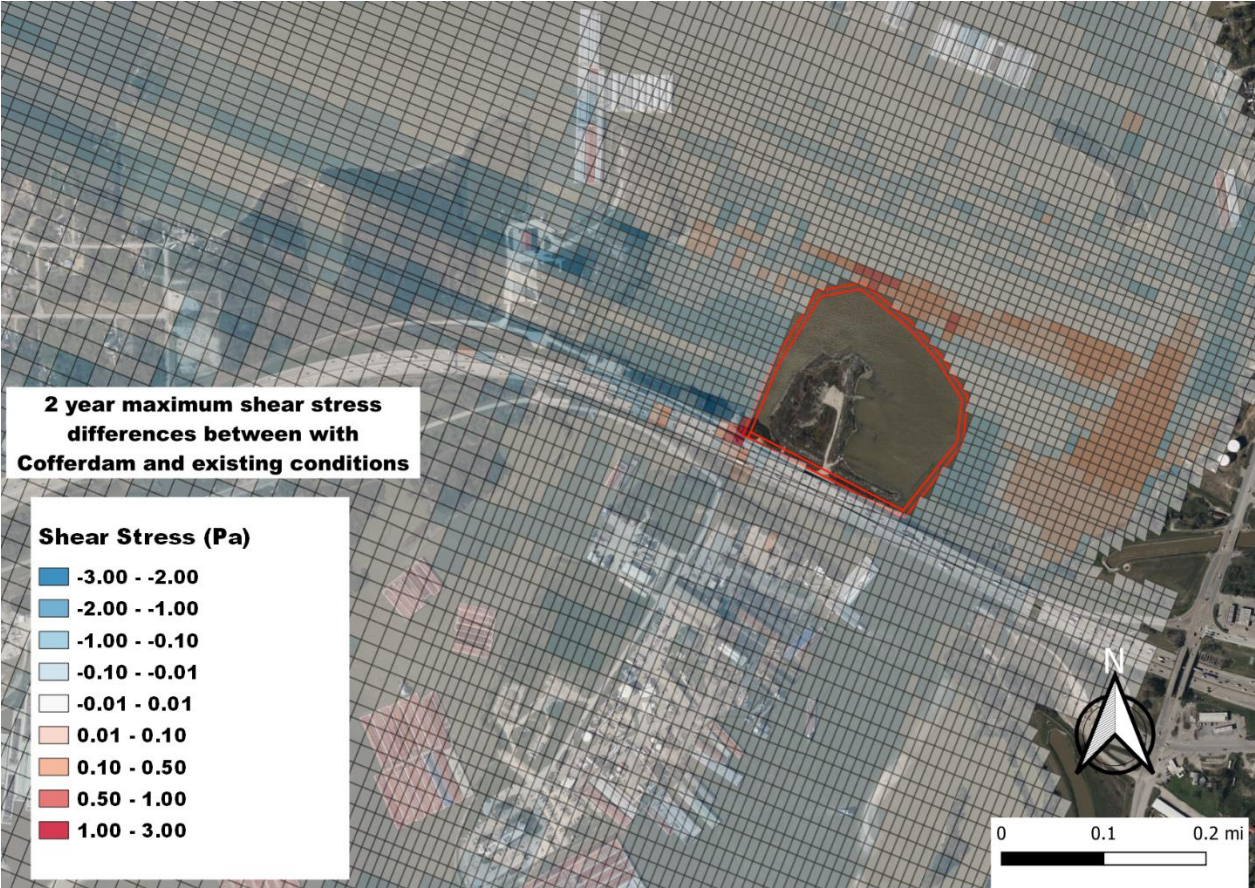


Appendix C - Shear Stress and Velocity Model Results for All Scenarios

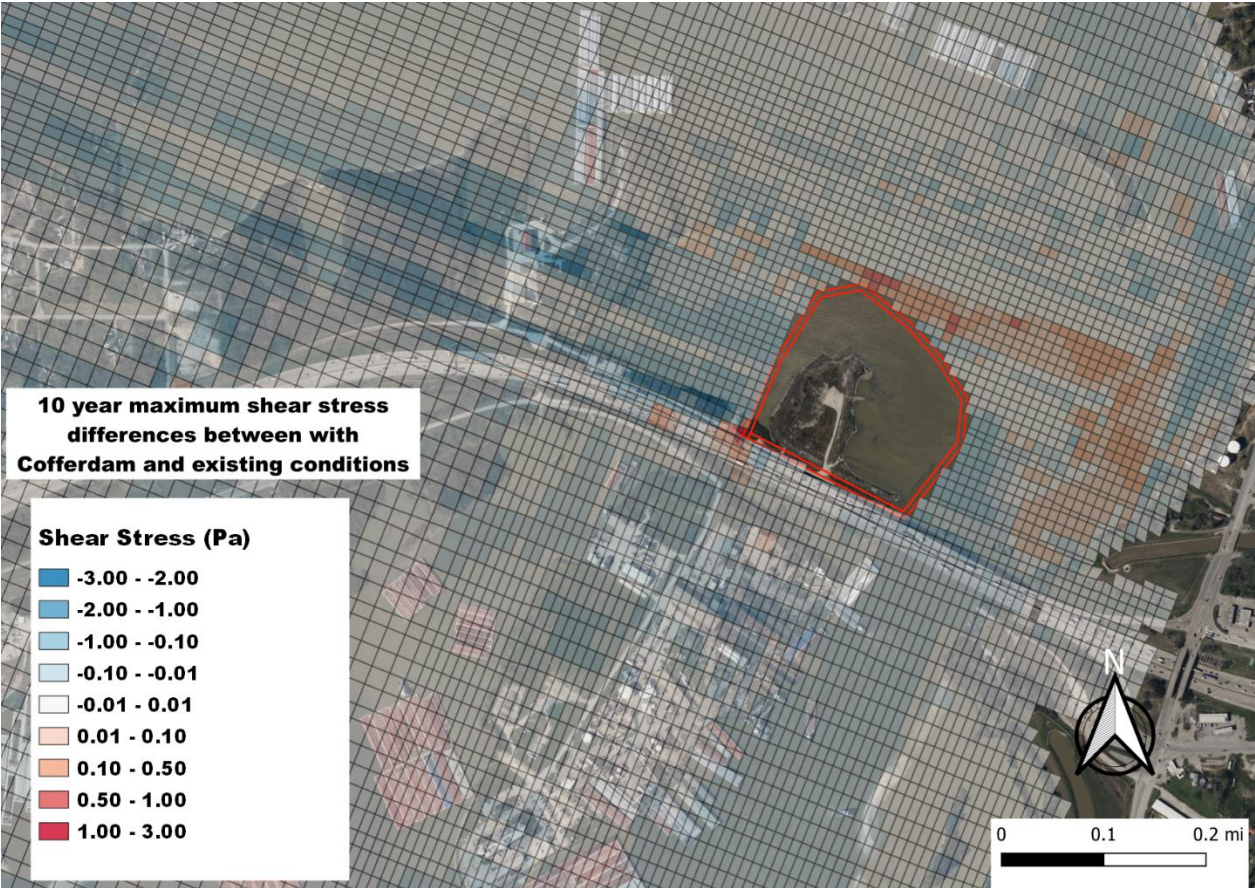


Shear Stress Difference Figures

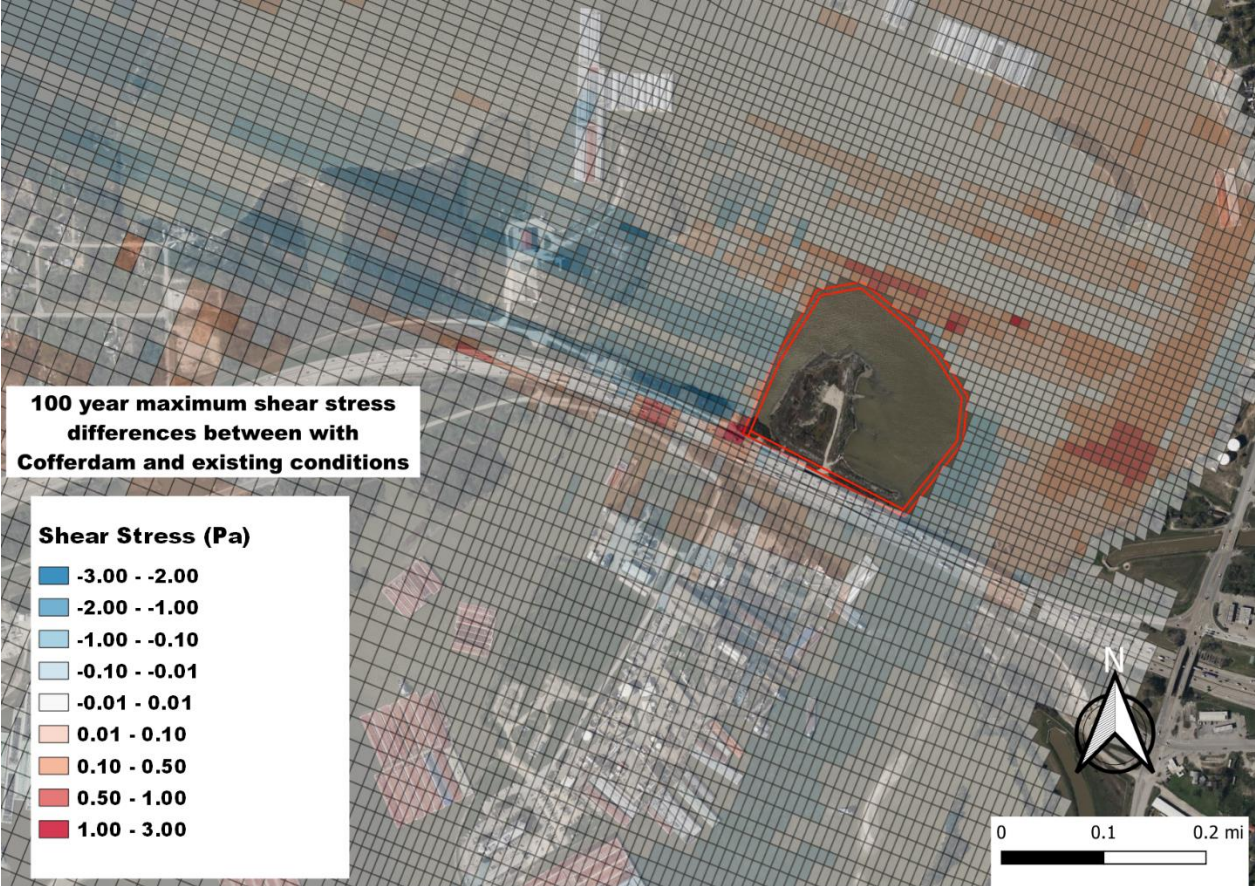
With Cofferdam Minus Existing Conditions



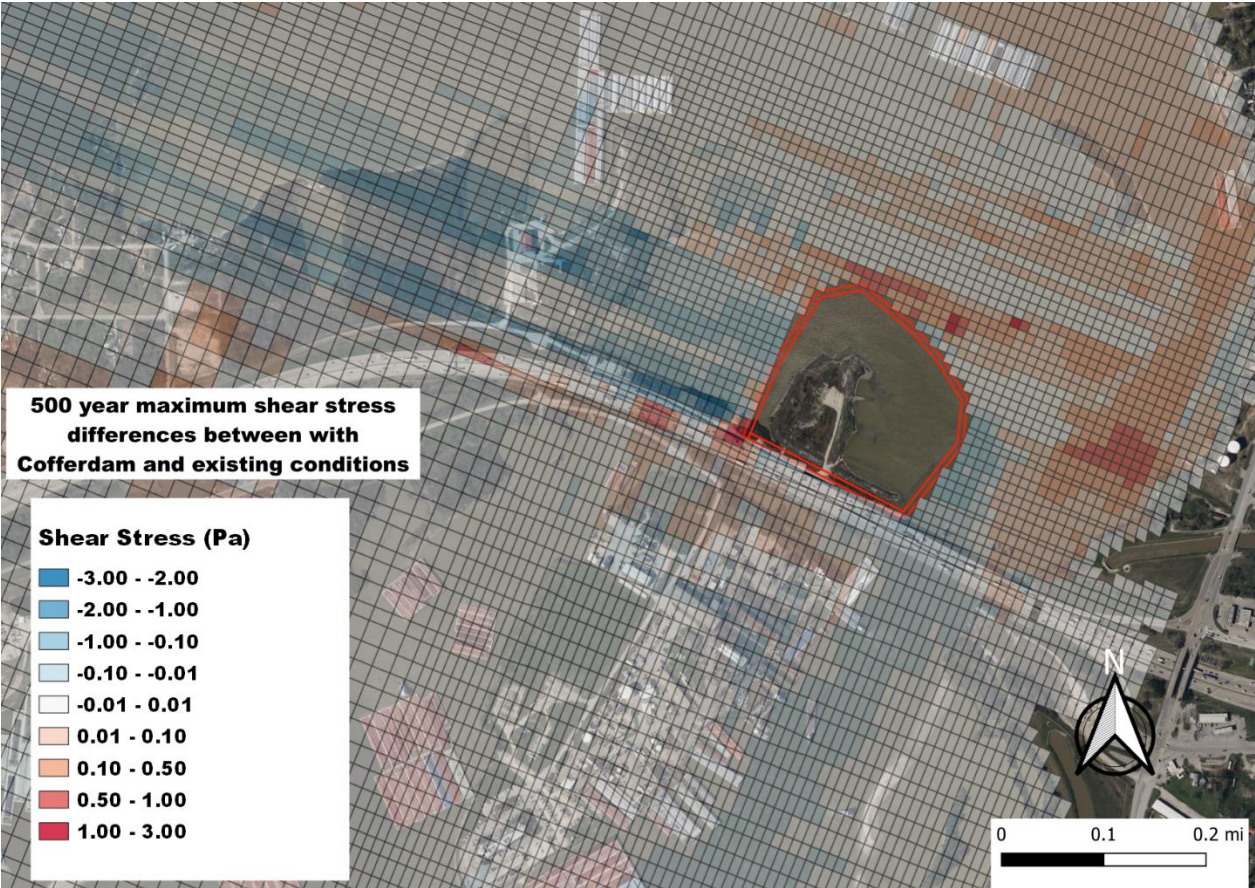
Appendix C - Shear Stress and Velocity Model Results for All Scenarios



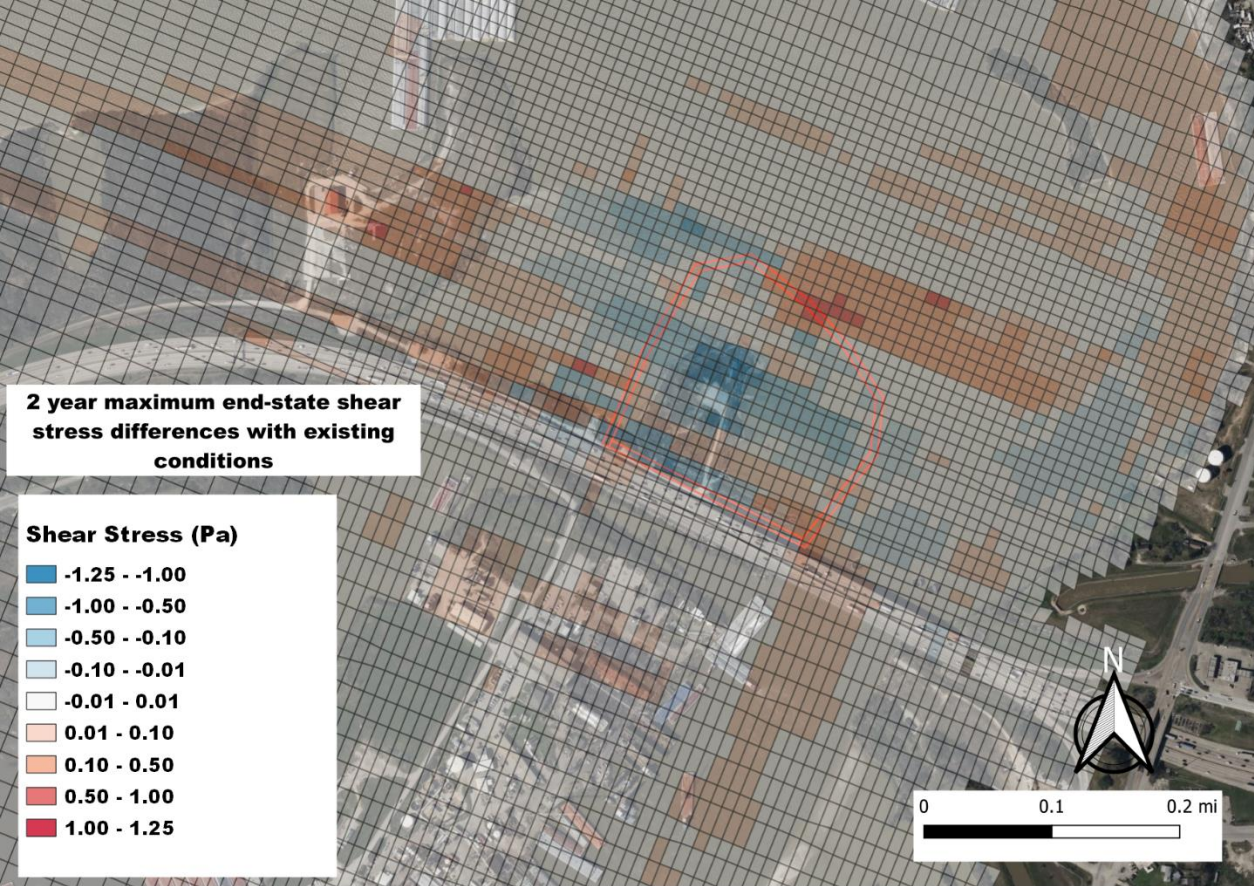
Appendix C - Shear Stress and Velocity Model Results for All Scenarios



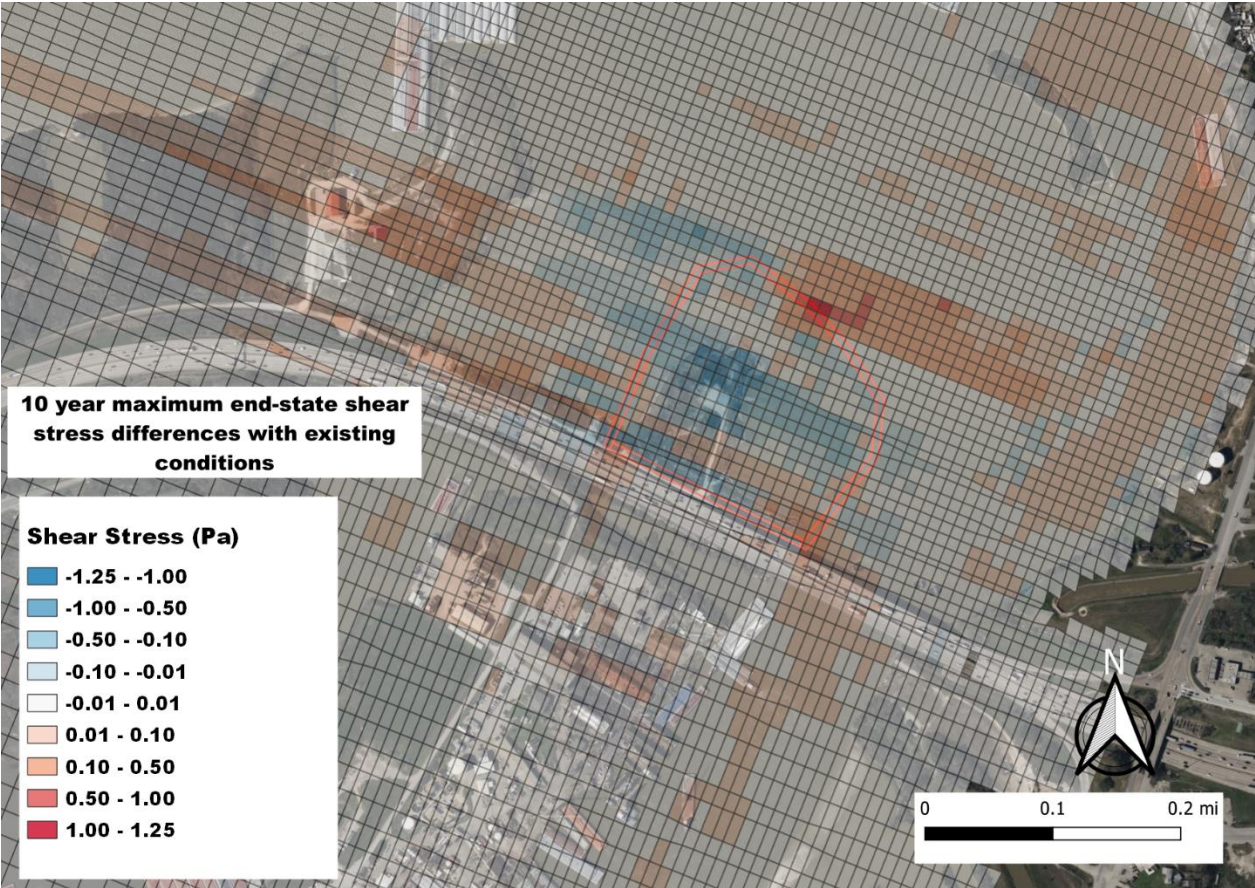
Appendix C - Shear Stress and Velocity Model Results for All Scenarios



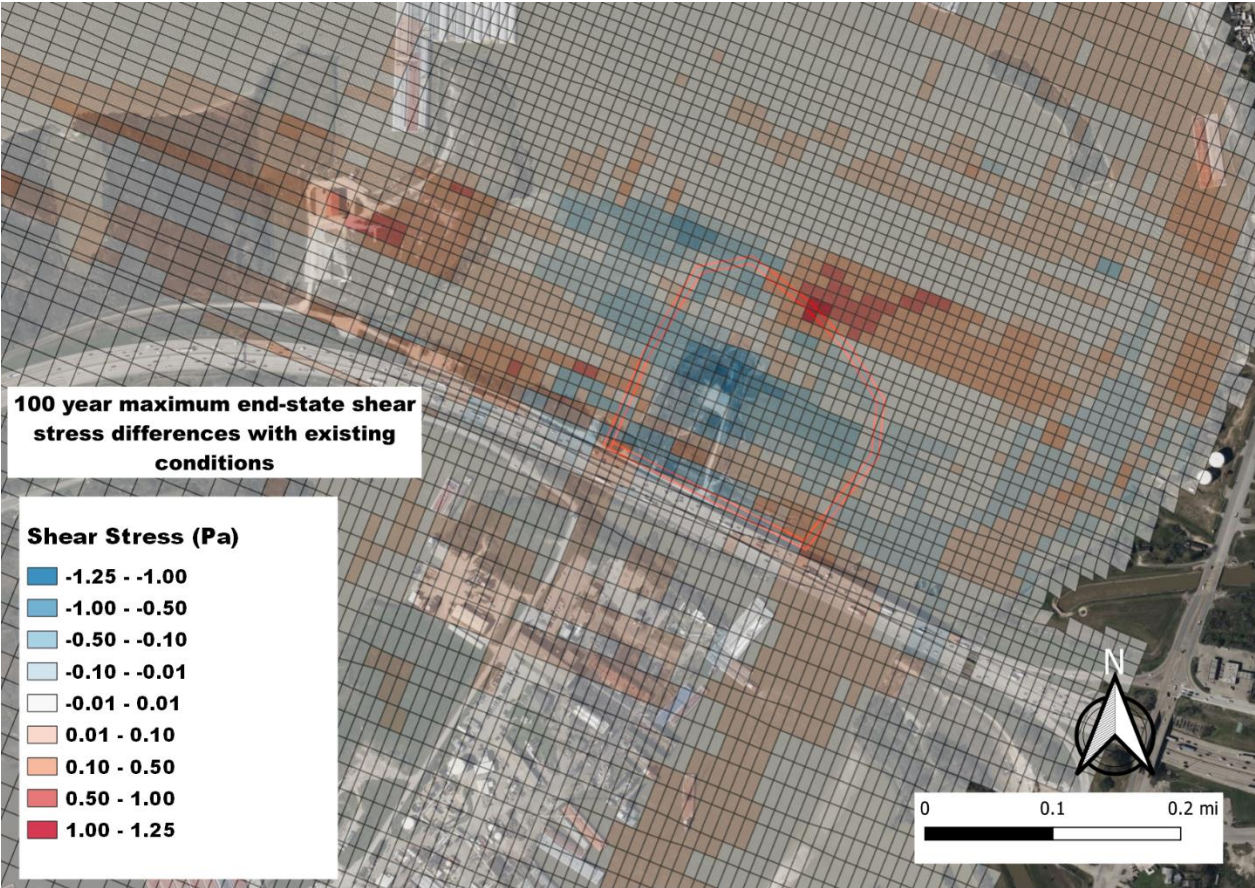
End-State Minus Existing Conditions



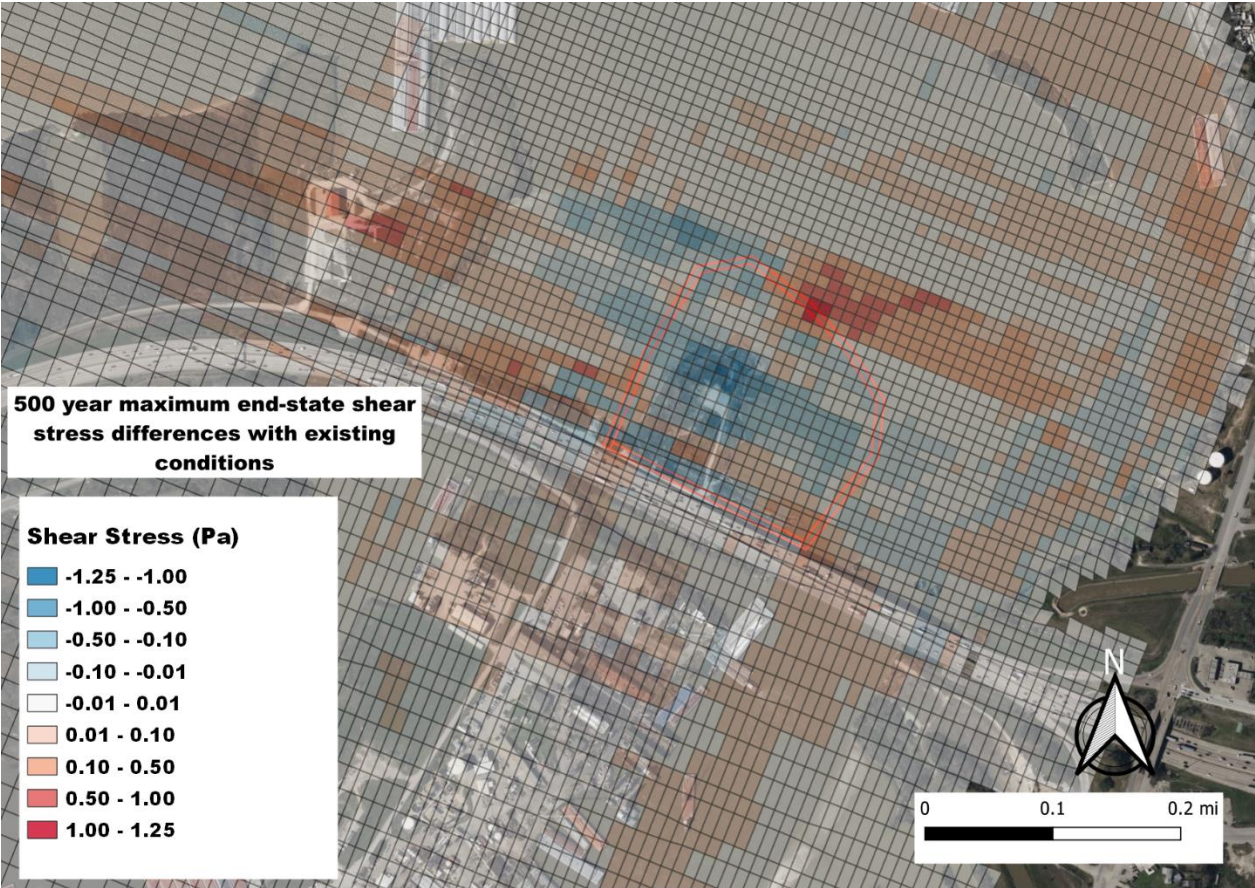
Appendix C - Shear Stress and Velocity Model Results for All Scenarios



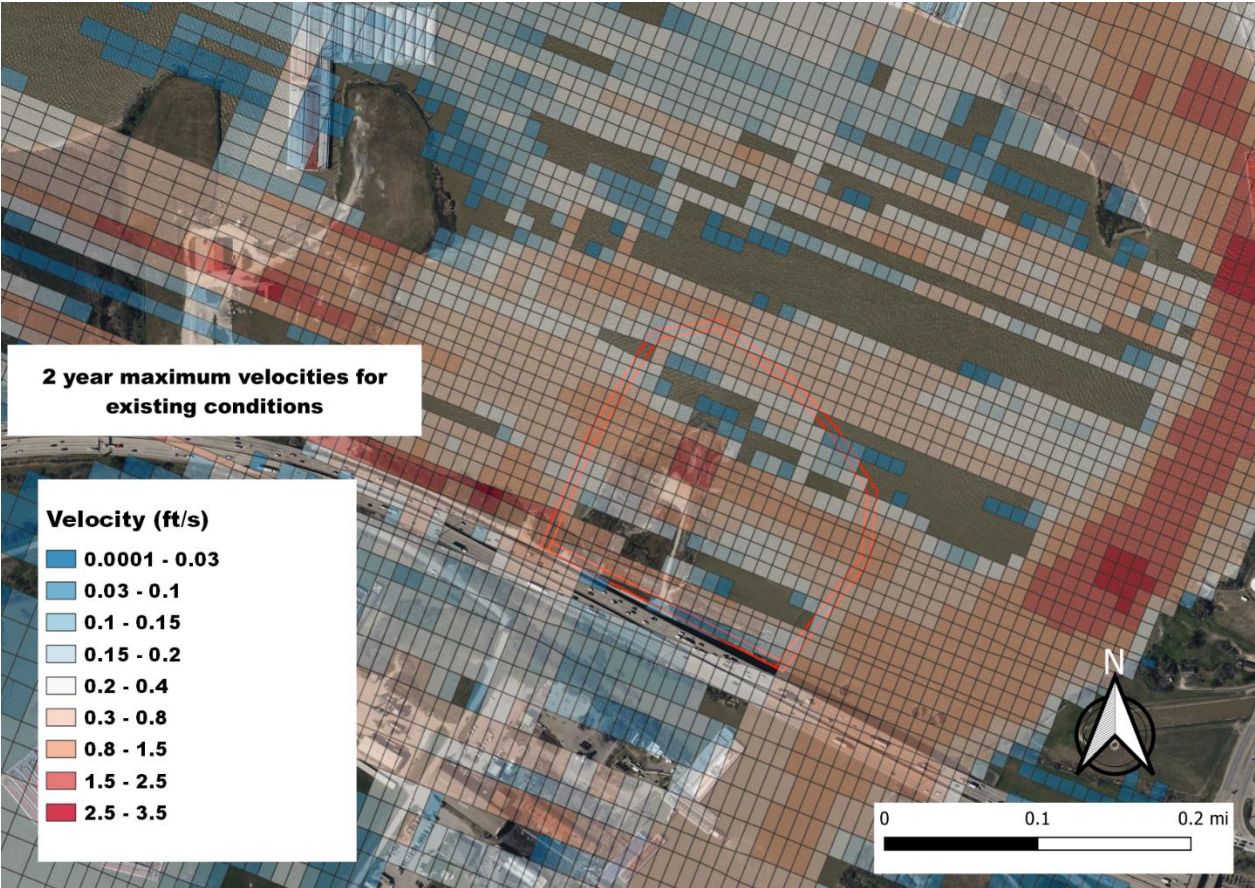
Appendix C - Shear Stress and Velocity Model Results for All Scenarios



Appendix C - Shear Stress and Velocity Model Results for All Scenarios



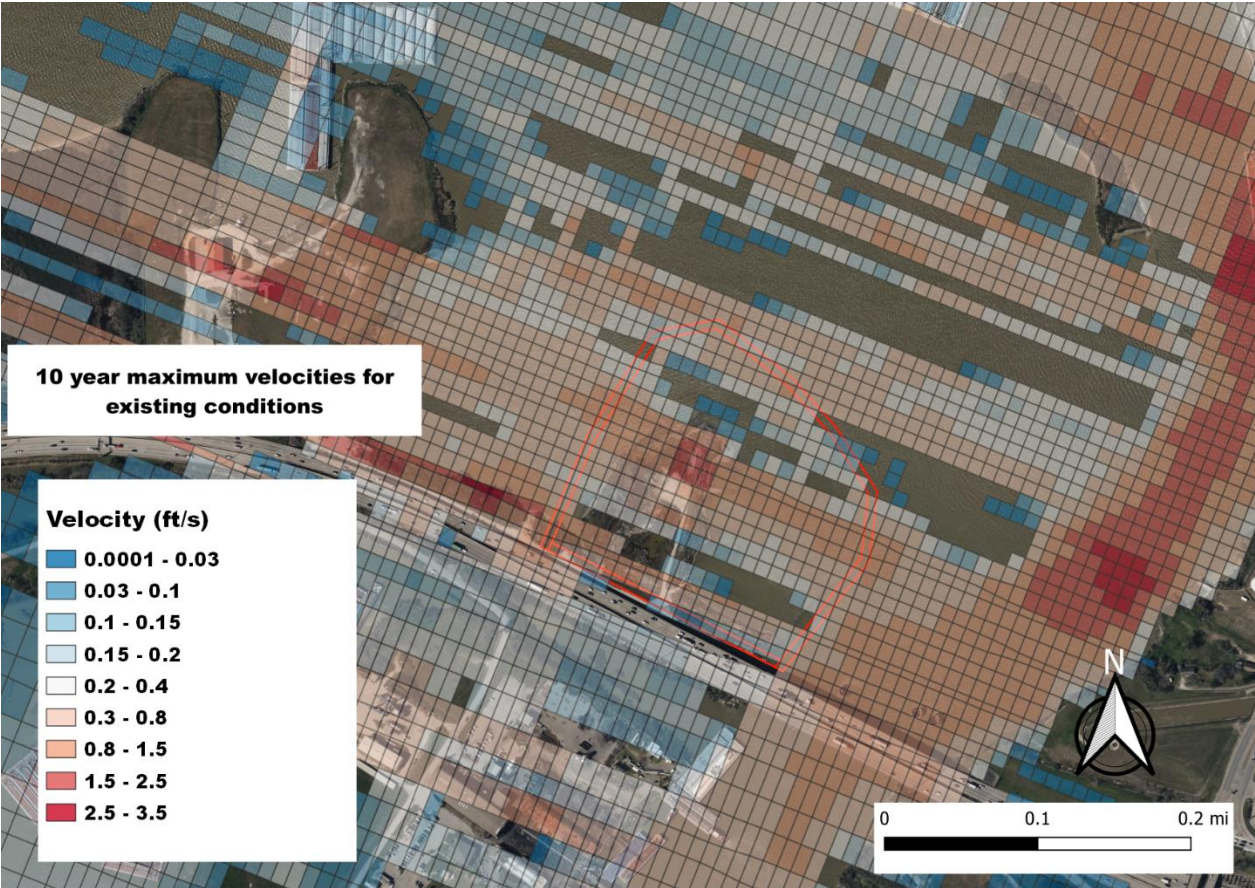
Velocity Figures Existing Conditions



Appendix C - Shear Stress and Velocity Model Results for All Scenarios



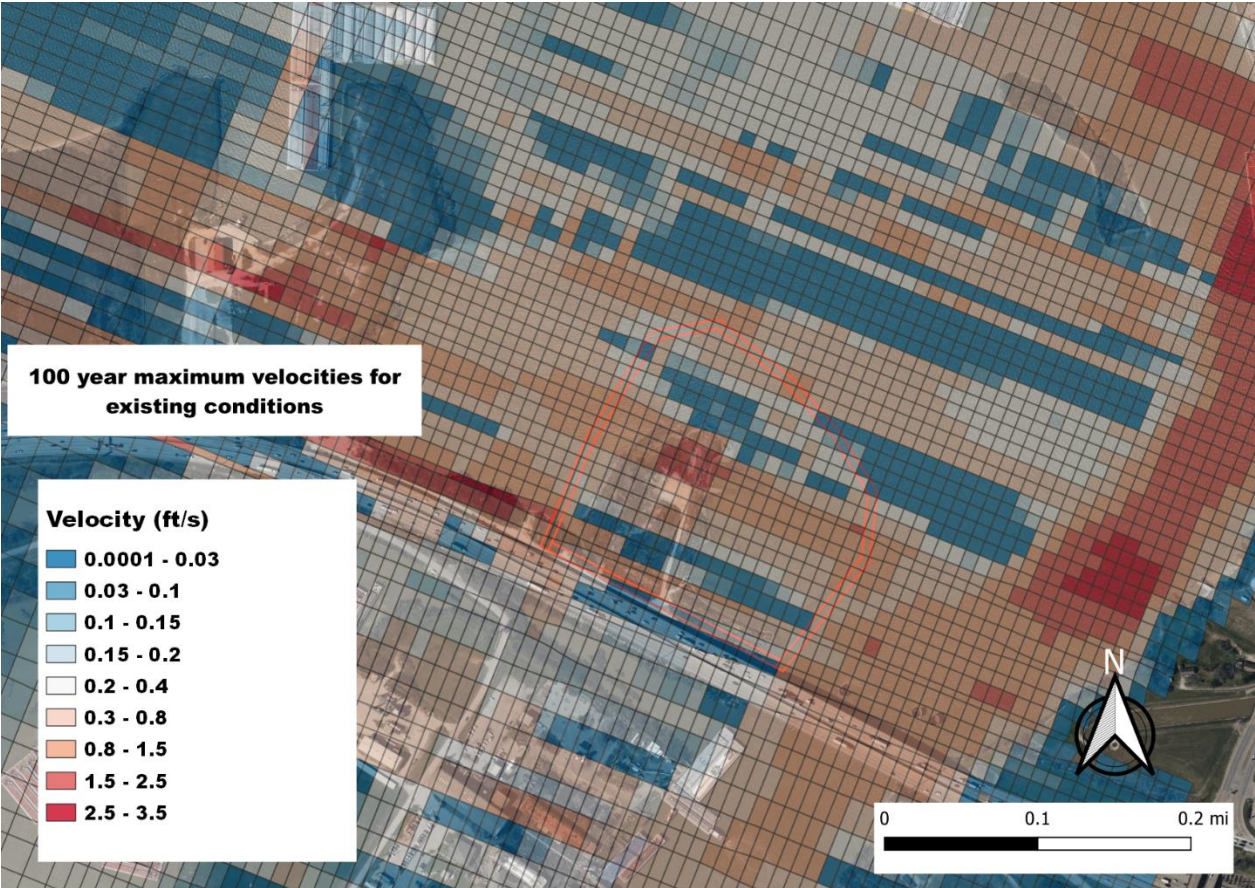
Appendix C - Shear Stress and Velocity Model Results for All Scenarios



Appendix C - Shear Stress and Velocity Model Results for All Scenarios



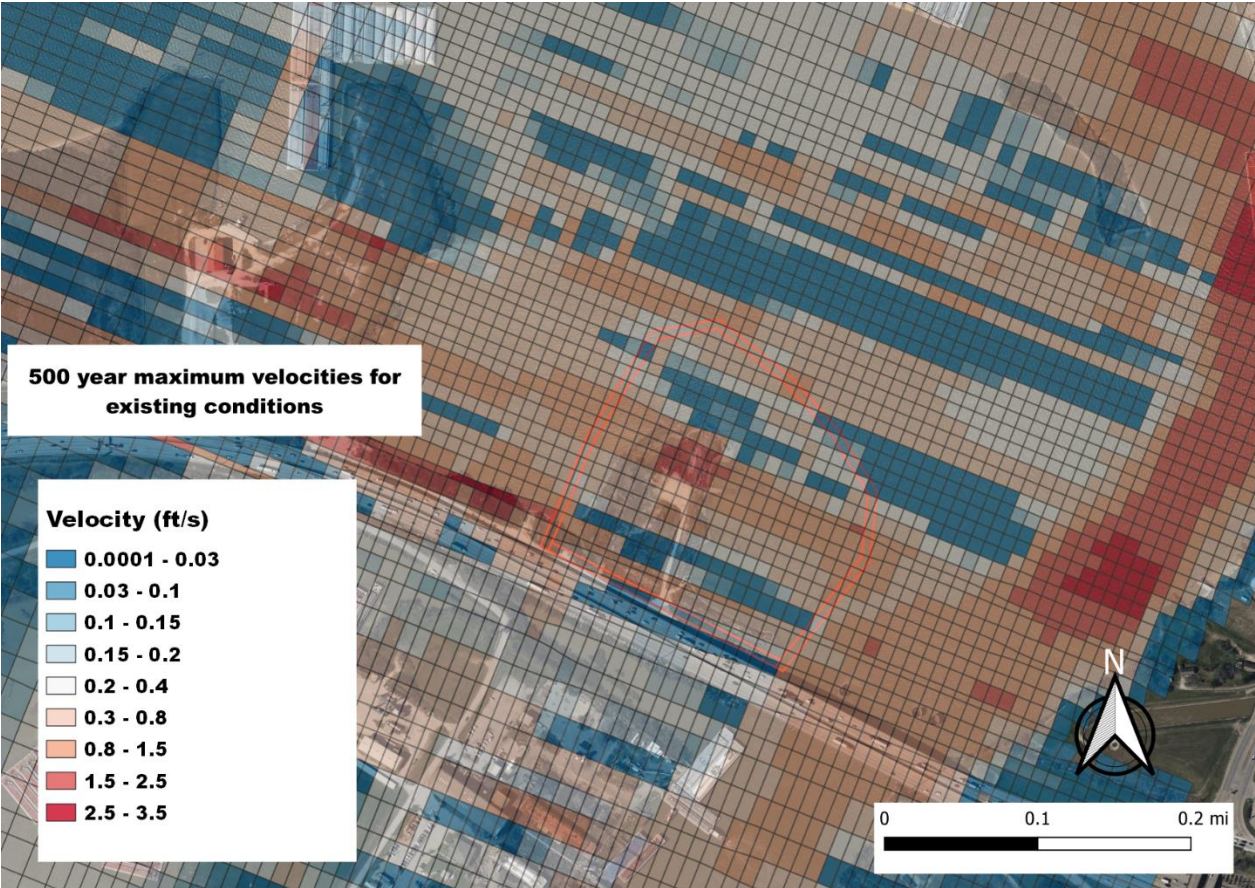
Appendix C - Shear Stress and Velocity Model Results for All Scenarios



Appendix C - Shear Stress and Velocity Model Results for All Scenarios



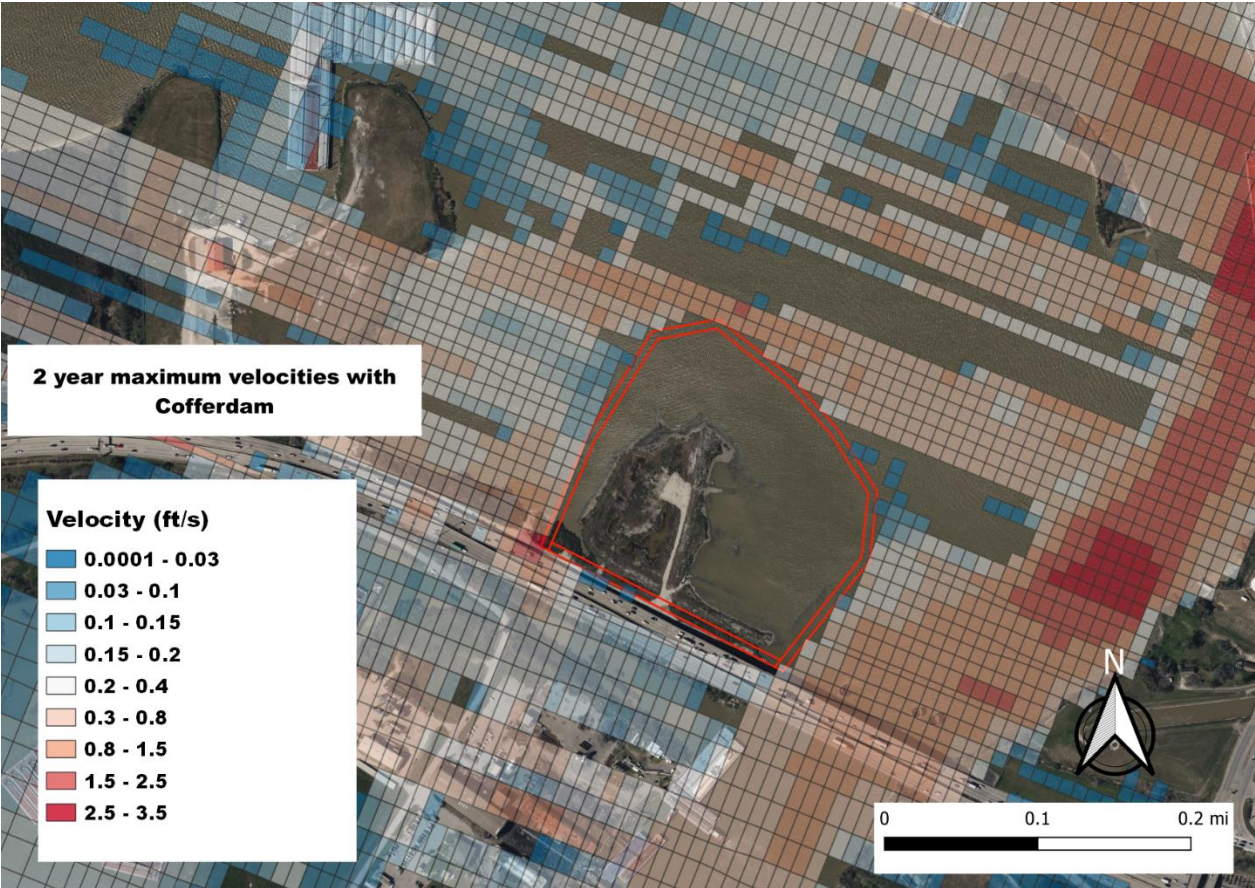
Appendix C - Shear Stress and Velocity Model Results for All Scenarios



Appendix C - Shear Stress and Velocity Model Results for All Scenarios



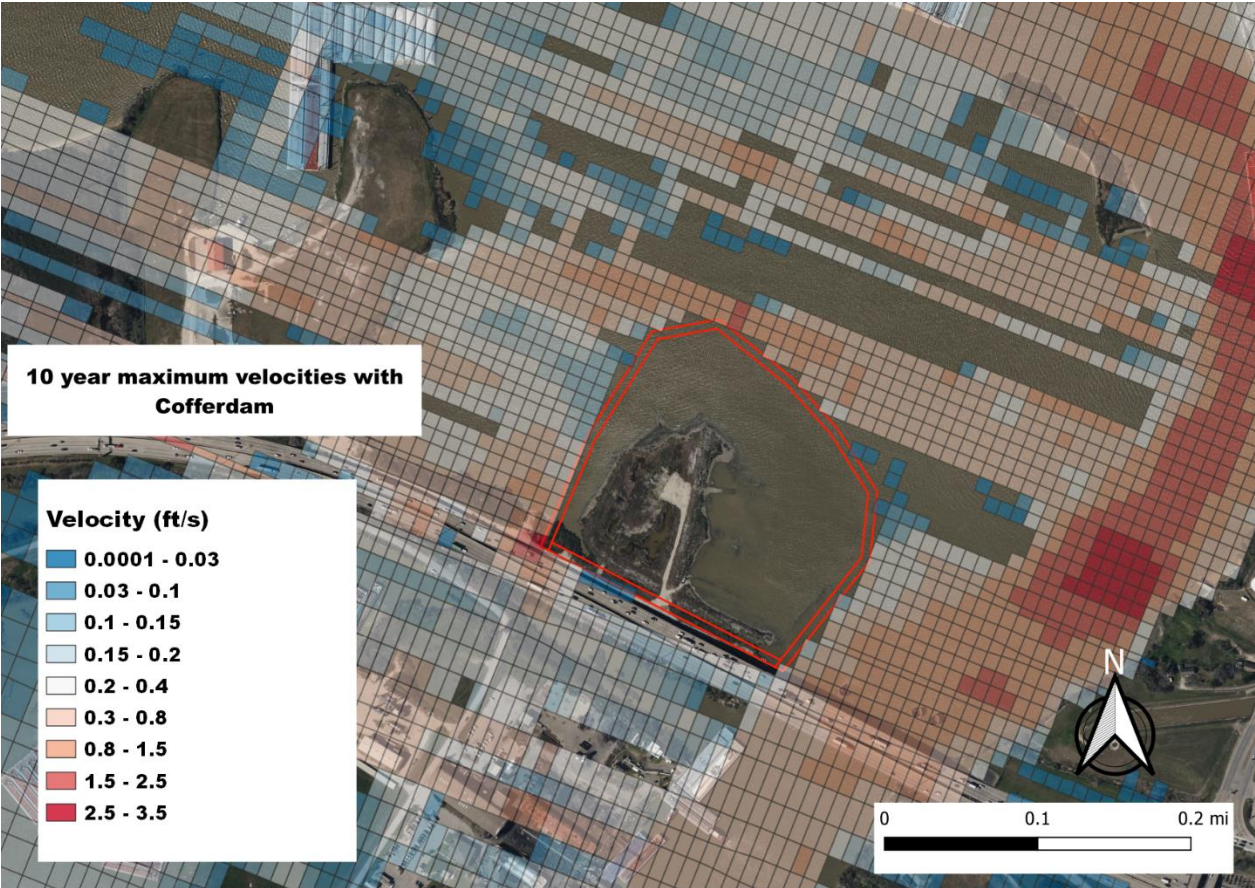
Velocity Figures with Cofferdam



Appendix C - Shear Stress and Velocity Model Results for All Scenarios



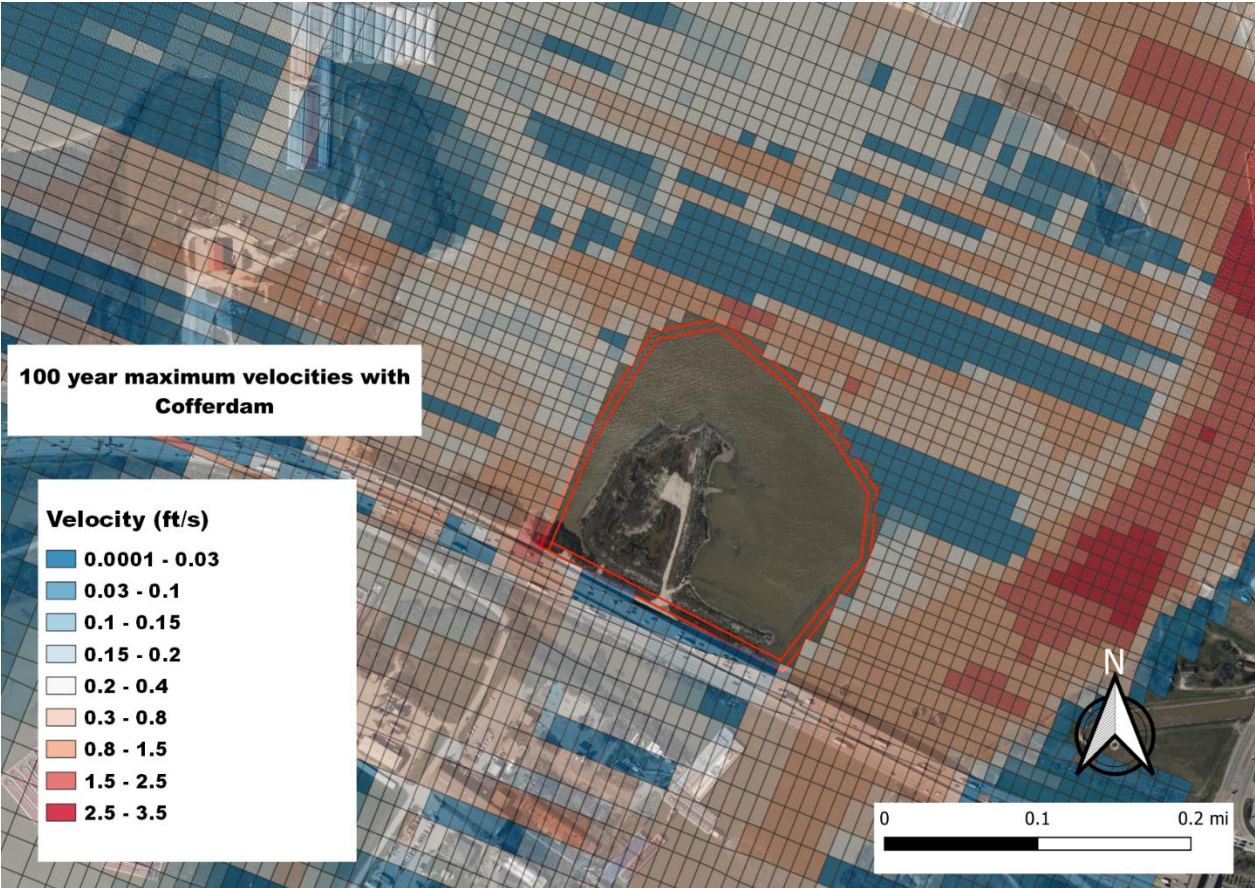
Appendix C - Shear Stress and Velocity Model Results for All Scenarios



Appendix C - Shear Stress and Velocity Model Results for All Scenarios



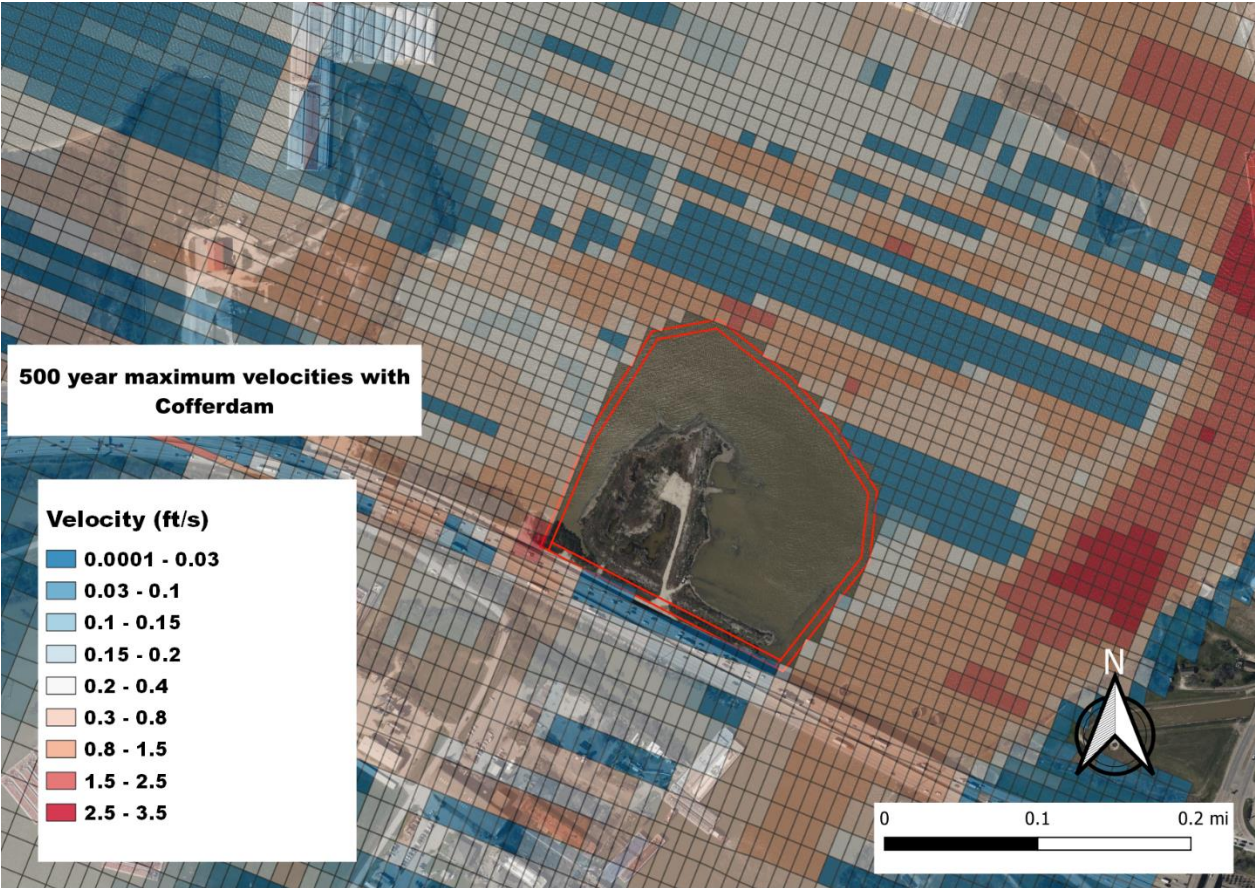
Appendix C - Shear Stress and Velocity Model Results for All Scenarios



Appendix C - Shear Stress and Velocity Model Results for All Scenarios



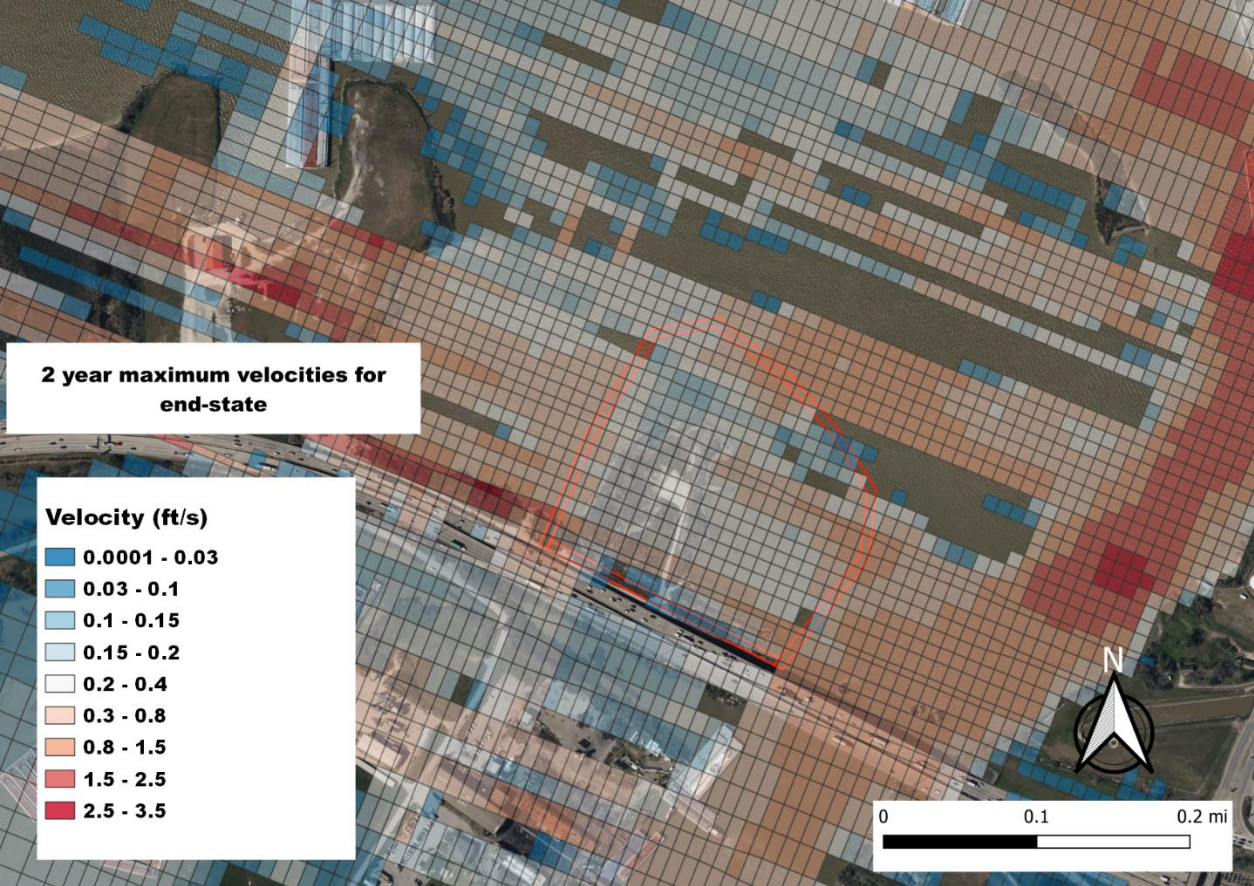
Appendix C - Shear Stress and Velocity Model Results for All Scenarios



Appendix C - Shear Stress and Velocity Model Results for All Scenarios



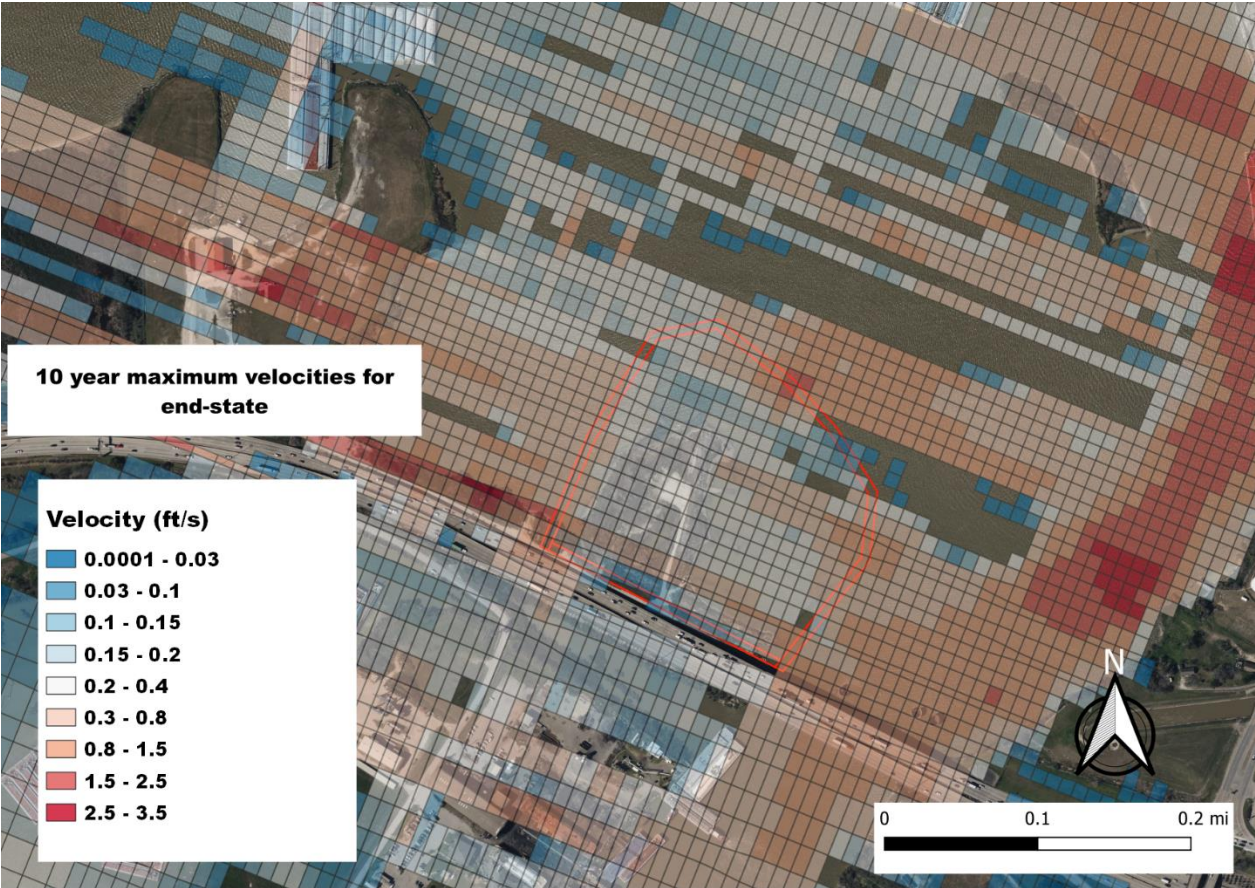
End-State Velocity Figures



Appendix C - Shear Stress and Velocity Model Results for All Scenarios



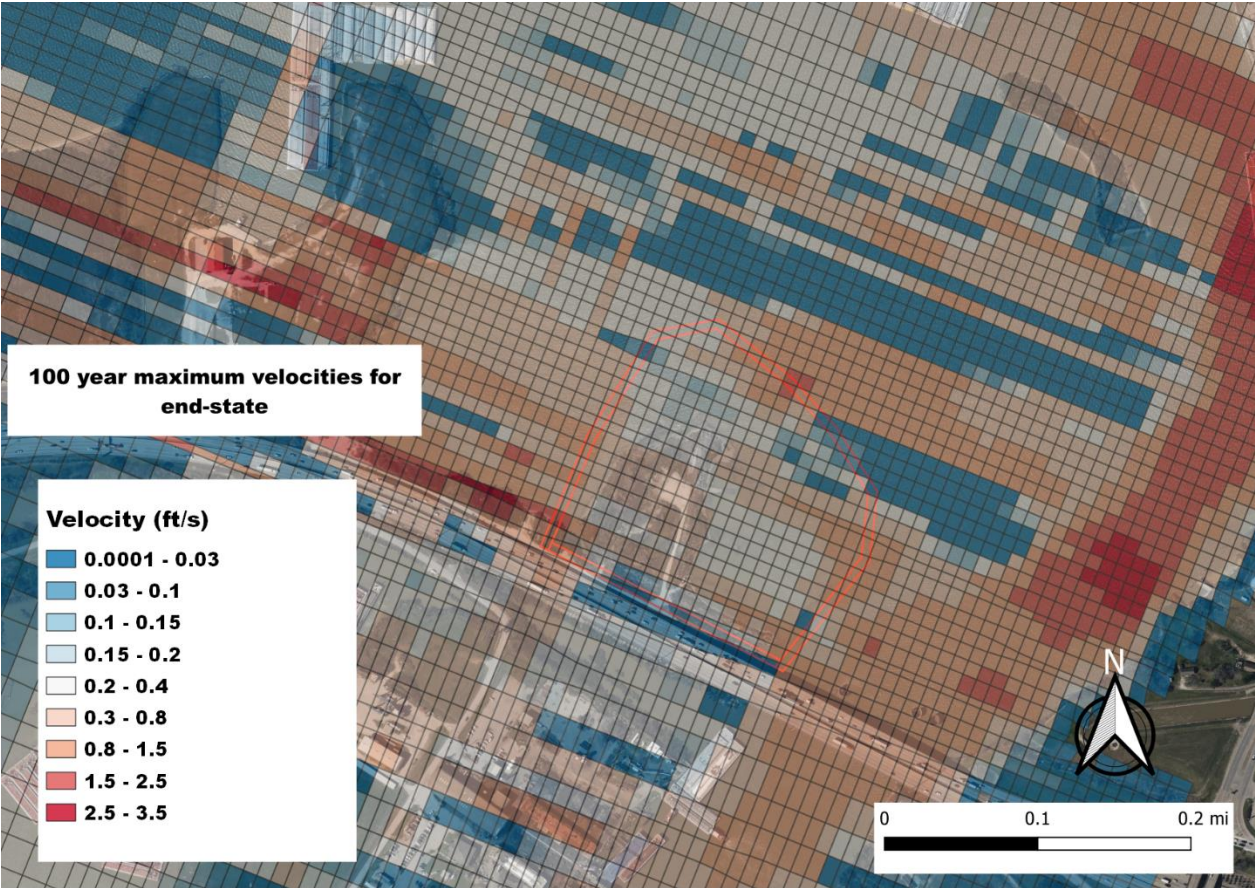
Appendix C - Shear Stress and Velocity Model Results for All Scenarios



Appendix C - Shear Stress and Velocity Model Results for All Scenarios



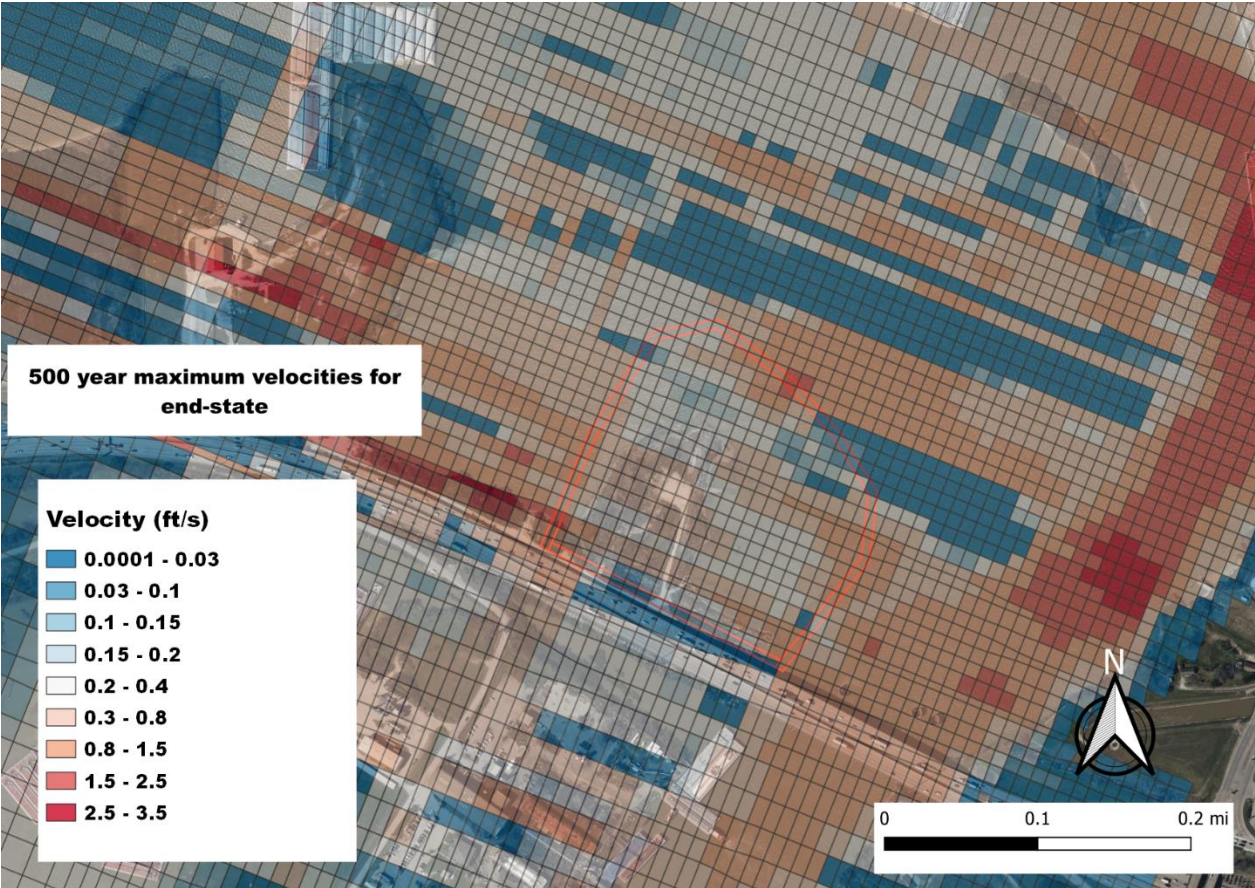
Appendix C - Shear Stress and Velocity Model Results for All Scenarios



Appendix C - Shear Stress and Velocity Model Results for All Scenarios



Appendix C - Shear Stress and Velocity Model Results for All Scenarios



Appendix C - Shear Stress and Velocity Model Results for All Scenarios



Velocity Difference Figures

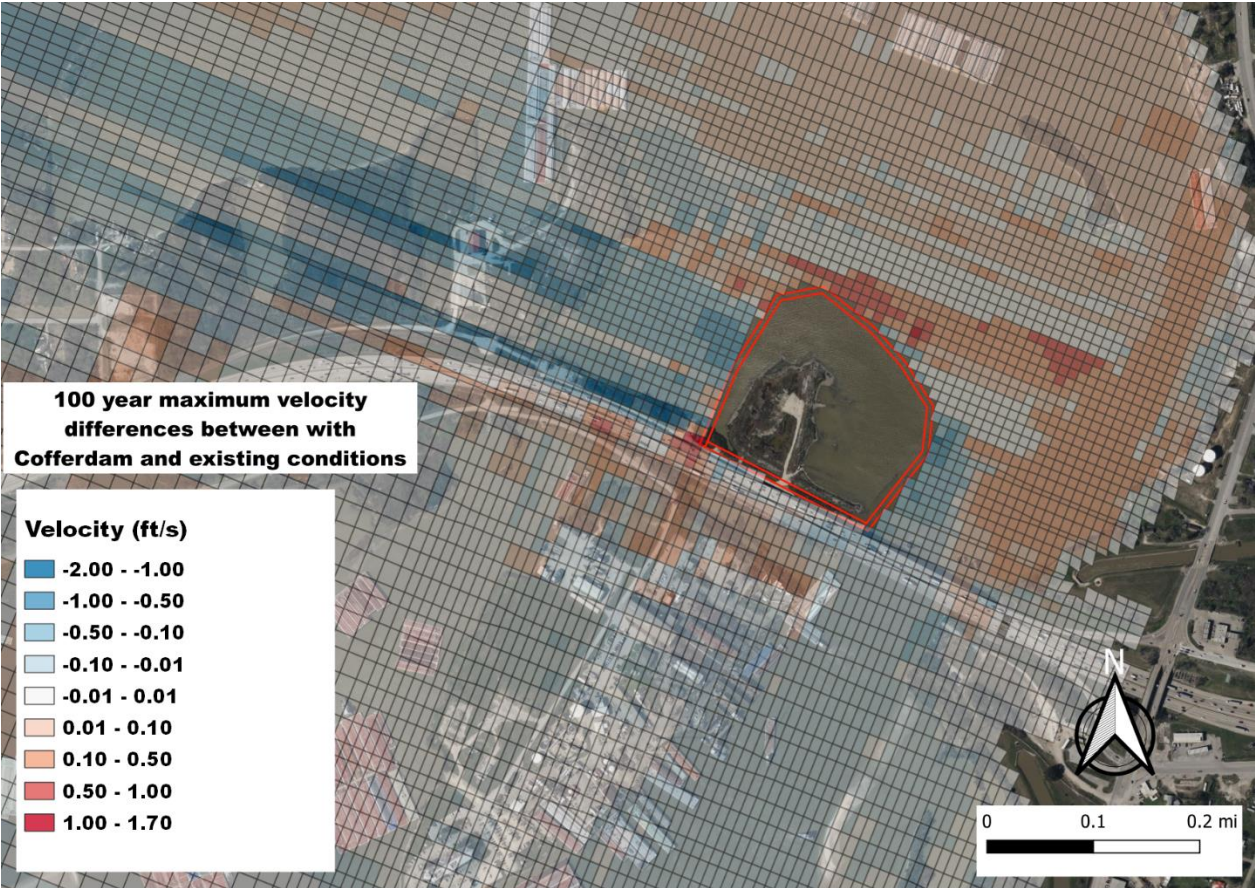
With Cofferdam Minus Existing Conditions



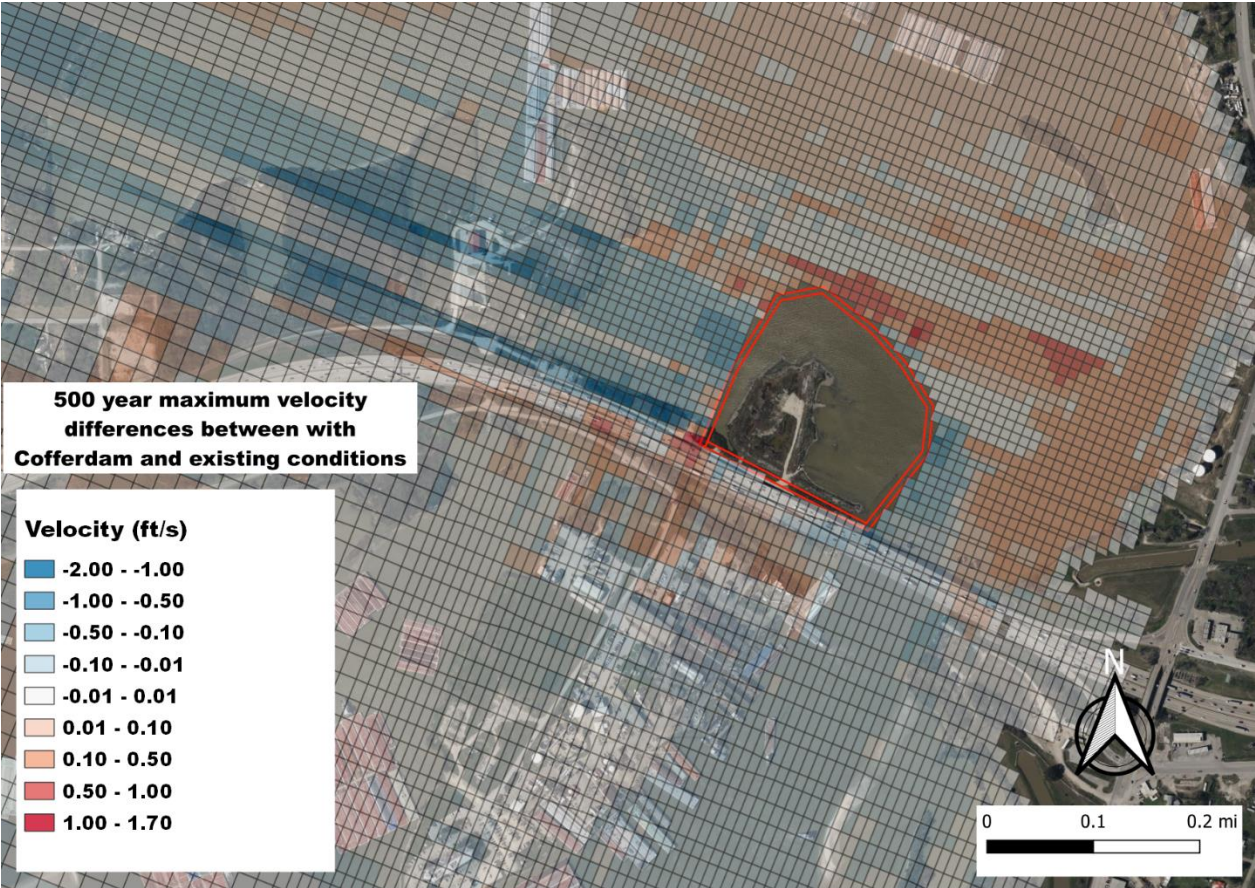
Appendix C - Shear Stress and Velocity Model Results for All Scenarios



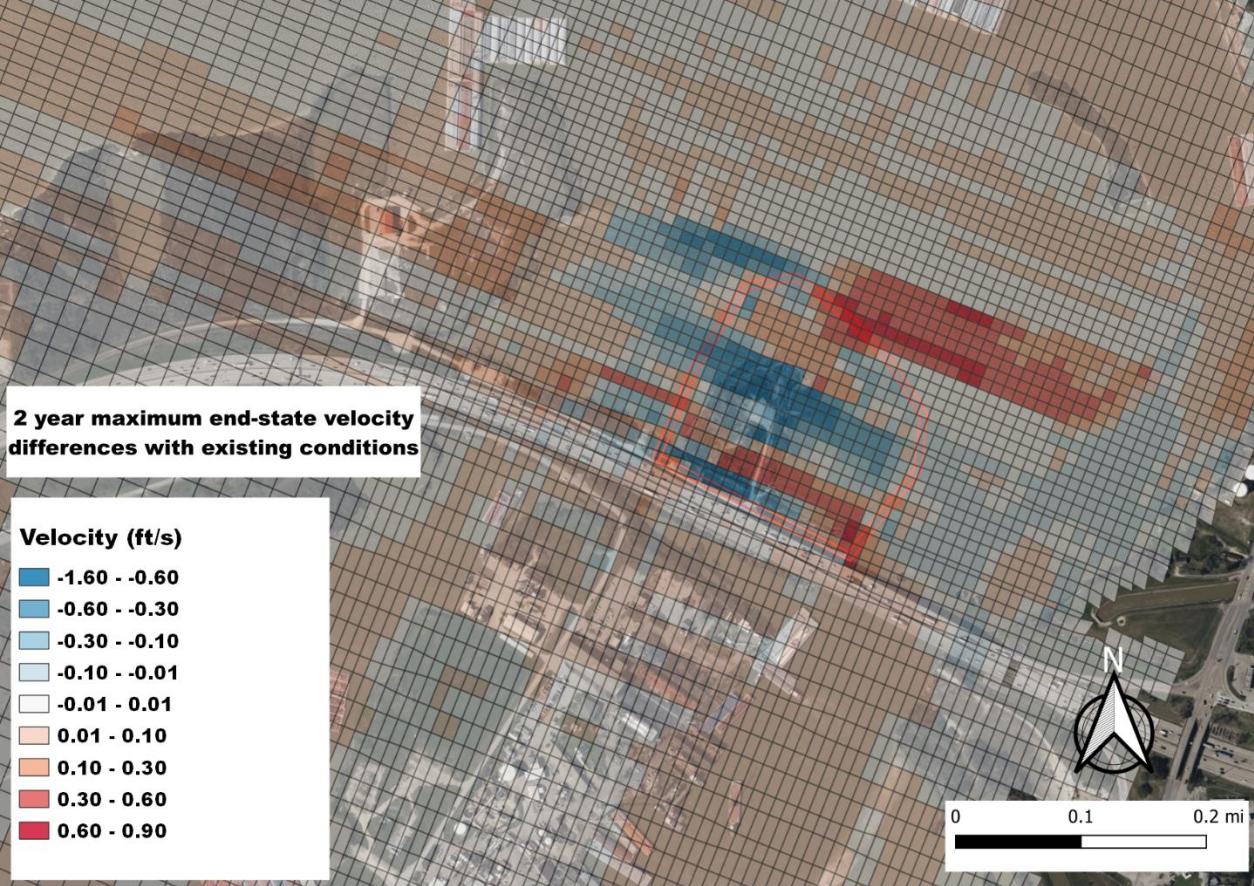
Appendix C - Shear Stress and Velocity Model Results for All Scenarios



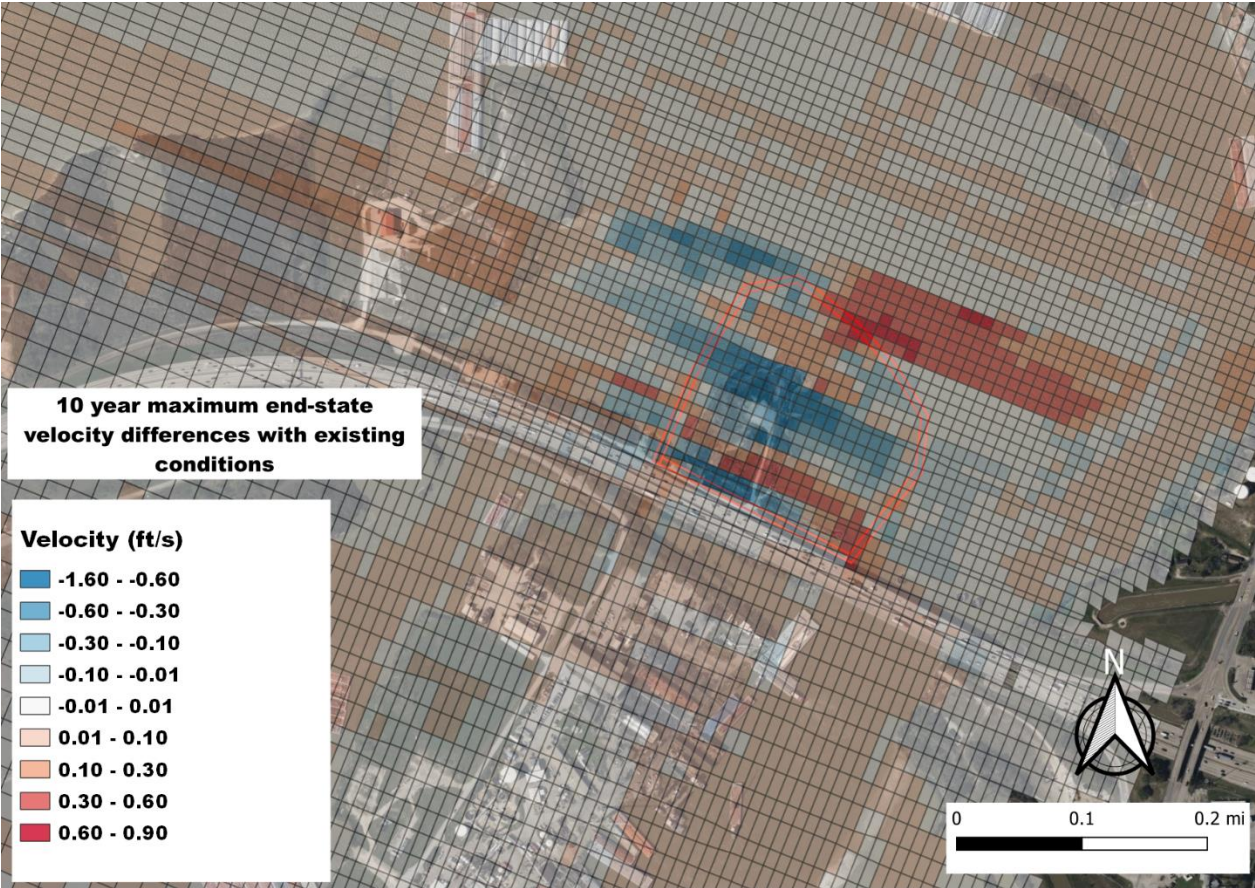
Appendix C - Shear Stress and Velocity Model Results for All Scenarios



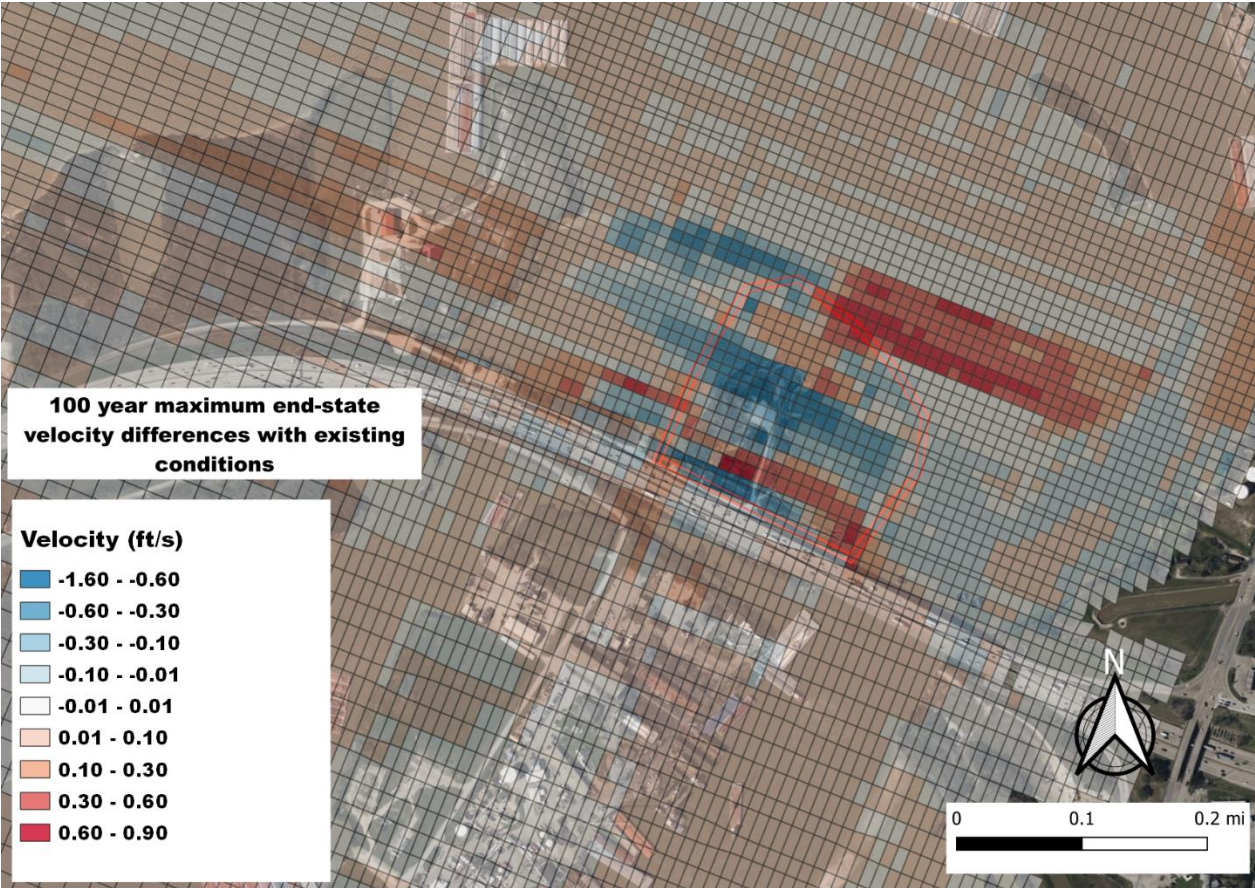
End-State Minus Existing Conditions



Appendix C - Shear Stress and Velocity Model Results for All Scenarios



Appendix C - Shear Stress and Velocity Model Results for All Scenarios



Appendix C - Shear Stress and Velocity Model Results for All Scenarios

